Etude des interactions du photosensibilisant méta-tétra(hydroxyphényl)chlorine avec les protéines de plasma et les cellules

Siarhei Sasnouski

UNIVERSITE HENRI POINCARE-NANCY I
FACULTE DE MEDECINE

THESE

pour obtenir le grade de

DOCTEUR DE L'UNIVERSITE HENRI POINCARE-NANCY I

Discipline : Bio ingénierie

Présentée et soutenue publiquement

par **Siarhei Sasnouski**

Le 23 octobre 2006

Etude des interactions du photosensibilisant méta-tétra(hydroxyphényl)chlorine
avec les protéines de plasma et les cellules

Directeurs de Thèse : Dr. L. Bezdetnaya-Bolotine
Dr. V. Zorin

JURY

Jury :   Dr. L. Bezdetnaya-Bolotine (CAV CRAN UMR CNRS 7039)

Dr. V. Zorin (BSU, Minsk)

Pr. A. Fedulov (BSMU, Minsk)

Pr. F. Guillemin (CAV CRAN UMR CNRS 7039)

Rapporteurs :   Dr. S. MacRobert (UCL, Londres)

Dr. D. Brault (BIOMOCETI, UMR CNRS 7033, Paris)

CAV, CRAN, UMR 7039 CNRS, UHP-NANCY I et INPL, BSU

SUMMARY

I GENERAL INTRODUCTION

Photodynamic therapy (PDT) has been developed as a treatment modality for a number of malignant and non-malignant disorders. PDT treatment is based on the presence of a drug with photosensitising and tumour localizing properties combined with visible light and oxygen. Separately, these three components are harmless, but in combination they may destroy tissue and inactivate cells.

It was shown that direct injection of sensitizers into the tumor is ineffective. Hence, the transport of photosensitizers (PSs) in the blood after intravenous injection seems to influence the photodynamic efficiency. In aqueous media like blood plasma, most of the tetrapyrrolic PSs form dimers and higher aggregates and as such are ineffective in producing singlet oxygen, thus resulting in a drop of their photosensitizing efficiency. Both aggregation and disaggregation of porphyrins occur in the blood circulation, and the competition between these processes could affect the in vivo PDT efficacy.

The PSs accumulation in cells can be realized by passive diffusion through plasmatic membrane or by various types of endocytosis. During interactions with plasma proteins hydrophobic sensitizers dissociate from an aggregate and bind to protein molecules. The type of protein-carrier governs the delivery of sensitizer to the tumor. In vivo transport of hydrophobic porphyrinoid derivatives is carried out by lipoproteins. Serum albumin serves as a carrier for amphiphilic and hydrophilic photosensitizers. The nature of the carrier protein also affects the drug localisation in the tumor with albumin primarily delivering bound drugs to the vascular stroma, while lipoproteins internalize sensitizers in malignant cells. Plasma proteins binding affinity for various photosensitizers can play an important role in drug distribution and photodynamic efficacy.

Accurate dosimetry is necessary to ensure complete treatment and to allow for consistent and reproducible patient outcome. It is accepted that the phototherapeutic effect of PDT is, in most cases, a result of singlet oxygen generation during activation of photosensitizer by light. The objective of PDT is to deliver a cytotoxic species dose that is sufficient to kill the malignant cells in a tumour. Dynamic variations and interrelationship of several parameters of PDT treatment, such as photosensitizer concentration, localization, photo-stability and aggregation state, optical properties of the tissue, characteristics of irradiation, make the treatment very complex. Therefore understanding of the influence of

these parameters on photodynamic toxicity may provide valuable information for optimization of the PDT treatment protocols.

Meta-tetra(hydroxyphenyl)chlorin (mTHPC) or Foscan® is a second-generation photosensitizer and is one of the most effective sensitizers studied to date. mTHPC has been granted European approval for palliative treatment of patients with advanced head and neck cancers and undergoes clinical open-label multicenter studies for the treatment of early squamous cell carcinoma. It is about two orders of magnitude more active compared to Photofrin.

The first objective of the present work was the study of the correlation between mTHPC-PDT efficiency and its biodistribution as a function of time. In a second part, we examined influence of the aggregation state of the photosensitizer on its interactions with plasma proteins. In a third part, we studied the kinetic characteristics and mechanism of sensitizer redistribution from the complexes with plasma proteins. The fourth part of the work consists of the assessment of mTHPC-PDT dosimetry and phototoxicity in vitro. The fifth part of the work was the study of electronic properties of sensitizer using Huckel-based quantum mechanical model of Van der Waals interactions and determination of mTHPC aggregates structure.

II INTRODUCTION

II.1. History and clinical applications of Photodynamic Therapy

Light has been employed in the treatment of disease since antiquity. Phototherapy has been applied by humans for 3000 years and was known by the Egyptians, the Indians and the Chinese (Spikes 1985). Herodotus (6C BC) is recorded as noticing the beneficial effect of sunlight on bone growth, and the eminent Hippocrates (460-375 BC) recommended the use of heliotherapy for various human diseases. But the first relevant "modern" scientist in the field of phototherapy was Niels Rydberg Finsen. From 1895 until 1903 he performed phototherapy on 800 patients, and in 1903 he was awarded the Nobel Prize for Physiology-Medicine for his work on the use of light from the carbon arc in the treatment of lupus vulgaris (skin tuberculosis) (Szeimies 2001). The concept of cell death being induced by the interaction of light and chemicals has first been reported by a German medical student Oscar Raab. In the winter semester of 1897-1898 he started an investigation on the toxicity of acridine to paramecia. This work was carried out under the direction of Professor Dr. Hermann von Tappeiner. Initially, Raab found that the apparent toxicity of low concentrations of acridine

varied significantly from day to day. However, he soon noted that the toxicity depended on the intensity of sunlight in the laboratory. He was then able to show that low concentration of acridine and some other colored dyes such as eosin, that had no effect in the dark, provoked the rapid killing of paramecia in the presence of light (Raab 1900). In 1902, C. Ledoux-Lebards observed that eosin killed paramecia more efficiently in open flask than in a closed bottle (Ledoux-Lebards 1902), and he postulated that the presence of oxygen is essential for photoinactivation. It is in 1904 that von Tappeiner and Jodlbauer coined the term "photodynamische Wirkung" (von Tappeiner and Jodlbauer 1904) which we translate as "photodynamic action" for oxygen-requiring photosensitized reactions in biological systems. Although the mechanism of action was still unknown, it did not take long until this new therapeutic approach was tried out on patients. The first paper reporting a clinical trial was published in November 1903 by von Tappeiner and Jesionek (von Tappeiner and Jesionek 1903). The photosensitizers used so far were dyes like chinidine, acridine and eosin, and further studies were devoted to develop new clinically relevant photosensitizers.

In 1911, Walter Hausmann injected 2 mg hematoporphyrin subcutaneously in mice, which were exposed to sunlight and he observed edema, erythema and skin necrosis (Haussman 1911). The first report on the use of hematoporphyrin in humans was done by Meyer-Betz who injected himself with 200 mg hematoporphyrin and became extremely photosensitive during more than two months (Meyer-Betz 1913). Accumulation and retention of hematoporphyrin in human neoplastic tissue was evidenced by Auler and Banzer in 1942 (Auler and Banzer 1942). Interrupted by the Second World War clinical studies on photodynamic treatment were not performed in a major organized way until the middle 70's, largely through the efforts of Dougherty.

Photodynamic therapy uses the combination of a photosensitizing drug and light to cause selective damage to the target tissue. Firstly, the sensitizer is injected into the bloodstream and it begins to redistribute to cells throughout the body. After certain period, when sensitizer retention in the tumor becomes greater than in normal tissue, the tumor region is illuminated with a light source with appropriate emission wavelength. Absorption of this light by tumor-localized sensitizer leads to generation of toxic free radicals and finally to destruction of malignant tissue (Henderson and Dougherty 1992). Tumor destruction can be realized both by direct cells killing or by photodamage of the tumor vasculature resulting in local hypoxia and indirect cells killing (Dougherty et al. 1998). Within a few hours after PDT tumor tissue exhibits extensive regions of necrosis and apoptosis. During the first 24 h the treated area shows evidence of swelling, infiltration of inflammatory cells and tissue

breakdown (Dougherty et al. 1998). After PDT treatment a large number of cytokines and inflammatory mediators are released (Gollnick et al. 1997). The enhanced immune response in the tumor area is necessary for complete elimination of the tumor tissue (Korbelik and Dougherty 1999).

Some advantages of PDT over other techniques include some degree of selectivity of PS binding to tumor tissue, the absence of systemic toxicity of the drug alone, the ability to focus the light on the tumor region. Moreover, the treatment can be repeated multiple times safely and can be used after surgery, chemotherapy or radiotherapy. PDT can induce a long-term anti-tumor immunity, a relatively unique response among anticancer therapies (MacDonald et al. 1999). As most of PSs are fluorescent the imaging and detection strategies can be applied in PDT protocols, known as photodetection or photodiagnosis. They may be used to detect otherwise hidden disease such as dysplasia, to delineate tumor borders, or to visualize disease in inaccessible areas such as the esophagus, bronchus or colon. Another application of fluorescent imaging and quantification is its ability to improve PDT dosimetry by measuring the amount of PS in the lesion before applying the appropriate illumination parameters. Among disadvantages of PDT are the prolonged skin photosensitivity, limited depth of light penetration (< 1 cm) and the possibility to treat only localized superficial tumors. The improved understanding of the tissue and cellular factors that control PDT and increased experience in the clinic has led to much larger, better-controlled clinical trials and the approval of drugs makes PDT a clinical reality.

Photofrin® was the first approved in 1993 in Canada, now approved in more than 40 countries (1995 approval in USA, Canada, Japan and Europe) for advanced and early lung cancer, superficial gastric cancer, oesophageal adenocarcinoma, cervical cancer, and bladder cancer. Then the Levulan® got the FDA approval in 1999 for actinic keratosis, followed in 2001 by mTHPC (approved for advanced head and neck cancer, Europe, Norway and Iceland). Currently, two derivatives of 5-ALA, methylaminolevulinate (MAL) and hexylaminolevulinate (HAL), gained marketing authorization from the regulatory offices in Europe and Australia. MAL is marketed under the trade name Metvix® for the treatment of actinic keratosis (AK) and difficult-to-treat basal cell carcinoma (BCC), HAL has recently been launched under the trade name Hexvix® for the improved diagnosis of superficial bladder cancer in Europe. PDT has also indications for non-oncological diseases, such as wet age related macular degeneration using benzoporphyrin derivative (Visudyne®, FDA and European approval in 2000). Also a number of other conditions have also been treated

including psoriasis, rheumatoid arthritis, menorrhagia and benign prostatic hyperplasia. In addition, PDT-mediated immune-modulation, bone marrow purging and PDT of certain bacterial, fungal and viral infections are being evaluated.

II.2. Photosensitization mechanisms

2.1. Pathway of molecular excitation and deactivation

The absorption of light by a chromophore is the initial step in all photophysical and photochemical reactions. The energy of the absorbed light promotes molecules from their ground state to states of higher energy (excited states). At room temperature, almost all the molecules are in their ground state S_0, which is the electronic state associated with the lowest energy and a configuration where all electrons are orbitally paired. During an electronic transition one of the electrons is excited from an initially occupied orbital of low energy to a previously unoccupied orbital of higher energy. The molecule undergoes transition from its ground state S_0 to an excited state S_1.

The excited state S_1 is energetically less preferable than S_0. Several physical pathways, leading to deactivation of excited state can be followed, represented in the Jablonski diagram (Fig. 2.1). A molecule in a high vibrational level of the excited electronic state S_n quickly falls to the lowest vibrational level (Vibrational Relaxation VR). Also, a molecule in a higher excited state S_n can fall to the first excited singlet state S_1 (Internal Conversion IC). Then, the singlet state S_1 can rapidly return to the ground state level S_0 by two mechanisms: a radiative process emitting a quantum of fluorescence or a non-radiative IC with dissipating the excitation energy into the heat (Table 2.1). Owing to IC and VR procceses, photons of fluorescence are generally emitted from the lowest vibrational sublevel of the excited singlet state (S_1) level. This implies that the form of fluorescence spectrum does not depend on the excitation wavelength (Vavilov's rule). Emitted photons have lower energy than absorbed photons, so fluorescence emission maximum is red-shifted as compared to the absorption maximum ($\lambda_{emission} > \lambda_{absorption}$, Stokes-Lommel's law).
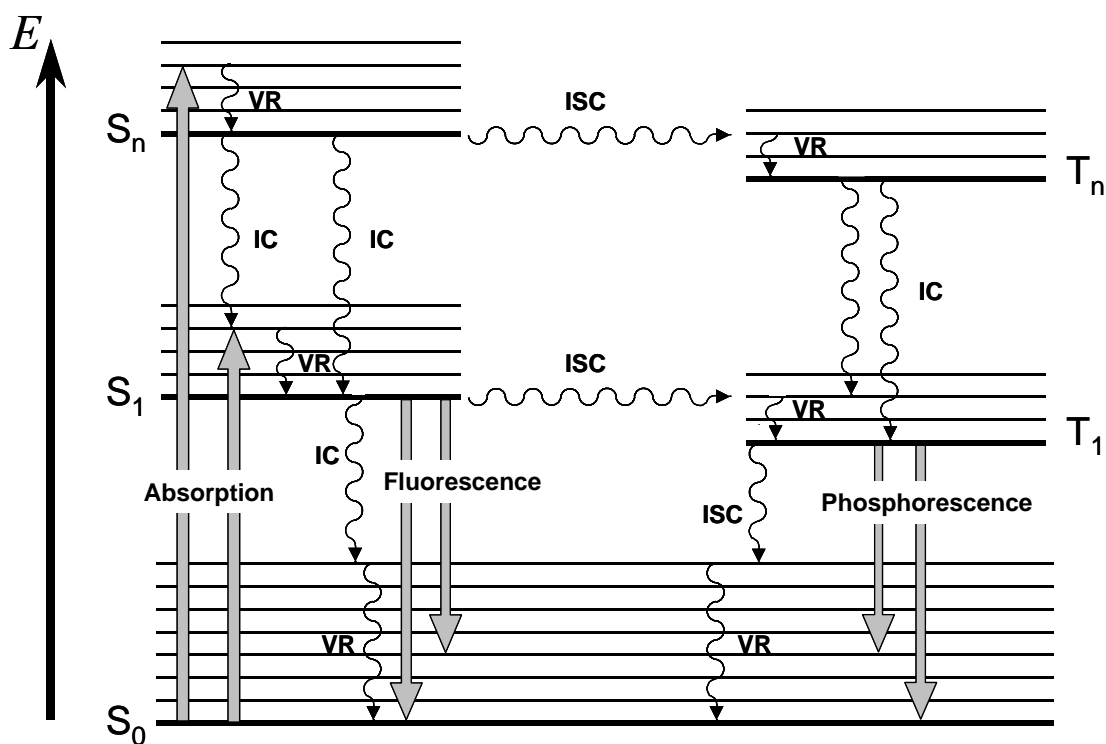
Figure 2.1 : Jablonski diagram, where IC stands for internal conversion, ICS for intersystem crossing and VR, for vibrational relaxation.

In addition to radiationless and radiative process, sensitizer molecule from the first exited singlet state can undergo a transition to a triplet state T_1 via intersystem crossing (ISC). The lifetime of the triplet state is much longer ($\tau \sim 10^{-3}$ - 10^{-7} s) than the lifetime of the singlet state ($\tau \sim 10^{-10}$ s), thus increasing dramatically the probability of interactions of neighbouring molecule with sensitizer in its triplet state. There are several pathways for the triplet state T_1 to return to a ground state S_0. De-excitation can occur with the emission of a photon, called phosphorescence, but at room temperature and due to Vavilov's rule phosphorescence intensity is weak and difficult to detect. The excited triplet state T_1 can be alternatively deactivated by undergoing intersystem crossing followed by vibrational relaxation (Fig. 2.1).

For most of the organic molecules, only the singlet state S_1 and triplet state T_1 of lowest energy can be considered as likely candidates for the initiation of photochemical and photophysical reactions. This is due to the fact that higher order electronic state ($n \geq 2$) undergos very rapidly internal conversion from S_n to S_1 and from T_n to T_1. This generalization (which was used here in the description of the Jablonski diagram Fig. 2.1) is known as Kasha's rule.

Table 2.1. : Photochemical processes involved in the activation and deactivation pathway of the photosensitizers and some of their characteristics

Processes	Reactions	Timescale	Constant
excitation	$h\upsilon + S_0 \rightarrow S_1, S_2,\ldots,S_n$	$\tau \sim 10^{-15}\text{-}10^{-12}$ s	k_{abs}
internal conversion	$S_n,\ldots,S_2 \rightarrow S_1$ + heat	$\tau \sim 10^{-13}\text{-}10^{-10}$ s	$k_{IC}[S_n]$
internal conversion	$S_1 \rightarrow S_0$ + heat	$\tau \sim 10^{-10}$ s	$k_{IC}[S_1]$
intersystem crossing	$S_1 \rightarrow T_1$ + heat	$\tau \sim 10^{-7}$ s	$k_{ISC}[S_1]$
photochemical reaction	$S_1 \rightarrow S_0$ + reaction		$k_R^{\,S}[S_1]$
fluorescence	$S_1 \rightarrow S_0 + h\upsilon_{fluor}$	$\tau \sim 10^{-11}\text{-}10^{-8}$ s	$k_F[S_1]$
intersystem crossing	$T_1 \rightarrow S_0$ + heat	$\tau \sim 10^{-2}\text{-}10^{2}$ s	$k_{ISC}^{\,T}[T_1]$
phosphorescence	$T_1 \rightarrow S_0 + h\upsilon_{phosphor}$	$\tau > 10^{-6}$ s	$k_{phosph}[T_1]$
chemiluminescence	Energy $+ S_0 \rightarrow S_1 \rightarrow S_0 + h\upsilon_{chemilum}$	$\tau > 10^{-6}$ s	$k_{chemilum}[S_1]$
photochemical reaction	$T_1 \rightarrow S_0$ + reaction		$k_R^{\,T}[T_1]$

2.2 Mechanism of photosensitized reactions

Photosensitized reaction can be defined as a process in which light activation of a chromophore induces chemical changes in another molecule than chromophore. The initial step of the reaction is the absorption of a photon by the photosensitizer, leading to the generation of molecules in excited triplet states (^{3}P*). The reaction can follow two competing pathways called Type I and Type II reactions (Sharman et al. 2000). According to the definition established by Foote (Foote 1991) and as shown in Fig. 2.2, a Type I mechanism involves the direct interaction of ^{3}P* with a substrate (S), whereas in a type II process, ^{3}P* reacts first with molecular oxygen to produce highly reactive oxygen intermediate that easily initiates further reactions.
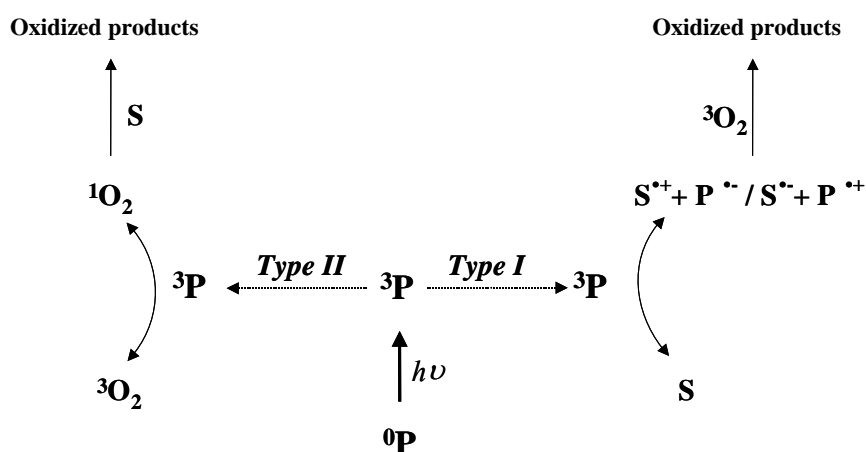
Figure 2.2. : Diagram of photosensitizations mechanisms occurring after absorption of a photon by photosensitizer.

2.2.1. Type I photosensitization processes

In a type I photochemical reaction, the exited triplet state of the photosensitizer ($^3P^*$) interacts directly with the substrate molecule (S) and leads to the formation of pairs of neutral radicals or radical ions following an electron or hydrogen transfer as shown in the Eqs 1 and 2 :

$$^3P^* + S \longrightarrow P^{\cdot -} + S^{\cdot +} \qquad (1)$$

$$^3P^* + S \longrightarrow P^{\cdot +} + S^{\cdot -} \qquad (2)$$
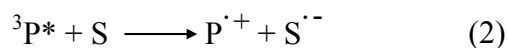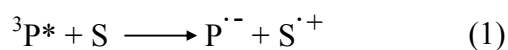
Both the excited photosensitizer and the ground state substrate can act as hydrogen donor or acceptor (Eq. 3-4).

$$^3PH^* + S \longrightarrow P^{\cdot} + SH^{\cdot} \qquad (3)$$

$$^3P^* + SH \longrightarrow PH^{\cdot} + S^{\cdot} \qquad (4)$$
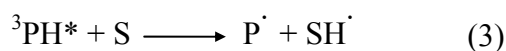
The resulting radical species from Type I primary processes can subsequently participate in different kinds of reactions. In the presence of oxygen, for example, oxidized forms of the sensitizer or of the substrate readily react with O_2 to give peroxyl radicals, thus initiating a radical chain auto-oxidation (Eqs 5 and 6).

11

$$S^{\cdot} + O_2 \longrightarrow SOO^{\cdot} \qquad (5)$$

$$SOO^{\cdot} + SH \longrightarrow S^{\cdot} + SOOH \qquad (6)$$
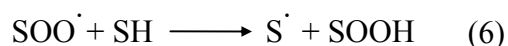
Semireduced forms of the photosensitizer or of the substrate also interact efficiently with oxygen and the electron transfer, which takes place between reactants, generate superoxide radical anion (eq 7).

$$\left. \begin{array}{l} S^{\cdot -} + O_2 \longrightarrow S + O_2^{\cdot -} \\ P^{\cdot -} + O_2 \longrightarrow P + O_2^{\cdot -} \end{array} \right\} \qquad (7)$$
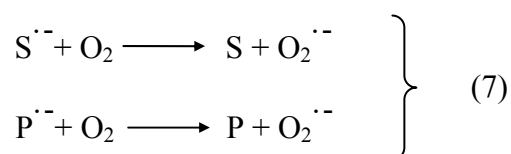
Any reaction that generates $O_2^{\cdot -}$ will also produce hydroperoxide H_2O_2 by spontaneous dismutation (eq 8) or one-electron reduction (eq 9).

$$O_2^{\cdot -} + O_2^{\cdot -} + 2H^+ \longrightarrow O_2 + H_2O_2 \qquad (8)$$

$$O_2^{\cdot -} + 2H^+ + e^- \longrightarrow H_2O_2 \qquad (9)$$
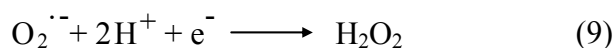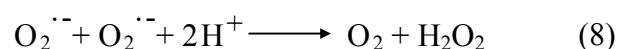
Hydroperoxide is a moderate oxidant, but when it accumulates, it can react with superoxide radical anion (eq 10) or undergo ferrous ion catalysed reduction to give rise to an extremely reactive hydroxyl radical (Haber-Weiss reaction)(eqs 11 and 12).

$$O_2^{\cdot -} + H_2O_2 \longrightarrow O_2 + OH^- + {}^{\cdot}OH \qquad (10)$$

$$\left. \begin{array}{l} O_2^{\cdot -} + Fe^{3+} \longrightarrow O_2 + Fe^{2+} \qquad (11) \\ H_2O_2 + Fe^{2+} \longrightarrow OH^- + {}^{\cdot}OH + Fe^{3+} \qquad (12) \end{array} \right\} \begin{array}{c} \text{Haber-Weiss} \\ \text{reaction} \end{array}$$
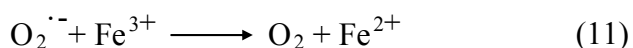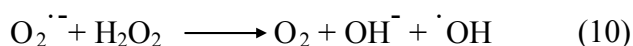
2.2.2. Type II photosensitization processes

This type of reaction requires the presence of molecular oxygen. In most cases, the reaction proceeds via non-radiative energy transfer from the excited triplet state

photosensitizer to the oxygen molecule in its triplet state. Singlet oxygen can only be generated by photosensitizer that has an energy gap between the ground state and the excited triplet state higher than the energy ΔE needed to excite oxygen into its singlet state (Fig. 2.3). ΔE being very low (94 kJ mol-1 (van Lier and Spikes 1989), almost all the tetrapyrrolic photosensitizers can mediate generation of singlet oxygen.
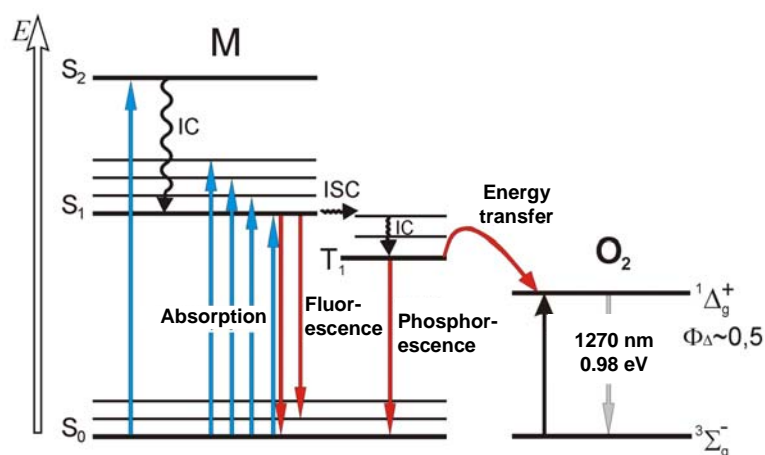
Figure 2.3. : Simplified Jablonski diagram, showing the
activation and deactivation pathways during a Type II reaction.

Due to the higher lifetime of triplet compared to the singlet state of porphyrin-like photosensitizers, photochemical reactions most likely occur with sensitizer in its triplet state. Energy transfer from the excited triplet state of the sensitizer to the ground state (triplet) oxygen is a spin allowed process and the molecule of oxygen undergoes transition from its ground triplet into excited (singlet) state:

$$P \xrightarrow{\ h\nu\ } {}^3P + O_2 \rightarrow P + {}^1O_2 \qquad (13)$$
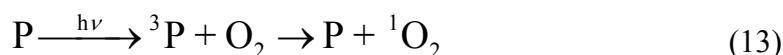
Two forms of singlet oxygen with different excited state energies are generated: ${}^1O_2$ (${}^1\Delta_g$, E = 94 kJ mol^{-1}) and ${}^1O_2$ (${}^1\sum_g$, E = 157 kJ mol^{-1}) (Lang et al. 1998). But ${}^1O_2$ (${}^1\sum_g$) form is rapidly transformed into ${}^1O_2$ (${}^1\Delta_g$) with almost unit efficiency. It was shown through a theoretical estimation based on oxygen diffusion in aqueous solution, that the lifetime of the intermediate to be attacked by oxygen must be at least 10^{-6} s (Imamura and Koizumi 1955). More recently, it was found that oxygen exerted no measurable effect on the short-lived excited singlet state of xanthene dyes even in oxygen-saturated solutions (Gollnick et al. 1992).

Quantum yield of singlet oxygen formation is defined as the ratio of triplet state deactivation rate, that leads to energy transfer to oxygen molecule and the sum of all deactivation rates, leading to triplet state deactivation, like phosphorescence and ISC. For pure Type II reaction, the quantum yield of singlet oxygen formation can be defined as (for constant description see Table 2.1.) :

$$\Phi_\Delta = \frac{k_R^T[T_1]\,[S]}{k_{phosph}[T_1] + k_{ISC}^{\ T}[T_1] + k_R^T[T_1]\,[S]} \tag{14}$$

Data on $^1O_2$ generation quantum yields in different media for some sensitizers are given in Table 2.2.

Table 2.2. Quantum yields of $^1O_2$ ($^1\Delta_g$) generation (Φ_Δ) by sensitizers.

Photosensitizer	Φ_Δ	Medium	Method	Reference
HP	0.53	methanol	1270 nm luminescence	(Chacon et al. 1988)
PPIX	0.56	PB/TX100	lysozyme sensitization	(Fernandez et al. 1997)
BPD-MA	0.77	benzene	1270 nm luminescence	(Aveline et al. 1994)
AlPcS$_4$	0.38	PB/TX100	lysozyme sensitization	(Fernandez et al. 1997)
mTHPP	0.46	air-saturated methanol	1270 nm luminescence	(Bonnett et al. 2001)
mTHPC	0.43	air-saturated methanol	1270 nm luminescence	(Bonnett et al. 2001)
mTHPBC	0.43	air-saturated methanol	1270 nm luminescence	(Bonnett et al. 2001)

In the presence of oxygen the observed quenching rate of PS triplet states is given by (Lang et al. 1998):

$$k_{ob} = k_{decay}^T + k_q[O_2] \tag{15}$$

where k_{decay}^T is the sum of all triplet states deactivation rate constants in the absence of oxygen, k_q is the bimolecular rate constant of triplet states quenching by oxygen, $[O_2]$ is the concentration of oxygen. As diffusion controlled value of k_q is about $10^9 - 10^{10}$ M^{-1}s^{-1} the value of k_{decay}^T is sensitive to small amounts of oxygen in the system and can be used as a direct measure of the oxygen.

The quantum yield of singlet oxygen formation Φ_Δ depends on the quantum yield of the triplet states Φ_T according to:

$$\Phi_\Delta = \Phi_T S_\Delta S_q \qquad (16)$$

where S_Δ is the fraction of triplet molecules quenched by oxygen and yielding $^1O_2$ and is given by

$$S_\Delta = \frac{k_{et}}{k_q} \qquad (17)$$

where k_{et} the rate constant of energy transfer leading to the formation of $^1O_2$ and S_q is the fraction of oxygen dependent triplet deactivations

$$S_\Delta = \frac{k_q[O_2]}{k_{decay}^T + k_q[O_2]} \qquad (18)$$

The denominator represents all pathways of triplet deactivations. For many porphyrins the value of S_Δ is about 0.75 (Keene et al. 1986).

Laser flash photolysis studies in vitro showed that oxygen and local PS concentrations influence the reaction mechanism and phototoxicity (Aveline et al. 1998). The authors observed the reduction of fluorescence and IC yields on increasing of the photosensitizer concentration. This phenomenon was explained as PS self-association leading to self-quenching of the triplet state. To obtain the values of k_{decay}^T and k_q constants the observed rate constant k_{ob} of PS triplet states quenching is measured as a function of oxygen concentration (eq. 15). The values of $k_{decay}^T = 6.6 \times 10^8$ M^{-1}s^{-1} and $k_q = 9 \times 10^3$ (corresponding to triplet state lifetime 110 μs) were observer for deuteroporphyrin (DP) in L1210 cells (Aveline et al. 1998). The comparable value of $k_{decay}^T = 5.5 \times 10^8$ M^{-1}s^{-1} was reported for zinc phthalocyanine in vitro (Firey et al. 1988). These values are significantly less than that normally found for oxygen quenching of such triplet states in aqueous solution $k_{decay}^T = 1.85 \times 10^9$ M^{-1}s^{-1} (Reddi et al. 1983). This can be explained by lower oxygen content in membrane compared to solution, by lowered diffusion rate of reactants and PS protein binding.

A plot of initial triplet state decay rate constant as a function of sensitizer concentration gave the value of rate constant of triplet state quenching by ground state DP $k_S = 10^6$ M^{-1}s^{-1} (Aveline et al. 1998). Low value of triplet self-quenching constant k_S compared to oxygen quenching constant k_{decay}^T means that the self-quenching can compete with the quenching of

triplet state by oxygen at high local PS concentration and such competition can exist in vitro as local PS content in lipid bilayer can reach an order of mM.

Moreover, the good correlation between calculated S_Δ values (eq. 18) and cellular phototoxicity with different oxygen levels was observed for DP proving that cell killing is due to singlet oxygen formation. Study of photophysical parameters of PSs in biosystems can give valuable information about reaction mechanism and sensitizer state and environment.

Singlet oxygen is a very reactive molecule. It is much more electrophilic than its ground state and can rapidly oxidize biomolecules. It is a metastable species with a lifetime varying from about 4 µs in water to 25-100 µs in non polar organic solutions (Kohen et al. 1995). The life time of singlet oxygen decreases in biological environment due to the presence of various quenchers, and is calculated to be about 170-330 ns (Baker and Kanofsky 1992). According to Moan and coworkers, this short lifetime allows the diffusion of singlet oxygen to a maximum distance of 50 nm at the sub-cellular level (Moan and Boye 1981; Moan 1990; Moan and Berg 1991). Singlet oxygen can be either deactivated by returning to the ground state, or react with electron-rich regions of biomolecules to give oxidized species. It should be mentioned that as emission of fluorescence and ISC are competitive processes there is an inverse negative relationship between the quantum yield of PS fluorescence and the quantum yield of triplet states formation. This implies that the more strong the fluorescence of PS makes is less efficient triplet states producer (Bonnett et al. 1989). As fluorescence is used for detection of PS in tissues the ratio of fluorescence and triplet states quantum yields Φ_f / Φ_{ISC} should be optimized.

2. 3. The properties of an ideal sensitizer

Haematoporphyrin derivative (HpD) has been for a very long time the only photosensitizer used in clinical PDT. It belongs to the so called first generation photosensitizers. It was the first photosensitizer to receive regulatory approval from the Canada in 1993, and it is now approved in more than 40 countries. Many clinical trials have been realized with this drug, so that there is now a very large experience and the benefit of hindsight. Despite these advantages HpD presents several major drawbacks. It is a complex mixture and its exact composition is rather difficult to reproduce. The absorption maximum of HpD in the red is at 630 nm, which is located at the start of the "therapeutic window" (Fig. 2.4), and the molar extinction coefficient is rather low (about 1170 $M^{-1}cm^{-1}$). Although its photodynamic activity is acceptable, it is still modest. The selectivity for the tumour versus

the healthy tissue is low, therefore inducing side effect such as skin sensitisation remaining for several weeks.

During the 80's it has becomes evident that HpD was not a perfect photosensitizer and several requirements for an ideal photosensitizer were established consequently (Bonnett et al. 1989; Allison et al. 2004):

- Strong absorption in the "optical window" of the visible spectrum, where absorption of tissue chromophores is minimal (Fig. 2.4)
- High quantum yield of triplet states formation, with a triplet energy greater than 94 kJmol^{-1}, the excitation energy for Δ_g singlet oxygen
- High singlet oxygen quantum yield
- Lack of dark toxicity
- Absence of mutagenicity/carcinogenicity
- Pharmacokinetic profile with rapid clearance from the body to prevent skin photosensitization
- High selectivity for the tumour tissue versus healthy tissue
- Uniform stable composition, and preferably a pure chemical substance
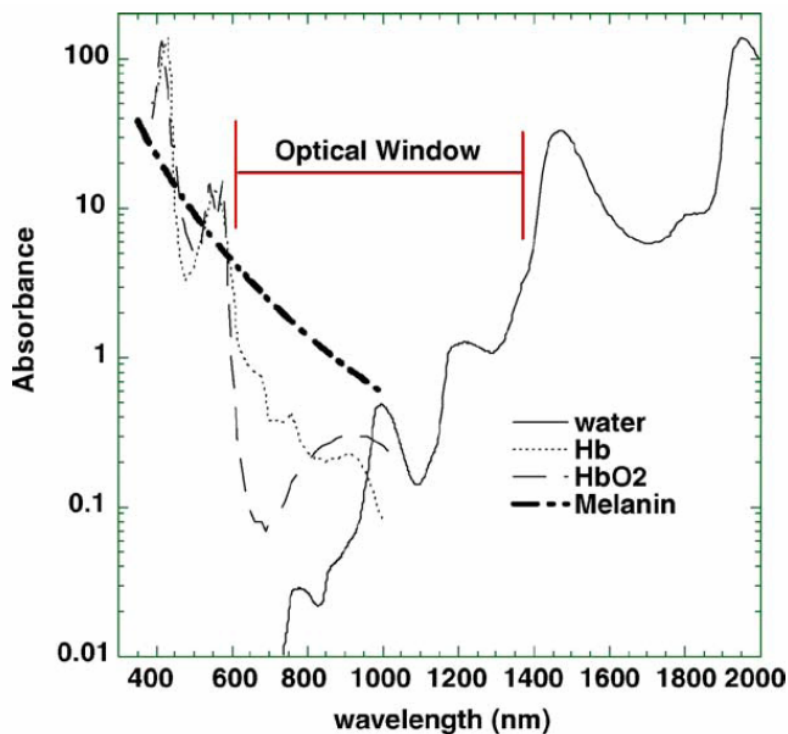
Figure 2.4. Optical window in tissue. Absorption spectra of important tissue chromophores such as water, oxy- and deoxyhemoglobin and melanin are plotted on a logarithmic scale.

2. 4. Tetraphenylchlorin series photosensitizers

Second generation photosensitizers have been developed so far as possible in agreement with the above requirements of the ideal photosensitizer. They are pure chemical substances with synthetic (Phthalocyanines, naphthalocyanines, benzoporphyrins, purpurins, chlorines and porphycenes) and natural porphyrinoids (pheophorbides, bacteriochlorins, bacterio-pheophorbides) origin. Most of the second generation photosensitizers are tetrapyrrolic compounds with side chains added so as to stabilize and improve the absorption in the red. Phthalocyanines are tetrapyrrolic compounds where pyrrole groups are condensed with a benzenic group and where a nitrogenous bridge replaces a methene one, thus enhancing the molar absorption coefficient of these molecules and with λ_{max} of absorption around 700 nm. Texaphyrins are also synthetic relatives of porphyrins, due to their side chains these molecules are water-soluble, and rapidly cleared from the circulation with a wide absorption band centred at 732 nm. However, one of the most active photosensitising agent appears to be 5,10,15,20-tetrakis(*m*-hydroxyphenyl)chlorin (mTHPC) (Fig. 2.5). This sensitizer requires very low drug (0.15 mg/kg) and light (20 J/cm^2) doses and strongly absorbs in the "therapeutic window" at 652 nm (Bonnett et al. 1989). Unfortunately 2nd generation sensitizers generally do not manifest a large tumour localizing selectivity. Therefore research has been focused on developing third generation photosensitizers. The 2nd generation photosensitizers are introduced in a vehicle (e.g. liposomes) which will drive the molecule until the desired target. Another method is to graft amino-acids, proteins, polymers, carbohydrates or anti-body on an existent photosensitizer (Moser 1998).

The photosensitizers of tetraphenylchlorin series derive from the meso-tetra(hydroxyphenyl)porphyrins, they are namely the meso-tetra(hydroxyphenyl)chlorin and the meso-tetra(hydroxyphenyl)-bacteriochlorin (mTHPBC) (Fig. 2.5). The discovery and the chemical synthesis pathway of these compounds was done by Bonnett et al. (Berenbaum et al. 1986; Bonnett et al. 1989). The meta isomer mTHPP was found to be the most active isomer in the in vivo assay (Berenbaum et al. 1986). The same meta isomer of the chlorin mTHPC was identified as the most active chlorin isomer (Bonnett et al. 1989).
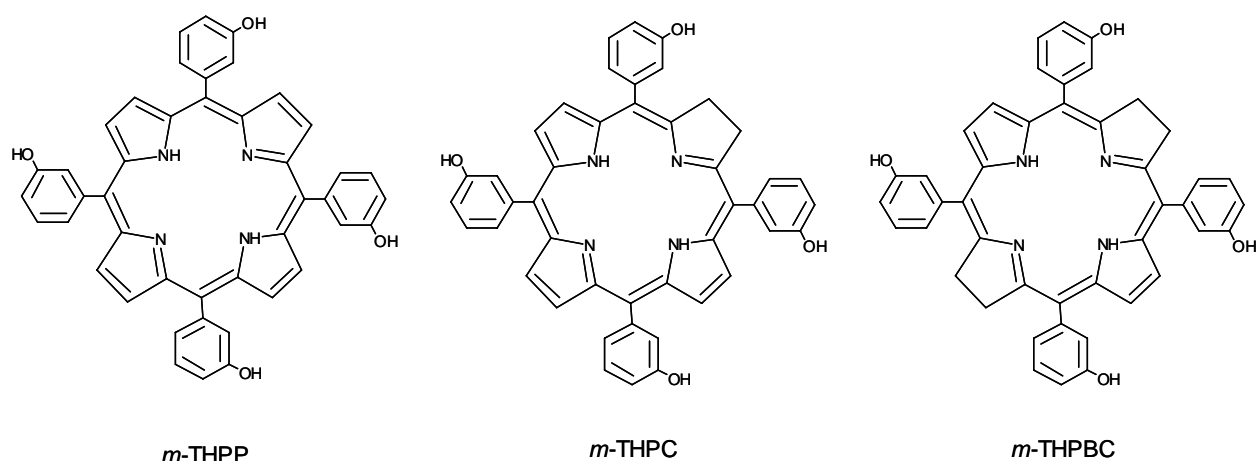
m-THPP *m*-THPC *m*-THPBC

Figure 2.5. : Molecular structures of mTHPP, mTHPC and mTHPBC.

The attractive properties of this series are the strong absorption in the far red region. Where the molar extinction coefficient in ethanol is 1170 $M^{-1}cm^{-1}$ for Photofrin® at 630 nm, it is 3400 $M^{-1}cm^{-1}$ at 644 nm for *m*-THPP, 29600 $M^{-1}cm^{-1}$ at 650 nm for mTHPC and 91000 $M^{-1}cm^{-1}$ at 735 nm for *m*-THPBC (Table 2.3). They have a high triplet states quantum yield formation ranging between 0.69-0.89 and a high quantum yield of singlet oxygen formation (0.43-0.45).

Owing to their photophysical properties these photosensitizers were expected to be valuable compounds for PDT. Actually it has been shown that mTHPP was 25-30 times as potent as haematoporphyrin derivative in sensitising tumours (Berenbaum et al. 1986), and mTHPC considering global photodynamic doses (light dose x photosensitizer dose) was found to be 100 to 200 times as potent as haematoporphyrin derivative (Savary et al. 1997; Savary et al. 1998).

Table 2.3. : Some photophysical properties of *m*-THPP, *m*-THPC and *m*-THPBC in methanol from (Bonnett, charlesworth et al. 1999).

	m-THPP	*m*-THPC	*m*-THPBC
λ_{max} Band I/nm	644	650	735
ε_{max}/M-1cm^{-1}	3400	29600	91000
λ_{max} fluorescence/nm	649, 715	653, 720	612, 653, 746
for excitation at λ/nm	415	415	500
Φ_f	0.12	0,089	0,11
Φ_T	0.69	0,89	0,83
τ_T/S	1.2×10^{-4}	$0,50 \times 10^{-4}$	$0,53 \times 10^{-4}$
O_2 quenching rate constant k_q/M^{-1}s^{-1}	1.9×10^9	$1,8 \times 10^9$	$2,5 \times 10^9$
Φ_Δ, air-saturated	0.46	0,43	0,43
Φ_Δ, oxygen-saturated	0.59	0,59	0,62

2. 4. 1. The 5,10,15,20-meta-tetra(hydroxyphenyl)chlorin

mTHPC is a second-generation photosensitizer (Bonnett et al. 1989) and is one of the most effective sensitizers studied to date (Dougherty et al. 1998). It mediates cell photodamage, principally through singlet oxygen formation (Melnikova, Bezdetnaya et al. 1999) and its efficacy is sensitive to oxygenation conditions (Coutier et al. 2002). mTHPC has been granted European approval for palliative treatment of patients with advanced head and neck cancers and undergoes clinical open-label multicenter studies for the treatment of early squamous cell carcinoma (Copper et al. 2003; Hopper et al. 2004).

mTHPC is introduced to patients intravenously. mTHPC's hydrophobic nature defines its affinity to plasma proteins. Hence, the interactions with plasma components and blood cells can play an important role in mTHPC-PDT efficacy. Studies on mTHPC interaction with plasma protein fractions are sparse (Michael-Titus et al. 1995; Hopkinson et al. 1999; Kessel 1999). mTHPC displays some unusual properties in vitro and in vivo compared with many other sensitizers. Gradient-density ultracentrifugation demonstrated the presence of weakly fluorescing aggregated mTHPC species in the regions of albumin or HDL/albumin (Hopkinson et al. 1999; Kessel and E. Sykes 1999). mTHPC forms large-scale aggregates in aqueous media that monomerize upon interaction with plasma proteins (Bonnett et al. 2001). This sensitizer is rigidly fixed in model membranes and strongly retained in cells in vitro (Ball et al. 1999; Bombelli et al. 2005). mTHPC displays an unusual pharmacokinetic behaviour in human and rabbit plasma with a secondary peak at about 10 and 6 h after in intravenous injection, respectively (Ronn et al. 1997; Glanzmann et al. 1998). These phenomena were supposed to be explained by initial retention of PS in the liver or sensitizer aggregates in the vasculature. Similar pharmacokinetic profile was reported only for hexyl-ether derivative of pyropheophorbide-a in mice (Bellnier et al. 1993). MTHPC has small initial volume of distribution with high retention in the vasculature together with two peaks of PDT efficacy (2h and 24h) in mice (Jones et al. 2003).

It has been demonstrated that the Golgi apparatus and endoplasmic reticulum (ER) are preferential sites of mTHPC accumulation in MCF-7 human adenocarcinoma cells after 3h of incubation (Teiten, Bezdetnaya et al. 2003). Golgi apparatus and ER were shown to be the primary PDT-induced damage sites as measured by enzymes photoinactivation technique (Teiten, Bezdetnaya et al. 2003; Teiten, Marchal et al. 2003). Damage to Golgi apparatus was confirmed by fluence-dependent alterations of Golgi apparatus and mitochondria morphology

(Melnikova, Bezdetnaya, Bour et al. 1999). Both apoptotic and necrotic pathway are implicated in mTHPC-mediated HT29 cell photoinactivation that is governed by mitochondrial membrane photodamage manifested by cytochrome C release and dissipation of mitochondrial membrane potential (Marchal et al. 2005).

During irradiation at 650 nm the absorption spectra of mTHPC in organic, PBS and PBS containing 10% FCS the major absorption bands at 380-450 and 650 nm decreased (Hadjur et al. 1998). A new absorption band was observed at 320 nm, attributed to the formation of a photoproduct. The spectra of mTHPC fluorescence also decreased upon irradiation but no fluorescent photoproducts were detected. A strong dependence of the photodegradation on oxygen concentration and the formation of photoproducts have been reported (Hadjur et al. 1998). Hadjur et al. determined the quantum yields of photobleaching Φ_{Pb} in aqueous solution containing 10 % FCS to be 1.54×10^{-5} for air saturated conditions and 1.8×10^{-6} after N_2 bubling. In aerobic conditions the photodegradation, as well as the formation of photoproducts, have been competitively inhibited by singlet oxygen quenchers. On the basis of photobleaching experiments Handjur et. al. also determined the quantum yield of singlet oxygen production (Φ_Δ) by mTHPC, which appeared to be 0.3 in ethanol and 0.01 in PBS suggesting that mTHPC is highly aggregated in aqueous media (Hadjur et al. 1998). Products of mTHPC oxidation irradiated in methanol have been separated and identified by high-performance liquid chromatography (HPLC). The major compound of oxygenation process has been described as β-hydroxy-mTHPC with an absorption band around 423 nm (Jones et al. 1996). MTHPC has been reported to be a moderately photolabile compound. A comparative study of mTHPBC and mTHPC in methanol–water (3:2, v/v) solution demonstrated a 90 fold greater mTHPBC photobleaching rate compared to mTHPC (Bonnett, Djelal et al. 1999). Rovers et al. in an in vivo study on Colo 26 tumour bearing mice showed that the rate of bleaching of mTHPBC was approximately 20 times greater than that of mTHPC (Rovers, de Jode, Rezzoug et al. 2000). The Φ_{Pb} value for mTHPC in PBS with 10 % FCS solution is an order of magnitude lower compared to BPD-MA ($\Phi_{Pb} = 2.07 \times 10^{-4}$) (Aveline et al. 1994).

mTHPC has a strong absorbance in the red region (650 nm) with high molar extinction coefficient (Table 2.2) (Bonnett, Djelal et al. 1999). This offers promising therapeutic perspectives for PDT of deep tumours and pigmented tissues. Pre-clinical studies have demonstrated that in female BALB/c mice bearing PC6 tumour cells the depth of necrosis was 3.79 ± 0.28 mm for mTHPC dose of administered photosensitizer 0.375 µmol/kg for mTHPC (Bonnett et al. 1989). Another *in vivo* study demonstrated that area of necrosis after

irradiation of mTHPC-sensitised liver is 26 ± 4 mm^2 (Rovers, de Jode and Grahn 2000). The absence of correlation between PS concentration in tumor and PDT efficiency was observed in vivo (Veenhuizen et al. 1997; Ris et al. 1998).

2. 5. Cells and tissue damage effects of PDT

PDT induces both direct and indirect antitumor effects (Castano et al. 2005). It can directly destroy tumor cells that undergo apoptosis and necrosis accompanied by induction of the inflammatory response and a slowly developing adaptive immunity that can potentiate local antitumor effects and might possibly induce systemic immunity. PDT together with inflammatory response can also damage tumor vasculature leading to the early vascular shutdown and ischemia-related cell death.

2. 5. 1. Vascular Shutdown and Inflammation

The alteration of endothelial cells during PDT treatment seems to be the origin of modifications observed in vasculature (Fingar et al. 2000). PDT provokes modifications of organisation of the proteins of cytoskeleton of endothelial human cells with consecutive induction of calcium influx in cells (Foster et al. 1991). The modifications of cytoskeletal proteins induce the changes of cells form and the loss of intracellular communications (Fingar et al. 2000). Such changes serve as a signal to the platelets and neutrophils activation which adhere on the vessel wall, roll toward the constriction and aggregate, at which point they migrate into the surrounding tissues following chemokine gradients (Steele et al. 1985). After adhesion platelets release a great quantity of vasoactive molecules such as thromboxan which amplify platelets aggregation being powerful vasoconstrictor (Fingar et al. 1992). In the region of injury cascades of eicosinoids lead to vessel constrictions. The formation of space between endothelial cells contribute to the reduction of tumoral perfusion and vascular permeability (McMahon et al. 1994; Zilberstein et al. 2001). It was demonstrated that vascular destruction occurred to a greater extent *in vivo* (Henderson et al. 1984). This cause the blood stasis and tumor cells starvation of oxygen and nutrients and reduce the survivability of cells *in vivo* (Henderson et al. 1985; Henderson and Fingar 1987; Fingar et al. 1992). It was reported that vascular destruction after PDT is accompanied by inflammatory response like after tissue injury (Korbelik 1996).

Different photosensitizers do not produce the same type of vascular response: NPe6-PDT produce blood stasis mainly due to platelets aggregated on the artery walls while SnEt$_2$ produces an inflammatory response without vessel constriction or platelet aggregation (McMahon et al. 1994). Vascular destruction is generally considered to be one of the major effects contributing to tumor destruction.

2. 5. 2. Direct cell destruction

One of the first who provided the evidence that cells may undergo two distinct types of cell death was Kerr (Kerr et al. 1972). The first type is known as necrosis, a violent and quick form of death affecting extensive cell populations, characterized by cytoplasm swelling, destruction of organelles and disruption of the plasma membrane, leading to the release of intracellular contents and inflammation. Necrosis has been referred to as accidental cell death, caused by physical or chemical damage and has generally been considered an unprogrammed process. During necrosis decomposition of cell is principally mediated by proteolytic activity (Castano et al. 2005).

Several types of cell death were termed apoptosis or programmed cell death (Agostinis et al. 2004; Almeida et al. 2004). They are identified in single cells usually surrounded by healthy-looking neighbors, and characterized by cell shrinkage, blebbing of the plasma membrane, the organelles and plasma membrane retain their integrity for quite a long period. As a rule the apoptotic program initiated by PDT is the rapid release of mitochondrial cytochrome C into the cytosol followed by activation of the apoptosome and procaspase 3. In vitro, apoptotic cells are ultimately fragmented into multiple membrane-enclosed spherical vesicles. In vivo, these apoptotic bodies are scavenged by phagocytes, inflammation is prevented. Apoptosis, requires transcriptional activation of specific genes, include the activation of endonucleases, consequent DNA degradation into oligonucleosomal fragments, and activation of caspases. Some alternative modes of cell death have bee described: mitotic cell death (Castedo et al. 2004), programmed necrosis (Bizik et al. 2004), cathepsin-mediated lysosomal death pathway (Leist and Jaattela 2001) and autophagic cell death (Yu et al. 2004).

Photosensitizers that localize in cellular organelles such as endoplasmic reticulum or mitochondry can induce apoptosis via photodamage of Bcl-2 and Bcl-xl proteins (Kessel and Luo 1999). With PS localized in the plasma membrane, the photosensitization process can be switched to the necrotic cell death likely due to loss of plasma membrane integrity and rapid depletion of intracellular ATP (Kessel and Poretz 2000; Agostinis et al. 2004). It is believed

that lower dose PDT leads to more apoptosis, while higher doses provoke more necrosis (Plaetzer et al. 2002). Cells sufficiently damaged by PDT are killed, regardless of the mechanism involved. This means that inhibition of apoptosis reorients cells to necrotic pathway, but cannot increase cell survival (Thibaut et al. 2002).

II. 3. Photophysical and photochemical properties of sensitizers

3. 1. Photobleaching of sensitizers

During the photodynamic treatment in addition to the reaction of PS with biological substrate, self-photosensitization occurs, the reactive oxygen intermediates can interact with the photosensitizer, leading to its transformation and/or destruction. This phenomenon is called photobleaching. Photobleaching is relevant to a variety of fields, from laser technology to photomedicine. The first observation of photobleaching in the photodynamic therapy field was made in 1986 by Moan (Moan 1986). Photobleaching is usually observed as lowering of the optical density or the fluorescence intensity of the solution during irradiation (Spikes 1992; Rotomskis et al. 1996). Two types of photobleaching can be considered (Bonnett and Martínez 2001):

- photomodification, where loss of absorbance or fluorescence during irradiation leads only to PS transformation into modified form.
- "true photobleaching", where chemical change is profound and results in small fragments that do not absorb in the visible spectral region.
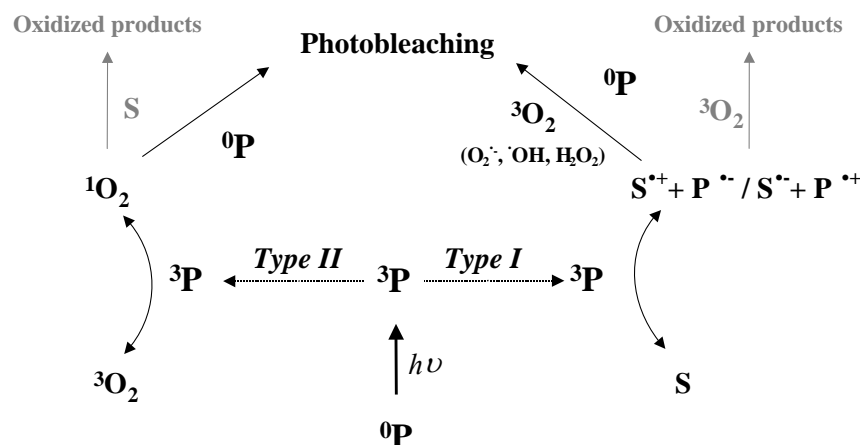
Figure 2.6. : Diagram of photobleaching mechanisms occurring after absorption of photons by photosensitizer.

The main reactions leading to photobleaching are presented in Fig. 2.6. Irradiation of medium containing photosensitizer leads to the production of reactive oxygen species. These oxygen radical species react with the neighbouring molecules, including the photosensitizers, leading to their destruction. Photobleaching can occur via two pathways, the Type I way involving reactive oxygen species and Type II way involving singlet oxygen.

The sensitivity of PS to photodegradation by light is determined by its photobleaching quantum yield. The photobleaching quantum yield (Φ_{Pb}) at time t of irradiation is determined as the number of moles of PS photobleached (n_{PS}) devided by the number of moles of photons absorbed (n_{Ph}) during the same time. For the case of irradiation of PS solution in the cuvette the Φ_{Pb} is expressed as (Aveline et al. 1994):

$$\Phi_{Pb} = \frac{(A_0 - A_t)V_S}{\varepsilon l N_{Ph} \int_0^t (1 - 10^{-A_0 \exp(-kt)})dt}, \text{ where } N_{Ph} = \frac{I_0 \lambda}{N_A hc} \qquad (19)$$

where A_0 and A_1 are optical densities of the PS before and after irradiation during time t, V_S is the volume of the sample (in liters), ε is the molar absorption coefficient (in $M^{-1}cm^{-1}$) at irradiation wavelength, l is the optical pathlength (in cm), k is photobleaching constant (s^{-1}), N_{Ph} is the photon flux at irradiation wavelength λ (in mol photons s^{-1}), N_A is Avogadro's number, h is Plank's number and c is the velocity of light.

There are large differences in the Φ_{Pb} of photosensitizers (Table 2.4). These differences are attributed to oxidation potential, lipophilicity, presence of a metallic ion, kind of reactions involved (Type I or II).

The differencies in Φ_{Pb} of photosensitizers can be explained in the basis of their redox potentials. In organic solvents sensitizers with the lowest redox potential show the most rapid photobleaching (Bonnett and Martínez 2001). The relative photobleaching rates of PSs are proportional to the values of their redox potentials (Chang et al. 1981). Thus the rates of oxygen-mediated photobleaching of sensitizers can be predicted on the basis of their redox potentials values.

Table 2.4. Photobleaching quantum yield of some photosensitizers in PBS

photosensitizer	Concentration (M)	Photobleaching quantum yield	References
MACE (Mono-L-aspartylchlorin e6)	5×10^{-6}	8.2×10^{-4}	(Spikes and Bommer 1993)
Sn aspartyl chlorin e6	5×10^{-6}	5.7×10^{-6}	(Spikes and Bommer 1993)
Zn aspartyl chlorin e6	5×10^{-6}	1.9×10^{-2}	(Spikes and Bommer 1993)
Chlorin e6	5×10^{-6}	1.9×10^{-3}	(Spikes and Bommer 1993)
Chlorin e6	10^{-4}	74.7×10^{-3}	(Rotomskis et al. 1997)
Sn chlorin e6	5×10^{-6}	1.3×10^{-5}	(Spikes and Bommer 1993)
Zn chlorin e6	5×10^{-6}	1.8×10^{-2}	(Spikes and Bommer 1993)
Hematoporphyrin	10^{-4}	1.05×10^{-3}	(Rotomskis et al. 1997)
Hematoporphyrin	5×10^{-6}	4.7×10^{-5}	(Spikes 1992)
Photofrin®	10^{-4}	9×10^{-5}	(Rotomskis et al. 1997)
Photofrin®	5×10^{-6}	5.4×10^{-5}	(Spikes 1992)
$TSPP_4$	10^{-4}	2×10^{-4}	(Rotomskis et al. 1997)
$TSPP_4$	5×10^{-6}	9.8×10^{-6}	(Spikes 1992)
Uroporphyrin I	5×10^{-6}	2.8×10^{-5}	(Spikes 1992)
BPD-MA		2.8×10^{-5}	(Aveline et al. 1994)

Kinetic parameters of photobleaching are mainly derived from spectroscopic measurements assessed by UV-Vis or fluorescence spectroscopy. Several important mechanistic issues of photobleaching were obtained from the detailed analysis of spectroscopic modifications. In the earlier studies on photobleaching of PSs the kinetic decay of photosensitizer was considered to be mono-exponential decay $e^{-\alpha D}$, where α stands for the photobleaching constant (s^{-1} or $J^{-1} \times cm^2$) and D stands for the fluence of irradiation ($J \times cm^{-2}$). As became clear later, the photobleaching kinetic is a complex phenomenon which cannot be described by a single exponential decrease (Sørensen et al. 1998; Moan et al. 2000). Several parameters can influence the kinetic decay such as the oxygen depletion during PDT and different types of binding sites for the sensitizer PS in cells and tissues. For some photosensitizers the decay rates have been shown to be practically independent of the concentration of the dye during illumination (Moan 1986; Mang et al. 1987; Sørensen et al. 1998); and thus exhibit a first order decay. However, for the majority of dyes the photobleaching decay is highly dependent on the initial concentration of the photosensitizer

(Moan et al. 1988), meaning that the photoproducts from the PS can cause the destruction of a neighboring molecules (Moan et al. 1997). For example, the values of Φ_{Pb} for the different concentrations of Ce6 are very different as for other dyes (PF, hematoporphyrin and TSPP$_4$) (Table 2.3). The deviation from the first-order photobleaching kinetics can be due to oxygen depletion during PDT, photochemical modifications of sensitizer, different types of sensitizer binding sites in tissues and relocalization of sensitizer during light exposure (Moan et al. 1997; Sorensen et al. 1998).

Photobleaching leads to important consequences for light dosimetry in PDT (Potter et al. 1987). Photodynamic dosimetry, based on calculation of the therapeutic dose, was first introduced by Potter et al in 1987 and modified by Robinson et. al. (Robinson et al. 1998). This model includes such parameters as sensitizer and oxygen concentration, illumination fluence rate and several photophysical constants of PS. Dysart et. al. have proposed an implicit approach to assessing PDT efficacy where changes of PS fluorescence during treatment are used to predict treatment outcome (Dysart et al. 2005). The starting point of the authors is the statement that if the biological response to PDT and photobleaching are both mediated by singlet oxygen, hence, photobleaching should yield information about the biological outcome of the treatment.

The photobleaching kinetics for ground-state PS undergoing singlet oxygen–mediated bleaching can be described by the differential equation that is based on homogenous distribution of sensitizer and oxygen (Georgakoudi et al. 1997):

$$\frac{d[S_0]}{dt} = -k_{os}[S_0][^1O_2] \qquad (20)$$

where $[S_0]$ and $[^1O_2]$ are concentrations of ground state PS and singlet oxygen, respectively; k_{os} is the bimolecular rate constant of $^1O_2$ reaction with ground state sensitizer S_0. In reality, if the concentration of PS is low enough, the only PS molecule with which the singlet oxygen can react is the parent PS molecule. For these low PS concentrations, the rate of photobleaching will depend only on the rate of singlet oxygen generation because the volume through which each singlet oxygen molecule can diffuse before reacting will contain exactly one PS molecule, independent of PS concentration. Taking into account the short lifetime and diffusion distance of singlet oxygen in biological media the eq. 20 can be modified by the addition of a constant, δ:

$$\frac{d[S_0]}{dt} = -k_{os}([S_0] + \delta)[^1O_2] \qquad (21)$$

δ is is effective minimum concentration of PS. It is determined by the distance of singlet oxygen diffusion befor reaction with adjacent PS molecule and is given by:

$$\delta = \frac{1}{N_A (6D\tau_\Delta)^{3/2}} \qquad (22)$$

where N_A is Avogadri's number, D is the diffusion coefficient of singlet oxygen in cells, τ_Δ is singlet oxygen lifetime. At constant oxygenetion during treatment the PDT dose (total amount of $^1O_2$ molecules generated) at time T may be expressed:

$$Dose = \frac{CS_\Delta}{\tau_\Delta k_{os}} \int_0^T \Phi(t)[S_0](t)dt \qquad (23)$$

where $\Phi(t)$ is the fluence rate of excitation light, C is a constant, S_Δ is the fraction of triplet molecules quenched by oxygen (eq. 17). If $\Phi(t)$ remaines constant during the treatment the singlet oxygen dose can be estimated directly from PS photobleaching curve $[S_0](t)$.

Using this model, Dysart et. al. have determined important photophysical and photobiological parameters of mTHPC in MLL cells (Dysart et al. 2005). The estimation of values $S_\Delta = 0.96 \pm 0.01$, $\delta = 33 \pm 6$ μM, $\tau_\Delta = 0.03 - 0.018$ μs, $k_{os} = (7.8 - 11.1) \times 10^6$ M^{-1}s^{-1} were obtained. Moreover, it was estimated that number of singlet oxygen molecules per cell required to reduce survival by 1/e is in the range $N_{1/e} = (7.6 - 11.1) \times 10^8$ for MLL cells with mTHPC. The proposed model explains the dependence of bleaching kinetics on PS concentration and shows the possibility of singlet oxygen concentration estimation on the basis of PS photobleaching kinetics without the need for measurements of ground-state oxygen concentrations or treatment fluence rate. Other authors have reported the values of $N_{1/e}$ to be 3.9×10^7 with ALA-induced PpIX in AML5 leukemia cells (Niedre et al. 2003) and 1.2×10^8 for TA-3 cells with HpD (Dougherty et al. 1976).

3. 1. 1. Parameters effecting photobleaching. Aggregation state, pH, ionic strength and oxygen concentration

Previous work in our laboratory demonstrated a different photosensitivity of monomeric and aggregated forms. In a first study Bezdetnaya et al. (Bezdetnaya et al. 1996) demonstrated that for HpD and PpIX quantum yield of photobleaching obtained by matching fluorescence where higher than that obtained by matching absorbance (10 and 11 times for HpD and PpIX respectively). The authors concluded that this difference reflected the

preferential photobleaching of photolabile monomeric forms compared to aggregates. In another study they confirmed this assumption using mTHPC (Belitchenko et al. 1998).

Several studies of Rotomskis and co-workers demonstrated that photobleaching efficiency of haematoporphyrin-like sensitizers seems to be consistent with their aggregation state and the presence of covalently linked structures. Dimethoxyhaematoporphyrin (DMHp) and Hp are present in an equilibrium of monomeric and aggregated forms in aqueous solution (Streckyte and Rotomskis 1993). Their absorption bleaching rate constants are two to four times higher than that of HpD, a sensitizer containing mostly linear structures of porphyrins linked by ether, ester and/or carbon-carbon bonds (Dougherty et al. 1984), and 10 to 20 times higher than that of Photofrin® (PF), which contains covalently linked "sandwich" type structure (Streckyte and Rotomskis 1993). In HpD, some of the side chains are involved in ether and ester linkages, and therefore this compound is more photostable than DMHp and Hp. In PF and Photosan-3 (PS) (highly aggregated "sandwich" type structure (Streckyte and Rotomskis 1993), almost all side chains are involved in covalently linked structures, probably accounting for the high photostability of these sensitizers. The presence of a certain amount of protoporphyrin in PS is probably responsible for its lower photostability compared to PF.

Lowering the pH value of a photosensitizer solution results in a shift of both the absorption and the fluorescence spectrum as well as in a decrease of the fluorescence intensity, indicating an aggregation at low pH values (pH < 5) (Cunderlikova et al. 1999). Reddi *et al.* (Reddi and Jori 1988) also demonstrated an aggregation of hematoporphyrin and Photofrin® when decreasing the pH from 7.4 to 5.0 and they also demonstrated the decrease of the photobleaching quantum yield to 70 % for hematoporphyrin and 30 % for Photofrin®, thus suggesting a resistance toward photobleaching of aggregated species.

Changing the ionic strength by varying the buffer concentration can affect the aggregation state of a sensitizer. An increase of the buffer concentration of a $TPPS_4$ solution increases the aggregation of the sensitizer and reduces the photobleaching quantum yield by 50 % (Davila and Harriman 1990). Thus, it follows from all this studies that the quantum yield of photobleaching is inversely proportional to the aggregation state of the photosensitizers.

It was observed that the quantum yield of photobleaching of several porphyrins in phosphate buffer is reduced with the lack of oxygen (using nitrogen bubbling) (Spikes 1992). Same observation was made for endogenously formed porphyrins in bacteria (Konig et al. 1993). An observation of the involvement of oxygen *in vivo* has been realised by Robinson and co-workers (Robinson et al. 1998). During a photobleaching experiment with ALA-

induced PpIX the mice died and they observed a slowdown of the photobleaching. They correlated this bleaching decrease to the oxygen decline in the skin, due to the death of the animal.

Several studies from the laboratory of T. H. Foster documented the oxygen depletion during PDT. Oxygen consumption model was refined by Georgakoudi and co-workers (Georgakoudi et al. 1997; Georgakoudi and Foster 1998) by taking into account the parameter of photobleaching of Photofrin in EMT6 spheroids. This improvement considerably changed the kinetic profile of the oxygen aspects of Photofrin-PDT. The authors observed a rapid decrease in oxygen concentration during irradiation followed by a progressive return to the values measured before the irradiation. The first phase is due to the photochemical oxygen consumption which is faster than the diffusion of the oxygen through the spheroid. The second phase, corresponding to the comeback of oxygen to the initial value, is due to a slowdown of the photochemical consumption of the oxygen explained by the decrease in photosensitizer concentration (photobleaching), together with the diffusion. This was in agreement with the mathematical model assuming that the photobleaching was based on a reaction between singlet oxygen and photosensitizer.

In their further studies Foster and co-workers investigated the impact of irradiance on photobleaching (Finlay et al. 2001; Finlay et al. 2002). In a study reporting the photobleaching of ALA-induced Protoporphyrin IX (Pp IX) in normal rat skin (Finlay et al. 2001) it was demonstrated that the photobleaching kinetics were different with the change of the irradiance. High irradiance led to rapid oxygen consumption and a slow down of the photobleaching. In a second study, Finlay *et al.* (Finlay et al. 2002) showed that photobleaching kinetics of *m*-THPC on normal rat skin exhibits two distinct phases. The first phase was shown to be irradiance independent, whereas the second phase revealed an irradiance dependency consistent with an oxygen-dependant reaction process. Using mathematical model of photobleaching based on selfsensitized singlet oxygen reactions the fluence rate dependence of the cell survival and of mTHPC photobleaching was due to photochemical oxygen consumption and a predominantly singlet oxygen-mediated mechanism of mTHPC photobleaching (Coutier et al. 2001). It was demonstrated that high fluence rates lead to rapid photochemical oxygen consumption in mTHPC-PDT, where at lower fluence rates intratumor oxygen content was maintaines at levels comparable to those measured before illumination (Coutier et al. 2002). The authors proposed that improved tumor destruction could be expected by reducing the rate and the extent of oxygen depletion during mTHPC photodynamic therapy using low fluence rates.

3. 2. Effect of aggregation state on photophysical and photochemical properties of sensitizers.

Hydrophobic PSs with high value of octanol-water partition coefficient form dimers and higher micelle-like aggregates in aqueous media and their physical and chemical properties differ noticeably from those of the monomeric sensitizer (Brown et al. 1976). The aggregated PSs are generally have much lower fluorescence and triplet states quantum yields that leads to lowering of the quantum yield of singlet oxygen production (Redmond et al. 1985; Tanielian et al. 2001) and drop of photosensitizing efficiency (Ma et al. 1994; Ball et al. 1998; Theodossiou et al. 2004). Action spectra have significantly greater resemblance to the fluorescence excitation spectra than to the absorption spectra of the HpD in cells (Moan and Sommer 1984) indicating that fluorescent monomeric species of sensitizer are more photodynamically active compared to aggregates.

The explanation of reduced singlet oxygen production by aggregates can be done taking into account that competition between the type I and II photosensitization mechanisms is substantially altered as a consequence of protein binding and dye aggregation, favoring type I mechanism by protection of triplet species against collisional oxygen quenching (Bartlett and Indig 1999). The limited access of oxygen to interact with PSs is due to stabilization of aggregated species by hydrophobic forces, hydrogen bonds and π-π interactions of the aromatic rings (Lang et al. 1998; Bonnett et al. 2001). When strong electronic coupling exists among PS molecules in an aggregate the resonance light scattering (RLS) can be detected from the solution of such aggregates. RLS effect is observed as increased scattering intensity at or very near the wavelength of absorption maximum of aggregated molecular species (Pasternack and Collings 1995; Collings et al. 1999). The intensity of scattering depends on the square of the volume of the aggregate and increases as a consequence of aggregation.

Hydrophobicity of PSs influences not only their aggregation state but also accumulation in cells. The strong linear correlation between PSs cell uptake and octanol-water partition coefficient was observed (Oenbrink et al. 1988). Aggregated PS species are assumed to internalize in cells via endocytotic pathway, whereas sensitizers in monomeric state can be transported by passive diffusion through plasmatic membrane or internalized in complexes with plasma proteins. After endocytosis aggregated PSs are believed to localize in lysosomes (Berg et al. 1993; MacDonald et al. 1999).

During interactions with plasma proteins the value ot the fluorescence yield of hydrophobic sensitizers augment with time (Belitchenko et al. 1998) that can be explained by

PS dissociation from an aggregate and binding to protein molecule. This may lead to increase of their photodynamic efficiency (Fiedler et al. 1997). Upon interaction with light a photo-induced disaggregation can occur that is accompanied by the rise of PS fluorescence quantum yield and relocalization of sensitizer (Ambroz et al. 1994; Moan et al. 1998).

3. 3. Photophysical properties of porphyrinoid sensitizer non-covalently bound to proteins.

Poor correlation between photophysical parameters sensitizer in solution and its photodynamic efficacy was observed (Aveline and Redmond 1999). This fact turned attention to the influence of the biological environment on PS properties as to be photodynamically active the sensitizer needs to be closely associated with the target. The influence of the environment can be attributed to non-covalent interactions of the sensitizer with surrounding molecules. Non-covalent interaction exerts great impact on photophysical properties of the sensitizer molecule (Henderson and Dougherty 1992; Ricchelli 1995; Aveline and Redmond 1999). The non-covalent complexation changes the PSs photophysical properties because the sensitizer molecule feels a different environment, usually less polar than in aqueous media, and because its internal movements are restricted. Conversely, the change of photophysical properties can be a useful tool for getting information on the topology of binding sites and on the nature of interactions of PS with host molecule. Knowledge of PSs photophysical characteristics in biological environment can help in the prediction of their photodynamic action.

Non-covalent interactions are weak binding forces responsible for assemblies of molecules. These forces govern the structure and stability of assemblies and play a decisive role in molecular recognition. The common features of non-covalent interactions are the distinctly lower bond energies than those of the covalent bonds. The values of bond energies for non-covalent interactions are as a rule < 100 kJ mol^{-1}, the weakest being of the order of kJ mol^{-1}. The interactions form two distinct groups: hydrophobic interactions and electronic interactions. Electronic interactions involve hydrogen bonds, Coulombic interactions, π interactions, charge-transfer interactions, and dispersion forces.

The non-covalent interactions between sensitizers and proteins are essential for understanding the mechanism and efficiency of photoreactions on molecular and cellular level. The serum proteins play an important role in transport of the sensitizers to the tumor

sites and in uptake by cells (Kessel 1986). A great number of studies are devoted to characterization of the binding process of porphyrinoid PS to serum proteins (Gantchev et al. 1999; Andrade and Costa 2002; Kubat et al. 2004). Proteins have single or multiple binding sites for porphyrins and phthalocyanines, including independent cooperative modes (Gantchev et al. 1999; Andrade and Costa 2002). Binding influences distribution, metabolism and the molecular form of the sensitizers, e.g. their protonation, aggregation state and the concentration of the free molecules. Binding can alter their photochemical properties and influence photosensitized reactions.

The electronic absorption spectra of porphyrins bound to proteins exhibit significant changes when compared with the corresponding monomer in an aqueous solution. The spectroscopic effects are due to changes in solvent–solute interactions as the polarity of the protein environment is lower than that of water. Binding is indicated by a red shift of the Soret band usually concomitant with some hypochromicity. For example, the Soret band of TPPS is shifted by 8 nm together with Q bands that are shifted from 633 to 646 nm (Lang et al. 1998).

The parameters of PSs fluorescence also undergo changes upon interaction with proteins. Binding of porphyrins and phthalocyanines to proteins increases the lifetime of the excited singlet states (Howe and Zhang 1998; Andrade and Costa 2002; Kubat et al. 2004). The decay of fluorescence is characterized by a single long-lived fluorescence component (Andrade and Costa 2002) or displays complex kinetics that can be fitted by two or three exponential functions (Beltramini et al. 1987; Ambroz et al. 1994). This could indicate presence of several populations of PSs that are located in different compartments within the protein matrix. The analysis of AlPcSn-HSA complex fluorescence decay led to the identification of three limiting environments (Ambroz et al. 1994; Foley et al. 1997): (i) excited AlPcSn molecules are in free contact with water ($\tau = 5.0$ ns); (ii) water molecules are excluded or preferentially solvate the constituents of protein ($\tau = 6.7$ ns); (iii) locations where additional quenching or interfacial effects occur ($\tau = 0.4 - 1.2$ ns). Contributions of the respective components depend on the number of sulfonate groups and can be correlated with the hydrophilicity of the molecules decreasing from $AlPcS_1$ to $AlPcS_4$. Consequently, the most hydrophobic $AlPcS_1$ partitions between the aqueous and protein phases, less hydrophobic $AlPcS_2$ and $AlPcS_3$ are bound at the protein surface and within hydrophobic sites protected from water, and hydrophilic $AlPcS_4$ is attached to the protein surface. The fluorescence quantum yields Φ_f of $AlPcS_2$ and $AlPcS_3$ are 0.4 irrespective whether bound to HSA or free in water, while Φ_f of bound AlPcS1 is considerably reduced. The shortest

fluorescence lifetime and the smallest Φ_f for bound AlPcS$_1$ suggest that an additional quenching process is due to exciton interaction between closely spaced PS molecules.

The lifetimes of the triplet states for protein-bound PSs in the absence of oxygen are much longer than the corresponding lifetimes of the free molecules in solution (Foley et al. 1997; Lang et al. 1998; Lang et al. 2004). The reason is that the sensitizers are bound within the environment in which the rate of solvent-enhanced deactivation of the triplet state is significantly lower than the rate in an aqueous solution. For example, the triplet state lifetime of AlPcS bound to BSA increase from 440 to 1160 µs (Lang et al. 2004). The kinetics of quenching the triplet states by dissolved oxygen (Fig. 2.2) can also be multi-phasic and best fitted by several exponential terms. This can be explained by the presence of several populations of protein-bound porphyrin molecules differing in oxygen accessibility. Generally, there is at least one population of the triplet states, well shielded from oxygen, that is quenched by oxygen with a rate constant of about one order of magnitude lower ($k_q = 10^8$ M^{-1} s^{-1}) than that of free porphyrin ($k_q = 10^9$ M^{-1} s^{-1}). For instance, for population of ^{3}TPPS that is buried deep in the protein matrix with a very low oxygen accessibility the constant of quenching by oxygen is about $k_q = 9 \times 10^6$ M^{-1} s^{-1} (Borissevitch et al. 1998). In general, binding of the sensitizers does not inhibit excitation to the triplet states, although it affects the rate constant k_q and hence the triplet lifetimes in the presence of oxygen. The reported values of Φ_T do not change upon binding indicating that the bound sensitizers retain their ^{1}O$_2$ producing capacity (Davila and Harriman 1990).

It can be concluded that the non-covalent interaction of the sensitizers does not restrict the formation of the excited singlet states, triplet states and hence the formation of ^{1}O$_2$. The binding influences spectroscopic properties and kinetic parameters, namely the lifetimes of the excited states and rate constants of collisional quenching. The fluorescence yield Φ_f, triplet state formation yield Φ_T and quantum yield of ^{1}O$_2$ formation Φ_Δ remain mostly unchanged. But the prediction of photosensitising efficacy in biological systems is difficult as overall effect of the photodynamic processes is affected by a combination of numerous, often oppositely acting factors as aggregation, monomerization, compartmentalization, and restriction of internal movements.

II. 3. 4. Electronic structure of porphyrinoid photosensitizers.

Free base porphin (FBP) is the basic unit from which porphyrins and their analogs derive (Fig. 2.7). The spectra of porphyrins have been extensively studied experimentally and theoretically. FBP, involving 24 π valence MOs and 26 π electrons, has been a challenge for ab initio theoretical work. Chlorin and bacteriochlorin rings have 24 and 22 π electrons, respectively. Only 18 π electrons satisfy the Huckel's rule. Even for the correct determination of the ground-state geometry, electron correlation effects for both s and p electrons have been demonstrated to be crucial (Merchan et al. 1994). It also holds for the computation of excitation energies. Indeed, the accurate determination of the electronic spectra of FBP, based solely on ab initio grounds, has become a milestone in theoretical spectroscopy. It is only recently that ab initio methods have been able to compute the excited states of FBP. These calculations have not been made without a number of problems, leading to different interpretations of the spectra.

The absorption spectrum of FBP is characterized by three regions (Nagashima et al. 1986). The lowest energy transitions of the spectra form the weak Q band in the visible region. This band is split into two components: Q_x (1.98 – 2.02 eV), parallel to the inner axis containing the pyrrolic hydrogens and Q_y (2.33 – 2.42 eV), perpendicular to that axis. The intense Soret (B band) region occurs in the near-UV region (3.13 – 3.33 eV) with two shoulders on its high-energy tail, the so-called N (3.65 eV) and L (4.25 eV) bands (Edwards et al. 1971). The Q and B bands are usually related to the $1^1B_{3u} – 1^1B_{2u}$ and $2^1B_{3u} – 2^1B_{2u}$ states, respectively. This traditional interpretation comes from the earliest attempts to explain those bands by the well-known four-orbital model developed by Gouterman and co-workers in the 1960s (Weiss et al. 1965).

Results for Ab initio study of the low-lying optically allowed valence excited states of the porphin molecule were reported and an interpretation of the porphin Q, B, N and L bands was proposed (Serrano-Andres et al. 1998). But the theoretical assignment of the spectrum of FBP is still under debate.
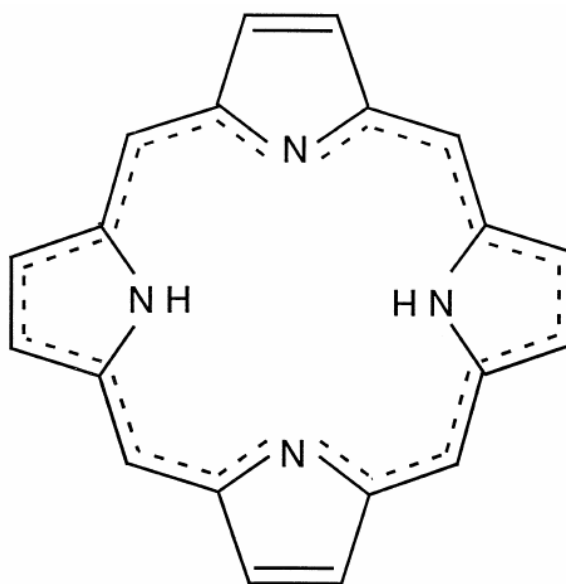
Figure 2.7. Delocalized D2h ground-state structure of FBP.

II. 4. PHOTOSENSITIZERS INTERACTIONS WITH PLASMA PROTEINS

Binding of photosensitizers to plasma proteins is the first important step for effective PDT as it determines PS delivery into sensitive sub-cellular sites. The importance of PSs interactions with plasma proteins is clear from the fact that direct injection of photosensitizers into the lesion was shown to be inefficient (Brown et al. 2004). As shown by the study of pharmacokinetics plasma proteins play an important role in PS transport and interactions in blood.

After PS injection into the bloodstream it passes through a number of transport stages that can take different time-spans for different PS (Castano et al. 2005):

a. PS must come to equilibrium with the components of the blood. This can involve the PS disaggregation or redistribution from its delivery vehicle and binding to various serum proteins and blood.

b. Circulating PS binds to the walls of the blood vessels. The process depends on the nature PS and on the characteristics of blood vessels in the tumor and normal tissues.

c. PS penetrates through the wall of the blood vessel at a rate depending on the strength of the initial binding to the vessel.

d. PS diffuses throughout the parenchyma of the organ or tumor to which it has been delivered. In the liver or other metabolically active organ the PS may

be subjected to changes by metabolic enzymes, but this is thought to be unlikely for most tetrapyrrole PS.

e.   PS is eliminated from the tissue by lymphatic drainage.

f.   PS is excreted from the body by the pathway from the liver into the bile and then to the intestine with subsequent elimination.

4. 1. Pharmacokinetics of sensitizers.

Various PSs have very different pharmacokinetics and biodistribution. With the possible exceptions of uroporphyrin and some of the larger aggregates present in Photofrin, all tetrapyrrole PSs, which have been suggested for use as PDT drugs are more or less firmly bound to serum proteins after intravenous injection. Three classes of these compounds, which have tumor localizing properties, can be delineated.

(a) relatively hydrophilic compounds, which are primarily bound to albumin (and possibly globulins) such as the tri and tetra-sulfonated derivatives of tetraphenylporphine ($TPPS_3$, $TPPS_4$) and chloroaluminum phthalocyanine ($ClAlPCS_3$, $ClAlPCS_4$);

(b) amphiphilic, asymmetric compounds, which are thought to insert into the outer phospholipids and apoprotein layer of lipoprotein particles, such as the adjacent disulfonates ($TPPS_{2a}$, $ClAlPCS_{2a}$), benzoporphyrin derivative monoacid (BPD), lutetium texaphyrin (LuTex) and monoaspartyl chlorin(e6) (MACE), which distributes between albumin and high-density lipoprotein (HDL);

(c) hydrophobic compounds, which require a solubilization vehicle such as liposomes, cremaphor EL or Tween 80. These are thought to localize in the inner lipid core of lipoproteins particularly low-density lipoprotein (LDL) (but also HDL and very low-density lipoprotein, VLDL). Examples of these compounds are unsubstituted phthalocyanines (ZnPC, ClAlPC) naphthalocyanines (isoBOSINC), tin-etiopurpurin (SnET2).

The type of protein-carrier governs the delivery of sensitizer to the tumor (Jori and Reddi 1993). As was mentioned above, in vivo transport of several porphyrinoid derivatives with a moderate and high degree of hydrophobicity is carried out by lipoproteins (Jori and Reddi 1993). Serum albumin, the most abundant protein in blood plasma, serves as a carrier for amphiphilic and hydrophilic photosensitizers (Kessel et al. 1987; Peters 1995). It has been suggested that PS delivery with various macromolecular systems may lead to differing mechanisms of tumor destruction as PS are delivered to different sites. Albumin and globulins

are believed to deliver PS mainly to the vascular stroma of tumors (Jori 1989), HDL delivers PS to cells via a non-specific exchange with the plasma membrane, LDL probably delivers a large fraction of the PS via an active receptor-mediated pathway (Morliere et al. 1987). Plasma proteins binding affinity for various photosensitizers can play an important role in drug distribution and photodynamic efficacy (Korbelik and Hung 1991; Kongshaug 1992; Obochi et al. 1993; Tsuchida et al. 1997). Another possible mechanism of sensitizer transport into cells and tissues is passive diffusion following the PS concentration gradient.

Many of the most effective PSs are too hydrophobic to dissolve in aqueous solvents. Therefore after injection they form aggregates that disaggregate upon interaction with plasma proteins. Disaggregation step leads to higher time-span to reach maximal PS accumulation in the tumor compared to monomeric PSs (Buchholz et al. 2005). This necessitates the use of a delivery vehicle to keep the molecules in disaggregated state to be able to cross the blood vessels and to diffuse into tumors. The choice of delivery vehicle can influence the tumor selectivity of the PS (Reddi 1997). In vivo delivery of PS incapsulated in liposomes has been shown to give advantages in either biodistribution or tumor destruction compared to non-liposomal delivery for Photofrin (Jiang et al. 1997), BPD (Richter et al. 1993) and Zn-PC (Polo et al. 1996). More rapid pharmacokinetics of liposomal mTHPC formulation (Fospeg) with maximal tumor accumulation 5.5 times earlier compared to mTHPC has been reported (Buchholz et al. 2005).

After penetration through the blood vessels the PSs accumulate in healthy and tumor tussues. An important parameter in clinical PDT, light-to-drug interval (LDI), is determined by preferentially localization of PS in tumors. The value of the "tumor to normal tissue" ratio, the ratio between the tumor and peritumoral/distant muscle or skin, should be maximal at the time of tumor irradiation. The mechanisms of establishing of PS preferential tumor localization depend on sensitizer type and their pharmacokinetics. The tumor localizing ability of the PS with the faster pharmacokinetics is probably due to selective accumulation in the tumor, while the localization of PS with slower pharmacokinetics is likely due to selective retention. In the selective accumulation model it is thought that the increased vascular permeability to macromolecules typical of tumor neovasculature is mainly responsible for the preferential extravasation of the PS. These quick acting PS frequently bind to albumin which is of ideal size to pass through the ''pores'' in the endothelium of the tumor microvessels (Yuan et al. 1993). The selective retention of PS in tumors can be achieved by enhanced accumulation of LDL-bound PS by tumor cells (Jori and Reddi 1993), by retention of protein-bound PS in the tumor extravascular space due to poorly developed lymphatic drainage

(Roberts and Hasan 1992), by macrophages infiltration into solid tumors, that accumulate up to 13 times the amount of PS compared to cancer cells (Korbelik and Krosl 1995) or by low pH in tumors that increase the accumulation of anionic PS (Pottier and Kennedy 1990).

The last step of PSs transport is elimination from the organism. This phenomenon influences the skin photosensitization after PDT and is studied by measuring sensitizer's pharmacokinetics in the blood. There has been a wide variation in blood pharmacokinetics reported for various PS in clinical and preclinical use. Bellnier and Dougherty (Bellnier and Dougherty 1996) studied pharmacokinetics of Photofrin in patients scheduled to undergo PDT for the treatment of carcinoma of the lung or the skin. They found a triexponential three-compartment pharmacokinetic model with half-lives of approximately 16 h, 7.5 days, and 155.5 days. Detectable Photofrin fluorescence was shown to persist in the serum for longer than one year. The pharmacokinetics of 2-[1-hexyloxyethyl]-2- devinyl pyropheophorbide-a (HPPH) was studied in cancer patients (Bellnier et al. 2003). A two-compartment model yielded alpha and beta half-lives of 7.77 and 596 h. Radiolabeled mTHPC pharmacokinetics was studied in tumor-bearing rats yielding a tri-exponential model with half-lives of 0.46, 6.91 and 82.5 h, respectively (Jones et al. 2003). Pharmacokinetics of the silicon phthalocyanine Pc4 were studied in non-tumor-bearing mice giving a twocompartment fit with alpha and beta half-lives of approximately 10 min and 20 h with some variation depending on injected dose and solvent (Boyle and Dolphin 1996; Egorin et al. 1999). The palladium bacteriopheophorbide PS known as TOOKAD has very rapid pharmacokinetics with alpha and beta half-lives of approximately 2 min and 1.3 h and in this case graphite furnace atomic absorption spectroscopy was used to quantify the palladium atom coordinated to the tetrapyrrole (Boyle and Dolphin 1996). Unusual pharmacokinetics of mTHPC was reported in human and rabbit plasma with a secondary peak at about 10 and 6 h after in intravenous injection, respectively (Ronn et al. 1997; Glanzmann et al. 1998). The possible explanation of such PS behavior was supposed to be connected with its aggregation. A similar pharmacokinetic profile was reported only for hexyl-ether derivative of pyropheophorbide-a in mice (Bellnier et al. 1993).

4.2. Kinetic and equilibrium characteristics of sensitizers interactions with proteins.

Equilibrium binding characteristics of photosensitizers to plasma proteins together with dynamic parameters of redistribution between plasma proteins and biomembranes define PSs interaction with cells, their intracellular localization and kinetics of sensitizers accumulation in

the tumour (Korbelik and Hung 1991; Obochi et al. 1993; Bonneau et al. 2004). The knowledge of PSs redistribution rates from different plasma proteins and membrane structures can be predictive of its pharmacokinetic behaviour.

4.2.1. Characteristics of PS redistribution between plasma proteins.

According to the value of octanol–buffer partition coefficient $P = C_{octanol}/C_{buffer}$ all sensitizers can be divided into lipophilic and hydrophilic with big and low P values, respectively. Evidently, hydrophilic sensitizers are much more solvable in aqueous media compared to lipophilic. Lipophilic PSs have high solubility in the membrane structures and are associated with the lipid bilayer in vitro (Fahr et al. 2005). Photosensitizers association with biomembranes in cells and plasma proteins plays an important role in their redistribution between these structures. Liposomes are used as model for biological membranes in studies of the inter-membrane drugs transfer phenomenon.

Two models to explain the transfer between two lipid domains of lipophilic membrane components were hypothesized. One model proposes a collision mechanism for phosphatidylcholine (Jones and Thompson 1989) and cholesterol transfer (Steck et al. 1988). The other model proposes redistribution through the water phase as demonstrated by cholesterol transfer (McLean and Phillips 1981; Lange et al. 1983) and phosphatidylcholine transfer studies (McLean and Phillips 1981). Others studies suppose that both mechanisms may simultaneously play a role, as demonstrated by the transfer of monoacylglycerols from small unilamellar vesicles (SUV) to brush border membrane vesicles (Schulthess et al. 1994). The mathematical equations describing a "First Order Model" (for lipid transfer between vesicles through the aqueous phase via desorption from the bilayer) and a "Second Order Model" (for transfer upon collision of donor and acceptor vesicles in addition to transfer to the aqueous phase) can be found in the work of Jones and Thompson (Jones and Thompson 1989).

4. 2. 1. 1. Collision mechanism

In the collision mechanism, photosensitizer transfer can be described in a simple reaction scheme:

$$A_{PS} + B \underset{k_{in}}{\overset{k_{out}}{\rightleftarrows}} A + B_{PS} \qquad (24)$$

where A_{PS} and B_{PS} stand for the complexes of photosensitizer with proteins A and B, respectively. Constants k_{in} and k_{out} stand for molecular rate constants of PS redistribution from the complexes with proteins to lecithin vesicles and contrariwise. The concentrations of protein and lecithin vesicles remain constant during the experiment, so that k_{in} and k_{out} become pseudo-first order constants. For this system, the change of the concentration of protein-photosensitizer complex as a function of incubation time is expressed as:

$$[A_{PS}](t) = \frac{k_{in}[A_{PS,0}][P]}{k} + C_0\, e^{-kt} \qquad (16)$$

where k defined as:

$$k = k_{in}[A] + k_{out}[B] \qquad (17)$$

where $A_{PS,0}$ stands for the concentration of the complex protein-photosensitizer at time t = 0. C_0 − constant, k is an experimentally measured apparent rate constant obtained by fitting of variations of measured signal (PS or label fluorescence intensity) with time using exponential rise or decay functions.

A collision mechanism implies an increase in the value of apparent rate constant k with increasing concentrations of donor and acceptor structures as we see from eq.17. For some PSs the rate-limiting step in the redistribution can be the release of the molecules to the surface of protein/lipoprotein to be able to interact with acceptor structures (Bonneau et al. 2002).

4. 2. 1. 2. Redistribution through the aqueous phase

In the aqueous phase redistribution model photosensitizer transfer can be described in a reaction scheme:

$$PS_A \underset{k_{onA}}{\overset{k_{offA}}{\rightleftarrows}} PS_f \underset{k_{offB}}{\overset{k_{onB}}{\rightleftarrows}} PS_B \qquad (18)$$

where PS_A, PS_B and PS_f are concentrations of sensitizer bound to protein A, protein B and non-bound PS in solution, respectively. The constants k_{oni} and k_{offi} (i = A, B) are the rate constants of PS binding and exit from proteins, respectively. The constants defined as $k_{onA} = k'_{onA}[A]$, $k_{onB} = k'_{onB}[B]$.

For such system of n successive reversible reactions, the evolution of the concentrations of all components as a function of time is described by a set of expressions including n exponential terms with the same exponential factors:

$$PS_{A,B,f} = A_{1,2,3} + B_{1,2,3}e^{-k_1t} + C_{1,2,3}e^{-k_2t} \qquad (19)$$

If the measured fluorescence intensity is the sum of contribution from all three species thus the observed fluorescence signal can be written as a sum of one constant and two exponential terms with the rate constants k_1 and k_2. The rate constants k_1 and k_2 are expressed through the combination of molecular rate constants k_{oni} and k_{offi} (i = A, B). Changing proteins contents and experimental conditions, such as temperature, pH and ionic strength, it is possible to determine the values of molecular redistribution rate constants.

The distribution of PS at equilibrium is determined by (eq.20):

$$\frac{d[PS_A]}{dt} = 0 \text{ hence } [PS_A] = \frac{k_{onA}[A]}{k_{offA}}[PS_f] \qquad (20)$$

where [A] is free protein concentration at equilibrium. Thus, the kinetic parameters of the system determine the equilibrium concentrations of free and protein-bound PS.

The limit value for a diffusion-controlled association constant between two species defined as k_{dif}, was determined using modified Smoluchowski equation (von Smoluchowski 1917; von Hippel and Berg 1989; Atkins 1990):

$$k_{dif} = 4\pi\chi(R_1+R_2)(D_1+D_2)N \qquad (21)$$

where R_1 and R_2 are radii of two proteins, respectively; D_1 and D_2 are their diffusion coefficients derived from Stockes-Einstein equation, respectively; N – Avogadro's number, χ – is dimensionless parameter to account for electrostatic interactions and geometrical peculiarities of interacting molecules (Xavier and Willson 1998). Stockes-Einstein relationship for the diffusion coefficient of species i :

$$D_i = \frac{k_bT}{6\pi\eta R_i} \qquad (22)$$

where k_b is Boltzmann's constant, T is the absolute temperature, η is the solvent viscosity, R_i is the radius of molecule. For diffusion-controlled reactions the value of experimental association constant is close to the limit value calculated according to (eq. 22).

Which mechanism plays a role under in vitro conditions is largely dependent on phospholipids concentration (Jones and Thompson 1989), pH and membrane configuration and hydrophobicity/lipophilicity of the molecule, which is subject of the transfer (Yang and Huestis 1993). Monomer transfer through the water phase predominates for less hydrophobic molecules at all values of pH and membrane concentrations, and for more hydrophobic compounds at very high membrane dilutions. Collision transfer contributes significantly to the rate for relatively hydrophobic compounds in concentrated donor–acceptor systems. The size and surface configuration of donor and acceptor membranes also influence the relative contributions of through-medium and collision transfer study (Yang and Huestis 1993). A collision mechanism implies an increase in the value of apparent rate constant k with increasing concentrations of acceptor structures (Thilo 1977; Roseman and Thompson 1980). Lipophilic drugs may also exchange between lipid domains in the same way as natural membrane components by collision transfer or monomeric diffusion transfer (Nichols 1988).

Several studies revealed the kinetic characteristics of sensitizer's redistribution between plasma proteins and artificial membranes. In the study of Kuzelova and co-workers the reported values of the rate constants of aqueous mediated deuteroporphyrin association and release from liposomes to be 9.2×10^6 $M^{-1}s^{-1}$ and 18.5 s^{-1} for 100 nm diameter DMPC liposomes, respectively (Kuzelova and Brault 1994). The rate of release of cis-di-sulfonated aluminium phthalocyanine from model membranes and LDL was around 5 s^{-1} and 1 s^{-1}, respectively (Bonneau et al. 2004). The rate of hydrophobic sensitizer Verteporfin transfer from lipid formulations was determined to be about 2×10^{-2} s^{-1} (calculated from (Chowdhary et al. 2003)). The rate of non-solvable in aqueous media Verteporfin release from liposomes is some orders of magnitude higher compared to hydrophilic PSs. Also, the values of rate constants of hemin association 5.7×10^9 $M^{-1}s^{-1}$, 1.5×10^9 $M^{-1}s^{-1}$, 6.5×10^6 $M^{-1}s^{-1}$ and dissociation 4.5×10^{-1} s^{-1}, 5.1×10^{-2} s^{-1} and 3.3×10^{-3} s^{-1} from the complexes with LDL, HDL and HAS, respectively, were reported (Miller and Shaklai 1999).

In a diffusion mechanism where the substance releases through an aqueous phase, the k value is independent of acceptor concentration, but the properties of the solvent considerably affect the redistribution process. Generally, a substantial energetic barrier exists for membrane-bound lipophilic drugs to partition into the aqueous phase (Fahr et al. 2005). Considerable decrease of entropy during PS transfer in aqueous medium points out that

sensitizer release is unfavorable. The collisional mechanism of transfer is predominant for this case. Indeed, the rate of non-polar compounds transfer through aqueous phase decreases exponentially with the solubility of the substances in the medium (Kim and Storch 1992). Lipophilic PSs accumulate preferentially in hydrophobic and lipid structures of plasma proteins and can be inserted deep in the bilayer thus restricting the transfer through aqueous phase. For lipophilic drugs with slow transferring properties due to the longer circulation time, the probability that the drug co-transfers with lipids or is taking up by macrophages increases. In addition, the transferring properties may be predictive to some extent for the distribution and retention kinetics of drugs in the biomembranes.

No data present in the literature about mTHPC redistribution between plasma proteins and biomembranes.

4. 2. Thermodynamics of PS redistribution between plasma proteins. Eyring theory.

The widely used model to describe the thermodynamics of chemical and transport reactions in solutions is Eyring transition state theory (Glasstone et al. 1941). In this model it is assumed that the reactants before transformation into the products form activated complex with high potential energy and that this step is rate limiting. Thermodynamic characteristics are connected with redistribution rates and can be used to study the mechanism of transfer.

It is found experimentally that the plot of lnk vs 1/T gives a straight line (Fig. 2.8, right). Here k is redistribution rate constant and T is incubation temperature. This behavior, known as the Arrhenius law, is commonly introduced by using two parameters, the intercept and the slope. These two parameters are used in the Arrhenius equation:

$$\ln k = \ln A - \frac{E_a}{RT} \text{ or } k = Ae^{-\frac{E_a}{RT}} \qquad (24)$$

The pre-exponential factor A in eq. 24 has the dimension of the frequency and is characterizes the effective frequency of molecular collisions. The activation barrier E_a is the minimum energy the reactants A and B (protein or sensitizer molecules) should possess to overpass the reaction activation barrier. In the condensed phase E_a is close to the enthalpy of activation ΔH. The fact that the slope gives the activation energy means that the temperature dependence becomes stronger for higher activation energies.

For thermodynamic description of kinetic processes Eyring transition state theory is used. Eyring theory describes the changes of reaction rate with temperature. It is a theoretical

construct, based on transition state model. According to the transition state theory, the reactants are getting over into an unsteady intermediate state (or activate complex, Fig. 2.8, left) on the reaction pathway:

$$A + B \xrightleftharpoons[k_{out}]{k_{in}} AB^* \xrightarrow{k_t} AB \tag{25}$$
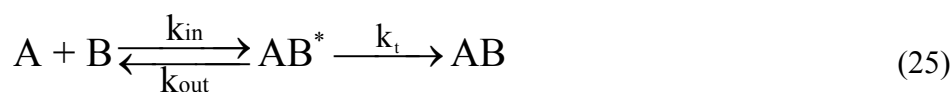
where k_{in} and k_{out} are association and dissociation redistribution constants, respectively, AB^* an AB are contents of activated complex and product, respectively. Constant k_t is universal constant for a transition state, it is determined by statistical mechanics to be:

$$k_t = \frac{k_b T}{h} \tag{26}$$

Fig. 2.8. A reaction profile (right): the horizontal axis is the reaction coordinate and the vertical axis is the potential/Gibbs energy. The transition state corresponds to the maximum of the Gibbs energy. Arrhenius plot (left). The intercept and the slope of linear curve are used to calculate the activation energy.

Then, k is defined as overall reaction rate constant (constant that is measured in experiment):

$$k = \frac{k_b T}{h} K \qquad (27)$$

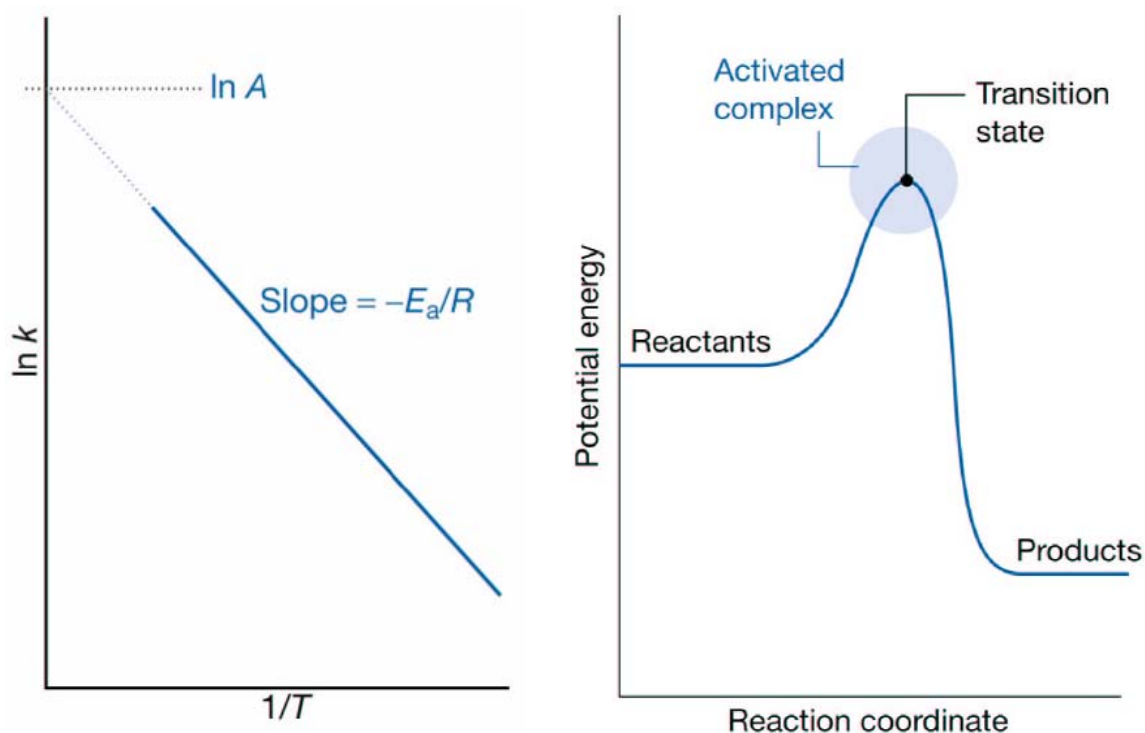where K is thermodynamic equilibrium constant of the reaction (eq. 25). Thermodynamics gives a further description of the equilibrium constant:

$$\Delta G = - RT\ln K \qquad (28)$$

Combining eq. 29 and eq. 30 we can find the free energy of activation ΔG:

$$\triangle G = RT \ln[(\frac{k_b T}{h})(\frac{1}{k})] \qquad (29)$$

The activation enthalpy ΔH, the enthalpy difference between transition state of the reaction and the ground state of the reactants, can be found from eq. 30:

$$\Delta G = \Delta H - T\Delta S \qquad (30)$$

Entropy of activation (ΔS) is determined from the equations:

$$\Delta S = 2.3R \log(\frac{NhX}{RT}) \text{, where } X = k\exp(\frac{\Delta H}{RT}) \qquad (31)$$

where R is the gas constant, T is the temperature, N - Avogadro's number, h – Planck's constant, k – redistribution rate constant. Thus activation parameters of redistribution can be obtained from the temperature dependence of apparent redistribution rate constant k using the Eyring equation (Glasstone et al. 1941; Eyring and Eyring 1963).

On the basis of different contributions of ΔS and ΔH into ΔG and their absolute values the mechanism of the transfer can be revealed. For collisional inter-membrane transfer the mobility of PS molecule does not change considerably, that leads to small entropy changes and little contribution of ΔS into ΔG. Aqueous transfer leads to comparable contribution into the free energy of activation as entropy changes are considerable during PS release from protein into aqueous medium (Thilo 1977; Roseman and Thompson 1980; Kuzelova and Brault 1994; Hsu and Storch 1996).

There is no data in literature about the mechanism of mTHPC redistribution between plasma proteins and biomembranes.

II. 5. Intracellular localization of photosensitizers.

The high reactivity and short half-life of singlet oxygen and hydroxyl radicals determine their localized action on biological molecules and structures close to the areas of PS localization. The radius of the action of singlet oxygen in biological environmeny is of the

order of 20 nm (Moan and Berg 1991). Sub-cellular localization is governed by the chemical nature of the PS, lipophilicity, amphiphilicity, ionic charge and protein binding characteristics, the concentration of the PS, the incubation time, the serum concentration and the type of the target cell (Rosenkranz et al. 2000). Precise way that PDT influences the pathways of cell death is also depend on PS intracellular localization (Kessel et al. 1997). Therefore, site of intracellular localization of PSs is an important parameter in PDT.

5. 1. Techniques to study sensitizer intracellular localisation and aggregation state.

Fluorescence microscopy is the main technique to study the intracellular localization of PSs as fluorescence intensity is dependent upon a variety of environmental influences, such as quenching by other molecules, aggregation, energy transfer, and refractive index effects (Suhling et al. 2005). Using this technique the fluorescence emission can be characterised by intensity and position, lifetime, polarization and wavelength. Fluorescence imaging techniques are powerful tools in the biological and biomedical sciences as they are minimally invasive and can be applied to live cells and tissues (Wouters et al. 2001). On the basis of confocal microscopy, the microspectrofluorimetry technique can be used to measure the spectrum of PS fluorescence in each pixel of the image. Using two-photon excitation the fluorescence signal from very thin layer can be measured excluding the excitation of adjacent areas and thus reducing the PS photobleaching and increasing light penetration in tissues.

New fluorescence microscopic techniques appeared enhancing the possibilities of simple confocal microscopy: fluorescence lifetime imaging microscopy (FLIM) (Suhling et al. 2005) have several advantages for characterisation of molecular microenvironment by measuring the fluorescence lifetime, second harmonic generation microscopy (Campagnola and Loew 2003), total internal reflection fluorescence microscopy (TIRF) (Schneckenburger 2005) allowing the measurement of the signal from a very thin layer of about 50 nm, fluorescence correlation spectroscopy (FCS) that gives the possibility to study quantitively the mobility and dynamics of fluorescent molecules in living cells (Berland 2004; Bacia et al. 2006).

5. 1. 1. Confocal laser scanning fluorescence microscopy.

The first technique to study the intracellular distribution of fluorescent molecules was epifluorescence microscopy. In the epifluorescence microscope, the light excitation pathway is the same as the observation optical pathway. The light sources used can be xenon lamps or

mercury arc lamps. The images obtained, using this technique, are contaminated by information from outside the focal plane, leading to a decrease in contrast and clarity of the picture. The irradiated area corresponds to the observed area and for the whole thickness of the sample, thus observation of light sensitive molecules such as photosensitizers can be difficult. This technique was used in several studies (Wood et al. 1997; Melnikova, Bezdetnaya, Bour et al. 1999; Bour-Dill et al. 2000; Morgan et al. 2000). Due to the major drawbacks of epifluorescence microscopy, confocal microscopy is now the preferred method to look at the intracellular fluorophores localisation.

The confocal microscope offers several advantages over the conventional epifluorescence microscope (Zucker and Price 2001). This includes the elimination of out-of-focus glare, the decrease of depth of field and the ability to collect serial optical sections from thick specimens. The illumination is achieved by scanning beams of light, usually from a laser, across the specimen, the configuration uses a pinhole placed in front of the light source, and another pinhole placed in front of the emission photomultiplier with the same focus as the first pinhole (the two are confocal). The pinholes prevent light originating from above or below the focal plane in the specimen from reaching the photomultiplier. The confocal microscope does not avoid photobleaching, but reduces the irradiated area and therefore enables the study of light sensitive molecules. Due to all these improvements confocal microscopy is preferred to epifluorescence microscopy in the localisation of photosensitizers (Scully et al. 1998; Chen et al. 2000; Delaey et al. 2001; Pogue et al. 2001; Zucker and Price 2001; Leung et al. 2002).

Microspectrofluorimetry is usually coupled to confocal microscopy. This technique enables the spectral study of the molecules in a focal plane of a confocal microscope. The topographic resolution is very small (less than 1 μm^2), therefore it is possible to study the spectral signature of a molecule in a localised area such as the organelles. In opposition to the imaging techniques such as epifluorescence and confocal microscope which gives subjective information, the microspectrofluorimetry gives objective data on the localisation or co-localisation of two fluorescent probes. Therefore, this technique has been widely used for the determination of the photosensitizers intra-cellular localisation sites (Morliere et al. 1998; Ouedraogo et al. 1999).

One of the most widely used technique to determine localization is double-label confocal fluorescence microscopy (Wilson et al. 1997). In this technique, a drug and an organelle-specific dye are both administered to a cell. The drug and organelle dye must have distinguishable fluorescence bands so that separate fluorescence images may be acquired of

the drug and dye colocalization within the same cell *via* double-label confocal microscopy. The fluorescence images of the drug and of the organelle-specific dye provide the sub-cellular distribution of the two compounds. The areas of overlap between the two images provide information about the spatial accumulation of the drug within different organelles. Co-localization can also be used to identify sites of damage after illumination (Melnikova, Bezdetnaya, Bour et al. 1999).

However, only qualitative assessment of the correlation between the two images in double-label confocal microscopy has been provided in the past (Enderle et al. 1997; Wilson et al. 1997). More accurate information about drug localization can be obtained through quantitative analysis. A quantitative assessment of fluorophore colocalization in confocal optical sections can be obtained using the information obtained from scatter-plots. Among the variables used to analyze the entire scatterplot is Pearson's correlation coefficient R, which is one of the standard techniques applied in pattern recognition for matching one image to another in order to describe the degree of overlap between the two patterns. The correlation coefficient measured the strength of the linear relationship between the two images (Trivedi et al. 2000).

5. 1. 2. Fluorescence lifetime imaging microscopy (FLIM).

Fluorescence lifetime imaging (FLIM) can report on photophysical events that are difficult or impossible to observe by fluorescence intensity imaging as the lifetime of excited state does not depend on PS content and photobleaching rates giving the possibility to exclude the influence of these parameters from analysis. FLIM is a time-resolved image acquisition method in which both the fluorescence intensity and lifetime is measures in each pixel. There are two main technologies for FLIM: confocal scanning (Sheppard 2003) or multiphoton excitation (Konig 2000) FLIM, where the image is acquired pixel-by-pixel using a non-imaging detector (photomultiplier), and wide-field camera-based FLIM (van Munster and Gadella 2005). The time-resolved information is obtained either in the time domain by exciting the sample with a short optical pulse and observing the decay of the fluorescence intensity using time-correlated single photon counting (TCSPC) technique, or in the frequency domain by modulating the excitation source intensity to calculate the fluorescence decay time from the demodulation and the phase shift of the fluorescence. In wide-field time-gated FLIM, 'snapshots' of the fluorescence emission are taken at various nanosecond delays after the excitation using high-speed gated image intensified cameras (Dowling et al. 1997).

This approach is fast, since all the pixels are acquired in parallel, but it lacks single photon sensitivity and accuracy, and its temporal resolution is about 10 ps (Cole et al. 2001). In confocal scanning or multiphoton excitation microscopes FLIM is essentially a series of single channel fluorescence lifetime measurements where the fluorescence decay can be acquired by TCSPC (Birch and Imhof 1991).

TCSPC is a mature and reliable technique which records the arrival time of single photons after an excitation pulse. The ease of reproducibility of measurements is due to the unique combination of advantages such as the unlimited dynamic range associated with photon counting techniques, linear recording characteristics independent of excitation intensity fluctuations and photobleaching, excellent signal to noise ratio and a high temporal (picosecond) resolution. As each photon is timed individually in each pixel of the image, the collection of many photons for a high statistical accuracy can be time-consuming (Becker et al. 2004). The maximum photon flux that can be timed using a single channel time to amplitude converter (TAC) and analogue to digital converter (ADC) is limited by photon pile-up and the dead time of the electronics to 10^6 photons s^{-1}. Time domain approach needs sufficient time (about 5τ) between excitation pulses for the sample fluorescence to completely decay in order to obtain accurate fluorescence lifetime values. In practice this implies using cavity-dumpers, lower repetition rate pulsed diode lasers (Elson et al. 2004) or appropriate fitting procedures to take residual fluorescence into account (Jo et al. 2004).

FLIM has a great number of biological applications. Measurements of fluorescence resonance energy transfer (FRET) between spectrally similar donor GFP and acceptor YFP have been used to monitor caspase activity in individual cells during apoptosis (Harpur et al. 2001). Application of FLIM in cell biology can be used for identification of FRET to probe intermolecular distances on the scale of the dimensions of the proteins themselves (Stryer 1978; dos Remedios and Moens 1995). It has a significant advantage over co-localization studies with two fluorophores which is limited by the optical resolution (approximately 200 nm laterally, 500 nm axially (Sheppard 2003). FLIM has been used to image the Ca^{2+} concentration in cells (Herman et al. 1997). The use of FLIM in these cases is more robust and reliable than fluorescence intensity-based imaging methods, since FLIM is unaffected by variations of illumination intensity, dye concentration or photobleaching. FLIM of a long-lived (decay time of 760 ns) ruthenium-based oxygen sensor has been used to map oxygen concentrations in macrophages (Gerritsen et al. 1997). FLIM has also been used to map the pH in single cells (Sanders et al. 1995; Lin et al. 2003). In this case the intensity-based fluorescence imaging of the pH probe could not have been used as the observation of a

variation in fluorescence intensity could be attributed to either a change in pH or a variation of the local probe concentration. FLIM of autofluorescence has been used to provide intrinsic contrast in unstained tissue (Tadrous et al. 2003; Elson et al. 2004). The combination of multiphoton excitation for deep, sectioned, tissue imaging with FLIM yields contrast not available with fluorescence intensity-based imaging.

FLIM has also been employed to study aggregation of sensitizers in photodynamic therapy (Scully et al. 1997; Scully et al. 1998; Connelly et al. 2001; Kress et al. 2003). Using this technique the changes of intracellular pH upon irradiation and detection of uroporphyrin III photoproducts was reported (Schneckenburger et al. 1995). The analysis of the $AlPcS_2$ intracellular concentration and aggregation state influence on its fluorescence lifetime was presented (Connelly et al. 2001). Endocytosis-mediated uptake and monomerization inside cells of pyropheophorbide-a and chlorine e6 derivatives using FLIM was reported (Kelbauskas and Dietel 2002). Preferential localization of aggregated sensitizers in lysosomes and endosomes was assumed. The reduction in fluorescence lifetime at higher concentrations was attributed to the quenching of monomers fluorescence by non-fluorescent aggregates. The decrease of mTHPC fluorescence lifetime in vitro from 7.5 to 5.5 ns during incubation from 1 to 6 hours was interpreted as aggregates formation (Kress et al. 2003). Two-exponential fitting analysis revealed that the slow component of mTHPC fluorescence decay completely vanishes upon irradiation suggesting the lower photobleaching rates of PS aggregated forms.

The impact of mTHPC's different aggregated species at various incubation time periods on cell viability has not been studied yet.

5. 2. Sub-cellular localisation and dynamics of sensitizers during PDT.

Intracellular distributions in vitro have been determined for a range of PS with widely differing structures. One of the most important structural parameters that influence the distribution are the ionic charge which can range from −4 to +4, the degree of hydrophobicity (octanol-water partition coefficient) and the degree of asymmetry present in the molecule. PS which are hydrophobic and have two or less negative charges can diffuse across the plasma membrane. These PS also tend to have the greatest uptakes into cells in vitro, especially when present in relatively low concentrations in the medium (<1 μM). Less hydrophobic and PSs that have more that two negative charges tend to be too polar to diffuse across the plasma membrane, and are therefore taken up by endocytosis. Some PS distribute very broadly in various intracellular membranes (Sun and Leung 2002). The charge, its sign and distribution,

and hydrophilicity or hydrophobicity of the sensitizer determine the mode of interaction with biomolecules and carriers, its photophysical properties and effectiveness of the sensitizer in a biological system. The amphiphilic sensitizers possess separated hydrophilic and hydrophobic regions that can independently interact with other adjacent molecules (Boyle and Dolphin 1996). Such sensitizers are photodynamically more active than symmetric hydrophilic or hydrophobic sensitizers (MacDonald and Dougherty 2001). The activity is not necessarily correlated with photophysical properties of the isolated molecule in solution. Systematic studies of variously sulfonated Al phthalocyanines AlPcSn and tetraphenylporphyrins (1 ≤ n ≤ 4, n is the number of the sulfonato groups) as model sensitizers have unambiguously shown maximal activity of unsymmetrical disulfonated compounds. Important amphiphilic sensitizers used in PDT are mTHPC and verteporphin (Boyle and Dolphin 1996; Bonnett, Djelal et al. 1999).

5. 2. 1. Sites of sub-cellular localization of hydrophilic and hydrophobic PSs.

Despite that many PSs localize in lysosomes (Geze et al. 1993) the efficiency of cell killing by such sensitizers is significantly lower that of PSs localized in other organelles (MacDonald et al. 1999). The explanation of this may be the tendency of PSs with greater degree of aggregation to localize in lysosomes. Aggregated hydrophobic photosensitizers enter the cell via endocytosis or pinocytosis and are transported to lysosomes. This has been observed for Photofrin (Morliere et al. 1987), HpD (Malik et al. 1992), aluminium sulphonated phthalocyanines AlPcS$_4$ and AlPcS$_2$ (Moan et al. 1989; Moan et al. 1994), and MACE. Study of intracellular localization of a series of HP and PPIX derivatives with different hydrophobic, anionic or cationic residues revealed that those with a net cationic character localized in mitochondria, while those with net anionic character localized in lysosomes (Woodburn et al. 1991). The initial lysosomal localization of PS may change upon application only a small amount of light. It was found that exposure of cells pre-incubated with anionic porphyrins to light resulted in relocalization of the sensitizers from the lysosomes to the cytoplasm and in the nucleus (Berg et al. 1991; Peng et al. 1991). This behavior was attributed to photodynamic permeabilization of the lysosomal membrane, thus allowing small molecules, including the PS to leak out into the cytoplasm. The photochemical inactivation of cells through such lysosome-localized PSs is assumed to realize due to the release of lysosomal hydrolases (Wilson et al. 1987).

Mitochondria have been found to be a very important sub-cellular target for many PSs used in PDT (Morgan and Oseroff 2001). This is related to the tendency of many PSs to produce apoptosis by mitochondrial damage after illumination. PSs with cationic charges and which are also hydrophobic can localize in mitochondria (Dummin et al. 1997) supposedly by the influence of the mitochondrial membrane potential as well as the lipid bilayer of the membrane (Rashid and Horobin 1990). Mitochondria have been shown to be a localisation site of many photosensitizers such as Photofrin (Singh et al. 1987; Sharkey et al. 1993; Wilson et al. 1997), ALA-PpXI (Iinuma et al. 1994; Wilson et al. 1997), benzoporphyrin derivative (BPD) (Runnels et al. 1999) and HpD (Kessel 1986). There is strong evidence that sensitizers with an acute localization in mitochondria promote the release of cytochrome c upon irradiation (Xue et al. 2001; Marchal et al. 2005). This loss of cytochrome c leads to disruption of the mitochondrial respiratory chain with the eventual reduction of cellular ATP levels or through caspase initiation with subsequent apoptotic cell death (Yow et al. 2000; Xue et al. 2001).

There are not a lot of PSs that localize in plasma membranes of cultured cells (Aveline and Redmond 1999). But all the sensitizers during intracellular transport pass through the plasma membrane. It has been observed that for the short incubation time (less than 1 h) the damage to the plasma membrane was more important compared to longer time spans. This is explained by the fact that, depending on the incubation time, the PS gets deeper in the cells as was shown for Photofrin (Morgan et al. 2000). Dynamics of Photofrin distribution in human carcinoma cells leads to preferential plasma membranes after short LDI (3 h) while the Golgi complex is affected after prolonged (24 h) (Hsieh et al. 2003).

The ER and the Golgi apparatus are closely linked not only by their localisation in the perinuclear area of the cytoplasm, but also as they interact together in protein synthesis. Therefore, damage to these compartments can be lethal for the cells. Some photosensitizers were found to localise in the ER and the Golgi, for example, Photofrin (Candide et al. 1989), some analogues of hypericin (Delaey et al. 2001) and a recent study in our laboratory demonstrated that mTHPC mainly localizes and induces damage to these compartments (Melnikova, Bezdetnaya, Bour et al. 1999; Teiten, Bezdetnaya et al. 2003). Trans-Golgi network have usually an acidic lumen with a pH of approximately 6 - 6.5. Therefore PSs with weak basic properties obtain higher charge and are trapped in this organelle (Berg and Moan 1997).

5. 2. 2. Relocalisation of sensitizers upon irradiation.

During light exposure, photosensitizers can move from one binding site to another. This is also called light induced re-localisation. This has been shown for lysosomotropic dyes such as $TPPS_4$ (Berg et al. 1991; Rück et al. 1992), nile blue (Lin et al. 1993), $AlPcS_4$ and $AlPcS_2$ (Rück et al. 1990; Peng et al. 1991; Rück et al. 1996), which display a granular lysosomial distribution in a discrete perinuclear region (Rück et al. 1996). Moreover Ambroz *et al.* (Ambroz et al. 1994) reported a fluorescence redistribution and a monomerization of $AlPcS_2$ during irradiation, which were coincidental with a change in the fluorescent decay from a bi-exponential to a mono-exponential one. Moan also underlined the capability for PpIX to re-localise during light irradiation in WiDr cells (Moan et al. 1997). The surviving fraction was plotted against the relative values of the integrated number of PpIX fluorescence photons emitted during the irradiation. Three concentrations of ALA-induced PpIX were tested. The authors postulated that if the PpIX molecules remained in their binding sites during light irradiation, the survival curves should be completely superimposable when plotted with exposures measured as the number of emitted photons. This was not what the authors observed, the survival curves became steeper than expected when the PpIX concentration was reduced, indicating a significant transfer of PpIX molecules from one binding site to another. Similar observations had been done earlier by Brun *et al.* on the transfer of PpIX from erythrocytes to other cells (Brun et al. 1990).

A remarkable transient relocalisation is observed when phthalocyanine sulphonates in tumor are exposed to light (Moan and Anholt 1990; Moan et al. 1990). Upon irradiation PSs relocalize to other subcellular sites during the period of some minutes (Wood et al, 1997). As a result of relocalization the fluorescence intensity of PS becomes brighter and localization pattern becomes more diffuse (Ruck et al. 1996; Wood et al. 1997; Kessel 2002). These data could be explained by PS release from cellular organelles into the cytoplasm, displacing the photosensitizer molecules from one type of binding site to another, and/or by photoinduced disaggregation. More recently, Finlay *et al.* (Finlay et al. 2002) hypothesize that the two phases of mTHPC photobleaching observed *in vivo* were due to a redistribution of the photosensitizer in the tissue. However, mTHPC re-distribution in vitro was not detected (Melnikova, Bezdetnaya et al. 1999).

III OBJECTIVES

The first part of the work was an investigation of the influence of mTHPC concentration in tumor, plasma and leukocytes on PDT response *in vivo* in respect of time after injection.

- Assessment of mTHPC pharmacokinetics in plasma, leukocytes and tumor.
- Correlation of PDT efficacy with mTHPC concentration in different compartments.

The second objective of our work was to study mTHPC interactions with plasma proteins and its aggregation state. For this purpose we have investigated the spectroscopic and kinetic properties of mTHPC in solutions containing plasma proteins. The study includes the measurements of:

- Absorption, fluorescence and resonance light scattering properties of mTHPC in different media.
- Kinetics of mTHPC disaggregation in solutions of BSA and lipoproteins.
- Gel filtration chromatograms of BSA solutions containing mTHPC with subsequent measurements of sensitizer fluorescence.

The third objective was to examine the kinetic and mechanism of mTHPC redistribution from the complexes with plasma proteins to model membranes. For this purpose we realized following measurements:

- Kinetics of mTHPC redistribution from the complexes with plasma proteins to lecithin vesicles based on FRET technique.
- Influence of lecithin vesicles concentration and temperature on mTHPC redistribution from HDL.
- The analysis of thermodynamic potentials and mechanism of photosensitizer transfer.

The fourth part of the work consisted in the study of mTHPC intracellular aggregation state as a function of incubation time and its influence on the quantum yield of cells inactivation. We were interested in:

- Intracellular localization and fluorescence lifetime imaging of mTHPC in MCF-7 cells.
- Determination of molar extinction coefficient of mTHPC in MCF-7 cells.
- Photobleaching of mTHPC in cells.
- Calculation of mTHPC absorbed dose in MCF-7 cells and comparison of mTHPC phototoxicity at different incubation times.

The fifth part of the work investigated mTHPC, mTHPP and mTHPBC solvatochromism in different solvents and determined their aggregates structure in aqueous media. For this reason we undertook:
- Development of qauntum mechanic semi-empirical method based on Huckel molecular orbital theory for calculation of the spectral shifts.
- Measurements of absorption spectra of the three compounds for determination of spectral shifts of Soret bands.
- Determination of PSs dimers structure in ethanol-water mixtures.

IV RESULTS

IV.1. Foscan®-based photodynamic treatment *in vivo:* Correlation between efficacy and Foscan accumulation in tumor, plasma and leukocytes

In the first part of the work we have investigated the influence of tumor, plasma and leukocyte concentrations of mTHPC at different times after photosensitizer delivery on PDT response. Both pharmacokinetic and tumor-response studies were carried out in nude mice bearing s.c. Colo26 tumors. Foscan accumulation in leukocytes matches perfectly PDT efficacy compared to tumor and plasma photosensitizer concentrations. This observation reveals the potential role of leukocytes at predicting Foscan-mediated tumoricidal effect and points out the prevalence of vascular photodamage. In the clinical context, the possibility to predict effective therapeutic outcome with Foscan-PDT based on the kinetics of Foscan accumulation in leukocytes, could result in modification of the current PDT treatment protocols.

This part of the work was published in the *Oncology Reports* and is presented thereafter in its published form.

Foscan®-based photodynamic treatment *in vivo:* Correlation between efficacy and Foscan accumulation in tumor, plasma and leukocytes

ESTELLE MAUGAIN[1], SIARHEI SASNOUSKI[1,2], VLADIMIR ZORIN[2], JEAN-LOUIS MERLIN[3], FRANÇOIS GUILLEMIN[1] and LINA BEZDETNAYA[1]

[1]Centre Alexis Vautrin, CRAN CNRS UMR 7039, Avenue de Bourgogne, 54511 Vandœuvre-Les-Nancy Cedex, France, [2]Laboratory of Biophysics and Biotechnology, Physics Faculty, Belorusian State University, Skarini 4 St., Minsk, 220080 Belarus, [3]Centre Alexis Vautrin, EA 3452, Avenue de Bourgogne, 54511 Vandœuvre-Les-Nancy Cedex, France

Abstract. The tumoricidal effect of Foscan-mediated photodynamic therapy may involve both vessel and tumor cell destruction. The relevant importance of each mechanism seems to be defined by the time interval between photosensitizer administration and illumination (drug-light interval, DLI). Short drug-light intervals favor vascular damage due to the preferential photosensitizer accumulation in the tumor vasculature, whereas long drug-light intervals trigger direct tumor cell damage due to the dye localization in the tumor. The purpose of this study was to investigate the influence of tumor, plasma and leukocyte concentrations of Foscan at different times after photosensitizer delivery on PDT response. Both pharmacokinetic and tumor-response studies were carried out in nude mice bearing s.c. Colo26 tumors. One to 96 h after i.v. injection of 0.5 mg/kg Foscan, animals were exposed to 10 J/cm^2 652-nm light delivered at 30 mW/cm^2. Mean tumor regrowth time was determined for each schedule of treatment and correlated to Foscan distribution in the compartments of interest at the time of illumination. PDT efficacy was greatest for irradiations performed at 6 and 12 h post Foscan injection and limited at 96 h. Unlike tumor and plasma Foscan concentrations, photosensitizer accumulation in leukocytes exhibited a good correlation with PDT efficacy. The results suggest that leukocytes could play an important role in the mechanism of PDT-induced vascular damage either by being one of the main effector compartments or by better reflecting Foscan accumulation in endothelial cells compared to plasma. The prevalence of indirect damage was highlighted by the fact that PDT efficacy was not modified by the use of a higher fluence rate of irradiation (160 mW/cm^2), which depleted intratumor oxygen and did not restrain PDT-induced cell toxicity.

Introduction

Photodynamic therapy (PDT) is an emerging modality for the treatment of cancers and other diseases (1,2). The principle of PDT consists in the uptake of a photosensitizer by a target tissue followed by illumination at a specific wavelength. The absorption of light energy by the photosensitizer induces oxygen-dependent photochemical reactions leading to damage of the illuminated tissue. Based on the localization/ biodistribution of the photosensitizer, PDT can have a direct action on tumor cell and/or an indirect action linked to vascular system alterations inducing vascular shut down and/or acute inflammatory reaction (3).

Photodynamic therapy with meta-tetra (hydroxyphenyl) chlorine (m-THPC, Foscan), one of the most powerful second generation photosensitizers (3,4) was approved in the EC countries for the palliative treatment of patients with advanced head and neck cancers (Biel et al, Proc Am Soc Oncol, 38th Annual Meeting, Orlando, FL, abs. 379, 2002). In a clinically relevant situation, Foscan may act by destroying both vessel walls and tumor cells. The relevant importance of either mechanism seems to be defined by the interval between photo-sensitizer administration and illumination (drug-light interval, DLI). Several studies in experimental animals have demonstrated than short DLIs (up to 48 h) favored vascular damage due to the preferential Foscan localization in association with the vasculature (5-7). Tissue-specific damage was observed with irradiation conducted at intervals ≥72 h (7,8). Clinical protocols for Foscan-based PDT recommend the drug-light interval of 96 h, assuming that long DLIs favor maximum differentiation between photosensitizer retention in the tumor and in surrounding normal tissue. However, there is increasing evidence of discrepancy between times of maximum Foscan uptake in the tumors, usually observed at long time intervals and optimal illumination times for PDT efficacy (9-11). Alternatively, Foscan-PDT response is enhanced at short drug light intervals, thus suggesting that

the presence of photosensitizer in the vasculature at early times is responsible for photo-induced damage. Endothelial cells have been proposed as a primary target of Foscan-PDT, based on the assumption that Foscan accumulation in plasma reflects endothelial-cell exposure. Nevertheless, even if PDT response could be better predicted by Foscan plasma levels than tumor levels, the pattern of PDT efficacy does not parallel the Foscan concentration in the plasma (9,12). Moreover, the study of Menezes da Silva and Newman reported a distinct decoupling between serum drug level and maximum of vessel occlusion in mice photosensitized with Foscan (13). The authors postulated that the vascular effect of Foscan-PDT is likely to be related to the drug accumulation in macrophages rather than in endothelial cells with the further implication of the former in photo-induced release of vasoactive substances and vessel occlusion. Given the important role of leukocytes in the PDT-induced vascular shutdown effect *in vivo* (14), Foscan accumulation in these cells could probably much better predict the Foscan-mediated PDT response.

Discrimination between *in vivo* direct and indirect damage based solely on pharmacokinetic parameters is not always allowed. In some cases, time intervals at which the photosensitizer is distinctly confined either to the tumor or to the vascular sites, result in quite similar PDT-induced tumor growth delay (10,15). An effective way to differentiate between direct and indirect damage could be an investigation of both PDT efficacy and intratumor oxygen partial pressure with respect to the fluence rate of irradiation. As has been demonstrated for several photosensitizers, high irradiation fluence rates provoke intratumoral oxygen depletion thus limiting photo-oxidative damage to tumor cells (16,17).

In this study we focused on the correlation between Foscan distribution in tumor, plasma and leucocytes at different times after drug delivery and PDT efficacy of grafted Colo26 tumors in mice over the same time course. We further attempted to differentiate the mechanisms involved in tumor destruction by measuring fluence-rate-dependent variations in intratumor oxygenation and PDT treatment outcome at a selected time interval.

Materials and methods

Experimental model. Studies were performed using female athymic Swiss nu/nu mice (Iffa Credo, L'Arbrelse, France). All animal experiments were carried out in compliance with the French Animal Scientific Procedures Act (from April 1988). Six to eight-week old mice weighing 22-24 g were inoculated subcutaneously into the left hind thigh with a suspension of Colo26 mouse colorectal carcinoma cells (0.1 ml of $2x10^7$ cells/ml in 0.9% NaCl). Experiments were performed 12-15 days later, when tumors reached a surface diameter of about 4-5 mm, and a thickness of 2-3 mm. At that time, histological studies demonstrated that tumors were free of evident necrosis.

Photosensitizer. Foscan® was provided by Biolitec Pharma Ltd. (Edinburgh, UK) and diluted in ethanol/polyethylene glycol 400/water solution (2/3/5) as recommended by the manufacturer. Mice were injected with 50 μl of Foscan (0.5 mg/kg) *via* the tail vein.

Pharmacological studies. Foscan plasma and tumor concentrations were assessed by spectrofluorimetry. Animals

were sacrificed by cervical dislocation 1, 6, 12, 24, 48, 72 or 96 h after Foscan injection. Tumors were rapidly removed and kept under –180 °C until analysis. Plasma and pellet of blood cells were isolated after blood centrifugation (5 min, 350 g) and immediately used for experiments. Plasma was diluted 400 times with PBS in order to maintain plasma absorption value under 0.1 at 420 nm. Fluorescence spectra of diluted plasma were then recorded by a SAFAS flx-Xenius spectrofluorimeter (λ_{ex}: 420 nm, λ_{em}: 652 nm) (SAFAS, Monaco).

Foscan tumor extraction was carried out as follows. 100 mg tissue were digested with 5 ml NaOH (0.2 N) in a 50~C water bath for 4 h, under regular shaking. After centrifugation (1600 g, 10 min), Triton X-100 and 1 N HCl were added to the supernatant (1:2:6, v:v:v) and subjected to fluorescence measurements.

For both plasma and tumor, the amount of dye was calculated from standard curve and expressed in ng of Foscan per g of plasma/tumor.

Anesthesia. The animals were anesthetized by an inhalation of isoflurane Forene 30 (Abbott France, Ringis, France) followed by intraperitoneal injection of a mixture of ketamine-xylazine (80 and 10 mg/kg body weight respectively). Supplemental injections were given at 10-20% of the initial dose, as needed.

Photodynamic treatment. The treatment was carried out under anesthesia 1, 6, 12, 24 or 96 h after sensitization of the mice. Irradiation was performed at 652 nm either by a dye laser (Spectra-Physics 375 B, Les Ulis, France) pumped with an argon laser for the high fluence rate or with a diode laser (Spectra-Physics 375 B, Les Ulis, France) for the low fluence rate. All irradiations were performed using the same optical fiber and frontal light diffuser. The wavelength was verified by a monochromator (Jobin-Yvon, Longjumeau, France) and laser output by an integrating sphere (Labsphere, Massy, France). Mouse tumors were exposed to a total light dose of 10 J/cm^2 delivered over a treatment field 1.5 cm in diameter, at a fluence rate of 30 or 160 mW/cm^2.

Assessment of tumor response. Mice were examined for tumor regrowth daily for 30 days after treatment, and two days a week thereafter for a total of 60 days. The tumor volume was calculated as V = 2/3 (a/2 x b/2 x c) where a and b are two perpendicular axes, and c is the height measured using a caliper. Eight to 15 animals were used per treatment group. Control group received drug but no light. Cures were defined as no visible or palpable tumor at 60 days after treatment.

Measurements of tumor pO$_2$. Intratumor pO$_2$ was measured polarographically using the Eppendorf pO$_2$ Histograph (Eppendorf, Hamburg, Germany). The thin needle was calibrated before and between the measurements in 0.9% saline bubbled alternatively with air and nitrogen to set to the 100% and 0% current. The average tumor temperatures and ambient air pressures were used to postcalibrate the data. The 300-μm-diameter polarographic needle probe was aligned at the tumor surface after creation of a pinpoint hole in the skin

Table I. Mean concentrations of Foscan® (± SD) in Colo26 tumors and in plasma after i.v. drug administration (0.5 mg/kg).

	1 h	6 h	12 h	24 h	48 h	72 h	96 h
Tumor	116±92	143±13	233±55	271±30	330±80	290±89	247±65
Plasma	2648±1119	435±97	361±91	183±32	135±41	89±11	64±23

Results are expressed in ng of Foscan per g of tissue.

covering the tumor. The probe was advanced one step to ensure that the tip was in the tumor and automatic probe advancement was started after the pO_2 values stabilized. Probe advancement consisted of a 0.7 mm forward motion and a 0.3 mm reverse motion for each reading. The probe track length was determined by the tumor dimensions, and the tracking was diagonal through the tumor. Oxygen partial pressure was measured for the 24-h-drug-light-interval immediately before illumination with 30 and 160 mW/cm^2, during the 10 J/cm^2 illumination at times corresponding to a light dose of 5 J/cm^2, and 5 min after irradiation. The time needed for the delivery of 5 J/cm^2 was 31 sec at 160 mW/cm^2 and 2 min 46 sec at 30 mW/cm^2. Since one track of pO_2 measurement takes approximately 10 sec, only one track could be measured during the irradiation of tumors treated with 160 mW/cm^2, while two tracks could be measured with 30 mW/cm^2. Ten animals were used per experimental group. Data were expressed as medians as well as percentages of very hypoxic fraction of values (≤ 2.5 mm Hg).

Foscan accumulation in leukocytes (monocytes, granulocytes, lymphocytes). Animals were sacrificed by cervical dislocation 1, 6, 12, 24, 48, 72 or 96 h after 0.5 mg/kg Foscan injection. Blood was immediately removed and centrifuged (5 min, 350 g). Leukocytes were isolated from pellet of blood cells by a 10 min-lysis of red blood cells: 100 μl of pellet from mice blood was incubated with 2 ml of Facs Lysing solution 1X (BD Biosciences, USA). After 10 min, the mixture was centrifuged (5 min, 350 g). Pellet containing white blood cells was washed twice by addition of PBS followed by centri-fugation (5 min, 350 g). Suspension of white blood cells in 500 μl PBS was examined for Foscan accumulation by flow cytometry (FACSCalibur™, BD Biosciences, USA) (λ_{ex} = 488 nm, λ_{em} = 652 nm). The background signal was subtracted after measuring the autofluorescence from control blood (PEG, no Foscan). Mean fluorescence values were calculated on at least 4 mice.

Statistical analysis. Results from pharmacological studies were compared with the Mann and Whitney statistical test.
Growth delay results are represented as a Kaplan-Meier curve. The statistical significance of difference in the tumor decupling times was assayed using the log-rank test. For oxygen partial pressure measurement, median pO_2 are represented as median values ± SD. Within each experimental group, the significance of the effect of fluence rate on pO_2 for various irradiation conditions was evaluated using the Wilcoxon test. p-values were calculated on the basis of paired analyses of pO_2 values obtained from individual tumors

before, during and after irradiation.
For all the statistical analysis, $p<0.05$ was considered to be significant.

Results

Assessment of Foscan concentration in plasma and tumor. Foscan concentrations in plasma and tumor at the various time points after drug administration are shown in Table I. Foscan plasma concentration was maximum at 1 h (2648±1119 ng/g) and decreased steadily thereafter. Foscan concentration in tumor reached a plateau at 12 h and remained constant until 96 h ($p<0.05$).
Several drug-light intervals were selected for further PDT studies: 1, 6, 12, 24 and 96 h. The short delays (1, 6 and 12 h) were characterized by tumor/plasma ratio ranging from 0.044 to 0.645. This ratio is inverse from 24 h on and amounted to 1.48, with a significantly higher Foscan concentration in tumor compared to that in plasma ($p=0.0045$).

Photodynamic treatment. Each tumor received a light dose of 10 J/cm^2 administrated at 30 mW/cm^2. The evolution of the growth of the tumors irradiated at different drug-light intervals is expressed as Kaplan-Meier curves where the percentage of tumors not having reached 10 times their initial volume is plotted against time after PDT (Fig. 1A). Fig. 1B displays the mean tumor decupling time and the number of tumor cures for all DLIs.
All schedules of treatment significantly delayed tumor growth but the results clearly demonstrate that shorter drug light intervals led to significantly longer tumor growth delay. The mean regrowth time for established tumors to increase by 10 mean volume (T_{10}) was 9.3±1.3 days (Fig. 1B). As follows from Fig. 1A, the PDT effect was heterogeneous at 1 h with a T_{10} of 14.9±6.3 days and equivalent to the response after illumination at 24 h (T_{10} = 14.6±3.9 days) ($p=0.990$). Illumination at 6 and 12 h after Foscan injection was significantly more effective than illumination at all other intervals ($p<0.05$) and was characterized by a T_{10} of 26.3±5.1 and 25.3±2.7 days respectively ($p=0.824$). Tumor cures were observed for all DLIs except for 96 h, which exhibited a weak anti-tumor effect with a T_{10} = 10.7±1.7 days. It should be noted that, except for 96 h, a pronounced edema and erythema at the tumor site accompanied all schedules of treatment in the hours following irradiation.
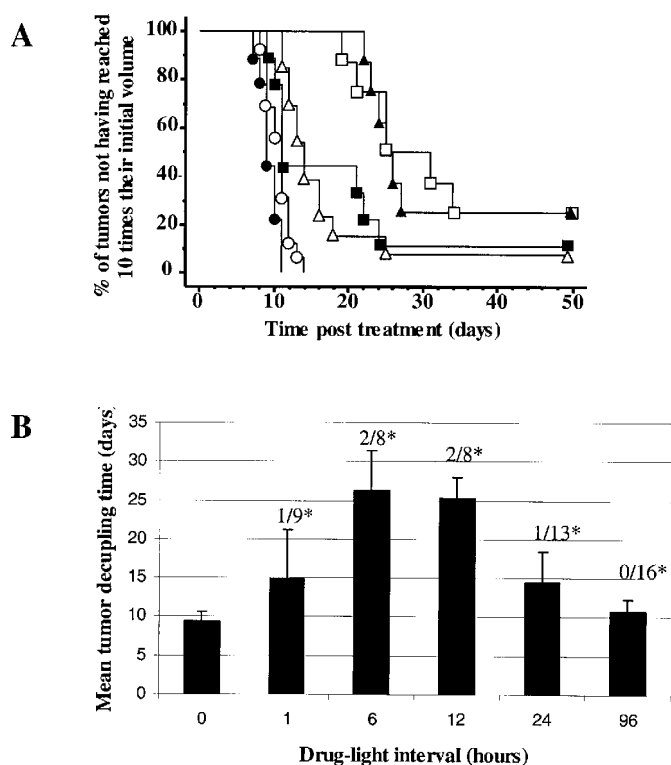
A

B

Figure 1. A, Kaplan-Meier curve of Colo26 tumor regrowth after PDT treatment with Foscan at different time points. The tumor-bearing mice were irradiated with a fluence of 10 J/cm^2 delivered at 30 mW/cm^2 (652 nm) at 1 (■), 6 (□), 12 (▲), 24 (△) and 96 h (○) after i.v. injection of 0.5 mg/kg Foscan. Control animals received drug, no light. B, Tumor regrowth time (mean ± SD) for different drug-light intervals (1, 6, 12, 24 and 96 h). Results were extrapolated from Kaplan-Meier curve A. *Cures/number of animal per experimental group.

Effect of fluence rate on the tumor oxygen partial pressure and tumor growth delay. The contribution of direct or indirect damage in the Foscan-based PDT was further addressed in a study of fluence-rate-dependent variations both in intratumor oxygen partial pressure and treatment outcome at 24 h post-injection. At this time point tumor Foscan concentration

exceeds that in the plasma (Table I) and thus may favor cellular PDT damage.

The tumors at 24 h post injection were treated with the light fluence of 10 J/cm^2 administered at fluence rates of 30 mW/cm^2 and 160 mW/cm^2. Intra-tumor oxygen partial pressure for each fluence rate was measured using the pO_2 Eppendorf histograph before, during and 5 min after illumination. Table II summarizes the effect of fluence rate on intra-tumor pO_2. The results are expressed as median pO_2 values as well as percentage of very hypoxic cell fraction ($pO_2 \leq 2.5$ mm Hg). Median pO_2 prior to illumination for each group of Colo26 tumors were comparable (p>0.05) and averaged to 2.18±0.2 mm Hg. A high fluence rate of irradiation led to a significant drop in the pO_2 values in the course of irradiation as well as a significant increase in the percentage of values ≤ 2.5 mmHg (Table II). Conversely, oxygen partial pressures were maintained at their initial level during irradiation at low fluence rate (30 mW/cm^2). The oxygen depletion resulting from high fluence rate irradiation was reversible (Table II). The values reached their initial level within 5 min after the end of illumination.

Increasing the fluence rate of irradiation from 30 mW/cm^2 to 160 mW/cm^2 did not affect tumor regrowth delay. The Kaplan-Meier curves established for both fluence rates follow the same profile and were not significantly different (p=0.0958) (Fig. 2).

Distribution of Foscan in leukocytes. Blood was removed from animals at different intervals after injection of Foscan and the photosensitizer fluorescence intensity was measured in leukocytes by flow cytometry.

Evolution of Foscan accumulation in leukocytes is displayed in Fig. 3. Foscan fluorescence intensity peaked at 6 and 12 h post-administration with no significant difference between the values (p=0.479) and progressively declines thereafter (Fig. 3). Foscan fluorescence intensity at 1 h was not different from that at 24 h (p=0.512), still both values are statistically higher than at 96 h (p=0.049).

The extent of Foscan accumulation in leukocytes at different time intervals exhibits very good correlation with the efficacy of PDT treatment (Figs. 1B and 3).

Table II. Effect of fluence rate on intra-tumor oxygen partial pressure.

	Treatment protocol	Median pO_2	Percentage of values ≤ 2.5 mm Hg	No. of mice
30 mW/cm^2	Before illumination	2.3±1.15	41.3	10
	During illumination	2.21±1.63	61.2	
	After illumination	2.56±1.22	55.34	
160 mW/cm^2	Before illumination	1.9±0.6	62.2	10
	During illumination	$0.7^a \pm 0.3$	89.6^a	
	After illumination	1.8±0.66	63.5	

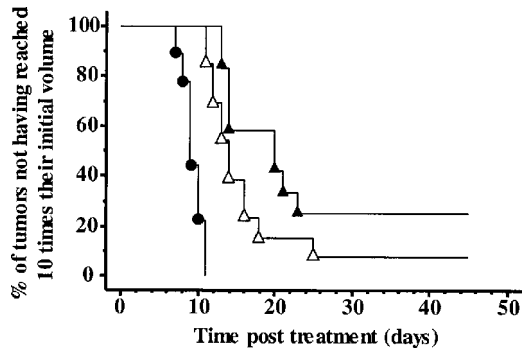[a]Values significantly different from control.

Figure 2. Kaplan-Meier curve of Colo26 tumor regrowth after PDT treatment with Foscan at different fluence rates. The tumors were irradiated 24 h after i.v. injection of 0.5 mg/kg Foscan with a fluence of 10 J/cm^2 delivered at 30 ($\triangle$) or 160 ($\blacktriangle$) mW/cm^2. Control animals ($\bullet$) received drug, no light.
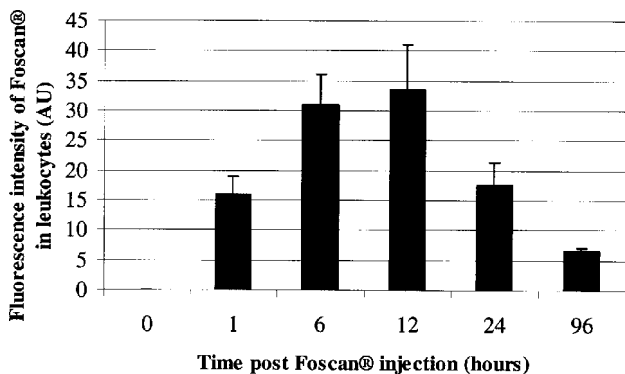

Figure 3. Kinetics of Foscan accumulation in leukocytes at different time intervals post sensitization (0.5 mg/kg) assessed by flow cytometry. Results are expressed as mean fluorescence intensities ± SD.

Discussion

Ample studies have aimed to relate Foscan pharmacokinetic parameters to the extent of PDT damage (8-12,18). Even if the prevalence of vascular damage at short drug-light intervals has been suggested, the direct correlation between plasma Foscan level and effective treatment outcome has not been established. Furthermore, the weak response of tumors illuminated at times corresponding to maximum plasma drug level argues against plasma being the effector compartment (10,12). The failure to establish a correlation between PDT efficacy and plasma sensitizer level encouraged a search of other vascular components, which could be more effective at predicting Foscan-mediated tumoricidal effect. Both endothelial cells and leukocytes such as macrophages have been proposed as possible PDT targets, but the relevance of these statements has not been tested (13).

The primary objective of the present study was to investigate the influence of Foscan distribution in tumor, plasma and white blood cells at different times after drug delivery on the PDT response of the tumor over the same time course using tumor growth delay as the end point.

Abundant *in vivo* pharmacokinetic studies reported that

Foscan plasma concentration is maximal immediately after injection and falls exponentially in mice and rats (9,10), whereas this immediate peak is followed by a second plasma peak between 4 and 24 h after sensitization in rabbits (19), in hamster (20) and in humans (21). The results from this study demonstrated that Foscan plasma concentration declines rapidly as the drug is taken up by the tumor (Table I). The pattern of Foscan concentration in plasma and in tumor assessed by spectrofluorimetry (Table I) is in very good agreement with the study of Whelpton and co-workers (22,23) on the pharmacokinetics of ^{14}C-labelled mTHPC in Colo26 tumor-bearing mice.

We observed a clear discrepancy between optimal intervals of Foscan-mediated tumor photodestruction and the highest concentrations of the photosensitizer in tumor and plasma. PDT response is maximum 6 h after Foscan administration and is not different from the 12 h-time point (Fig. 1). Both these time intervals are characterized by moderate Foscan plasma concentrations, which are 5-6 times lower compared to the maximum drug level at 1 h post-injection (Table I). Neither does the DLI of 6 h correspond to the maximum photosensitizer concentration in the tumor that reaches its highest value at 12 h post-administration and does not vary significantly until 96 h time interval (Table I). Furthermore, the progressive decrease in PDT efficacy over the time span of maximum tumor uptake (12-96 h) accentuates major discrepancies between tumor tissue drug loading and optimal PDT interval. This observation is consistent with several other studies in rodent tumors and human xenografts grown in nude mice (5,6,11,24). Thus, Foscan accumulation in the tumor cannot be a predictive factor of the extent of photo-induced damage. We note that the weakest anti-tumor effect was exhibited at the DLI of 96 h (Fig. 1). Consistent with other studies (9), the decreased PDT response at long DLIs may be a consequence of tumor cell proliferation. The rapid doubling time of Colo26 tumors (2.6 days) could contribute to both a diluting effect on photo-sensitizer levels per cell and to cells distancing from well-oxygenated regions, located close to the vessels.

There was a better correlation between Foscan concentration in plasma and PDT response if the 1 h time point is excluded (Table I, Fig. 1). Other studies also established a better correspondence between plasma drug level and the degree of tumor photo-damage excluding the initial distribution time (9,11,12). The authors suggested that the lack of correlation between plasma photosensitizer level and PDT response at early times could be related to the particular pattern of Foscan distribution in the plasma immediately after injection. As can be extrapolated from *in vitro* binding studies (25), shortly after injection Foscan persists in highly aggregated inactive form, whereas 6-8 h later the aggregates split up and active monomer Foscan species redistribute in the vascular compartments. If this holds true *in vivo*, Foscan uptake in the target cell population will require a certain delay. Hypothesizing that sensitizer accumulation in white blood cells could better predict tumor response to photosensitization, we further addressed the kinetics of Foscan deposition in this compartment and compared it with post-PDT tumor growth delay. A remarkable correlation was observed between Foscan

accumulation in white blood cells and PDT response (Figs. 1 and 3). A possible explanation could be offered, if we consider that endothelial cells are the vascular target and that Foscan accumulation in these cells is reflected by the dye accumulation in leukocytes. Studies in rodent models demonstrated that Foscan distributes in endothelial cells within certain delay after drug administration and the highest Foscan levels were registered between 8 and 24 h (21,27). Even if direct correlation between kinetics of the photosensitizer deposition in endothelial cells and photo-induced damage has not been established, the key role of endothelial cells at controlling PDT efficacy has been proposed in several studies (9,12). Another explanation could be related to the possible role of photoactivated leukocytes in Foscan-PDT damage. This presumption is supported by our previous demonstration of Foscan sensitized macrophages activation at sub-curative light doses (27). The macrophages activation was accompanied by the release of nitric oxide (NO) and tumor necrosis factor-α (TNF- α), the role of both these mediators in tumor regression through the effects on microvasculature has been widely acknowledged (28,29). Further, the important role of activated mononuclear cells in PDT-triggered vascular shut-down with the first generation photosensitizer has been recently highlighted in a study of Takahashi and co-workers (14). Their concept was based on two observations: *in vitro* mononuclear cells activation by photogenerated reactive oxygen species (ROS) with the subsequent generation of ROS (in particular superoxide anion radical, $O_2^{\cdot-}$) by monocytes themselves and *in vivo* demonstration that singlet oxygen ($^1O_2$) and $O_2^{\cdot-}$ influence all processes of the PDT-mediated vascular shut-down effect (30). The question on the impact of leukocytes in PDT induced vascular damage remains open, and this field of research definitively deserves further investigations.

In the present study, Foscan-based PDT efficacy was evaluated by measuring tumor regrowth delay as an endpoint. This kind of measurement is insensitive to the type of damage triggered by PDT and does not allow to discriminate the prevalence of direct or indirect mechanism. Even if a close correlation between Foscan levels in leukocytes and PDT efficacy supports the prevalence of vascular effects in PDT outcome, the impact of direct damage cannot be ruled out. According to pharmacokinetics studies (Table I), Foscan concentration reaches a plateau in tumors at 12 h, and there could be a complex interplay between direct tumor cell kill and damage to vasculature from 12 h on, when Foscan concentration in tumor exceeds that in plasma. The relevance of direct and indirect damage in Foscan-based PDT was further investigated in the study of the influence of photo-induced intratumor oxygen depletion on PDT efficacy. As has been demonstrated for several photosensitizers that low fluence rates of irradiation preserve tumor oxygenation thus improving the tumor response, while intratumor oxygen depletion with a concomitant decrease in PDT efficacy was recorded by applying high irradiation fluence rates (16,17). Consistent with our recent study on Foscan-sensitized xenografted HT29 tumors (16), irradiation of Colo26 tumors with the same light fluence but delivered at a higher fluence rate (160 mW/cm^2), resulted in the decrease in tumor pO$_2$ during irradiation (Table II). However, unlike photosensitization with Foscan of xenografted HT29 tumors, this photo-induced intratumoroxygen depletion did not influence tumor growth delay in our experimental model (Fig. 2). Assuming that the

fluence rate effect is closely linked to direct photocytotoxicity and based on the observations of the fluence rate-dependent variations in oxygenation (Table II), but not in photocytotoxicity (Fig. 2), we confirm the pre-dominance of indirect, vascular damage.

In conclusion, the present study reports that Foscan accumulation in leukocytes matches perfectly PDT efficacy compared to tumor and plasma photosensitizer concentrations. This observation reveals the potential role of leukocytes at predicting Foscan-mediated tumoricidal effect and points out the prevalence of vascular photodamage. In the clinical context, the possibility to predict effective therapeutic outcome with Foscan-PDT based on the kinetics of Foscan accumulation in leukocytes, could result in modification of the current PDT treatment protocols.

Acknowledgements

References

1. Okunaka T and Kato H: Potential applications of photodynamic therapy. Rev Contemp Pharmacother 10: 59-68, 1999.
2. Dougherty TJ: An update on photodynamic therapy applications. J Clin Laser Med Surg 20: 3-7, 2002.
3. Dougherty TJ, Gomer CJ, Henderson BW, *et al:* Photodynamic therapy. J Natl Cancer Inst 90: 889-905, 1998.
4. Van Geel IP, Oppelaar H, Oussoren YG, *et al:* Photosensitizing efficacy of MTHPC-PDT compared to Photofrin-PDT in the RIF1 mouse tumor and normal skin. Int J Cancer 60: 388-394, 1995.
5. Ris HB, Altermatt HJ and Nachbur B, *et al:* Effect of drug-light interval on photodynamic therapy with metatetrahydro-xyphenylchlorin in malignant mesothelioma. Int J Cancer 53: 141-146, 1993.
6. Van Geel IP, Oppelaar H, Oussoren YG, *et al:* Mechanisms for optimising photodynamic therapy: second-generation photo-sensitisers in combination with mitomycin C. Br J Cancer 72: 344-350, 1995.
7. Andrejevic-Blant S, Hadjur C, Ballini JP, *et al:* Photodynamic therapy of early squamous cell carcinoma with tetra(m-hydroxyphenyl)chlorin: optimal drug-light interval. Br J Cancer 76: 1021-1028, 1997.
8. Westerman P, Glanzmann T, Andrejevic S, *et al:* Long circulating half-life and high tumor selectivity of the photosensitizer metatetrahydroxyphenylchlorin conjugated to polyethylene glycol in nude mice grafted with a human colon carcinoma. Int J Cancer 76: 842-850, 1998.
9. Cramers P, Ruevekamp M, Oppelaar H, *et al:* Foscan uptake and tissue distribution in relation to photodynamic efficacy. Br J Cancer 88: 283-290, 2003.
10. Jones HJ, Vernon DI and Brown SB: Photodynamic therapy effect of m-THPC (Foscan) *in vivo:* correlation with pharmacokinetics. Br J Cancer 89: 398-404, 2003.
11. Veenhuizen RB, Ruevekamp MC, Oppelaar H, *et al:* Foscanmediated photodynamic therapy for a peritoneal-cancer model: drug distribution and efficacy studies. Int J Cancer 73: 230-235, 1997.
12. Veenhuizen R, Oppelaar H, Ruevekamp M, *et al:* Does tumor uptake of Foscan determine PDT efficacy? Int J Cancer 73: 236-239, 1997.
13. Menezes da Silva FA and Newman EL: Time-dependent photodynamic damage to blood vessels: correlation with serum photosensitizer levels. Photochem Photobiol 61: 414-416, 1995.

63

14. Takahashi M, Nagao T, Imazeki Y, *et al:* Roles of reactive oxygen species in monocyte activation induced by photo-chemical reactions during photodynamic therapy. Front Med Biol Eng 11: 279-294, 2002.

15. Chen B, Pogue BW, Goodwin IA, *et al:* Blood flow dynamics after photodynamic therapy with verteporfin in the RIF-1 tumor. Radiat Res 160: 452-459, 2003.

16. Coutier S, Bezdetnaya LN, Foster TH, *et al:* Effect of irradiation fluence rate on the efficacy of photodynamic therapy and tumor oxygenation in meta-tetra (hydroxyphenyl) chlorin (mTHPC)-sensitized HT29 xenografts in nude mice. Radiat Res 158: 339-345, 2002.

17. Sitnik TM, Hampton JA and Henderson BW: Reduction of tumor oxygenation during and after photodynamic therapy *in vivo:* effects of fluence rate. Br J Cancer 77: 1386-1394, 1998.

18. Morlet L, Vonarx-Coinsmann V, Lenz P, *et al:* Correlation between meta(tetrahydroxyphenyl)chlorin (m-THPC) bio-distribution and photodynamic effects in mice. J Photochem Photobiol B 28: 25-32, 1995.

19. Ronn AM, Nouri M, Lofgren LA, *et al:* Human tissues levels and plasma pharmacokinetics of temoporfin (Foscan, mTHPC). Lasers Med Sci 11: 267-272, 1996.

20. Blant SA, Glanzmann TM, Ballini JP, *et al:* Uptake and localisation of mTHPC (Foscan) and its ^{14}C-labelled form in normal and tumor tissues of the hamster squamous cell carcinoma model: a comparative study. Br J Cancer 87: 1470-1478, 2002.

21. Glanzmann T, Hadjur C, Zellweger M, *et al:* Pharmacokinetics of tetra(m-hydroxyphenyl)chlorin in human plasma and individualized light dosimetry in photodynamic therapy. Photochem Photobiol 67: 596-602, 1998.

22. Whelpton R, Michael-Titus AT, Basra SS, *et al:* Distribution of temoporfin, a new photosensitizer for the photodynamic therapy of cancer, in a murine tumor model. Photochem Photobiol 61: 397-401, 1995.

23. Whelpton R, Michael-Titus AT, Jamdar RP, *et al:* Distribution and excretion of radiolabeled temoporfin in a murine tumor model. Photochem Photobiol 63: 885-891, 1996.

24. Ris HB, Li Q, Krueger T, *et al:* Photosensitizing effects of m-tetrahydroxyphenylchlorin on human tumor xenografts: correlation with sensitizer uptake, tumor doubling time and tumor histology. Int J Cancer 76: 872-874, 1998.

25. Hopkinson HJ, Vernon DI and Brown SB: Identification and partial characterization of an unusual distribution of the photosensitizer meta-tetrahydroxyphenyl chlorin (temoporfin) in human plasma. Photochem Photobiol 69: 482-488, 1999.

26. Andrejevic Blant S, Ballini JP, van den Bergh H, *et al:* Time-dependent biodistribution of tetra(m-hydroxyphenyl)chlorin and benzoporphyrin derivative monoacid ring A in the hamster model: comparative fluorescence microscopy study. Photochem Photobiol 71: 333-340, 2000.

27. Coutier S, Bezdetnaya L, Marchal S, *et al:* Foscan (mTHPC) photosensitized macrophage activation: enhancement of phagocytosis, nitric oxide release and tumor necrosis factor-alpha-mediated cytolytic activity. Br J Cancer 81: 37-42, 1999.

28. Asher A, Mule JJ, Reichert CM, *et al:* Studies on the anti-tumor efficacy of systemically administered recombinant tumor necrosis factor against several murine tumors *in vivo.* J Immunol 138: 963-974, 1987.

29. Korbelik M: Induction of tumor immunity by photodynamic therapy. J Clin Laser Med Surg 14: 329-334, 1996.

30. Imazeki Y, Nagao T, Saito K, *et al:* Vascular shut down effect in photodynamic therapy-mechanism of platelets thrombus formation by photochemical reaction. Microcirculation Annu 16: 69-70, 2000.

IV.2. Investigation of Foscan® interactions with plasma proteins

The purpose of this study was the examination of Foscan® interaction with plasma albumin and lipoproteins and assessment of sensitizers aggregation state in aqueous media. Spectroscopic studies indicated the presence of monomeric and aggregated Foscan® species upon addition to plasma protein solutions. Kinetics of Foscan® disaggregation in albumin-enriched solutions were very sensitive to the protein concentration and incubation temperature. Disaggregation considerably increased with the temperature rise from 15 °C to 37 °C. Compared to albumin, Foscan® disaggregation kinetics in the presence of lipoproteins displayed poorer dependency on lipoprotein concentrations and smaller variations in disaggregation rate constants. Gel-filtration chromatography analysis of Foscan® in albumin solutions demonstrated the presence of aggregated fraction of free, non-bound to protein Foscan® and monomeric Foscan®, bound to protein.

This part of the work was published in the *Biochimica et Biophysica Acta - General Subjects* and is presented thereafter in its published form.

Investigation of Foscan® interactions with plasma proteins

Siarhei Sasnouski[a,b], Vladimir Zorin[b], Ivan Khludeyev[b], Marie-Ange D'Hallewin[a], François Guillemin[a], Lina Bezdetnaya[a,]*

[a]Centre Alexis Vautrin , CRAN UMR 7039 CNRS-INPL-UHP, Avenue de Bourgogne, 54511 Vandœuvre-Les-Nancy cedex, France
[b]Laboratory of Biophysics and Biotechnology, Physics Faculty, Belorussian State University, Skarini 4 St., Minsk 220080, Belarus

Abstract

The present study investigates the interaction of the second generation photosensitizer Foscan® with plasma albumin and lipoproteins. Spectroscopic studies indicated the presence of monomeric and aggregated Foscan® species upon addition to plasma protein solutions. Kinetics of Foscan® disaggregation in albumin-enriched solutions were very sensitive to the protein concentration and incubation temperature. Kinetic analysis demonstrated that two types of Foscan® aggregated species could be involved in disaggregation: dimers with a rate constant of $k_1 = (2.3\pm0.15) \times 10^{-3}$ s^{-1} and higher aggregates with rate constants varying from $(0.55\pm0.04) \times 10^{-3}$ s^{-1} for the lowest to the $(0.17\pm0.02) \times 10^{-3}$ s^{-1} for the highest albumin concentration. Disaggregation considerably increased with the temperature rise from 15 °C to 37 °C. Compared to albumin, Foscan® disaggregation kinetics in the presence of lipoproteins displayed poorer dependency on lipoprotein concentrations and smaller variations in disaggregation rate constants. Gel-filtration chromatography analysis of Foscan® in albumin solutions demonstrated the presence of aggregated fraction of free, non-bound to protein Foscan® and monomeric Foscan®, bound to protein.
© 2005 Elsevier B.V. All rights reserved.

Keywords: Photodynamic therapy (PDT); Foscan®; Disaggregation; Bovine serum albumin (BSA); Lipoprotein; Gel-filtration chromatography

1. Introduction

Photodynamic therapy (PDT) involves the administration of a photosensitizer followed by the exposure of tumors to light of a specific wavelength. Photosensitizer absorbs light and generates cytotoxic-reactive oxygen species leading to cellular damage [1]. The phototoxic effect of photosensitizer is influenced by its photophysical properties, pharmacokinetics and intratumoral uptake.

One of the parameters largely influencing photophysical and pharmacological behaviour of photosensitizers is their aggregation state. In aqueous media, most of the tetrapyrrolic photosensitizers form dimers and higher micellelike aggregates and as such are ineffective in producing

singlet oxygen ($^1O_2$) [2,3], thus resulting in a drop of their photosensitizing efficiency [4,5]. Considering that tetrapyrrolic sensitizers may aggregate at very low concentrations and that the dissociation of these aggregates does not occur readily even in the presence of plasma, it is clear that both aggregation and disaggregation of porphyrins occurs in the blood circulation [6], and the competition between these processes could affect the in vivo PDT efficacy.

During interactions with plasma proteins, a hydrophobic sensitizer dissociates from an aggregate and binds to protein molecule. The type of protein-carrier governs the delivery of sensitizer to the tumor [7]. In vivo transport of several porphyrinoid derivatives with a moderate and high degree of hydrophobicity is carried out by lipoproteins [7]. Serum albumin, the most abundant protein in blood plasma, serves as a carrier for amphiphilic and hydrophilic photosensitizers [8,9]. The nature of the carrier protein also affects the drug localisation in the tumor with albumin primarily delivering bound drugs to the vascular stroma, while lipoproteins

internalise sensitizers in malignant cells [9]. Plasma proteins binding affinity for various photosensitizers can play an important role in drug distribution and photodynamic efficacy [10–13].

Foscan® or meta-tetra(hydroxyphenyl)chlorin (mTHPC) is a second-generation photosensitizer [14] and is one of the most effective sensitizers studied to date [15]. Foscan® has been granted European approval for palliative treatment of patients with advanced head and neck cancers and undergoes clinical open-label multicenter studies for the treatment of early squamous cell carcinoma [16,17].

Studies on Foscan® interaction with plasma protein fractions are sparse [18–20]. Foscan® displays some unusual properties in vitro and in vivo compared with many other sensitizers. Gradient-density ultracentrifugation demonstrated the presence of weakly fluorescing aggregated Foscan® species in the regions of albumin or HDL/albumin [18,21]. This binding pattern was transient and re-distributed among plasma proteins with increase in incubation time.

The present study addresses the kinetics of Foscan® disaggregation on plasma proteins (albumin and lipoproteins) and investigates the distribution of different aggregated fractions of Foscan® in bovine serum albumin (BSA) solution.

2. Materials and methods

2.1. Chemicals

The photosensitizer Foscan® (mTHPC, temoporfin) was kindly provided by Biolitec AG (Jena, Germany). Stock solution was made by dissolving the powder in 100% ethanol. Phosphate-buffered saline ((PBS), without $CaCl_2$ and $MgCl_2$; pH 7.4) was obtained from Invitrogen. Gels Sephadex G-100 and Sephadex G-200, sodium azide (NaN_3), t-Octylphenoxypolyethoxyethanol (Triton® X-100), bovine serum albumin (BSA) and lipoproteins from bovine plasma were obtained from Sigma.

According to the manufacturer (Sigma), lipoproteins' purity was confirmed by both immunoelectrophoresis and agarose electrophoresis. Stock solution of lipoproteins (20 mg protein/mL in 10 mM sodium bicarbonate, pH 7.4) were kept at 4 - C with EDTA (0.01% by mass) to exclude oxidative processes. Lipoproteins and BSA were dissolved in PBS solution to appropriate concentrations immediately before measurements. BIO-RAD DC Protein Assay was obtained from BIO-RAD Laboratories.

2.2. Spectroscopic measurements

Twenty AL of Foscan®-ethanol stock solution was added to 2 mL of PBS, PBS containing BSA or PBS containing lipoproteins to reach a final Foscan® concentration of 3×10^{-6} M. Absorption spectra were recordedon a Perkin-Elmer Lambda Bio 9 spectrophotometer, using a 10-mm quartz cuvette. Steady-state emission spectra of Foscan® were

carried out using a 10-mm pathlength quartz cuvette in a computer-controlled Perkin-Elmer LS50B luminescence spectrometer, equipped with a xenon discharge lamp and a red-sensitive photomultiplier (Hamamatsu R 928). Emission spectra were collected for the wavelength range between 600 and 700 nm (bandpasses of both excitation and emission slits were 10 nm; photomultiplier voltage 775 V). The fluorescence intensity was measured with excitation at 420 nm and emission at 655 nm. Kinetics of Foscan® disaggregation after injection in BSA and lipoproteins solutions were performed by the continuous monitoring of its fluorescence intensities at a fixed wavelength of emission (λ = 655 nm). To dissociate weakly-fluorescent aggregates, a neutral detergent Triton X-100 (0.2% v/v) was added to each sample at the end of incubation period. The temperature was kept constant with a water thermostat and was controlled using Testo 110 thermometer (Radiospares, Germany). All kinetic measurements were fitted by biexponential curves using modified Levenberg–Marquardt non-linear fitting program.

Resonance Light Scattering (RLS) spectra were conducted on Perkin-Elmer LS50B luminescence spectrometer using 10 mm pathlength quartz cuvette in the synchronous scanning mode in which the emission and excitation monochromators are preset to identical wavelengths.

2.3. Gel filtration experiments

All the gel filtration experiments were performed with 2.5×50 cm Sephadex G-100 or Sephadex G-200 gels columns in the dark at 24T1-C. The entrance of the column was connected to a peristaltic pump with capillary silicon tubing and equilibrated at 20 mL/h with PBS. Sample volumes were 1.8–2.5 mL and elutions were performed at a flow rate 8–18 mL/h. Ten μL of a Foscan® ethanol solution (10^{-6}–10^{-5} M) was added to 1 mL of PBS containing BSA (1.47×10^{-4} M) and incubated during 1 or 24 h. Between each new run, the column was washed with 500 mL PBS containing NaN_3 (0.1% m/m) at flow rate 20 mL/h. Concentrations of BSA in column fractions were determined using BIO-RAD DC Protein Assay on Multiscan Ascent plate reader (Labsystems, Finland) photometer with 690 nm bandpass filter in 96-well plates Microtest (Becton Dickinson, USA). Monomeric BSA was prepared by using gel filtration of BSA (3×10^{-4} M) on the Sephadex G-200 column and was further isolated according to the molecular weight of 70 kDa.

Foscan® fluorescence was measured in each chromatographic fraction with and without Triton X-100 (0.2% v/v) on a SAFAS flx-XENIUS spectrofluorimeter. The fluorescence intensity was measured with excitation at 420 nm and emission at 655 nm.

3. Results

3.1. Spectroscopic and RLS properties of Foscan® in different media

In organic solvents Foscan® has a typical absorption spectrum of chlorin-type compounds with two main peaks at 416 nm (Soret band) and 650 nm (red region) (Fig. 1A). Changes, corresponding to aggregation, were observed after injection of Foscan® ethanol solutions in PBS (Fig. 1A, Table 1). The aggregated species are characterized by a broadening of Soret band and a shift of its peak to $\lambda = 433$ nm with a concomitant decrease of extinction in all bands
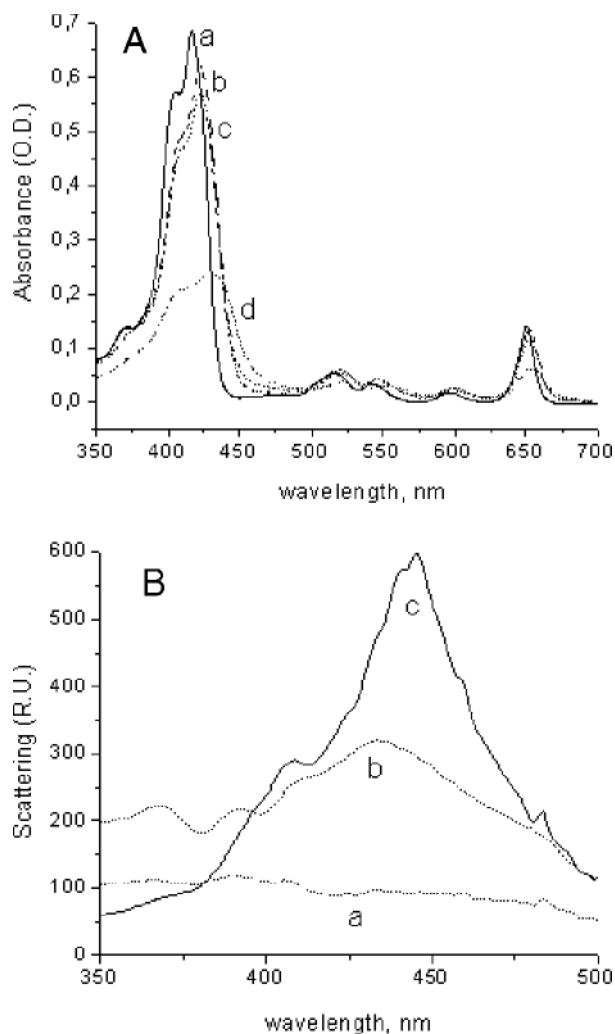

Fig. 1. Absorption and Resonance Light Scattering spectra of Foscan® in different media. Absorption spectra (A) of Foscan® (3×10^{-6} M) in ethanol solution (trace a), in PBS solution containing lipoproteins of 1.47×10^{-5} M(trace b); in PBS solution containing BSA of 1.47×10^{-4} M (trace c), in PBS solution (trace d). All spectra were registered immediately after Foscan® injection. Resonance Light Scattering spectra (B) of Foscan® (3×10^{-6} M) in PBS +2% Triton X-100 solution (trace a); in PBS solution containing BSA of 1.47×10^{-4} M(trace b); in PBS solution (trace c). All spectra were registered immediately after Foscan® injection.

Table 1
Foscan® (3×10^{-6} M) absorption maxima ($\lambda_{max,}$ nm) and Soret band bandwidths (cm^{-1}) in ethanol, PBS and PBS containing proteins solutions

Medium	Absorption maxima (nm)		Soret band half height bandwidths (cm^{-1})
	Soret	Red region	
Ethanol	416	650	1940
PBS	433	653	3500
PBS–BSA[a]	421	653	2240
PBS–lipoproteins[b]	420	652	2140

[a] PBS containing BSA of 1.47×10^{-4} M.
[b] PBS containing lipoproteins in a concentration 1 mg/mL (by protein).

(Fig. 1A). The half height bandwidth of Foscan® Soret band undergoes substantial increase upon introduction of sensitizer into aqueous medium (Table 1). The spectroscopic properties of Foscan® in the presence of BSA and lipoproteins displayed transitional features between aqueous and organic media (Fig. 1A, Table 1). Compared to ethanol, Foscan® absorption spectra in both BSA and lipoproteins were characterized by bathochromic shift and broadening in Soret band and in the first Q-band. Also, in these media half height bandwidths of Soret bands were considerably reduced compared to PBS solution, and were closer to Foscan® ethanol solution. Spectral modifications of Foscan® in different environment (Table 1) demonstrate that all these changes are more pronounced in BSA than in lipoproteins solutions.

Fluorescence yields are very sensitive to aggregation state of porphyrin-like sensitizers with the monomeric species solely responsible for fluorescence [4,22]. In proteins-enriched solutions, Foscan® fluorescence yield is nearly three orders of magnitude greater than in Foscan® PBS solutions, but still is lower compared to monomeric Foscan® ethanol solution (data not shown). Thus, both absorption and fluorescence measurements indicate that Foscan® in protein-containing milieu exists as a mixture of monomers and aggregates.

The presence of aggregates was further evidenced by using resonance light scattering (RLS) spectroscopy. RLS effect is observed as increased scattering intensity at or very near the wavelength of absorption maximum of aggregated molecular species [23,24]. The intensity of scattering depends on the square of the volume of the aggregate and increases as a consequence of aggregation. The scattering properties of Foscan® in different media are displayed in the Fig. 1B. The maxima in the scattering peaks of Foscan® in PBS ($\lambda_{max} = 445$ nm) and PBS–BSA solutions ($\lambda_{max} = 433$ nm) are located close to their respective absorption maxima in the Soret bands ($\lambda = 433$ nm and $\lambda = 421$ nm, Table 1). The peak of Foscan® aggregates scattering in PBS is twice as big as in BSA solution (Fig. 1B). Consistent with the studies [23,24], this strong peak in scattering spectrum of sensitizer in aqueous solutions could be indicative of an intensive electronic coupling between Foscan® molecules in aggregates. The interactions between Foscan® molecules are supposed to be carried out by
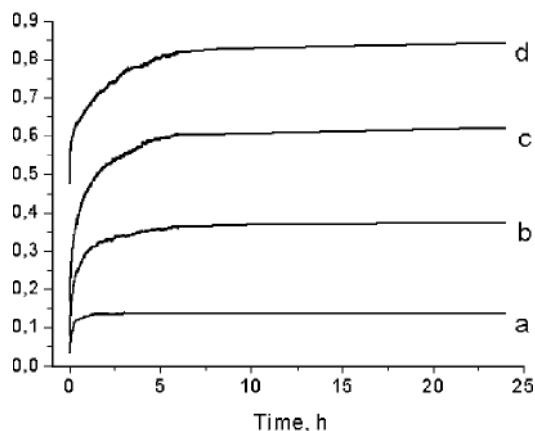
Fig. 2. Kinetics of Foscan® disaggregation in the solutions of the different concentrations of BSA. Foscan® (3×10^{-6} M) was incubated in PBS solutions containing BSA of 1.47×10^{-6} M (trace a), 4.41×10^{-6} M (trace b), 1.47×10^{-5} M (trace c) and 1.47×10^{-4} M (trace d) during 24 h at 25 °C. Foscan® fluorescence intensities were measured continuously at the wavelength of emission λ_{em}=655 nm (λ_{ex}=420 nm). At the end of incubation period Triton X-100 (0.2% v/v) was added to each sample. The ratio between Foscan® fluorescence intensity before (I) and after addition of Triton (I_T) represents the monomeric fraction of Foscan® and is displayed at the Y-axis.

hydrogen bonding between its phenolic groups, k–k interactions between the aromatic rings and hydrophobic forces in aqueous media, which form less-polar exterior inside aggregate and determine its very low solubility in aqueous media [25]. Addition of Triton X-100 as monomer-izing agent results in the disappearance of RLS peaks thus pointing out the rupture of interactions between Foscan® molecules as a consequence of disaggregation (Fig. 1B). Measurements of RLS spectra of Foscan® in lipoproteins solution encountered difficulties related to very intense scattering from lipoproteins particles and therefore could not be reported.

3.2. Study of Foscan® disaggregation kinetics in solutions of BSA and lipoproteins

Foscan® behaviour in solutions of plasma proteins was assessed by measuring the kinetics of sensitizer fluorescence intensities in the response to various protein concentrations and incubation temperatures. For each experimental condition, Foscan® fluorescence intensities were measured continuously at the wavelength of emission (655 nm) and at the end of 24 h incubation period, Triton was added. Assuming that only monomers fluoresce, the ratio between Foscan® fluorescence intensity before (I) and after addition of Triton (I_T) represents the monomeric fraction of sensitizer.

Kinetics of Foscan® disaggregation in BSA solutions are greatly influenced by protein concentration (Fig. 2). Depending on BSA concentrations, the parameter I/I_T achieved a plateau after 0.3–6 h incubation, thus indicating an equilibrium between aggregates and monomers of the

sensitizer at these time points. In the presence of low BSA concentrations (1.47×10^{-6} M and 4.41×10^{-6} M) the main part of Foscan® is still aggregated after 24 h incubation and less than 35% undergoes disaggregation. Foscan® disaggregation increases with increasing BSA concentration. Already at BSA concentration of 1.47×10^{-5} M Foscan® monomerization reaches about 60% after 6 h incubation and remains stable till the end of the incubation period. In the presence of 1.47×10^{-4} M, albumin monomerization reached 80% (Fig. 2). Even at concentrations of albumin equal to that in human plasma (6×10^{-4} M) the ratio I/I_T at equilibrium does not exceed 80% (data not shown).

The kinetics of disaggregation are very sensitive to temperature changes (Fig. 3). An incubation of Foscan® with the fixed BSA concentration of 1.47×10^{-4} M at 15 °C required more than 24 h in order to reach the equilibrium, whereas the equilibrium was obtained in 1 h upon an incubation at 37 °C.

The processes of Foscan® disaggregation in lipoproteins solutions differ from that of BSA solutions (Fig. 4). After addition of Foscan® ethanol solutions in lipoproteins the equilibrium was obtained 7 to 8 h after injection with the disaggregation between 70% for the lowest lipoproteins concentrations (0.1 mg/mL) and 80% for the highest ones (3 mg/mL).

Foscan® disaggregation rate constants for every BSA and lipoproteins concentration were obtained by bi-exponential fitting of the plots from the Figs. 2 and 4, respectively. The rate constants of the first rapid phase (k_1), which dominates immediately after injection, was (2.3 ± 0.15) $\times 10^{-3}$ s^{-1} at 25 °C regardless the BSA and lipoproteins concentrations. The rate constant of the slower
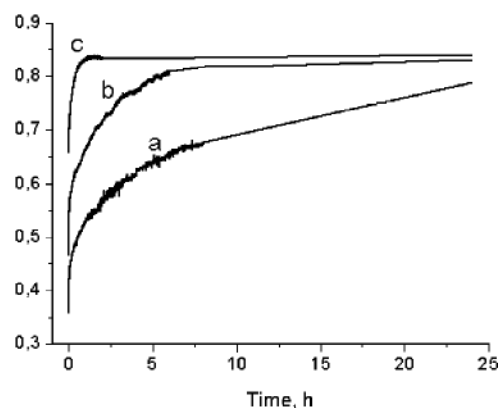
Fig. 3. Kinetics of Foscan® disaggregation in solutions of BSA at different incubation temperatures. Foscan® (3×10^{-6} M) was incubated in PBS solutions containing BSA of 1.47×10^{-4} M during 24 h at the incubation temperatures of 15 °C (trace a), 25 °C (trace b) and 37 °C (trace c). Foscan® fluorescence intensities were measured continuously at the wavelength of emission λ_{em}=655 nm (λ_{ex}=420 nm) at indicated temperatures. At the end of incubation period Triton X-100 (0.2% v/v) was added to each sample. The ratio between Foscan® fluorescence intensity before (I) and after addition of Triton (I_T) represents the monomeric fraction of Foscan® and displayed at the Y-axis.

phase (k_2), displayed in Fig. 5, decreases about 3 times upon a 100-fold increase in BSA concentration. The values of k_2 when plotted against lipoproteins concentration (Fig. 5) demonstrated a 2 times increase upon 30-fold increase in lipoproteins content.

3.3. Gel filtration of Foscan® BSA solutions

In the next step, we investigated the re-partition of different Foscan® fractions in BSA solution with gel-chromatography. The samples of Foscan® (5×10^{-6} M) solutions incubated in the presence of BSA for 1 and 24 h were eluted through the column filled with gelSephadex G-100 and Foscan® fluorescence was measured in every eluted fraction of 2 mL. In order to investigate the aggregation state of Foscan®, the fluorescence of each fraction was measured directly in chromatographic fractions and after addition of Triton X-100. Protein content was also measured in every chromatographic fraction.

Foscan® elution profiles after 1 h incubation with BSA at 37 °C demonstrated two main bands with the peaks in the first rapid fraction (elution volume V_e=106 mL) and in the slow second one (V_e=135 mL) (Fig. 6A). Upon addition of the surfactant, we observed a very large increase in sensitizer fluorescence intensity in the rapid fraction with little change in the fluorescence of the second slow fraction (Fig. 6A). Calibration of G-100 gel column demonstrated the presence in the first rapid fraction of aggregated protein with a molecular weight (M.W.) approximately 400 kDa and aggregated Foscan® with a M.W. about 600 kDa, whereas in the second fraction, we detected a 70-kDa monomeric protein. An increase in incubation time till 24 h (Fig. 6B) or a decrease in Foscan® concentration from 3×10^{-6} to 10^{-6}

Fig. 5. Rate constant k_2 of Foscan® disaggregation with respect to different concentrations of BSA and lipoproteins. The rate constants for every BSA and lipoproteins concentration were deduced from the biexponential fitting of the plots from Fig. 2 and from Fig. 4, respectively. The rate constant k_2 stands for the slow phase of disaggregation. Biexponential fitting was performed using modified Levenberg–Marquardt non-linear fitting program.

M (Fig. 6C) resulted in a considerable reduction of the first peak of the sensitizer, especially in the case of low Foscan® concentration.

The maximum level of Foscan® fluorescence in the first elution peak after addition of surfactant does not coincide with the elution volume of maximal protein content (Fig. 6A). This issue was further assessed by chromatography of Foscan® solution with pre-incubated for 1 h at 37 °C monomeric BSA solution using gel Sephadex G-200. Before addition of Triton, the only one fluorescent peak was recorded with a V_e=46 mL (Fig. 7). Surfactant addition significantly increased the fluorescence of this peak. Protein content analysis demonstrated the presence of monomeric protein in this fraction, thus assuming that the latter consists of monomeric BSA together with monomeric and aggregated sensitizer. A striking observation was the appearance of huge Foscan® fluorescence in the elution volume 25–32 mL with a peak at 30 mL upon Triton addition.

4. Discussion

There are several investigations on Foscan® photophysical properties [25,26] and the influence of its aggregation state on photodynamic activity [5,27]. Studies with cultured cells demonstrated better photosensitizing efficacy for monomeric fluorescence species [4,27]. At the same time, certain photobiological activity was also attributed to aggregated form of sensitizer [22].

Spectroscopic studies of Foscan® placed in solutions of BSA and lipoproteins (Fig. 1A, Table 1) demonstrated the presence of monomeric along with aggregated species. As lipoproteins are a more hydrophobic environment than BSA, the spectral properties that evidence sensitizer
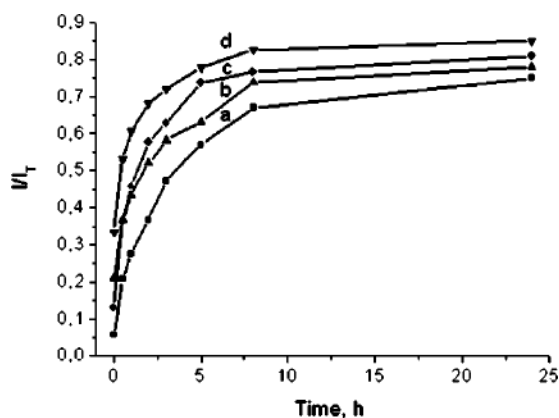
Fig. 4. Kinetics of Foscan® disaggregation in lipoproteins solutions. Foscan® (3×10^{-6} M) was incubated in PBS containing lipoprotein in the concentrations (by protein) of 0.1 mg/mL (trace a), 0.3 mg/mL (trace b), 1 mg/mL (trace c) and 3 mg/mL (trace d) during 24 h at 25 °C. Foscan® fluorescence intensities were measured continuously at the wavelength of emission λ_{em}=655 nm (λ_{ex}=420 nm). At the end of incubation period Triton X-100 (0.2% v/v) was added to each sample. The ratio between Foscan® fluorescence intensity before (I) and after addition of Triton (I_T) represents the monomeric fraction of Foscan® and is displayed at the Y-axis.
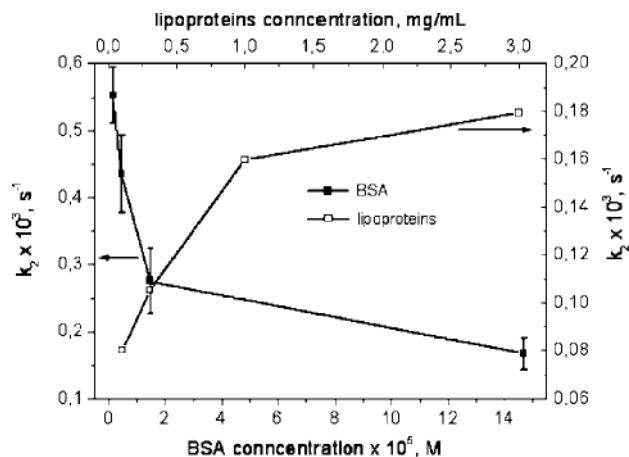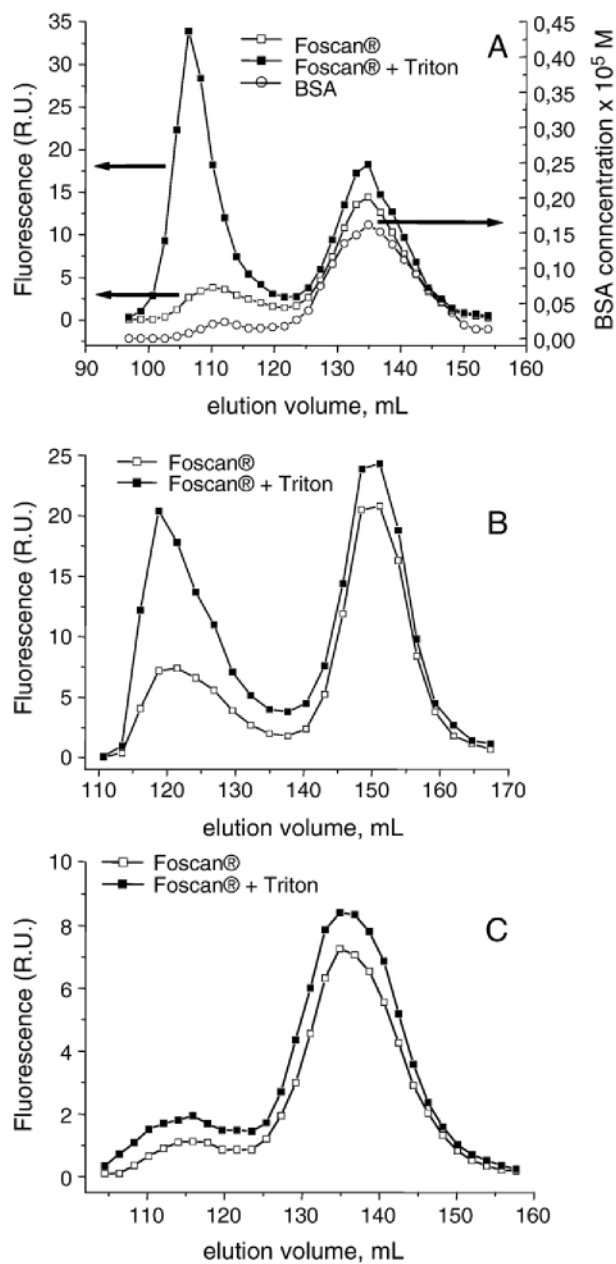
Fig. 6. Gel chromatography elution profiles of Foscan® with BSA solution. Foscan® (5×10^{-6}) was incubated with BSA (1.47×10^{-4} M) 1 h(A) or 24 h (B) at 37 °C. (C) Foscan® (10^{-6} M) was incubated with BSA (1.47×10^{-4} M) 1 h at 37 °C. After incubation, all samples were eluted through the 2.5×50 cm Sephadex G-100 gel column with the subsequent measurements of Foscan® fluorescence (λ_{em}=655 nm, λ_{ex}=420 nm) in every eluted fraction of 2 mL without (in A–C) and after addition of Triton X-100 (in A–C). Protein content was measured in every fraction (in A) using BIO-RAD DC protein assay.

aggregation are more strongly pronounced for the latter medium (Fig. 1A). The presence of Foscan® aggregated species in protein enriched aqueous solutions was proposed by other authors [25,22]. RLS studies further confirmed the different aggregation state of the sensitizer in various media. Foscan® RLS peak in PBS solution containing BSA is about half of the intensity of that in PBS only. Disappearance of RLS peak (Fig. 1B) together with considerable

increase in sensitizer fluorescence upon addition of Triton X-100 clearly indicate sensitizer monomerization.

It is established that the presence of proteins results in monomerization of chlorin-type compounds [28]. During the process of interactions between Foscan® and BSA, the sensitizer molecules in aggregated form bind to proteins and become monomeric. This process is accompanied by an increase in fluorescence quantum yield. At low BSA concentration, the fluorescence intensities at the equilibrium are considerably lower than at higher concentrations therefore indicating a higher degree of aggregation (Fig. 2). The shift of equilibrium between sensitizer aggregates and albumin-bound monomers could be explained by stronger interactions of sensitizer molecules in large aggregates and low albumin binding capacity [25,29]. Indeed, despite that albumin is the most abundant protein in circulation, the number of binding sites it has for tetrapyrrolic drugs is limited [6,29]. The dependencies of disaggregation on protein content were further subjected to kinetic analysis.

The kinetics of Foscan® disaggregation in BSA solutions were fitted by bi-exponential equation. The first rapid phase of Foscan® disaggregation kinetics in BSA solution ($k_1 = (2.3\pm0.15) \times 10^{-3}$ s^{-1}) is relatively constant at all BSA concentrations, whereas the second slower phase is dependent on the substrate concentration (Fig. 5). Consistent with the study of Kuzelova and co-workers [30], where the authors obtained the rate constants of heme dissociation in protein solutions of $(3–4) \times 10^{-3}$ s^{-1} and $(0.17–0.49) \times 10^{-3}$ s^{-1} for dimers and larger aggregates, respectively, we postulate that the first rapid phase of Foscan® disaggregation kinetics in BSA solution ($k_1 = 2.2 \times 10^{-3}$ s^{-1}) is due to the dissociation of sensitizer dimers, where the second slower phase is determined by sensitizer release from bigger aggregates ($k_2 = (0.17–0.55) \times 10^{-3}$ s^{-1}). With increasing BSA concentrations,
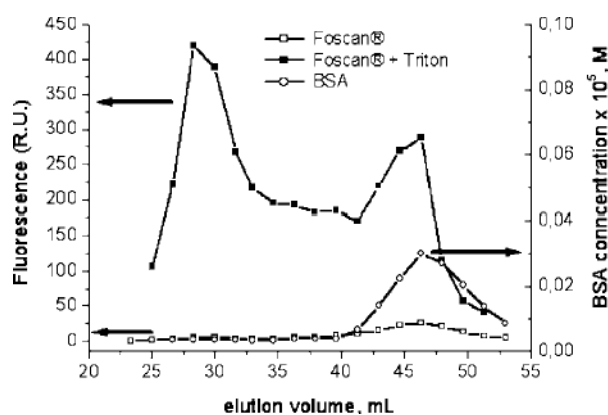
Fig. 7. Gel chromatography elution profiles of Foscan® with monomeric BSA solution. Foscan® (5×10^{-6}) was incubated with monomeric BSA of 1.47×10^{-5} M 1 h at 37 °C. After incubation the samples were eluted through the 2.5×50 cm Sephadex G-200 gel column with the subsequent measurements of Foscan® fluorescence (λ_{em}=655 nm, λ_{ex}=420 nm) in every eluted fraction of 2 mL without and after addition of Triton X-100. Protein content was measured in every fraction (o) using BIO-RAD DC protein assay.

the initial formation of aggregates with lower number of sensitizer molecules increases. Thus the decrease in k_2 values with increasing BSA concentrations (Fig. 5) could be explained by the increase in the amount of small aggregates involved in disaggregation and a decrease in larger aggregates fraction.

With temperature rise from 15 °C to 37 °C in Foscan® BSA solution, the time required to reach an equilibrium, considerably decreases (Fig. 3). Kinetic analysis demonstrated that both values k_1 and k_2 increase with increasing incubation temperature. The rate constant k_1 increases from 1.8×10^{-3} s^{-1} to 15.5×10^{-3} s^{-1} with a temperature rise from 15 °C to 37 °C. The k_2 underwent even greater increase from 0.07×10^{-3} s^{-1} to 1.0×10^{-3} s^{-1} for the same temperatures interval. Such changes could be attributed to an increased diffusion mobility of sensitizer aggregates and BSA molecules and/or to a weakening of the interactions between sensitizer molecules within the aggregate.

Foscan® has higher affinity for lipoproteins than for albumin [18–20]. Increasing the lipoproteins concentration by a factor 30 induces the increase of the k_2 value only about 2 times (Fig. 5). The poor dependency of Foscan® disaggregation kinetics on lipoproteins concentration (Fig. 3) can be explained by their much higher binding capacity compared to BSA [29]. It has been suggested that the process of interaction of porphyrins with lipoprotein solutions could be better viewed as a solubilization of sensitizer in lipoproteins lipid phase [31]. The lower values of Foscan® dissociation rate constants in lipoproteins as compared to those in BSA solutions could be explained by the full monomerization of all aggregated species.

Substances with higher molecular mass have smaller elution volume in gel-filtration chromatography and, thus, it can be assumed that the first peak in the chromatogram of Foscan® BSA solutions (Fig. 6A) represents oligomeric fraction of BSA together with the Foscan® aggregates while the second peak consists of monomeric Foscan® bound to monomeric BSA. Gel filtration of BSA solution containing Foscan® after 24 h incubation at 37 °C shows that the Foscan® content in the first peak decreases (Fig. 6B). We can conclude that after 24 h incubation some part of the sensitizer becomes monomeric and thus redistributes from the first (Foscan® aggregates with aggregated BSA) to the second (monomeric BSA) chromatographic fraction. This is in accordance with the results on disaggregation kinetics of Foscan® in BSA solutions (Fig. 2). Using smaller sensitizer concentration, we obtained a considerable decrease of Foscan® content in the first peak with a concomitant increase in the second (Fig. 6C). These data confirm the previous observations that sensitizer concentration has great influence on monomers-aggregates equilibrium and kinetic characteristics of Foscan® in protein solutions [25].

To study aggregated Foscan® in the first more rapid peak (Fig. 6A) the sensitizer was incubated with a monomeric BSA solution for 1 h at 37 °C before being subjected to gel-

chromatography. Fluorescence measurements in the elution samples after Foscan® chromatography with monomeric BSA revealed the presence of strongly aggregated not bound to protein sensitizer in the first peak (Fig. 7). Thus, our data suggest that only a minor fraction of Foscan® elutes through the column bound to BSA molecules (V_e=135 mL) (Fig. 6A) and as such monomerized, whilst the majority of the drug, being strongly aggregated, elutes in the first broad peak (V_e =106 mL).

From our experiments, we can reasonably assume that non-fluorescent product, which has been observed in several studies shortly after Foscan® injection in the plasma [18,21] consists of Foscan® aggregates that are not bound to albumin or other plasma components. Importantly, the factors that favor monomerization such as sensitizer, ethanol and protein content, temperature and incubation time would substantially reduce the intensity of first peak. As a matter of fact, an establishment of the exact profile of Foscan® repartition among plasma proteins deduced from the in vitro studies is not obvious and large discrepancies between different investigation groups may be noted. These differences arise from the use of different experimental conditions, including lipoprotein purity as well as their origin (bovine or human). For several other tested photosensitizers, a fluorescence steady-state was reached almost immediately after mixing with plasma [21].

The sensitizers binding to plasma proteins could have great influence on their transport, distribution and PDT efficacy [9,11,32]. Foscan® displays an unusual pharmacokinetic behaviour in human and rabbit plasma with a secondary peak at about 10 and 6 h after in intravenous injection, respectively [33,34]. Our study did not fully mimic the clinical situation since the major component of lipoproteins in man is LDL, and not HDL as is the case in bovine plasma. Nevertheless, according to our results Foscan® may form large-scale aggregates and precipitates just after injection, which may be retained in the vasculature leading to the exponential decrease of sensitizer concentration in blood. Following aggregates interaction with plasma proteins Foscan® can monomerize and will thus be released into the bloodstream and provoke the appearance of a delayed secondary peak of sensitizer concentration in plasma.

5. Conclusion

There are several confirmations of Foscan® aggregates existence in protein solutions: low fluorescence yield, enhanced RLS signals with the peak near absorption maximum and chromatographic data. The process of Foscan® disaggregation in solutions of plasma components is concentration and temperature dependent. The main result of our study is that part of Foscan® after injection into the albumin solution exists in free, non-bound to protein aggregated form. This can imply that in clinically relevant

conditions, the sensitizer persists partially in aggregated form in circulation, and this fact should be considered in designing clinical and dosimetry protocols.

Acknowledgements

References

[1] B.W. Henderson, T.J. Dougherty, How does photodynamic therapy work? Photochem. Photobiol. 55 (1992) 145–157.

[2] R.W. Redmond, E.J. Land, T.G. Truscott, Aggregation effects on the photophysical properties of porphyrins in relation to mechanisms involved in photodynamic therapy, Adv. Exp. Med. Biol. 193 (1985) 293A–302A.

[3] C. Tanielian, C. Schweitzer, R. Mechin, C. Wolff, Quantum yield of singlet oxygen production by monomeric and aggregated forms of hematoporphyrin derivative, Free Radical Biol. Med. 30 (2001) 208–212.

[4] L. Ma, J. Moan, K. Berg, Evaluation of a new photosensitizer, meso-tetra-hydroxyphenyl-chlorin, for use in photodynamic therapy: a comparison of its photobiological properties with those of two other photosensitizers, Int. J. Cancer 57 (1994) 883–888.

[5] D.J. Ball, S.R. Wood, D.I. Vernon, J. Griffiths, T.M. Dubbelman, S.B. Brown, The characterisation of three substituted zinc phthalocyanines of differing charge for use in photodynamic therapy. A comparative study of their aggregation and photosensitising ability in relation to mTHPC and polyhaematoporphyrin, J. Photochem. Photobiol., B Biol. 45 (1998) 28–35.

[6] R.K. Chowdhary, I. Sharif, N. Chansarkar, D. Dolphin, L. Ratkay, S. Delaney, H. Meadows, Correlation of photosensitizer delivery to lipoproteins and efficacy in tumor and arthritis mouse models; comparison of lipid-based and Pluronic P123 formulations, J. Pharm. Pharm. Sci. 6 (2003) 198–204.

[7] G. Jori, E. Reddi, The role of lipoproteins in the delivery of tumour-targeting photosensitizers, Int. J. Biochem. 25 (1993) 1369–1375.

[8] T. Peters, All About Albumin, Academic Press, San Diego, 1995.

[9] D. Kessel, P. Thompson, K. Saatio, K.D. Nantwi, Tumor localization and photosensitization by sulfonated derivatives of tetraphenylporphine, Photochem. Photobiol. 45 (1987) 787–790.

[10] M. Korbelik, J. Hung, Cellular delivery and retention of Photofrin II: the effects of interaction with human plasma proteins, Photochem. Photobiol. 53 (1991) 501–510.

[11] M. Kongshaug, Distribution of tetrapyrrole photosensitizers among human plasma proteins, Int. J. Biochem. 24 (1992) 1239–1265.

[12] M.O. Obochi, R.W. Boyle, J.E. van Lier, Biological activities of phthalocyanines. XIII. The effects of human serum components on the in vitro uptake and photodynamic activity of zinc phthalocyanine, Photochem. Photobiol. 57 (1993) 634–640.

[13] T. Tsuchida, G. Zheng, R.K. Pandey, W.R. Potter, D.A. Bellnier, B.W. Henderson, H. Kato, T.J. Dougherty, Correlation between site II-specific human serum albumin (HSA) binding affinity and murine in vivo photosensitizing efficacy of some Photofrin components, Photochem. Photobiol. 66 (1997) 224–228.

[14] R. Bonnett, R.D. White, U.J. Winfield, M.C. Berenbaum, Hydro-porphyrins of the meso-tetra(hydroxyphenyl)porphyrin series as tumour photosensitizers, Biochem. J. 261 (1989) 277–280.

[15] T.J. Dougherty, C.J. Gomer, B.W. Henderson, G. Jori, D. Kessel, M. Korbelik, J. Moan, Q. Peng, Photodynamic therapy, J. Natl. Cancer Inst. 90 (1998) 889–905.

[16] M.P. Copper, I.B. Tan, H. Oppelaar, M.C. Ruevekamp, F.A. Stewart, Meta-tetra(hydroxyphenyl)chlorin photodynamic therapy in earlystage squamous cell carcinoma of the head and neck, Arch. Otolaryngol., Head. Neck. Surg. 129 (2003) 709–711.

[17] C. Hopper, A. Kubler, H. Lewis, I.B. Tan, G. Putnam, mTHPC-mediated photodynamic therapy for early oral squamous cell carcinoma, Int. J. Cancer 111 (2004) 138–146.

[18] H.J. Hopkinson, D.I. Vernon, S.B. Brown, Identification and partial characterization of an unusual distribution of the photosensitizer meta-tetrahydroxyphenyl chlorin (temoporfin) in human plasma, Photochem. Photobiol. 69 (1999) 482–488.

[19] D. Kessel, Transport and localisation of m-THPC in vitro, Int. J. Clin. Pract. 53 (1999) 263–267.

[20] A.T. Michael-Titus, R. Whelpton, Z. Yaqub, Binding of temoporfin to the lipoprotein fractions of human serum, Br. J. Clin. Pharmacol. 40 (1995) 594–597.

[21] D. Kessel, E. Sykes, Transport, localization, and phototoxicity of m-THPC, Proc. SPIE 3592 (1999) 37–42.

[22] I. Belitchenko, V. Melnikova, L. Bezdetnaya, H. Rezzoug, J.L. Merlin, A. Potapenko, F. Guillemin, Characterization of photodegradation of meta-tetra(hydroxyphenyl)chlorin (mTHPC) in solution: biological consequences in human tumor cells, Photochem. Photobiol. 67 (1998) 584–590.

[23] R.F. Pasternack, P.J. Collings, Resonance light scattering: a new technique for studying chromophore aggregation, Science 269 (1995) 935–939.

[24] P.J. Collings, E.J. Gibbs, T.E. Starr, O. Vafek, C. Yee, L.A. Pomerance, R.F. Pasternack, Resonance light scattering and its application in determining the size, shape, and aggregation number for supramolecular assemblies of chromophores, J. Phys. Chem., B 103 (1999) 8474–8481.

[25] R. Bonnett, B.D. Djelal, N. Angelina, Physical and chemical studies related to the development of m-THPC (FOSCAN®) for the photodynamic therapy (PDT) of tumours, J. Porphyrins Phthalocyanines 5 (2001) 652–661.

[26] R. Bonnett, P. Charlesworth, B.D. Djelal, S. Foley, D.J. McGarvey, T.G. Truscott, Photophysical properties of 5,10,15,20-tetrakis(m-hydroxyphenyl)porphyrin (m-THPP), 5,10,15,20-tetrakis(m-hydroxyphenyl)chlorin (m-THPC) and 5,10,15,20-tetrakis(m-hydroxyphenyl)bacteriochlorin (m-THPBC): a comparative study, J. Chem. Soc., Perkin Trans. 22 (1999) 325–328.

[27] D.M. Fiedler, F. Wierrani, G. Schnitzhofer, J.C. Stewart, K. Gharehbaghi, W. Grunberger, B. Krammer, Does the in-vitro efficiency of meso-tetrahydroxy-phenyl-chlorin depend on pre-treatment of sensitizer?, J. Photochem. Photobiol., B Biol. 38 (1997) 241–244.

[28] B.M. Aveline, T. Hasan, R.W. Redmond, The effects of aggregation, protein binding and cellular incorporation on the photophysical properties of benzoporphyrin derivative monoacid ring A(BPDMA), J. Photochem. Photobiol., B Biol. 30 (1995) 161–169.

[29] V. Rosenberger, R. Margalit, Thermodynamics of the binding of hematoporphyrin ester, a hematoporphyrin derivative-like photosensitizer, and its components to human serum albumin, human highdensity lipoprotein and human low-density lipoprotein, Photochem. Photobiol. 58 (1993) 627–630.

[30] K. Kuzelova, M. Mrhalova, Z. Hrkal, Kinetics of heme interaction with heme-binding proteins: the effect of heme aggregation state, Biochim. Biophys. Acta 1336 (1997) 497–501.

[31] S. Bonneau, C. Vever-Bizet, P. Morliere, J.C. Maziere, D. Brault, Equilibrium and kinetic studies of the interactions of a porphyrin with low-density lipoproteins, Biophys. J. 83 (2002) 3470–3481.

[32] M. Kongshaug, J. Moan, S.B. Brown, The distribution of porphyrins with different tumour localising ability among human plasma proteins, Br. J. Cancer 59 (1989) 184–188.

[33] A.M. Ronn, J. Batti, C.J. Lee, D. Yoo, M.E. Siegel, M. Nouri, L.A. Lofgren, B.M. Steinberg, Comparative biodistribution of meta-Tetra(Hydroxyphenyl) chlorin in multiple species: clinical implications for photodynamic therapy, Lasers Surg. Med. 20 (1997) 437–442.

[34] T. Glanzmann, C. Hadjur, M. Zellweger, P. Grosiean, M. Forrer, J.P. Ballini, P. Monnier, H. van den Bergh, C.K. Lim, G. Wagnieres, Pharmacokinetics of tetra(m-hydroxyphenyl)chlorin in human plasma and individualized light dosimetry in photodynamic therapy, Photochem. Photobiol. 67 (1998) 596–602.

IV.3. Redistribution of Foscan® from plasma proteins to model membranes

Present study investigates the kinetics of Foscan® release from plasma proteins to model membranes using fluorescence resonance energy transfer (FRET) from label, covalently bound to protein, to sensitizer. We have demonstrated very slow kinetics of Foscan® release from protein complexes with rate constants of $(1.7 \pm 0.1) \times 10^{-3}$ s^{-1} for albumin and $(1.6 \pm 0.3) \times 10^{-4}$ s^{-1} for high-density lipoproteins (HDL). Foscan® redistributes by both collision and diffusion-mediated transfer from complexes with HDL, with bimolecular rate constant $k_{out} = (8.8 \pm 1.4) \times 10^{-2}$ M^{-1}s^{-1}. Thermodynamic considerations proposed that sensitizer release from HDL into the aqueous medium is unfavourable and collision mechanism appeared to be a preferred mode of transfer in biological environment. Slow rates of Foscan® redistribution from plasma proteins should be considered while planning dosimetry protocol of Foscan®-PDT.

This part of the work was published in the *Photochemical and Photobiological Sciences* and is presented thereafter in its corrected proofs form.

Redistribution of Foscan® from plasma proteins to model membranes

Siarhei Sasnouski [a,b], Dzmitry Kachatkou [b], Vladimir Zorin [b], François Guillemin [a] and Lina Bezdetnaya [a*]

Photodynamic therapy (PDT) is a comparatively novel modality of superficial tumours treatment that includes simultaneous action of photosensitizers, light and oxygen. Photosensitizer redistribution between plasma proteins and biomembranes define photosensitizers interaction with cells, their intracellular localization and kinetics of sensitizers accumulation in the tumour. Present study investigates the
10 kinetics of Foscan® release from plasma proteins to model membranes using fluorescence resonance energy transfer (FRET) from label, covalently bound to protein, to sensitizer. We have demonstrated very slow kinetics of Foscan® release from protein complexes with rate constants of $(1.7 \pm 0.1) \times 10^{-3}$ s^{-1} for albumin and $(1.6 \pm 0.3) \times 10^{-4}$ s^{-1} for high-density lipoproteins (HDL). Foscan® redistributes by both collision and diffusion-mediated transfer from complexes with HDL, with bimolecular rate constant $k_{out} = (8.8 \pm 1.4) \times 10^{-2}$ M^{-1}s^{-1}. Thermodynamic considerations proposed that sensitizer release from HDL into the aqueous medium is unfavourable and collision
15 mechanism appeared to be a preferred mode of transfer in biological environment. Slow rates of Foscan® redistribution from plasma proteins should be considered while planning dosimetry protocol of Foscan®-PDT.

1. Introduction

Photodynamic therapy (PDT) uses the combination of a
20 photosensitizing drug and light to cause damage to pathological proliferating tissues, including tumours. Photosensitizer (PS) activation by visible light results primarily in singlet-oxygen mediated photodamage [1, 2]. Binding of photosensitizers to serum proteins followed by its delivery into sensitive subcellular sites
25 seems essential for effective PDT, since direct injection of photosensitizers into the lesion has been unsuccessful [3]. Equilibrium binding characteristics of photosensitizers to plasma proteins together with dynamic parameters of redistribution between plasma proteins and biomembranes define
30 photosensitizers interaction with cells, their intracellular localization and kinetics of sensitizers accumulation in the tumour [4-6].

The redistribution of PS can be carried out either by the collisions between carrier proteins or via monomeric diffusion
35 through the medium. Porphyrin-like sensitizers and some phthalocyanines have been shown to redistribute from the complexes with plasma proteins and artificial biomembranes through the aqueous phase with typical release times from several to tens of seconds [4, 7].

40 Foscan® or meta-tetra(hydroxyphenyl)chlorin (mTHPC) is a second-generation photosensitizer [8] and is one of the most effective sensitizers studied to date [1]. It mediates cell photodamage principally through singlet oxygen formation [9] and its tumoricidal effect appears to be very sensitive to oxygenation
45 conditions [10, 11]. Foscan® has been granted European approval for palliative treatment of patients with advanced head and neck cancers. Recent clinical open-label multicenter studies also reported the efficacy of Foscan®-PDT in the treatment of early

[a] Centre Alexis Vautrin , CRAN UMR 7039 CNRS - INPL –UHP, Avenue de Bourgogne, 54511 Vandœuvre-Les-Nancy cedex, France

[b] Laboratory of Biophysics and Biotechnology, Physics Faculty, Belorussian State University, Nezalegnasti 4 st., Minsk, 220080 Belarus

* Corresponding author. Centre Alexis Vautrin , CRAN UMR 7039 CNRS - INPL –UHP, Avenue de Bourgogne, 54511 Vandœuvre-Les-Nancy cedex, France
Tel +33 3 83 59 83 06, fax +33 3 83 44 60 71
E-mail address: l.bolotine@nancy.fnclcc.fr

squamous cell carcinoma [12, 13].

50 Plasma distribution of Foscan® in vitro demonstrated that in equilibrium, the major part of photosensitizer (up to 73 %) associates with high density lipoproteins, whereas about 20 % of Foscan® form non-fluorescent complex with an unidentified protein fraction [14, 15]. Recently we have demonstrated that this
55 non-fluorescent complex consists of free, non-bound to proteins, Foscan® aggregates, which further disaggregate upon binding to albumin and lipoproteins [16]. Disaggregation kinetics were faster on lipoproteins compared to albumin [16].

The present study examines the mechanism of Foscan®
60 redistribution from the complexes with plasma proteins to model membranes. Given the major role of HDL in Foscan® transport [14, 15], this study focuses on the redistribution kinetics of this photosensitizer from the complexes with HDL. The dynamic of Foscan® redistribution was assessed with a fluorescent method,
65 based on the fluorescence resonance energy transfer (FRET). The work revealed very slow kinetics of Foscan® release from protein complexes compared to other photosensitizers. We further demonstrated the occurrence of both collision and diffusion-mediated transfer of Foscan® from complexes with HDL,
70 however the collision mechanism appeared to be a preferred mode of transfer in biological environment.

2. Materials and methods

2.1. Chemicals

The photosensitizer Foscan® (mTHPC, temoporfin) was kindly
75 provided by Biolitec AG (Jena, Germany). Stock solution was made by dissolving the powder in 100 % ethanol. Phosphate buffered saline (PBS, without CaCl$_2$ and MgCl$_2$; pH 7.4) was obtained from Invitrogen. HDL, lipoproteins from human plasma (total fraction), bovine serum albumin (BSA),
80 ethylenediaminetetraacetic acid (EDTA), hydroxylamine hydrochloride, gel Sephadex G-100, sodium azide (NaN$_3$), t-Octylphenoxypolyethoxyethanol (Triton® X-100) were purchased from Sigma.

According to the manufacturer (Sigma), lipoproteins' purity was
85 confirmed by both immunoelectrophoresis and agarose electrophoresis. HDL fraction was of 95 % purity. Stock solutions of liporoteins were kept at 4°C with 0.01 % (m/m) EDTA to exclude oxidative processes. Lipoproteins, HDL and BSA were dissolved in PBS to appropriate concentrations
90 immediately before measurements.

Fluorescent label Alexa fluor 350 carboxylic acid, succinimidyl ester (2H-1-Benzopyran-6-sulfonic acid, 7-amino-3-[2-[(2,5-dioxo-1-pyrrolidinyl)oxy]-2-oxoethyl]-4-methyl-2-oxo-) was obtained from Invitrogen (USA). Chemical structure is provided in the "Handbook of fluorescent probes", Invitrogen (http://probes.invitrogen.com). BIO-RAD DC Protein Assay was purchased from BIO-RAD Laboratories (USA). Egg lecithin (10 % ethanol solution) was purchased from Biolik (Kharkov, Ukraine). The purity was 95 %.

2.2. Covalent binding of label to plasma proteins

Covalent binding of Alexa fluor 350 (Molecular probes, USA) to plasma proteins was done according to the manufacturer recommendations for covalent binding of amine-reactive probes to proteins (Molecular Probes, USA). Succinimidyl esters produce stable carboxamide bonds with proteins.

Briefly, 10 mg of protein were dissolved in 1 ml of 0.1 M sodium bicarbonate buffer (pH 8.3) and 50 µl of Alexa fluor 350 in DMSO solution (10 mg/ml) was added. The solution was incubated for 1 hour at room temperature under continuous stirring. The reaction was stopped by adding 0.1 ml of freshly prepared 1.5 M hydroxylamine solution (pH 8.5). After binding, the labelled proteins were separated from free label by passing the solution through the column with a gel Sephadex G-100. The resulting sample was kept at 4 °C with 2×10^{-3} M sodium azide and 0.01 % (m/m) EDTA to prevent protein oxidation. The degree of labelling (label concentration/protein concentration) was determined by spectrophotometric analysis using Alexa fluor 350 extinction coefficient at 350 nm (ε_{350}) of 19.000 $M^{-1}cm^{-1}$, whereas protein concentration was defined with BIO-RAD DC Protein Assay. For HDL the average molecular mass of 260.000 Da and the percentage of protein in HDL equal to 50 % (m/m) were used. The degree of HDL labelling computed in such way was 4.2. For BSA the average molecular mass of 70.000 Da was used. The degree of BSA labelling computed in such way was 1.5.

This low degree of labelling along with the huge difference in molecular weights of lipoproteins compared to Alexa Fluor 350 (260 kDa and 70 kDa *versus* 410 Da) are, in all probability, insufficient to change the properties of the proteins, thereby affecting their kinetic parameters.

2.3. Spectroscopic measurements

Absorption spectra were recorded on a Perkin-Elmer Lambda Bio 9 spectrophotometer, using a 10 mm quartz cuvette. Steady-state emission spectra were carried out using a 10 mm path length quartz cuvette in a computer-controlled Perkin-Elmer LS50B luminescence spectrometer. Except for the lipoproteins, kinetics of Foscan® redistribution were performed by the continuous monitoring of the fluorescence of Alexa fluor 350 at a fixed wavelength of emission (λex = 350 nm, λ em = 450 nm, bandpasses for excitation and emission slits were 5 nm and 10 nm, respectively). Kinetics of Foscan® redistribution from lipoproteins were measured at fixed time points under the similar experimental conditions. Foscan® fluorescence was monitored at the emission wavelength of 655 nm (λex = 420 nm). Data were collected with a 1 s interval during 4 h. At each time point, the signal was integrated for 1 s.

2.4. Vesicle preparation.

Lipid vesicles were prepared using the injection method [17]. Briefly, 350 µl of egg lecithin ethanol solution (30 mM) was added into 5 ml of PBS at a rate of 1 µl/s. The suspension of vesicles was held at 4 °C for several weeks. The size of lyposomes was measured using Photon Correlation Spectroscopy technique using a Zetasizer 3000 HSA (Malvern, UK). Using monomodal analysis the average hydrodynamic diameter of liposomes was computed as D_H = 116 nm. This value was used in further kinetic calculations.

2.5. Release of Foscan® from plasma proteins to lipid vesicles.

Kinetics of Foscan® redistribution from the donor complexes with BSA, HDL or total lipoprotein fraction to acceptor lipid vesicles was assessed using FRET from the label Alexa fluor 350, covalently linked with the studied protein, to photosensitizer. The energy transfer from the donor complex Alexa-protein to photosensitizer is possible as evidenced by the significant overlap between Foscan® absorption and Alexa fluorescence spectra (Fig. 1).

Ten µl of Foscan® ethanol solution (initial concentration 3×10^{-5} M) was added to 1 ml PBS containing Alexa-labelled proteins (BSA, HDL or total lipoprotein fraction) and was incubated 1 hour at 37 °C. The respective concentrations of BSA, HDL and lipoproteins bound to Alexa were 1.3×10^{-7} M, 4.3×10^{-7} M and 10^{-2} mg/ml (by protein). Upon binding to protein-Alexa complexes, Foscan® quenches the label fluorescence. Afterwards, one ml of PBS with different concentrations of lecithin vesicles was added to these solutions and the kinetics of increase of label fluorescence intensity were recorded during photosensitizer release from the protein-Alexa complexes to the vesicles. The ethanol content in the final sample was less than 0.5 %. Experiments were conducted under continuous stirring. To verify whether label fluorescence was quenched only by Foscan®, a full dissociation of photosensitizer from the complexes with HDL was achieved at the end of experiment by adding neutral detergent Triton X-100 to each sample (0.2 % v/v). The temperature was kept constant with a water thermostat and was controlled using Testo 110 thermometer (Radiospares, Germany).

2.6. Thermodynamic parameters of Foscan® transfer from HDL to lipid vesicles

In the study of the influence of temperature on kinetics of Foscan® redistribution, the activation energy (E_a) of the process was calculated from the slope of an Arrhenius plot of the data. For determination of thermodynamic parameters, the Eyring rate theory was used [18, 19]. Enthalpy (ΔH) of Foscan® transfer from HDL-Alexa was determined from the equation $\Delta H = E_a - RT$, where R is the gas constant, T is the temperature. Free energy of transfer (ΔG) and entropy (ΔS) were calculated as $\Delta G = \Delta H - T\Delta S$ and $\Delta S = 2.3R \log(NhX/RT)$, where N - Avogadro's number, h – Planck's constant, X = k/exp($-\Delta H/RT$), k – redistribution rate constant of Foscan® transfer from HDL-Alexa to lecithin vesicles at 25 °C (see equation 6 below).

2.7. Theory approach in determination of redistribution rate constants

In the collision mechanism, photosensitizer release can be described in a simple reaction scheme:

$$P_{PS} + L \underset{k_{in}}{\overset{k_{out}}{\rightleftharpoons}} L_{PS} + P \qquad (1)$$

where P_{PS} and L_{PS} stand for the concentrations of the complexes protein-photosensitizer and liposome-photosensitizer respectively. P and L represent the concentrations of free protein and lecithin vesicles respectively. The constants k_{in} and k_{out} stand for molecular rate constants of Foscan® redistribution from the complexes with proteins to lecithin vesicles and contrariwise.

The rate of change of P_{PS} concentration in the above scheme is given by:

$$\frac{d[P_{PS}]}{dt} = k_{in}[L_{PS}][P] - k_{out}[P_{PS}][L] \qquad (2)$$

L_{PS} was defined as:

$$[L_{PS}] = [P_{PS,0}] - [P_{PS}] \qquad (3)$$

where $P_{PS,0}$ stands for the concentration of the complex protein-photosensitizer at time t = 0. The concentrations of protein and lecithin vesicles remain constant during the experiment, so that k_{in} and k_{out} become pseudo-first order constants. For this system, the change of the concentration of protein-photosensitizer complex as a function of incubation time is expressed as:

$$[P_{PS}](t) = \frac{k_{in}[P_{PS,0}][P]}{k} + C_0 \exp(-kt) \qquad (4)$$

with k defined as:

$$k = k_{in}[P] + k_{out}[L] \qquad (5)$$

where C_0 – constant, k is an experimentally measured apparent rate constant obtained by fitting of variations of label fluorescence intensity with time using modified Levenberg-Marquardt non-linear fitting in Origin 7.5 program according to the equation:

$$F(t) = A + B(1-\exp(-kt)) \qquad (6)$$

where F(t) – Alexa fluor 350 fluorescence intensity, t – time, A and B – constants; k stands for the apparent redistribution rate constant.

Considering that P << L and that k_{in} and k_{out} are comparable values, the first component of equation (5) can be neglected. Then:

$$k = k_{out}[L] \qquad (7)$$

As follows from Eq. (7), the value of k depends linearly on vesicles concentration. This dependence, subjected to linear fitting, gives the molecular rate constant k_{out} of the photosensitizer transfer.

3. Results

3.1. Spectroscopic properties of HDL-Alexa complexes

Kinetics of Foscan® redistribution from the complexes with HDL to lipid vesicles was assessed using FRET between the label and sensitizer. The administration of Foscan® in PBS containing HDL-Alexa results in the decrease of label fluorescence intensity in the course of photosensitizer binding to lipoprotein particles (Fig. 2, curve 1). This quenching was accompanied by an increase in Foscan® fluorescence (Fig. 2, curve 2), likely indicating photosensitizer monomerisation. The increase in photosensitizers fluorescence quantum yields upon addition to proteins has been reported earlier in several studies including ours [16, 20, 21]. Based on this observation we speculate that predominantly monomer forms of photosensitizer quench the fluorescence of Alexa. It is worth to note that the quenching of label fluorescence was not due to the screening effect as the value of optical density of the sample did not exceed 0.05. Moreover, addition of Triton X-100 to the final solution at the end of incubation period resulted in the full restoration of initial level of Alexa fluorescence (data not shown).

Increase in photosensitizer concentration leads to progressive quenching of label fluorescence in HDL-Alexa complexes (Fig. 2 B). This quenching depends considerably on the conditions of incubation. Immediately after Foscan® administration about 30 % of Alexa fluorescence was quenched at the photosensitizer concentration of 10^{-6} M (curve 1), whereas after 3 hours incubation at 37°C the same degree of label fluorescence quenching was achieved at 10^{-8} M of sensitizer (curve 2). Hence, the incubation leads to an essential increase of the degree of quenching of label fluorescence, which reaches a plateau (80 %) at Foscan® concentration of 3×10^{-7} M. Together with the increase in Foscan® fluorescence during incubation (Fig. 2A), the observed greater quenching of label fluorescence in incubated Foscan®/HDL-Alexa solution is consistent with the differences in the photosensitizer aggregation state. Quenching of

label fluorescence upon addition of Foscan® to other plasma protein-Alexa complexes was similar (data not shown).

3.2. Kinetics of Foscan® redistribution from the complexes with plasma proteins to lecithin vesicles

Upon administration of biological substrate that can bind Foscan®, photosensitizer molecules will be subjected to redistribution. As a result, the efficiency of the label fluorescence quenching will decrease due to the uncoupling of donor (Alexa) and acceptor (Foscan®) molecules. Since in our conditions the label fluorescence intensity is inversely proportional to the quantity of Foscan® molecules bound to proteins, the increase in the fluorescence intensity of the label indicates the rate of Foscan® redistribution.

Upon addition of an excess of lecithin vesicles to BSA-Alexa solution, containing Foscan®, the sensitizer redistributes from BSA-Alexa to liposomes, and the label fluorescence intensity increases with time (Fig. 3, curve 1) reaching an equilibrium after 1h incubation. Compared to BSA, redistribution kinetics from HDL and total lipoprotein fraction were considerably slower (Fig. 3, curves 2, 3). Experimental plots displayed in Fig. 3 were fitted using mono-exponential function, from which the values of Foscan® redistribution apparent rate constants k were derived (Equation 6). The experimental results and theoretical plots for all proteins were in good agreement. Fig. 4 displays an example of this fitting for HDL-Alexa ($R^2 > 0.99$). The computed values of apparent constants k for BSA, HDL and lipoproteins were respectively $(1.69 \pm 0.09) \times 10^{-3}$ s^{-1}, $(1.60 \pm 0.30) \times 10^{-4}$ s^{-1} and 1.84×10^{-5} s^{-1}.

In the rest of our study we focused on HDL-Alexa complexes, considering the high affinity of Foscan® for this protein.

3.3. Influence of lecithin vesicles concentration on Foscan® redistribution from HDL-Alexa complexes

To discriminate between Foscan® transfer occurring by aqueous diffusion or during collisional interactions of the photosensitizer with acceptor membranes Foscan® redistribution from HDL complexes was examined as a function of increasing acceptor lipid membranes concentration. If the collision process is occurring, the transfer rate should increase with increasing concentration of acceptor molecules and should be independent of photosensitizer solubility in the medium. In opposition, if transfer is diffusion-mediated, the transfer rate should be independent of acceptor concentration.

The values of apparent redistribution rate constant k increase with increasing vesicles concentration (Fig. 5). Experimental values were best fitted by a linear function ($R^2 > 0.98$). As shown in Figure 5, the intercept of this curve with Y axe is above zero ($k_a = (6 \pm 2) \times 10^{-6}$ s^{-1}), pointing out to the transfer of Foscan® from HDL-Alexa in liposomes-free medium, supposedly by aqueous diffusion transfer. It is worth to note that the values of apparent rate constants did not depend on variations of HDL-Alexa concentration (data not shown), thus supporting unidirectionality of Foscan® transport from HDL-Alexa to liposomes.

3.4. Influence of temperature on Foscan® redistribution from the complexes with HDL-Alexa

The rate of Foscan® transfer from HDL-Alexa to lecithin vesicles is very sensitive to incubation temperature. The influence of temperature (15-37°C) on Foscan® apparent redistribution constant, presented in the form of an Arrhenius plot, is shown in Fig. 6. The thermodynamic parameters at 25°C were calculated as described in 2.6 and are presented in Table I. Both entropy and enthalpy processes contribute substantially to the free energy (ΔG) of activation for the transfer of Foscan® from HDL-Alexa complexes.

4. Discussion

345 Upon photosensitizer administration in the bloodstream it first encounters plasma proteins. Affinity of photosensitizers to plasma proteins thus plays an important role in drug distribution and photodynamic outcome [5, 6, 22, 23]. Since the release from the complexes with plasma proteins is an important step in the inter-
350 membrane transfer of lipophilic drugs, the assessment of release kinetics can be predictive for the adsorption parameters of the drugs [24]. Foscan® is a highly lipophilic photosensitizer, characterized by 1-Octanol–buffer partition coefficient ($C_{octanol}$ / C_{buffer}) of 3.3×10^5 at pH 7.0 [25]. We have previously demonstrated
355 different disaggregation kinetics of Foscan® in lipoproteins and albumin solutions with a lower value of Foscan® dissociation rate constant in lipoproteins [16]. The present study has been conceived in continuity with the previous one and addresses the kinetics and mechanisms of Foscan® redistribution from the
360 complexes with plasma proteins, with a particular interest for HDL being the major carriers of Foscan® in the blood [14]. Foscan® release was assessed by the fluorescent method based on the quenching of Alexa fluor 350 fluorescence by sensitizer.

All studied proteins were characterized by very slow
365 redistribution rates (Figures 3 and 4). Whereas about 600 s required for the release of Foscan® from BSA ($k = (1.69 \pm 0.09) \times 10^{-3}$ s^{-1}), one or two order of magnitude greater times were needed for the redistribution from HDL ($k = (1.60 \pm 0.30) \times 10^{-4}$ s^{-1}) and total lipoprotein fraction ($k = 1.84 \times 10^{-5}$ s^{-1}). Such
370 differences between proteins can be partially explained by much higher binding capacity of plasma lipoproteins compared to albumin [26]. Another factor that can influence the rates of Foscan® redistribution is its deep penetration into the lipid bilayer [4] of lipoproteins thus increasing transfer time [4]. Similar dependences
375 of redistribution of Foscan® from all studied proteins were observed at the incubation temperature of 37°C, except that all kinetic processes were accelerated (data not shown).

In the study of Kuzelova and co-workers the reported value of the rate constant of deuteroporphyrin release from
380 liposomes was 20 s^{-1}, thus four orders of magnitude higher than the rate of Foscan® release from HDL [27]. The rate of release of cis-di-sulfonated aluminium phthalocyanine from model membranes and LDL was around 5 s^{-1} and 1 s^{-1}, respectively [4]. The rate of Verteporfin transfer from lipid formulations was
385 determined to be about 2×10^{-2} s^{-1} (calculated from [28]). Also, the values of dissociation rate constants of hemin from the complexes with LDL, HDL and BSA at 37°C were reported to be 4.5×10^{-1} s^{-1}, 5.1×10^{-2} s^{-1} and 3.3×10^{-3} s^{-1} [29]. Low redistribution rates of Foscan® as compared to other sensitizers are consistent with
390 Foscan®'s unique binding properties. Ball et al. have reported that compared to Photofrin, Foscan® has a considerably greater ability to be sequestered in cells and remain tightly bound to them [30]. This tight binding to membrane structures could explain the fact that Foscan® has been shown to have a small initial
395 distribution volume *in vivo*, which was hypothesized to be the vascular compartment [31]. Upon administration in the bloodstream, Foscan® aggregates monomerize upon binding to different plasma proteins [16] and redistribute but remain tightly bound to lipoproteins and HDL. These large complexes prevent a
400 rapid diffusion through the vessel wall into the surrounding tissue, thus supporting the long retention of the photosensitizer in the vasculature [31]. Low rates of Foscan® redistribution from biomembranes could partially explain the unusual pharmacokinetics of this sensitizer in humans, which consist in
405 the second peak of the drug at 10 hours after its injection [32].

In the next step we studied the mechanism of Foscan® redisitribution from plasma proteins. A collision mechanism implies an increase in the value of apparent rate constant k with increasing concentrations of acceptor structures. In a diffusion
410 mechanism where the substance releases through an aqueous phase, the k value is independent of acceptor concentration, but the properties of the solvent considerably affect the redistribution process. The mobility of photosensitizer molecules undergoes significant changes and the entropy component contributes to the
415 change of the free energy of the system [27, 33-35].

In our study the apparent transfer constant k increases linearly with an increase in lecithin liposomes concentration, suggesting collisional Foscan® transfer (Fig. 5). The intercept of the linear curve with Y axis results in a non-zero value of
420 redistribution constant $k_a = (6 \pm 2) \times 10^{-6}$ s^{-1} at a zero value of vesicles concentration. Therefore k_a could be attributed to Foscan® transfer through aqueous phase. The contribution of k_a into k is important at low lecithin concentration (initial part of the curve in Fig. 5), but at higher vesicles concentrations its
425 contribution is negligible. Considering that in physiological conditions plasma lipid concentration is around 10 mg/ml, the collisional mechanism of Foscan® transfer is favoured over transfer through aqueous phase. Together with a slow release rates, the collision mode of Foscan® transfer from HDL and thus
430 the presence of large complexes containing the photosensitizer, lead to an increased probability of photosensitizer endocytosis into the cells and as such influence drug intracellular localization.

Using the Equation 7 we obtained the value of molecular rate constant $k_{out} = (8.8 \pm 1.4) \times 10^{-2}$ M^{-1}s^{-1}. The bimolecular
435 transfer constant k_{out} reflects the rate of collisions (effective association rate constant) between HDL and vesicles leading to transfer of sensitizer molecules. The limit value for a diffusion-controlled association between two species, HDL and vesicles, defined as k_{dif}, was determined using Smoluchowski equation [36,
440 37]:

$$k_{dif} = 4\pi(R_{HDL} + R_{LIP})(D_{HDL} + D_{LIP})N \qquad (8)$$

where R_{HDL} and R_{LIP} are HDL and liposomes radii, respectively, D_{HDL} and D_{LIP} are HDL and liposomes diffusion coefficients
445 derived from Stockes-Einstein equation, respectively; N – Avogadro's number. Assuming R_{HDL} and R_{LIP} of 10 nm and 58 nm, respectively, and diffusion coefficients D_{LIP} and D_{HDL} of 3.8×10^{-12} m^{2}s^{-1} and 22×10^{-12} m^{2}s^{-1}, the value of diffusion-controlled redistribution rate constant k_{dif} is 1.3×10^7 M^{-1}s^{-1}.

450 The value of k_{dif} is several orders of magnitude higher than experimental value of bimolecular transfer constant k_{out} (8.8×10^{-2} M^{-1}s^{-1}) indicating that the collisional efficiency of Foscan® transfer is very low. The possible explanation could be related to high Foscan® affinity to lipid bilayers due to hydrophobic
455 interactions with hydrocarbon core of the membrane. Rigid fixation of Foscan® in the hydrocarbon part of lipid bilayers was confirmed by the high value of its fluorescence polarization in lipoproteins (P = 25 %) along with a high fluorescence lifetime (10.2 ns) (V. Zorin, in preparation). Likewise, recent studies
460 reported deep location of this photosensitizer within lipid bilayer and its extremely low mobility in membrane structures [38, 39].

The changes of thermodynamic potentials are important characteristics of photosensitizer transfer providing addition information concerning the mechanism of redistribution. Both
465 enthalpy (ΔH = 10.7 kcal/mol) and entropy components (TΔS = -11.9 kcal/mol) contribute considerably to the free energy of activation (ΔG = 22.6 kcal/mol) (Table1) confirming the existence of a combined collision and diffusion mode of transport. Partial Foscan® release through aqueous phase is
470 supported by the transfer of this photosensitizer in the absence of lipid vesicles (Fig 5). The high value of the free energy of activation, which determines the energy required for Foscan®

dissociation from protein, is consistent with very low sensitizer redistribution rates. Generally, a substantial energetic barrier exists for membrane-bound lipophilic drugs to partition into the aqueous phase [24]. Considerable decrease of entropy points out that sensitizer release in aqueous medium is unfavourable. Indeed, the rate of non-polar compounds transfer through aqueous phase decreases exponentially with the solubility of the substances in the medium [40]. Therefore, low rate of Foscan® transfer through aqueous media could be related to its feeble hydrophilicity and solubility in the medium. Previous studies have reported that Foscan® forms large-scale aggregates in aqueous environment even at relatively low concentrations and exists predominantly as a mixture of free aggregates and protein-bound forms [16, 41].

5. Conclusion

We have addressed the kinetics and mechanism of Foscan® redistribution from the complexes with different plasma proteins. For this purpose we have developed the method of registration of transfer kinetics based on FRET. The results of the present study demonstrated that compared to other sensitizers Foscan® is characterized by a low rate of redistribution from all studied proteins. This could indicate that Foscan® is incorporated in the endothelial cells only after several hours after administration and as such should be taken into account when considering shortening the drug-light interval in pre-clinical trials, in order to enhance vascular PDT effects. Both collisional and aqueous phase mediated redistribution of Foscan® from HDL was postulated with a former mechanism as a major one. Based on the observance of tight complexes with HDL, the HDL-mediated endocytosis is proposed as a central mode of Foscan® transport in cells. Studies to explore the mechanism of Foscan® endocytosis and the subsequent intracellular targeting would be very useful.

Acknowledgments

References

1. T. J. Dougherty, C. J. Gomer, B. W. Henderson, G. Jori, D. Kessel, M. Korbelik, J. Moan and Q. Peng, Photodynamic therapy, *J. Natl. Cancer Inst.*, 1998, **90**, 889-905.
2. Q. Peng and J. M. Nesland, Effects of photodynamic therapy on tumor stroma, *Ultrastruct. Pathol.*, 2004, **28**, 333-340.
3. S. Brown, Brown EA and W. I., The present and future role of photodynamic therapy in cancer treatment., *Lancet Oncol.*, 2004, **5**, 497-508.
4. S. Bonneau, P. Morliere and D. Brault, Dynamics of interactions of photosensitizers with lipoproteins and membrane-models: correlation with cellular incorporation and subcellular distribution, *Biochem. Pharmacol.*, 2004, **68**, 1443-1452.
5. M. Korbelik and J. Hung, Cellular delivery and retention of Photofrin II: the effects of interaction with human plasma proteins, *Photochem. Photobiol.*, 1991, **53**, 501-510.
6. M. O. Obochi, R. W. Boyle and J. E. van Lier, Biological activities of phthalocyanines. XIII. The effects of human serum components on the in vitro uptake and photodynamic activity of zinc phthalocyanine, *Photochem. Photobiol.*, 1993, **57**, 634-640.
7. N. Maman, S. Dhami, D. Phillips and D. Brault, Kinetic and equilibrium studies of incorporation of di-sulfonated aluminum phthalocyanine into unilamellar vesicles, *Biochim. Biophys. Acta*, 1999, **1420**, 168-178.
8. R. Bonnett, R. D. White, U. J. Winfield and M. C. Berenbaum, Hydroporphyrins of the meso-tetra(hydroxyphenyl)porphyrin series as tumour photosensitizers, *Biochem. J.*, 1989, **261**, 277-280.
9. V. O. Melnikova, L. N. Bezdetnaya, A. Y. Potapenko and F. Guillemin, Photodynamic properties of meta-tetra(hydroxyphenyl)chlorin in human tumor cells, *Radiat. Res.*, 1999, **152**, 428-435.
10. S. Coutier, L. N. Bezdetnaya, T. H. Foster, R. M. Parache and F. Guillemin, Effect of irradiation fluence rate on the efficacy of photodynamic therapy and tumor oxygenation in meta-tetra (hydroxyphenyl) chlorin (mTHPC)-sensitized HT29 xenografts in nude mice, *Radiat. Res.*, 2002, **158**, 339-345.
11. S. Coutier, S. Mitra, L. N. Bezdetnaya, R. M. Parache, I. Georgakoudi, T. H. Foster and F. Guillemin, Effects of fluence rate on cell survival and photobleaching in meta-tetra-(hydroxyphenyl)chlorin-photosensitized Colo 26 multicell tumor spheroids, *Photochem. Photobiol.*, 2001, **73**, 297-303.
12. M. P. Copper, I. B. Tan, H. Oppelaar, M. C. Ruevekamp and F. A. Stewart, Meta-tetra(hydroxyphenyl)chlorin photodynamic therapy in early-stage squamous cell carcinoma of the head and neck, *Arch. Otolaryngol. Head Neck Surg.*, 2003, **129**, 709-711.
13. C. Hopper, A. Kubler, H. Lewis, I. B. Tan and G. Putnam, mTHPC-mediated photodynamic therapy for early oral squamous cell carcinoma, *Int. J. Cancer*, 2004, **111**, 138-146.
14. H. J. Hopkinson, D. I. Vernon and S. B. Brown, Identification and partial characterization of an unusual distribution of the photosensitizer meta-tetrahydroxyphenyl chlorin (temoporfin) in human plasma, *Photochem. Photobiol.*, 1999, **69**, 482-488.
15. D. Kessel, Transport and localisation of m-THPC in vitro, *Int. J. Clin. Pract.*, 1999, **53**, 263-267.
16. S. Sasnouski, V. Zorin, I. Khludeyev, M. A. D'Hallewin, F. Guillemin and L. Bezdetnaya, Investigation of Foscan interactions with plasma proteins, *Biochim. Biophys. Acta*, 2005, **1725**, 394-402.
17. J. M. Kremer, M. W. Esker, C. Pathmamanoharan and P. H. Wiersema, Vesicles of variable diameter prepared by a modified injection method, *Biochemistry*, 1977, **16**, 3932-3935.
18. H. Eyring, The activated complex in chemical reactions, *J. Chem. Phys.*, 1935, **3**, 107-115.
19. S. Glasstone and H. E. K.J. Laidler, The Theory of Rate Processes, *McGraw-Hill, New York*, 1941.
20. L. Ma, J. Moan and K. Berg, Evaluation of a new photosensitizer, meso-tetra-hydroxyphenyl-chlorin, for use in photodynamic therapy: a comparison of its photobiological properties with those of two other photosensitizers, *Int. J. Cancer*, 1994, **57**, 883-888.
21. I. Belitchenko, V. Melnikova, L. Bezdetnaya, H. Rezzoug, J. L. Merlin, A. Potapenko and F. Guillemin, Characterization of photodegradation of meta-tetra(hydroxyphenyl)chlorin (mTHPC) in solution: biological consequences in human tumor cells, *Photochem. Photobiol.*, 1998, **67**, 584-590.
22. M. Kongshaug, Distribution of tetrapyrrole photosensitizers among human plasma proteins, *Int. J. Biochem.*, 1992, **24**, 1239-1265.
23. T. Tsuchida, G. Zheng, R. K. Pandey, W. R. Potter, D. A. Bellnier, B. W. Henderson, H. Kato and T. J. Dougherty, Correlation between site II-specific human serum albumin (HSA) binding affinity and murine in vivo photosensitizing efficacy of some Photofrin components, *Photochem. Photobiol.*, 1997, **66**, 224-228.
24. A. Fahr, P. van Hoogevest, S. May, N. Bergstrand and S. L. ML, Transfer of lipophilic drugs between liposomal membranes and biological interfaces: consequences for drug delivery, *Eur. J. Pharm. Sci.*, 2005, **26**, 251-265.
25. B. Cunderlikova, O. Kaalhus, R. Cunderlik, A. Mateasik, J. Moan and M. Kongshaug, pH-dependent modification of

lipophilicity of porphyrin-type photosensitizers, *Photochem Photobiol*, 2004, **79**, 242-247.

26. V. Rosenberger and R. Margalit, Thermodynamics of the binding of hematoporphyrin ester, a hematoporphyrin derivative-like photosensitizer, and its components to human serum albumin, human high-density lipoprotein and human low-density lipoprotein, *Photochem. Photobiol.*, 1993, **58**, 627-630.
27. K. Kuzelova and D. Brault, Kinetic and equilibrium studies of porphyrin interactions with unilamellar lipidic vesicles, *Biochemistry*, 1994, **33**, 9447-9459.
28. R. K. Chowdhary, I. Sharif, N. Chansarkar, D. Dolphin, L. Ratkay, S. Delaney and H. Meadows, Correlation of photosensitizer delivery to lipoproteins and efficacy in tumor and arthritis mouse models; comparison of lipid-based and Pluronic P123 formulations, *J. Pharm. Pharm. Sci.*, 2003, **6**, 198-204.
29. Y. I. Miller and N. Shaklai, Kinetics of hemin distribution in plasma reveals its role in lipoprotein oxidation, *Biochim. Biophys. Acta*, 1999, **1454**, 153-164.
30. D. J. Ball, D. I. Vernon and S. B. Brown, The high photoactivity of m-THPC in photodynamic therapy. Unusually strong retention of m-THPC by RIF-1 cells in culture, *Photochem. Photobiol.*, 1999, **69**, 360-363.
31. H. J. Jones, D. I. Vernon and S. B. Brown, Photodynamic therapy effect of m-THPC (Foscan) in vivo: correlation with pharmacokinetics, *Br. J. Cancer*, 2003, **89**, 398-404.
32. T. Glanzmann, C. Hadjur, M. Zellweger, P. Grosiean, M. Forrer, J. P. Ballini, P. Monnier, H. van den Bergh, C. K. Lim and G. Wagnieres, Pharmacokinetics of tetra(m-hydroxyphenyl)chlorin in human plasma and individualized light dosimetry in photodynamic therapy, *Photochem Photobiol*, 1998, **67**, 596-602.
33. K. T. Hsu and J. Storch, Fatty acid transfer from liver and intestinal fatty acid-binding proteins to membranes occurs by different mechanisms, *J. Biol. Chem.*, 1996, **271**, 13317-13323.
34. L. Thilo, Kinetics of phospholipid exchange between bilayer membranes, *Biochim. Biophys. Acta*, 1977, **469**, 326-334.
35. M. A. Roseman and T. E. Thompson, Mechanism of the spontaneous transfer of phospholipids between bilayers, *Biochemistry*, 1980, **19**, 439-444.
36. M. von Smoluchowski, Veruch einer mathematischen theorie der koagulationskinetik kolloider losungen., *Z. Phys. Chem. Leipzig.*, 1917, **92**, 129-168.
37. P. W. Atkins, Physical Chemistry (4th ed.), *Oxford Univ. Press, Oxford*, 1990.
38. D. Knyazev, S.Sosnovsky, V. Zorin, L. Bolotine and F. Guillemin, Evaluation of meta-tetra (hydroxiphenil)chlorin incorporation into lipid bilayer, *Joint Conference of the German Society of Applied Optics and the Section of Optics of the Polish Physical Society. Wroclaw, Poland, Abstract*, 2005, 26-27.
39. C. Bombelli, G. Caracciolo, P. Di Profio, M. Diociaiuti, P. Luciani, G. Mancini, C. Mazzuca, M. Marra, A. Molinari, D. Monti, L. Toccacieli and M. Venanzi, Inclusion of a photosensitizer in liposomes formed by DMPC/gemini surfactant: correlation between physicochemical and biological features of the complexes, *J. Med. Chem.*, 2005, **48**, 4882-4891.
40. H. K. Kim and J. Storch, Free fatty acid transfer from rat liver fatty acid-binding protein to phospholipid vesicles. Effect of ligand and solution properties, *J. Biol. Chem.*, 1992, **267**, 77-82.
41. R. Bonnett, B. D. Djelal and N. Angelina, Physical and chemical studies related to the development of m-THPC (FOSCAN®) for the photodynamic therapy (PDT) of tumours, *J. Porphyrins Phthalocyanines*, 2001, **5**, 652-661.

Figures

Table 1. Thermodynamic parameters of Foscan® transfer from HDL-Alexa to lecithin vesicles.

Characteristics	value
E_a	11.3 ± 0.2 kcal/mol
ΔH	10.7 ± 0.2 kcal/mol
$T\Delta S$	-11,9 ± 0.2 kcal/mol
ΔG	22,6 ± 0.4 kcal/mol

From the rate constants over a temperature range of 15-37°C (Fig. 7), the activation energy Ea was obtained. ΔG, ΔH and $T\Delta S$ of the activated state were calculated at 25°C as described under "Methods and Materials". Results are average of 3 experiments.
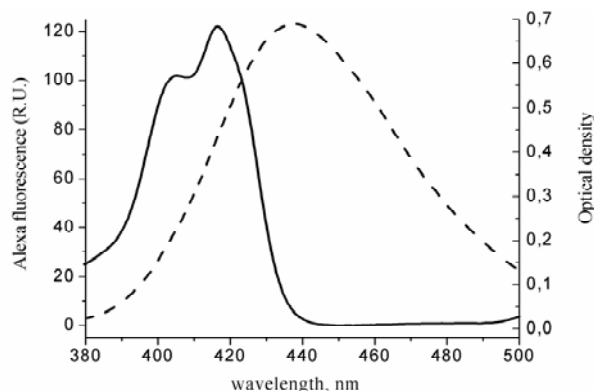

Fig. 1. Normalized fluorescence spectrum (dashed line) of Alexa Fluor 350 (10^{-7} M) covalently bound to HDL (2.6×10^{-8} M) and the absorption spectrum (solid line) of Foscan® (2.3×10^{-5} M) in ethanol. The excitation wavelength was set at 350 nm.

Fig. 3. Kinetics of Foscan® redistribution from the complexes with different plasma proteins to lecithin vesicles.

Time dependent changes in the intensity of fluorescence of preloaded with Foscan® Alexa Fluor 350 (10^{-7} M) solution covalently bound to BSA (1.3×10^{-7} M) (1, axis Y_1), HDL (2.6×10^{-8} M) (2, axis Y_2) and total lipoprotein fraction (10^{-2} mg/ml by protein) mg/ ml (3, axis Y_3) upon addition of lecithin vesicles (6.8×10^{-4} M).

Foscan® concentration 1.5×10^{-7} M. Label fluorescence was monitored at λem = 450 nm (λex = 350 nm). Experiments were conducted under continuous stirring. Temperature T = 25 °C.

Fig. 2. A. Changes in fluorescence intensity of the label fluorescence (1) and Foscan® (2) versus time recorded upon incubation of Alexa-HDL (2.6×10^{-8} M) with Foscan® (1.5×10^{-7} M).

Label fluorescence was monitored at λem = 450 nm (λex 350 nm); Foscan® fluorescence was registered at λem = 655 nm (λex 420 nm). Incubation temperature 25 °C. Experiments were conducted upon continuous stirring.

B. Changes in fluorescence intensity of Alexa fluor 350 (10^{-7} M) bound to HDL (2.6×10^{-8} M) versus Foscan® concentrations. Fluorescence was registered either immediately upon Foscan® administration (curve 1) or after 3h incubation with Foscan® at 37 °C (curve 2). Label fluorescence was monitored at λem = 450 nm (λex = 350 nm). Temperature T = 25°C.

Fig. 4. Experimental and theoretical Foscan® redistribution curves from the complexes with Alexa-HDL to lecithin vesicles.

Experimental plot for Alexa-HDL was fitted using non-linear mono-exponential function, from which the values of Foscan® redistribution apparent rate constants k were derived according to Equation 6. Fitting quality is characterised by $R^2 > 0.99$.

Inset shows the residuals from a mono-exponential fit of the signal. Conditions are the same as indicated in the Fig. 3.
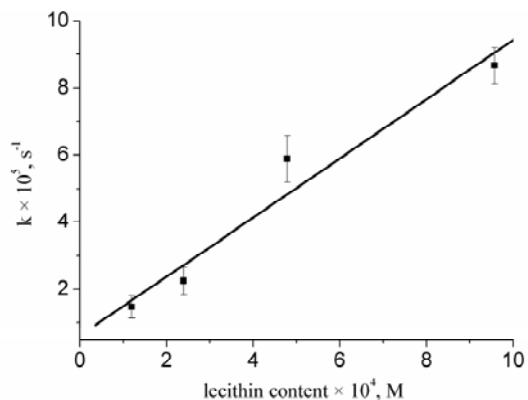
Fig. 5. Dependence of the Foscan® apparent redistribution rate
740 constant k on lecithin vesicles concentration.
The slope of a linear fit gives bimolecular rate constant for
Foscan® (1.5×10^{-7} M) transfer from the complexes with Alexa
(10^{-7} M)-HDL (2.6×10^{-8} M) to lecithin vesicles. Fitting quality
is characterised by $R^2 > 0.98$.
745 Label fluorescence was monitored at $\lambda em = 450$ nm ($\lambda ex = 350$
nm). Experiments were conducted under continuous stirring.
Average rates from three different experiments ± S.D. are shown.

750
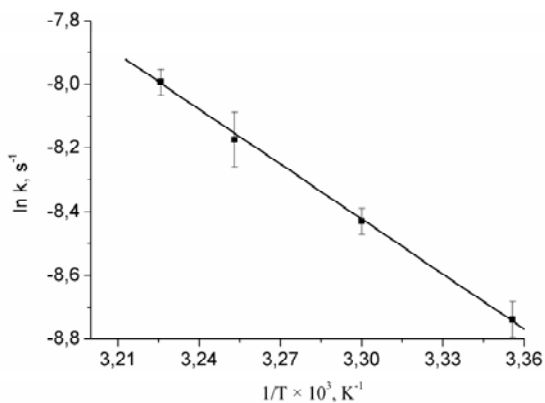
Fig. 6. Arrhenius plots of redistribution rate constant k for the
transfer of Foscan® from HDL-Alexa to lecithin vesicles.
755 Transfer of Foscan® (1.5×10^{-7} M) from Alexa fluor 350 (10^{-7}
M)-HDL (2.6×10^{-8} M) complexes to lecithin vesicles (6.8×10^{-4}
M) was monitored at 5-8 °C intervals from 15-37 °C in PBS.
Label fluorescence was monitored at $\lambda em = 450$ nm ($\lambda ex = 350$
nm). Experiments were conducted under continuous stirring.
760 Fitting quality is characterised by $R^2 > 0.99$.
Average rates from three different experiments ± S.D. are shown.

To complete our work we have also conducted the measurements of Foscan® redistribution kinetics from the complexes with low density lipoproteins (LDL). LDL are also important carriers of Foscan® in the blood as about 8 % of sensitizer is bound to these lipoproteins (Hopkinson et al, 1999).

765 Foscan® redistribution kinetic curve from the complexes with Alexa-LDL to lecithin vesicles at 37°C is presented in the Fig. 7. The apparent redistribution rate constant was calculated to be 8.0×10^{-5} s^{-1}. This value is lower compared to that for HDL 1.6×10^{-4} s^{-1} and can be explained by higher LDL mean diameter.

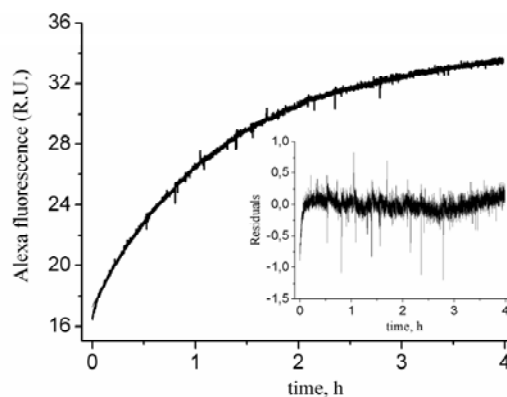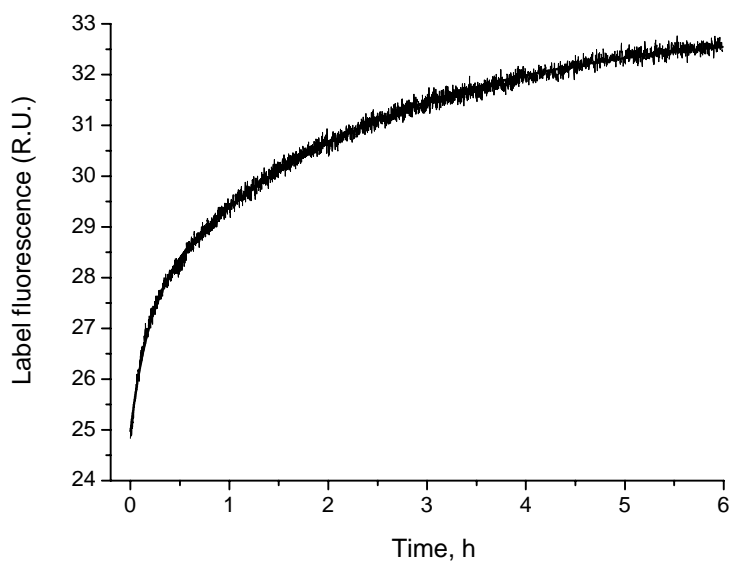770 **Fig. 7.** Experimental Foscan® redistribution curve from the complexes with Alexa-LDL to lecithin vesicles. Experimental plot for Alexa-HDL was fitted using non-linear mono-exponential function, from which the values of Foscan® redistribution apparent rate constants k were derived according to Equation 6. Fitting quality is characterised by $R^2 > 0.99$. Temperature T = 25°C. Conditions are the same as indicated in the Fig. 3.

775 Taken as a whole, the study of Foscan® redistribution from the complexes with different plasma proteins show that typically the redistribution rates of this sensitizer are 1.69×10^{-3} s^{-1}, 1.60×10^{-4} s^{-1}, 8.0×10^{-5} s^{-1} and 1.84×10^{-5} s^{-1} from BSA, HDL, LDL and lipoproteins, respectively.

IV.4. Calculation of quantum yield of MCF-7 cells inactivation by mTHPC-PDT: influence of incubation time and sensitizers localization

Foscan photophysical properties greatly depend on the time of incubation with cells. This effect can be explained on the basis of different PS localization patterns and concentration in cells. After 3 h incubation mTHPC has diffuse and relatively homogenous localization pattern in MCF-7 cells. The higher PS intracellular content after 24h incubation leads to the appearance of "bright spots". This is accompanied with the substantial decrease of absorbance in the Soret band, more slow and bi-exponential kinetics of photobleaching and reduces values of fluorescence lifetimes compared to 3h point. The lifetimes of mTHPC were 8.7 ns at 3h point and 3.9 and 2.0 ns in the diffuse and spots regions at 24 h point, respectively. The absolute photosensitising efficiency of mTHPC at 24h was determined by clonogenic assay to be 3 times greater compared to 3h time point. To compare the quantum yields of sensitizer in cells at different incubation times the number of absorbed photons by intracellular PS was calculated as a function of irradiation time. Owing to PS self-quenching and aggregation due to its high intracellular concentration the PDT efficiencies calculated from transformed cell survival curves 3 times higher at 3h incubation time point compared to 24h. The results point out the great influence of sensitizer intracellular content and aggregation state on its photodynamic efficiency in vitro.

This part of the work is in preparation.

Calculation of quantum yield of MCF-7 cells inactivation by mTHPC-PDT: influence of incubation time and sensitizer localization

Siarhei Sasnouski [a,b], Emilie Pic [a], Dominique Dumas [c], Vladimir Zorin [b], MA. D'Hallewin [a], François Guillemin [a] and Lina Bezdetnaya [a*]

[a] *Centre Alexis Vautrin , CRAN UMR 7039 CNRS - INPL –UHP, Avenue de Bourgogne, 54511 Vandœuvre-Les-Nancy cedex, France*

[b] *Laboratory of Biophysics and Biotechnology, Physics Faculty, Belorussian State University, Nezalegnasti 4 st., Minsk, 220080 Belarus*

[c] *LEMTA, Equipe Mécanique et Ingénierie Cellulaire et Tissulaire-Service Imagerie Cellulaire, IFR 111 and UMR CNRS 7563 CNRS-INPL-UHP, Faculté de Médecine, BP 184, 54505 Vandœuvre-les-Nancy, France*

* Corresponding author. Centre Alexis Vautrin , CRAN UMR 7039 CNRS - INPL –UHP, Avenue de Bourgogne, 54511 Vandœuvre-Les-Nancy cedex, France

Tel +33 3 83 59 83 06, fax +33 3 83 44 60 71

*E-mail address***:** l.bolotine@nancy.fnclcc.fr

Abstract

Measurements of mTHPC photophysical properties in MCF-7 cells have revealed several features of progressive sensitizer aggregation with increase of incubation time. This was accompanied by the change of mTHPC diffuse localization pattern at 3 h incubation into inhomogeneous sensitizer distribution at 24 h, connected with the formation of highly fluorescent regions. Substantial decrease of absorbance in the Soret band, bi-exponential kinetics of photobleaching and reduction of fluorescence lifetimes at 24 h compared to 3h point were explained by the higher sensitizer intracellular content and different localization pattern. Assessement of PDT efficiency by clonogenic assay have shown 3 times higher at 24 h. After transformation of abscissa axis into the absorbed dose 2 times higher efficiency was obtained at 3h incubation time point compared to 24h. The results were interpreted as drop of mTHPC photosensitizing efficiency upon aggregation.

1. Introduction

Photodynamic therapy (PDT) uses the combination of a photosensitising drug and light to cause damage to pathologically proliferating tissues, including tumours. Photosensitizer activation by visible light results primarily in singlet-oxygen mediated photodamage (Dougherty et al. 1998; Peng and Nesland 2004).

Foscan® or meta-tetra(hydroxyphenyl)chlorin (mTHPC) is a second-generation photosensitizer (Bonnett et al. 1989) and is one of the most effective sensitizers studied to date (Dougherty et al. 1998). It mediates cell photodamage principally through singlet oxygen formation (Melnikova et al. 1999) and its tumoricidal effect appears to be very sensitive to oxygenation conditions (Coutier et al. 2001; Coutier et al. 2002). Fluorescence microscopy studies in monoculture cells showed intense fluorescence in the perinuclear region (Foster et al. 2005) with a significant mTHPC accumulation in the endoplasmic reticulum and Golgi apparatus (Teiten et al. 2003). mTHPC has been granted European approval for palliative treatment of patients with advanced head and neck cancers and is considered as a valuable therapeutic option for localized oesophageal neoplasia (Lovat et al. 2005) and organ confined prostate cancer (Moore et al. 2006).

One of the parameters largely influencing photophysical behavior of sensitizers is their aggregation state. Aggregated photosensitizers generally have much lower fluorescence and triplet states quantum yields, resulting in reduced quantum yield of singlet oxygen production (Redmond et al. 1985; Tanielian et al. 2001) and drop of photosensitizing efficiency (Ambroz et al. 1994; Ball et al. 1998; Theodossiou et al. 2004). Both monomer and aggregated forms of photosensitizers are present in cells. Time-resolved fluorescence spectroscopy demonstrated that there is a considerable amount of aggregated porphyrin species in biomembranes (Ricchelli 1995) Furthermore, it has been observed that porphyrin monomers tend to aggregate in large clusters after prolonged incubation within the cells (Borovkov et al. 1996). Similar to porphyrins, an increase in incubation time also influences aggregation state of chlorine-type compounds. mTHPBC has been reported to exist in several aggregated forms after 24h incubation with tumor culture cells (Grahn et al. 1997). Fluorescence lifetime imaging (FLIM) measurements in cells demonstrated the decrease of mTHPC fluorescence lifetime from 7.5 to 5.5 ns with increasing incubation from 1 to 6 hours. This was interpreted as an enhanced formation of aggregates during incubation.

Within this work we addressed the impact of different aggregation states of mTHPC on cell phoinactivation yield. Different aggregation states were obtained by varying incubation times of mTHPC with MCF-7 cells. Photoxicity of mTHPC at different incubation times was

computed in function of the number of absorbed light photons. For this purpose we have used the parameters of mTHPC intracellular absorption, photobleaching kinetics of mTHPC in cells and the intracellular concentration of photosensitizer.

2. Materials and methods

2.1. Chemicals and photosensitizer

The photosensitizer mTHPC was kindly provided by Biolitec AG (Jena, Germany). Stock solution was made by dissolving the powder in 100 % ethanol at a concentration of 3 mM and was kept at 4°C in the dark. Further dilution was performed in RPMI 1640 (Gibco, Cergy Pontoise, France) supplemented with 2% heat inactivated fetal calf serum (FCS) (PAN Biotech GmbH, Aidenbach, Germany). The final photosensitiser concentration was 1.5 μM or 7.5 μM. Phosphate buffered saline (PBS, without $CaCl_2$ and $MgCl_2$; pH 7.4) was obtained from Invitrogen. Hepes and Crystal violet were purchased from Sigma (France).

2.2. Cell culture

The human breast adenocarcinoma cell line MCF-7, was grown in phenol red free RPMI 1640 medium (Invitrogen, Cergy Pontoise, France) supplemented with 9% heat-inactivated fetal calf serum (FCS) (PAN Biotech GmbH, Aidenbach, Germany), 1% penicillin (10 000 IU) streptomycin (10 000 μg/ml) and 1% glutamin 200 mM (Invitrogen, Cergy Pontoise, France). Cells were kept as monolayer culture in a humidified incubator (5% CO_2 in air at 37°C). Cell cultures were re-seeded every week to ensure an exponential growth.

2.3. Photodynamic treatment

Cells (10^4 cells/ml) were seeded in 50 mm Petri dishes containing 4 ml of RPMI 1640 with 9% FCS. After 4 days, cells were washed twice and incubated with fresh medium containing 2% FCS with 1.5 μM mTHPC for 3h or 24h. Before photosensitization, cells were washed three times, incubated with RPMI 9% FCS then irradiated with a 650 nm laser diode (F-System, Coherent, Saclay, F) at a fixed fluence rate of 2.12 mW/cm^2.

2.4. Fluorescence photobleaching experiments.

For photobleaching experiments the cells were preincubated in medium containing 2% FCS with 1.5 μM mTHPC for 3h or 24h. After photosensitization, the mTHPC fluorescence emission spectra were recorded on SAFAS Xenuis spectrofluorometer using microplate reader (Monaco). Excitation wavelength was set at 420 nm. No photobleaching effects were observed due to the spectrofluorometer excitation source. Cells were irradiated with a 650 nm laser diode (F-System, Coherent, Saclay, F) at a fixed fluence rate of 2.12 mW/cm^2. The acquired data were treated with background subtraction of a control sample (drug-free cells).

The value of fluorescence intensity at 650 nm was registered after each irradiation time and the photobleaching curves were constructed from these points. Fitting of data was performed using modified Levenberg-Marquardt non-linear fitting algorithm in Origin 7.5.

2.5. Cell viability assay

Cell viability was assessed by clonogenic assay. Logarithmically growing MCF-7 cells were collected from the monolayer with trypsin immediately after PDT, seeded in triplicate into 6-well plates at a density of 500 cells per well. Nine days after treatment, the medium was removed, colonies were fixed with 70% ethanol and stained with 1% crystal violet (Pointet Girard, Cuchy, F) for 5 minutes. Sensitizer excess was carefully washed off and colonies composed of more than 50 cells were counted with a robotized image analysis system (Techlab, Ca). Each experiment was done at least three times. Cell death percentage was obtained by referring treated samples to non-irradiated culture (drug, no light).

2.5. mTHPC intracellular extraction

Cells were incubated with 7.5 µM or 1.5 µM of mTHPC during 3h and 24 h. After incubation, cells were washed with cold PBS, tripsinised, washed in PBS, re-suspended in RPMI 1640 and centrifuged twice at 1500 rpm for 5 minutes. Cells were further re-suspended in RPMI 1640 and their concentration was determined using Thoma cells. Two mL of cell suspension was afterwards centrifuged at 1500 rpm for 5 minutes. The supernatant was poured out and 3 mL of methanol was added to the pellet. The resulting samples were sonicated for 10 minutes using Bransonic B-1200 E3 ultrasonic cleaner (Roucaire, France) and centrifuged at 3500 rpm for 5 minutes. After centrifugation, one mL of supernatant from each sample was added to two mL of methanol and the resulting mixture was introduced into 10x10 mm quartz cuvette. Emission spectra were carried out using Perkin-Elmer LS 50B luminescence spectrometer. Spectra were collected between 600 and 700 nm (excitation wavelength 422 nm; photomultiplier voltage 650 V). Fluorescence from the cells lysates was measured with respect to a calibration curve using mTHPC molar extinction coefficient in methanol of $\varepsilon_{650} = 29.600$ M^{-1}cm^{-1} (Bonnett et al. 2001).

2.6. mTHPC absorption spectra

Cells were incubated with 7.5 µM of mTHPC during 3h, 12h and 24 h. The suspension of intact cells was obtained as described in *2.5*. Three ml of mTHPC-loaded cells were introduced into 10x10 mm quartz cuvette and the absorption spectra of mTHPC were recorded using a Perkin Elmer Lambda 35 spectrophotometer equipped with an integrating sphere RSA-PE-20 (Labsphere). An integrating sphere was used to obtain a true absorption

spectrum of mTHPC in a scattering milieu such as cell suspensions. For calculating true absorbances we applied the method proposed by Merzlyak and Naqvi (Merzlyak and Naqvi 2000). This approach consists in the estimation of the true absorbance from a pair of absorption spectra obtained by positioning the sample at two different distances from the outer entrance of the sphere. Acccording to Merzlyak et al (Merzlyak and Naqvi 2000) apparent absorption spectra of mTHPC in cells were measured at two distances, $d_1 = 7$ mm and $d_2 = 2$ mm .and for further calculations of true absorbances we used equation (1):

$$D_{abs}(\lambda) = D_{ext}(\lambda,d_1) - L(d_1, d_2) \times \{D_{ext}(\lambda,d_1) - D_{ext}(\lambda,d_2)\} \qquad (1)$$

where $D_{abs}(\lambda)$ - true absorbance; $D_{ext}(\lambda, d_1)$ and $D_{ext}(\lambda, d_2)$ - apparent absorbances measured at d_1 and d_2 respectively; $L(d_1, d_1)$ – proportionality factor, defined as

$$L(d_1,d_2) = \frac{D_{ext}(\lambda_0,d_1)}{[D_{ext}(\lambda_0,d_1) - D_{ext}(\lambda_0,d_2)]} \qquad (2)$$

where λ_0 - wavelength where mTHPC does not absorb light.

Considering that the last absorption band of mTHPC peaks at 650 nm, we have chosen λ_0 of 800 nm in our measurements. $D_{ext}(\lambda_0, d_1)$ and $D_{ext}(\lambda_0, d_2)$ are the apparent absorbances measured at λ_0. As an example, Figure 1 displays apparent absorption spectra of mTHPC at d_1 (curve 1) and d_2 (curve 2) together with the reconstructed true absorption spectrum of mTHPC in cells (curve 3). It is important to note, that in a parallel set of experiments we demonstrated the linearity between mTHPC apparent absorption at 650 nm and cell content in the range (3 - 25) x 10^4 cells/ml (data not shown). According to Merzlyak et al (Merzlyak and Naqvi 2000), this linearity allows safely assume that the reconstructed absorption spectrum is a very good approximation of a "true" absorption spectrum. Reference spectra of mTHPC in methanol were measured on a Perkin Elmer Lambda 35 spectrophotometer without integrating sphere.

2.7. Laser Confocal Scanning Microscopy (LCSM).

MCF-7 cells (1×10^4 cells/ml) were plated into eight-well chambers Slideflask (Nunc), incubated in the dark at 37°C with 1.5 μM mTHPC for 3 h and 24h, rinsed in the medium and immediately examined with a confocal laser scanning microscope (SP-2 AOBS LCSM, Leica microsystem, Germany). An optimal pinhole size of 60.64 μm was used to exclude fluorescence light emitted from out-of-focus plane above and below the focusing plane. An oil immersion objective (x 63) was used to capture each image of 512 x 512 pixels size. mTHPC was excited with a Helium/Neon laser at 633 nm. mTHPC fluorescence was detected in the range 640-660 nm using an acousto-optical beamsplitter (AOBS).

2.8. Fluorescence lifetime measurements

Cells (1×10^4 cells/ml) were inoculated into Labtek dishes and 4 days later were incubated with 7.5 µM mTHPC for 3h or 24h at 37°C. After incubation, the cells were washed twice with RPMI 1640. For FLIM two-photon excitation, we used a mode-locked Ti:sapphire laser (MIRA 900F, Coherent) pumped with an 8 W argon-ion laser (Verdi, Coherent), which delivers a pulse width from 120 fs with a repetition rate of 76 MHz. sUsing a cavity dumpe,r the repetition rate was reduced to 2.76 MHz. The power of the excitation light in the focus was 5 mW. The detection was performed in a non-descanted mode (NDD-PMT). Time-correlated single photon counting was used for lifetime imaging. SPC-730 TCSPC photon counting module (Becker&Hickl) was interfaced to the scan controller of the Leica SP2 CLSM laser scanning microscope (Leica Microsystems, Germany) equipped with AOBS. The PMT was built-in the microscope attached to the non-descanted port, without discrimination for the different emission wavelengths of the different probes. Images at a 0.195 nm (x,y) pixel size were obtained for each case in 512 x 512 matrices at x63 magnification (numerical aperture = 1.32). The decay analysis was performed using the SPCImage Version 2.8.3 software (Becker&Hickl). Every pixel of the fluorescence lifetime image was achieved by software binning of 4×4 pixels of the image. The instrument response function was measured on erythrosine (full width half maximum equal to 220 ± 15 ps) and used for deconvolution.

2.9. Calculation of mTHPC absorbed dose in MCF-7 cells

The number of absorbed photons was computed according to Theodossiou and MacRobert (Theodossiou and MacRobert 2002). mTHPC molecular absorption rate (AR) in photons per molecule per second (photons/molecule/s), is expressed as :

$$AR = I_0 \times \sigma \qquad (3)$$

where σ - molecular absorption cross section (cm^2/molecule), I_0 - incident light intensity (photons/cm^2/s).

Considering that σ is related to ε as

$\sigma = 3.82 \times 10^{-21} \times \varepsilon$ (Lakowicz 1999), Equation (3) turns into :

$$AR = 3.82 \times 10^{-21} I_0 \times \varepsilon \qquad (4)$$

where ε - molar extinction coefficient of photosensitizer (M^{-1}cm^{-1}). The intensity of incident light I_0 does not considerably change during its diffusion through cells in monolayer and, as such, can be considered as constant. Since a linear correlation between mTHPC intracellular concentration and its fluorescence intensity was established (data not shown), the mTHPC

intracellular fluorescence measured in photobleaching experiments, could be used as a measure of mTHPC content. Accordingly, the average number of absorbed photons by a single mTHPC-loaded cell after irradiation time (t) can be expressed as:

$$D_{abs}(photons/cell) = AR \times N_0 \times F_{mono/bi}(t) \qquad (5)$$

where N_0 - initial number of mTHPC molecules in a single cell, defined as

$$N_0 = C \times N_A \qquad (6)$$

where C - average number of sensitizer moles per cell, N_A – Avogadro's number; function $F_{mono/bi}(t)$ - mono-and-biexponential sensitizer photobleaching and is defined as:

$$F_{mono}(t) = \frac{(1 - \exp(-k_1 t))}{k_1} \qquad F_{bi}(t) = \frac{A_1(1 - \exp(-k_1 t))}{k_1} + \frac{A_2(1 - \exp(-k_2 t))}{k_2} \qquad (7)$$

where k, k_1 and k_2 - photobleaching rate constants for mono and bi-exponential decays respectively; A_1 and A_2 - fractions of sensitizer fluorescence that photobleach with k, k_1 and k_2 constants.

Therefore, equation 5 turns into:

$$D_{abs}(photons/cell) = 3.82 \times 10^{-21} I_0 \times \varepsilon \times C \times N_A \times F_{mono/bi}(t) \qquad (8)$$

3. Results

3.1. Intracellular absorption properties of mTHPC

Figure 2 displays the intracellular extinction spectra of mTHPC in methanol and after 3h, 12h and 24h incubation of 7.5 μM mTHPC with MCF-7 cells. The molar extinction coefficients were calculated from Lambert-Beer's law using optical densities from reconstructed absorption spectra (as in Fig. 1) and intracellular mTHPC concentration after chemical extraction in cells incubated with 7.5 μM mTHPC. The mTHPC intracellular concentrations at each incubation time are provided in Table1. Compared to the reference spectrum of mTHPC in methanol, all intracellular mTHPC spectra were red shifted (Figure 2). Spectra at 3h and 12h incubation were very similar, while mTHPC spectrum at 24h post incubation was characterized by a significant decreased extinction in the Soret band.

The values of molar extinction coefficients in Soret band and at 650 nm at all experimental conditions are summarized in Table 1. The mTHPC molar extinction coefficient after 24h incubation was about 1.5 times lower compared to 3h incubation. Changes in the spectral band at 650 nm were much less pronounced, still ε_{650} was lower (by 17%) at 24h

compared to 3h. The mTHPC spectral characteristics observed after 24h incubation are consistent with the crude indications of aggregation. Since mTHPC spectra after 3 and 12h incubation were very similar (Figure 2, Table 1) we chose two incubation times, 3h and 24h for the rest of the study.

3.2. Intracellular localization and fluorescence lifetime imaging of mTHPC

After 3 h incubation mTHPC has a diffuse and relatively homogenous localization pattern (Fig. 3). After 24 h incubation we observe the appearance of mTHPC spots with high fluorescence intensity. FLIM measurements were performed at both incubation times. Decay analysis demonstrated two-exponential decay for both 3 and 24h incubation. Fig. 4 represents mTHPC (7.5 µM) confocal fluorescence images in MCF-7 cell at 3 h (a) and 24 h (b) incubation times together with corresponding histograms of mTHPC fluorescence lifetime distribution as a function of the number of detected photons for the field of view (FOV). The different colours on the images at the left correspond to various lifetimes as shown in histograms at the right. The average value of the lifetime for FOV decreases from 8.5 ns at 3 h to 2.5 ns at 24 h incubation time.

The value of 100 ps, obtained for the first lifetime component at 3 h point (Table 2) must probably be attributed to contamination by the excitation laser. The second lifetime at 3 h appeared to be 8.7 ns (Table 2). Due to mTHPC heterogeneous localization pattern at 24 h post-incubation, FLIM measurements were performed at two distinct localization sites, namely in diffuse regions and in the bright spots. mTHPC lifetimes τ_{1} and τ_{2} in diffuse regions are about 1 and 4 ns, and even lower in the fluorescent spots(0.3 and 2 ns, respectively). Since 0.3 ns is very close to the resolution limit of the system (0.25 ns) it was discarded in the further analysis.

3.3. Photobleaching of mTHPC

After 3 h incubation we observed an increase of mTHPC fluorescence during the first 30 seconds of irradiation, followed by mono-exponential decrease (Fig. 5), characterized by the rate constant of $(6.4 \pm 0.4) \times 10^{-3}$ s^{-1} (Table 2). mTHPC photobleaching after 24h incubation best fitted a bi-exponential decay (Fig. 5, Table 2) with a very rapid first rate constant $(78 \times 10^{-3}$ $s^{-1})$ and a slow second one $(0.6 \times 10^{-3}$ $s^{-1})$.

3.4. Yields of mTHPC induced cell photoinactivation at different incubation times

MCF-7 cells were incubated with 1.5 µM mTHPC for 3h or 24h, subjected to irradiation with different light fluences and their photocytotoxicity was further assessed by colony forming assay. Figure 6 displays the photocytotoxicity plotted in a function of either

irradiation time (Fig. 6A) or of a number of absorbed photons (Fig. 6B). Considerably greater cell photoinactivation was observed after 24h incubation at all applied fluences (Fig. 6A). For instance, the PDT efficiency at LD_{63} at 24 h incubation was about 3 times higher compared to that of 3 h (Fig. 6A).

Photocytotoxicity data were re-plotted, with the abscissa giving the values of the numbers of absorbed photons calculated according to the Eq. 8. Photophysical parameters as extinction coefficient ε, intracellular concentration C, photobleaching rate constants k, k1 and k2 for both incubation times were taken from Tables 1 and 2. The re-plotted curves (Fig. 6B) demonstrated results completely different from these depicted in Figure 6A. Three hours incubation yielded much better photoinactivation compared to 24h. Photoinactivation yield was further estimated by fitting of these plots (Fig. 6B) according "Single hit multiple target Model" (Fowler 1964). In this model the dependence of survival fraction on absorbed dose is presented as:

$$N = N_0 \{1 - (1 - exp^{-D/D_0})^n\} \tag{10}$$

where N stands for the number of live cells after irradiation, N_0 – initial number of live cells, D_0 is a light dose required to reduce the survival fraction by 1/e in the linear portion of the curve, D – absorbed light dose and n stands for the parameter that determine the threshold dose (width of the shoulder on the survival curve). Assuming the efficiency of PDT as $1/D_0$, we find that this parameter at 3h is twice higher than at 24h. In other words at 3h incubation mTHPC inactivates 2 times more cells compared to 24h, upon absorption of the same number of photons.

4. Discussion

Hydrophobic sensitizers form dimers and higher micelle-like aggregates in aqueous media and their physical and chemical properties differ noticeably from those of the monomeric sensitizer (Brown et al. 1976). Generally, monomeric forms of photosensitizer have a higher photodynamic efficacy compared to aggregated ones (Ma et al. 1994; Ball et al. 1998; Theodossiou et al. 2004).

The increase of incubation time of mTHPC with MCF-7 cells leads to an enhanced accumulation of aggregated species as can be deduced from this study. Absorption spectroscopy shows a bathochromic shift of Soret band maxima (420 nm) after 24 h incubation compared to that in methanol solution (415 nm) confirming sensitizer aggregation.

Secondly, we observe a considerable reduction of molar extinction coefficient of Soret band at 24 h compared to 3 and 12 h (Fig. 2, Table 1). Also, the increase of Soret band half height bandwidth at 24 h incubation (2040 cm^{-1}) relative to that at 3 h (1740 cm^{-1}) can be considered as another sign of aggregation.

Another parameter that is very sensitive to molecular aggregation state is fluorescence lifetime (Lakowicz 1999). There are several reports on the use of FLIM technique to study aggregation state of sensitizers (Scully et al. 1997; Scully et al. 1998; Connelly et al. 2001; Kress et al. 2003). The influence of AlPcS$_2$ intracellular concentration and aggregation state on its fluorescence lifetime demonstrated the reduction in fluorescence lifetime at higher concentrations and was attributed to the quenching of monomers fluorescence by non-fluorescent aggregates (Connelly et al. 2001). Likewise, the *in vitro* decrease of mTHPC fluorescence lifetime during incubation was attributed to formation of aggregates (Kress et al. 2003). We performed FLIM measurements of mTHPC in MCF-7 cells at 3 h and 24 h incubation times. For 24 h incubation the values of lifetime were calculated separately in the regions with diffuse localization and in the regions of high fluorescence intensity (Fig. 3). Our results demonstrate that the fluorescence intensity in the latter regions is an order of magnitude higher compared to diffuse regions. The lifetime of mTHPC at 3 h incubation appeared to be 8.7 ns (Table 2), and is consistent with that of mTHPC monomers in ethanol (10 ns) (Howe et al. 1999). General fluorescence lifetime decays at 24h are considerably faster compared to 3h and as such the lifetimes after prolonged incubation are much lower. The lower lifetimes at 24h could be the result of sensitizer self-quenching due to its high concentration and aggregation or due to interactions with cellular components and specific intracellular medium properties (Table 2). The changes in mTHPC aggregation state measured by FLIM confirm the absorption spectroscopy data on the increased aggregation with the increase in incubation time (Table 1). Both FLIM data and absorption spectroscopy data are consistent and suggest increasing presence of mTHPC aggregates with prolonged incubation.

mTHPC has been reported to be a moderately photolabile compound (Bonnett et al. 1999) and photodegradation and the formation of photoproducts is oxygen dependent. (Hadjur et al. 1998). The preferential photobleaching of photolabile monomeric forms of mTHPC compared to aggregates have been proposed (Belitchenko et al. 1998). Hence, photobleaching can serve as another indicator of aggregation state. The initial increase of sensitizer fluorescence intensity at 3 h incubation is probably connected to the rapid change of mTHPC localization pattern (Fig. 5A). At 3 h incubation primary sites of mTHPC localization and

photodamage in MCF-7 cells are the endoplasmic reticulum (ER) and Golgi apparatus (Teiten et al. 2003), whereas at 24 h the primary mTHPC localization site is ER (Marchal, submitted). This prolonged incubation was accompanied by the progressive exclusion of mTHPC from Golgi apparatus. Based on this observation, we speculate that energy delivered in course of irradiation could promote re-distribution between ER and Golgi apparatus and eventual location of the photosensitizer in the sites favoring higher fluorescence yield. Initial increase in fluorescence intensity is followed by a decrease which is best fitted by mono-exponential equation, thus suggesting the presence of only one type of photosensitizer species, presumably monomeric. This proposition is also consistent with the FLIM results after 3h incubation. The kinetics of photobleaching at 24 h incubation becomes bi-exponential with a very rapid first phase (Fig. 5B, Table 2). This rapid phase can be attributed to highly photolabile monomeric mTHPC fraction. The photobleaching rate constant of the second phase at 24 h is an order of magnitude lower than the constant at 3 h, thus suggesting the formation of sensitizer aggregated species upon prolonged incubation (Table 2). The increase of sensitizer intracellular content can also lead to the change of photobleaching mechanism.

Taking as an example fluorescein, it was demonstrated that the triplet excited state molecules are photoinactivated via two major pathways: the reaction of triplet either with another triplet or a ground state dye molecule; and the reaction between a triplet dye molecule and an oxygen molecule (Lindqvist 1960). These two mechanisms were re-examined by Usui et al. and were called D-D (dye-to-dye) and D-O (dye-to-oxygen) mechanisms, respectively (Usui et al. 1965). In the absence of D-D reactions the bleaching behavior is a single-exponential process. Simulation of fluorescein in solution showed that when dye content is much lower than oxygen concentration the probability of a reaction between dye molecules is very low (Song et al. 1995). This probability increases with increasing dye concentration. Therefore, it can be proposed that at 3h the mono-exponential photobleaching kinetic is consistent with predominantly D-O mechanism (Fig. 5). In the course of mTHPC intracellular accumulation the probability of D-D reactions between its molecules increases resulting in more complicated photobleaching profile at 24 h. This complex photobleaching behavior of mTHPC could also be anticipated based on the FLIM data after 24h incubation (Table 2) where several lifetime components were registered.

The reduction of fluorescence and IC yields with increasing sensitizer concentration were also observed for deuteroporphyrin (Aveline et al. 1998). This phenomenon was explained as sensitizer self-association, leading to self-quenching of the triplet state. Self-quenching can play a significant role at high local sensitizer concentration and such

conditions can be achieved *in vitro* since local sensitizer concentration in lipid bilayers can reach an order of mM.

The observed value of mTHPC photodynamic efficacy ($1/LD_{63}$) at 24 h incubation is about 3 times higher compared to 3 h (Fig. 6A). It should be noted that this is not proportional to the increase of sensitizer intracellular content which is about 15 times (Table 1). But in order to compare the real yields of cells photoinactivation at different incubation times, and thus different intracellular concentration,aggregated state and intracellular localization, the number of absorbed photons per sensitizer molecule should be calculated. After calculation of photodynamic efficacy ($EP = 1/D_0$) values, based on absorbed dose, the EP_{3h} appeared to be about 2 times superior to EP_{24h}. These results indicate that mTHPC aggregated species have lower photodynamic activity compared to monomers. In other words, increase of photosensitizer intracellular content can lead to the formation of photodynamically inactive sensitizer fraction. Therefore, intracellular content and localization of the photosensitizer can influence its photophysical characteristics and the phototoxicity outcome.

From a clinical point of view, it appears that small light-drug intervals may be beneficial, apart from reducing hospital stay. As it appears from Fig. 5, more rapid photobleaching kinetics at 3 h light-drug interval, together with much lower initial intracellular sensitizer content would probably lower skin photosensitivity. Together with the enhanced mTHPC vascular effect at small light-drug intervals (Triesscheijn et al. 2005), rapid sensitizer photobleaching and rather good photosensitizing efficiency propose short intervals as perspective tools for PDT.

5. Conclusion

mTHPC photophysical properties greatly depend on the time of incubation with cells. This effect can be explained on the basis of different sensitizer localization patterns and concentration in cells. The higher sensitizer intracellular content and appearance of highly fluorescent regions at 24h are accompanied by the substantial decrease of absorbance in the Soret band, bi-exponential kinetics of photobleaching and reduced values of fluorescence lifetimes compared to 3h point. Owing to sensitizer self-quenching and aggregation due to its high intracellular concentration, PDT efficacy calculated from re-plotted clonogenic assay curves is 2 times higher at 3h incubation time point compared to 24h.

Figures
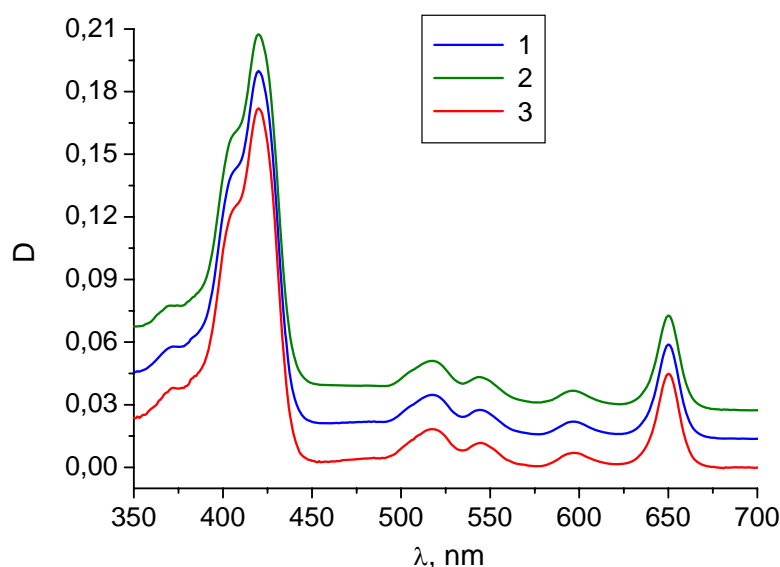
Fig. 1 mTHPC (7.5 μM) extinction spectra measured at different distances between integrating sphere and cuvette (1 − d = 2 mm, 2 − d = 7 mm) and calculated absorption spectrum (Eq. 1) in the suspension of MCF-7 cells. Incubation 24 h at 37 °C, $C_{cells} = 5.6*10^5$ cells/mL.

Table 1. Parameters of mTHPC absorption and accumulation in MCF-7 cells at different incubation times.

Parameter	ε, $M^{-1}cm^{-1}$	C (1.5 μM), mole/cell	C (7.5 μM), mole/cell
3 h	$\varepsilon_{650} = 30.000 \pm 1000$ $\varepsilon_{419} = 144.700 \pm 4.800$	$(1.6 \pm 0.4)*10^{-17}$	$(8.6 \pm 3.3)* 10^{-16}$
12 h	$\varepsilon_{650} = 29.300 \pm 600$ $\varepsilon_{420} = 139.900 \pm 4.800$	$(1.7 \pm 0.9)*10^{-16}$	$(1.0 \pm 0.2)*10^{-15}$
24 h	$\varepsilon_{650} = 25.500 \pm 900$ $\varepsilon_{420} = 97.700 \pm 3.800$	$(2.4 \pm 0.4)*10^{-16}$	$(3.3 \pm 0.8)* 10^{-15}$
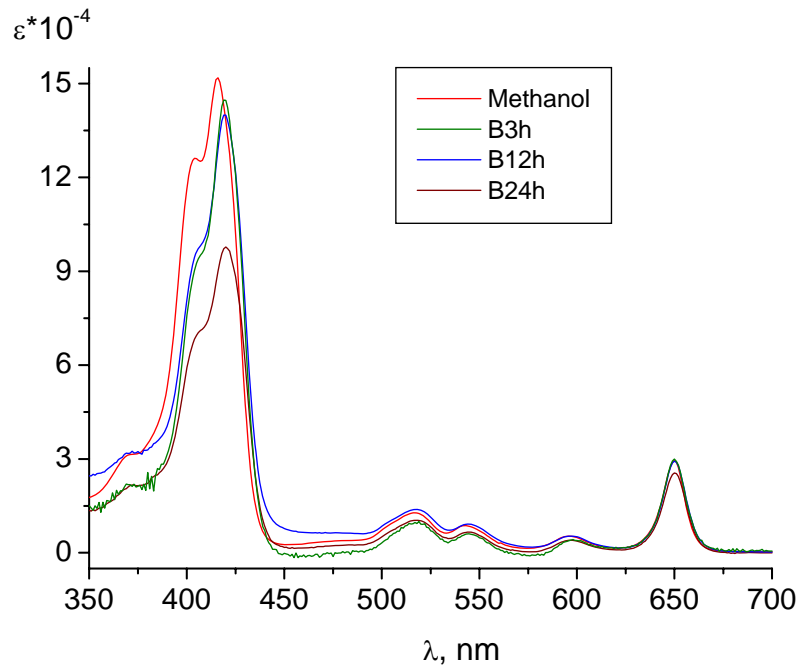
Fig. 2 mTHPC (7.5 μM) reconstructed absorption spectra in the suspensions of MCF-7 cells at different incubation times and in methanol. Incubation 3 h, 12 h and 24 h at 37 °C, C_{cells} = $5.6*10^5$ cells/mL.
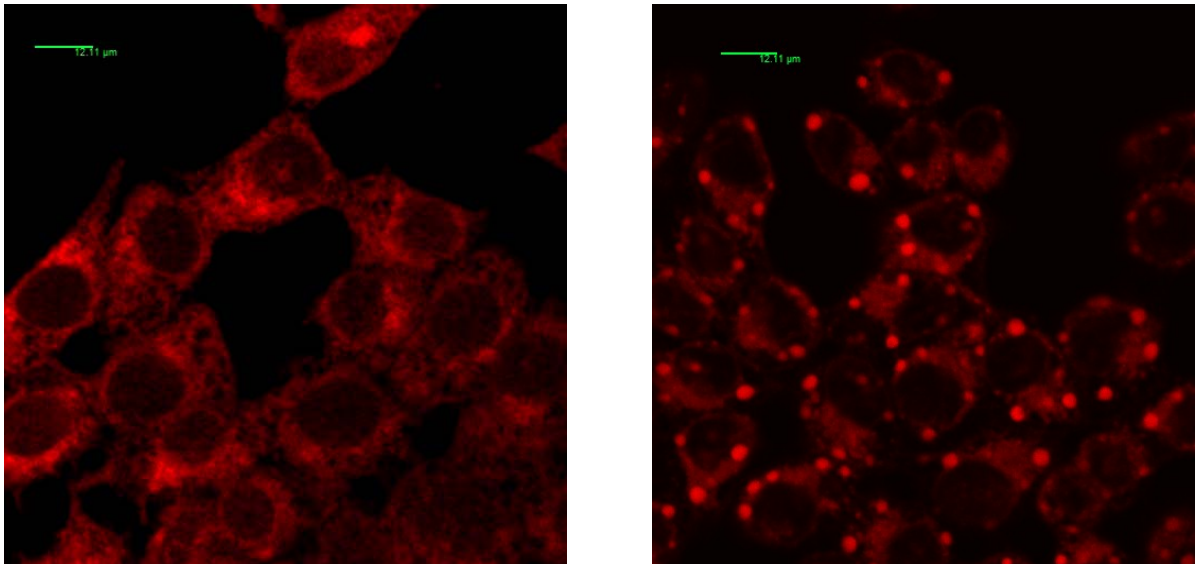
Fig. 3 mTHPC (1.5 μM) confocal fluorescence images in MCF-7 cell at 3 h (left) and 24 h (right) incubation times. Incubation at 37 °C.

a)

3h

b)

24h
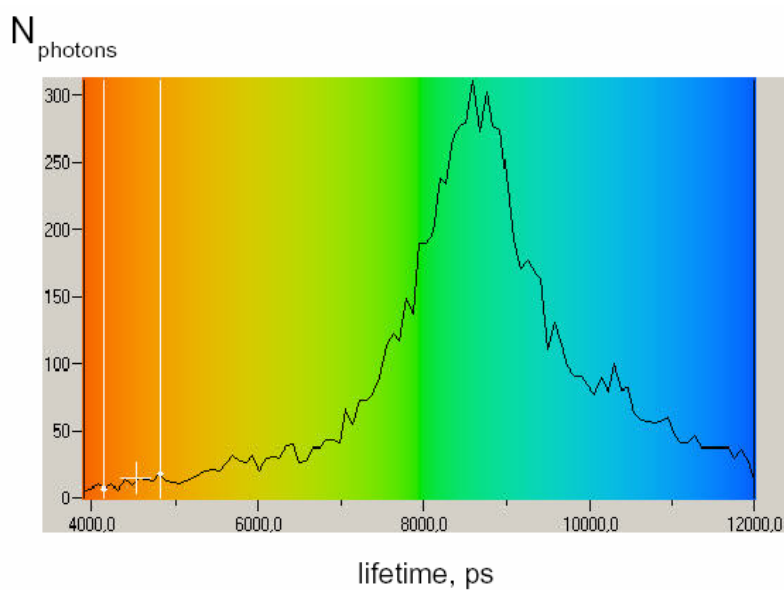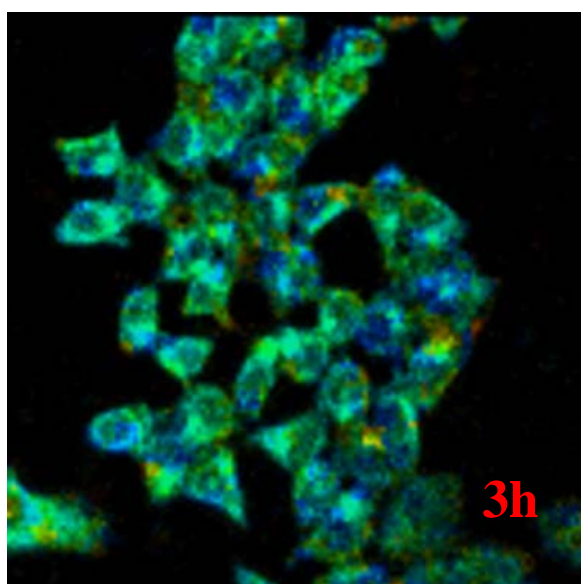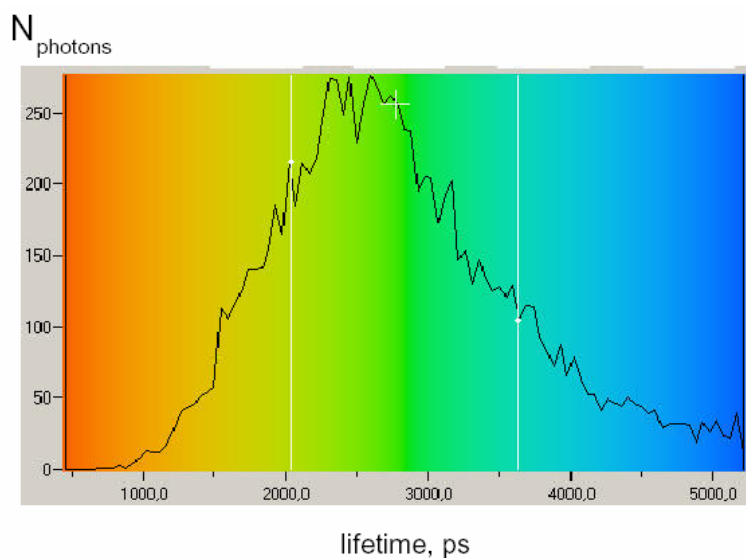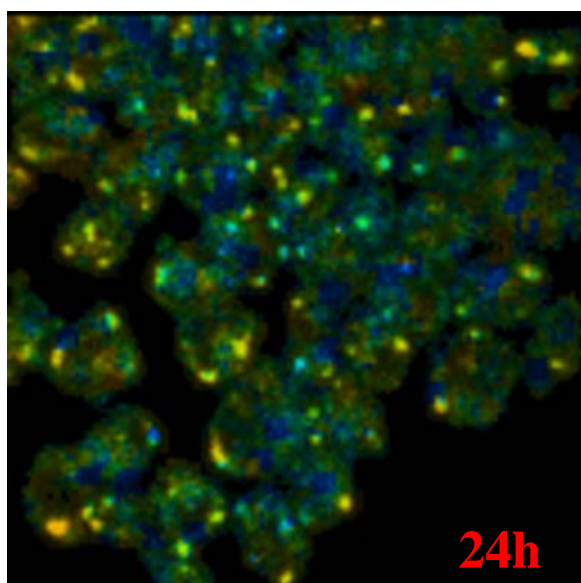
Fig. 4 mTHPC (7.5 µM) confocal fluorescence images in MCF-7 cell at 3 h (up) and 24 h (down) incubation times (left). Histograms of mTHPC fluorescence lifetime distribution as a function of the number of detected photons for the field of view (right). Incubation at 37 °C. The different colours on the images to the left correspond to various lifetimes as shown in histograms.

Table 2. Fluorescence lifetimes and photobleaching constants of mTHPC in MCF-7 cells at different incubation times.

Lifetimes		
3 h	24 h	
	diffuse	spots
$\tau_1 = 0.10 \pm 0{,}003$ ns (0.35)[*] $\tau_2 = 8.69 \pm 0{,}41$ ns (0.65)	$\tau_1 = 1{,}03 \pm 0{,}37$ ns (0.63) $\tau_2 = 3.92 \pm 0{,}54$ ns (0.37)	$\tau_1 = 0.31 \pm 0{,}22$ ns (0.55) $\tau_2 = 1.97 \pm 0{,}35$ ns (0.45)
Photobleaching		
3 h	24 h	
$k = (6.4 \pm 0.4) \times 10^3$ s^{-1}	$k_1 = (78 \pm 34) \times 10^3$ s^{-1} $k_2 = (0.6 \pm 0.2) \times 10^3$ s^{-1} [**]	

[*] The pre-exponential factors.

[**] The pre-exponential factors are $A_1 = 0.2 \pm 0.09$ and $A_2 = 0.8 \pm 0.08$.
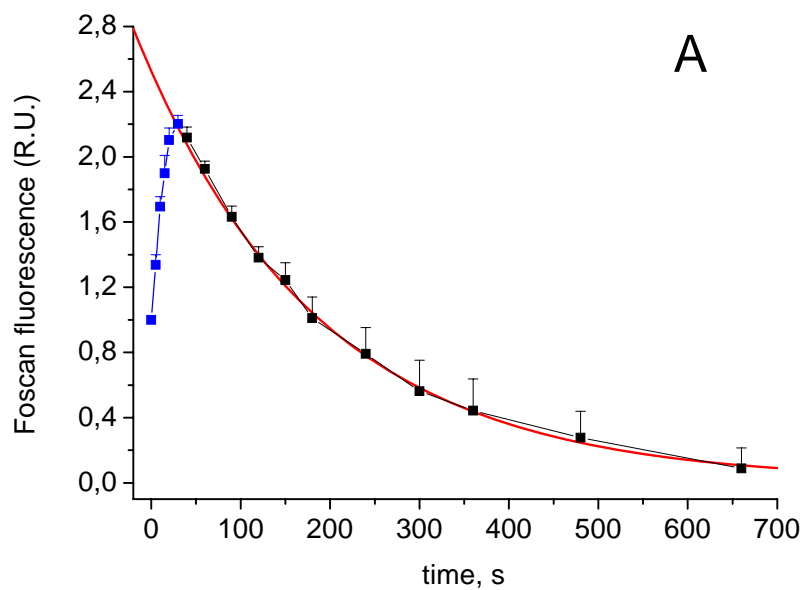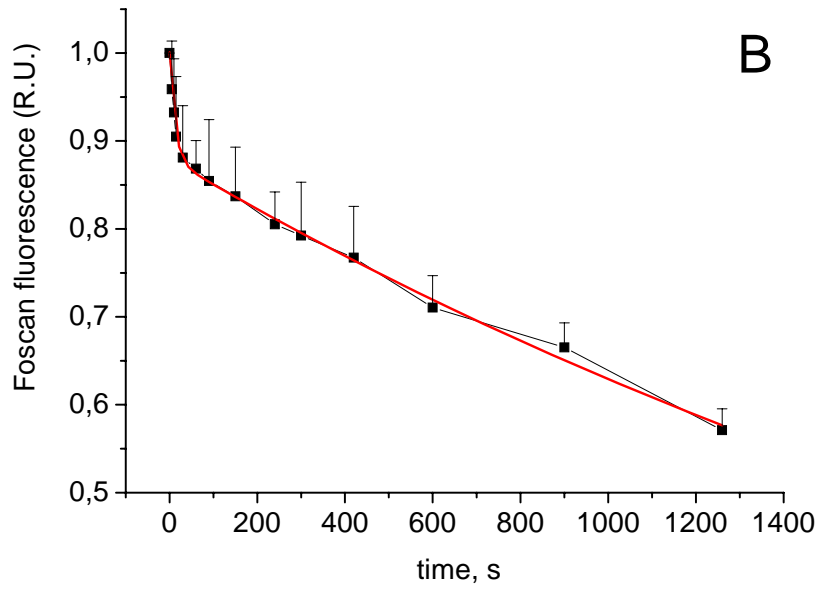
Fig. 5 Photobleaching kinetics of mTHPC (1.5 µM) in MCF-7 cells monolayers. A – incubation 3 h, B - incubation 24 h. Photobleaching parameters are presented in Table 2.
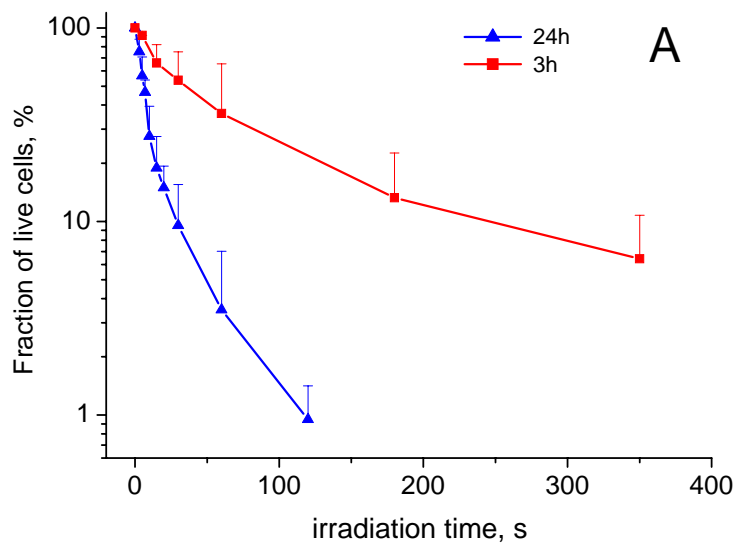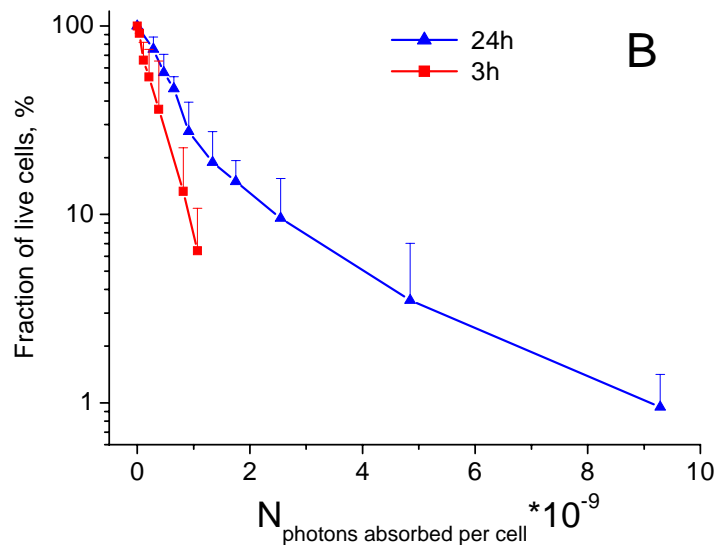
Fig. 6. The MCF-7 cell survival curves at 3h and 24h pre-incubation times (clonogenic assay) after mTHPC -PDT (1.5 µM) treatment (laser diode 650 nm, 2.12 mW/cm^2 in monolayer) as a function of irradiation time (A) and number of absorbed photons per cell by intracellular sensitizer (B).

References

Ambroz, M., A. J. MacRobert, J. Morgan, G. Rumbles, M. S. Foley and D. Phillips (1994). "Time-resolved fluorescence spectroscopy and intracellular imaging of disulphonated aluminium phthalocyanine." J. Photochem. Photobiol. B **22**(2): 105-17.

Aveline, B. M., R. M. Sattler and R. W. Redmond (1998). "Environmental effects on cellular photosensitization: correlation of phototoxicity mechanism with transient absorption spectroscopy measurements." Photochem Photobiol **68**(1): 51-62.

Ball, D. J., S. R. Wood, D. I. Vernon, J. Griffiths, T. M. Dubbelman and S. B. Brown (1998). "The characterisation of three substituted zinc phthalocyanines of differing charge for use in photodynamic therapy. A comparative study of their aggregation and photosensitising ability in relation to mTHPC and polyhaematoporphyrin." J. Photochem. Photobiol. B **45**(1): 28-35.

Belitchenko, I., V. Melnikova, L. Bezdetnaya, H. Rezzoug, J. L. Merlin, A. Potapenko and F. Guillemin (1998). "Characterization of photodegradation of meta-tetra(hydroxyphenyl)chlorin (mTHPC) in solution: biological consequences in human tumor cells." Photochem Photobiol **67**(5): 584-90.

Bonnett, R., B. D. Djelal and N. Angelina (2001). "Physical and chemical studies related to the development of m-THPC (FOSCAN®) for the photodynamic therapy (PDT) of tumours." J. Porphyrins Phthalocyanines **5**(8): 652-661.

Bonnett, R., B. D. Djelal, P. A. Hamilton, G. Martinez and F. Wierrani (1999). "Photobleaching of 5,10,15,20-tetrakis(m-hydroxyphenyl)porphyrin (m-THPP) and the corresponding chlorin (m-THPC) and bacteriochlorin(m-THPBC). A comparative study." J. Photochem. Photobiol. B **53**(1-2): 136-143.

Bonnett, R., R. D. White, U. J. Winfield and M. C. Berenbaum (1989). "Hydroporphyrins of the meso-tetra(hydroxyphenyl)porphyrin series as tumour photosensitizers." Biochem J **261**(1): 277-80.

Borovkov, V. V., M. Anikin, K. Wasa and Y. Y. Sakata (1996). "Structurally controlled porphyrin-aggregation process in phospholipid membranes." Photochem. Photobiol. **63**(4): 477–482.

Brown, S. B., M. Shillcock and P. Jones (1976). "Equilibrium and kinetic studies of the aggregation of porphyrins in aqueous solution." Biochem. J. **153**(2): 279-285.

Connelly, J. P., S. W. Botchway, D. P. L. Kunz, A. W. Parker and A. J. MacRobert (2001). "Time-resolved fluorescence imaging of photosensitiser distributions in mammalian cells using a picosecond laser line-scanning microscope." J. Photochem. Photobiol. A Chem. **142**: 169–175.

Coutier, S., L. N. Bezdetnaya, T. H. Foster, R. M. Parache and F. Guillemin (2002). "Effect of irradiation fluence rate on the efficacy of photodynamic therapy and tumor oxygenation in meta-tetra (hydroxyphenyl) chlorin (mTHPC)-sensitized HT29 xenografts in nude mice." Radiat Res **158**(3): 339-45.

Coutier, S., S. Mitra, L. N. Bezdetnaya, R. M. Parache, I. Georgakoudi, T. H. Foster and F. Guillemin (2001). "Effects of fluence rate on cell survival and photobleaching in meta-tetra-(hydroxyphenyl)chlorin-photosensitized Colo 26 multicell tumor spheroids." Photochem Photobiol **73**(3): 297-303.

Dougherty, T. J., C. J. Gomer, B. W. Henderson, G. Jori, D. Kessel, M. Korbelik, J. Moan and Q. Peng (1998). "Photodynamic therapy." J Natl Cancer Inst **90**(12): 889-905.

Foster, T. H., B. D. Pearson, S. Mitra and C. E. Bigelow (2005). "Fluorescence anisotropy imaging reveals localization of meso-tetrahydroxyphenyl chlorin in the nuclear envelope." Photochem Photobiol **81**(6): 1544-7.

Fowler, J. F. (1964). "Differences in Survival Curve Shapes for Formal Multi-target and Multi-hit Models." Phys. Med. Biol. **9**(2): 177–188.

Grahn, M. F., A. McGuinness, R. Benzie, R. Boyle, M. L. de Jode, M. G. Dilkes, B. Abbas and N. S. Williams (1997). "Intracellular uptake, absorption spectrum and stability of the bacteriochlorin photosensitizer 5,10,15,20-tetrakis (m-hydroxyphenyl)bacteriochlorin (mTHPBC). Comparison with 5,10,15,20-tetrakis(m-hydroxyphenyl)chlorin (mTHPC)." J. Photochem. Photobiol. B **37**(3): 261-266.

Hadjur, C., N. Lange, J. Rebstein, P. Monnier, H. van den Bergh and G. Wagnières (1998). "Spectroscopic studies of photobleaching and photoproduct formation of meta(tetrahydroxyphenyl) chlorin (m-THPC) used in photodynamic therapy. The production of singlet oxygen by m-THPC." J. Photochem. Photobiol. B **45**(2-3).

Howe, L., A. Sucheta, O. Einarsdottir and J. Z. Zhang (1999). "Time-resolved studies of the excited-state dynamics of meso-tetra(hydroxylphenyl)chlorin in solution." Photochem Photobiol **69**(6): 617-23.

Kress, M., T. Meier, R. Steiner, F. Dolp, R. Erdmann, U. Ortmann and A. Ruck (2003). "Time-resolved microspectrofluorometry and fluorescence lifetime imaging of photosensitizers using picosecond pulsed diode lasers in laser scanning microscopes." J Biomed Opt **8**(1): 26-32.

Lakowicz, J. R. (1999). "Principles of Fluorescence Spectroscopy." Kluwer.

Lindqvist, L. (1960). "A flash photolysis study of fluorescein." Arkiv for Kemi. **16**: 79-138.

Lovat, L. B., N. F. Jamieson, M. R. Novelli, C. A. Mosse, C. Selvasekar, G. D. Mackenzie, S. M. Thorpe and S. G. Bown (2005). "Photodynamic therapy with m-tetrahydroxyphenyl chlorin for high-grade dysplasia and early cancer in Barrett's columnar lined esophagus." Gastrointest Endosc **62**(4): 617-23.

Ma, L., J. Moan and K. Berg (1994). "Evaluation of a new photosensitizer, meso-tetra-hydroxyphenyl-chlorin, for use in photodynamic therapy: a comparison of its photobiological properties with those of two other photosensitizers." Int. J. Cancer **57**(6): 883-888.

Melnikova, V. O., L. N. Bezdetnaya, A. Y. Potapenko and F. Guillemin (1999). "Photodynamic properties of meta-tetra(hydroxyphenyl)chlorin in human tumor cells." Radiat Res **152**(4): 428-35.

Merzlyak, M. N. and K. R. Naqvi (2000). "On recording the true absorption spectrum and the scattering spectrum of a turbid sample: application to cell suspensions of the cyanobacterium Anabaena variabilis." J Photochem Photobiol B **58**(2-3): 123-9.

Moore, C. M., T. R. Nathan, W. R. Lees, C. A. Mosse, A. Freeman, M. Emberton and S. G. Bown (2006). "Photodynamic therapy using meso tetra hydroxy phenyl chlorin (mTHPC) in early prostate cancer." Lasers Surg Med **38**(5): 356-63.

Peng, Q. and J. M. Nesland (2004). "Effects of photodynamic therapy on tumor stroma." Ultrastruct Pathol **28**(5-6): 333-40.

Redmond, R. W., E. J. Land and T. G. Truscott (1985). "Aggregation effects on the photophysical properties of porphyrins in relation to mechanisms involved in photodynamic therapy." Adv. Exp. Med. Biol. **193**: 293-302.

Ricchelli, F. (1995). "Photophysical properties of porphyrins in biological membranes." J Photochem Photobiol B **29**(2-3): 109-18.

Scully, A. D., R. B. Ostler, A. J. MacRobert, A. W. Parker, C. de Lara, P. O'Neill and D. Phillips (1998). "Laser line-scanning confocal fluorescence imaging of the photodynamic action of aluminum and zinc phthalocyanines in V79-4 Chinese hamster fibroblasts." Photochem Photobiol **68**(2): 199-204.

Scully, A. D., R. B. Ostler, D. Phillips, P. O'Neill, A. W. Parker and A. J. MacRobert (1997). "Application of fluorescence lifetime imaging microscopy to the investigation of intracellular PDT mechanisms." Bioimaging **5**: 9–18.

Song, L., E. J. Hennink, I. T. Young and H. J. Tanke (1995). "Photobleaching kinetics of fluorescein in quantitative fluorescence microscopy." Biophys. J. **68**(6): 2588-600.

Tanielian, C., C. Schweitzer, R. Mechin and C. Wolff (2001). "Quantum yield of singlet oxygen production by monomeric and aggregated forms of hematoporphyrin derivative." Free Radic Biol Med **30**(2): 208-12.

Teiten, M. H., S. Marchal, M. A. D'Hallewin, F. Guillemin and L. Bezdetnaya (2003). "Primary photodamage sites and mitochondrial events after Foscan photosensitization of MCF-7 human breast cancer cells." Photochem Photobiol **78**(1): 9-14.

Theodossiou, T. and A. J. MacRobert (2002). "Comparison of the photodynamic effect of exogenous photoprotoporphyrin and protoporphyrin IX on PAM 212 murine keratinocytes." Photochem. Photobiol. **76**(5): 530-7.

Theodossiou, T., M. D. Spiro, J. Jacobson, J. S. Hothersall and A. J. Macrobert (2004). "Evidence for intracellular aggregation of hypericin and the impact on its photocytotoxicity in PAM 212 murine keratinocytes." Photochem. Photobiol. **80**(3): 438-43.

Triesscheijn, M., M. Ruevekamp, M. Aalders, P. Baas and F. A. Stewart (2005). "Outcome of mTHPC mediated photodynamic therapy is primarily determined by the vascular response." Photochem. Photobiol. **81**(5): 1161-7.

Usui, Y., K. Itoh and M. Koizumi (1965). "Switch-over of the mechanism of the primary rocesses in the photo-oxidation of xanthene dyes as revealed by the oxygen consumption experiments." Bull. Chem. Soc. Jpn. **38**: 1015-1022.

IV.5. Theoretical and experimental study of the effects of solvent on the electronic structure of tetrapyrrole compounds: application for the determination of the structure of aggregates

INTRODUCTION

The ω-technique (Wheland and Mann 1949) is a modified version of the Hückel molecular orbitals theory (MOH) (Hückel 1931). This method takes into account the relationship between calculated parameters and physico-chemical properties of atoms in molecules, such as electronegativity (Streitwieser 1961). In many works the reactive field of solvents is estimated with the help of additional induction parameters (Streitwieser 1961), that were introduced as corrections to coloumb integrals of carbon atoms, that are themselves connected with heteroatoms. Regardless of the fact that corrections were added using simple MOH theory, in many cases the results were consistent with those obtained using self consisted field (SCF) methods (Streitwieser 1961; Murrell et al. 1970). Hence, the influence of universal interactions (UI) (Reichardt 1988) on a molecule surrounded by solvent shell, can be taken into account as corrections to coloumb integrals of the molecule in question.

The compounds investigated in this study (meta-tetra(hydroxyphenyl)porphine (mTHPP), meta-tetra(hydroxyphenyl)bacteriochlorin(mTHPBC)and meta-tetra (hydroxyphenyl)chlorin (mTHPC)) are second-generation photosensitizers, which are used in photodynamic therapy (PDT). Photodynamic therapy (PDT) is a treatment modality based on the cytotoxic effect occurring on the target tissues by interaction of a photosensitizer with light in the presence of oxygen (Henderson and Dougherty 1992). The aggregation state of the photosensitizer is very important since it has been shown that aggregates have a reduced photodynamic activity as opposed to monomers (Bezdetnaya et al. 1996). In aqueous media, most of the tetrapyrrolic photosensitizers form dimers and higher micelle-like aggregates (Redmond et al. 1985). Depending on the steric factors and the origin of interactions between tetrapyrrolic molecules, several types of aggregates can be formed. The most widely reported are H-and J-aggregates (Parkash et al. 1998).

The present study, based on the application of a modified ω-technique as published previously by Krivulko et al (Krivulko and Klishchenko 2006), aims to define the electronic properties of tetrapyrrole compounds in different solvents and to determine the structure of their aggregates. This theoretical model utilizes a supermolecular approach, where the solute-solvent complex, with a fixed geometry consisting of a central solute molecule surrounded by

solvent molecules, can be treated as one supermolecule (Freitas et al. 1992). In this study we have proposed a slightly modified model in order to establish the relationship between the structure and the electronic spectra of tetrapyrroles in solution.

THEORETICAL MODEL

1 Universal interactions in the context of ω-technique.

In ω-technique (first approximation of SCF method) the values of coloumb integrals of atoms α are determined as follows:

$$\alpha = \alpha_0 + \omega_0 \beta_0 (n-q), \tag{1}$$

where α_0 – initial value of coloumb integral, dependent on electronegativity of an isolated atom, n - number of π - electrons, provided by an atom to a conjugated system of molecule, q - π-electron charge on the atom, β_0 – resonance integral for C-C bonds in benzole, ω_0 - parameter characterizing the one-center integral of inter-electron repulsion in the atom (Streitwieser 1961).

We first consider the interaction of a solute molecule with a dipole solvent molecule (Fig. 1). We propose ion-dipole interactions between solute atoms (ions) and solvent molecules (dipoles) since the size of tertrapyrroles is much larger than that of solvent molecules.
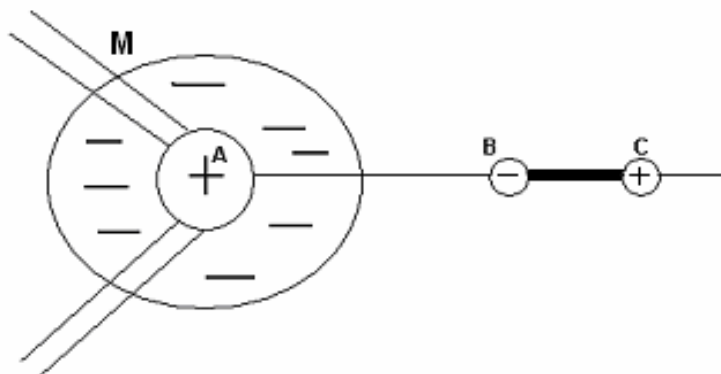
Figure 1. Scheme of solvent molecule interaction with sensitizers atom. M - molecule, A - atom of the molecule, B and C are the negative and positive poles of solvent molecule

When the positive pole of a dipole approaches molecule M, the electron density on atom A increases. Inversely, when the negative pole approaches M, the electron density on the neighboring atom will decrease. Thus, the value of the coloumb integral of the neighboring atom changes and eq. 1 becomes eq. 2 :

$$\alpha = \alpha_0 + \omega_0\beta_0(n-(1+\eta)q) \qquad (2)$$

where η – relative charge change (RCC) on atom A due to the external dipole. The parameter η can be represented as the sum:

$$\eta = \eta_{or} + \eta_{ind} + \eta_{disp} \qquad (3)$$

where η_{or}, η_{ind}, η_{disp}, –RCC on atom A due to orientation, induction and dispersion interactions respectively. When we assume that the RCC value, determined by an interaction, is proportional to the energy of this interaction, η_{or} will be defined as:

$$\eta_{or} = -sd(n-(1+\eta_{or}+\eta_{ind}+\eta_{disp})q) \qquad (4)$$

where d – dipole moment of the solvent, s – positive constant that determines the sign of η with different dipole orientations. From our previous work (Krivulko and Klishchenko 2006) the value of constant s = 0.0867 Debye^{-1} was obtained. A combination of eq. 2 and eq. 4 results in eq. 5 as follows:

$$\alpha = \alpha_0 + \omega_0\beta_0(n-(1+\eta_{ind}+\eta_{disp})q)/(1-sdq) \qquad (5)$$

For the atoms of the molecule M in an excited state a similar equation can be proposed:

$$\alpha = \alpha_0 + \omega\beta_0(n-(1+\eta_{ind}^*+\eta_{disp}^*)q)/(1-sdq) \qquad (6)$$

where η_{ind}^*, η_{disp}^*, – RCC of atom A in the excited state determined, by induction and dispersion interactions respectively, ω – parameter that determines the interelectron repulsion in the molecule M in the excited state. The value of ω in the ground and in the second exited states (Soret band) were 0.42 and 0.25, respectively.

In this model we use four parameters η_{ind}, η_{disp}, η_{ind}^*, η_{disp}^* to describe induction and dispersion interactions of molecule M with a solvent molecule. However, since we use the difference between molecular orbital (MO) energies for the calculation of electronic transitions, it can be assumed that the values of parameters η_{ind}, η_{disp} are equal to zero. Therefore the parameters η_{ind}^*, η_{disp}^* will characterize the influence of induction and dispersion interactions both in ground state and excited state.

Many dye molecules form H-bonds with the shell of polar solvents. As H-bonds have a partially covalent nature, they exhibit similar properties to simple chemical bonds, particularly the existence of an overlap between electron shells of interacting atoms (Pimentel and McLellan 1960). In the MOH theory the values of resonance integrals (RI) β are evaluated from the overlap of π–electron shells of atoms that form π-bonds (Dewar 1969). In most cases there exists a proportionality between β and overlap integral (OI) S (Streitwieser 1961). The values of OI and RI for $2p_z$ atom orbitals of two carbon atoms in the form of Hartree-Fock as a function of bond length has been calculated by Mulliken et al (Mulliken et al. 1949). For other atom pairs, like N-N or O-O pairs, the value of RI decreases faster with

interatom distance being about 80 % lower at the same distance for C-C pair (Mulliken et al. 1949). Taking into account that in most cases H-bond length varies from 2.5Å to 2.8 Å (Pimentel and McLellan 1960; Terenin 1967), it can be concluded that RI values for donor and acceptor atoms of hydrogen bonds are within the interval $0.10\beta_0$ - $0.20\beta_0$, (β_0 - standard resonance integral for C-C bond in benzole).

We have previously applied an ion-dipole model in order to assess 3-aminophthalimide absorption spectra in different solvents (Krivulko and Klishchenko 2006). This study allowed to obtain the values of different RI as shown in Table 1. It should be noted that the values of RI found experimentally (Table 1) are in good agreement with that evaluated from OI (Mulliken 1949), thus confirming the validity of modified ω-technique.

The energy of the first electron transition (0-0) depends linearly on the difference between MO energy levels:

$$\Delta E = \beta_0 \Delta x + \gamma \qquad (7)$$

where Δx – difference between the highest and lowest occupied MO energy levels (HOMO, LUMO), γ – parameter determined by the magnitude of singlet - triplet splitting of molecular energy levels in the first excited states and by effects of configuration interactions between energy levels (Streitwieser 1961). The coefficients β_0 and γ are semiempiric parameters, whose values give the best description of the characteristics of solute molecules. Direct calculations of 3-aminophthalimide in heptan using the proposed modified ω-technique show that the frequency of 0-0 transition $\Delta\nu_{0-0}$ depends linearly on $\eta_S = \eta_{ind}^* + \eta_{disp}^*$ and can be approximated as (Krivulko and Klishchenko 2006):

$$\Delta x = a(sd,\sigma_i,\delta_j)\eta_S + b(sd,\sigma_i,\delta_j) \qquad (8)$$

where $a(sd,\sigma_i,\delta_j)$, $b(sd,\sigma_i,\delta_j)$ – functions that depend on the product $s \times d$ and on RI of all intramolecular σ_i $i \in [1,I]$ and intermolecular δ_j $j \in [1,J]$ H-bonds in a molecule-solvent complex. The particular structure of these two functions depends on the effective electronic Hamiltonian of the molecular complex in question. The calculated (points) and linear fit (line) data are presented in the Fig. 2.
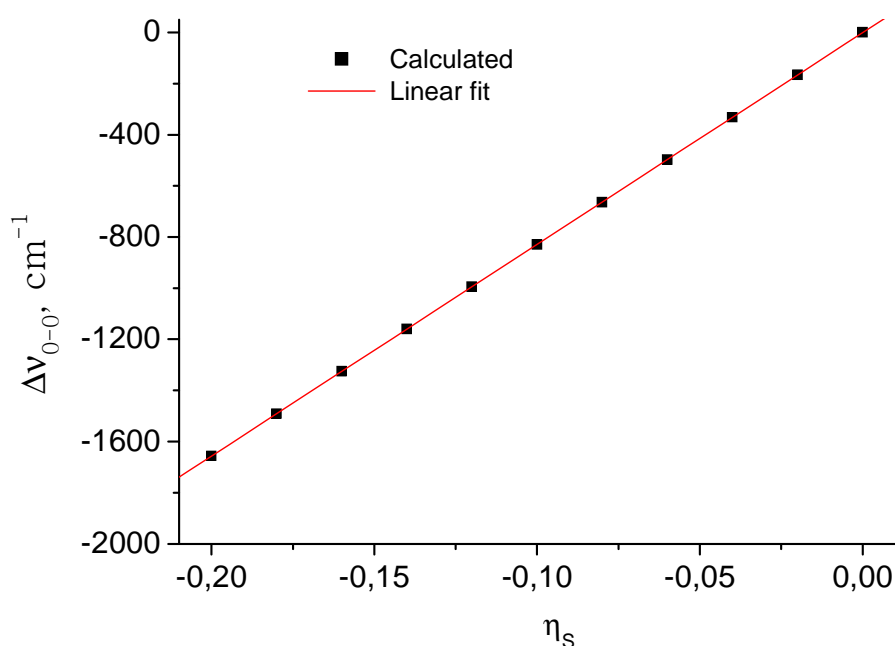
Figure 2. The frequency of 3-aminophthalimide 0-0 transition in heptan as a function of η_S.

A combination of eq. 8 and eq. 7 results in eq.9:

$$\Delta E = \beta(a(sd,\sigma_i,\delta_j)\eta_S + b(sd,\sigma_i,\delta_j)) + \gamma \qquad (9)$$

Using eq. 9 the magnitude of spectral shift of 0-0 transition $\Delta\nu$ of a molecule after transfer from the gas phase into the solvent is determined as eq 10:

$$\Delta\nu = \beta\{a(sd,\sigma_i,\delta_j)\eta_S + b(sd,\sigma_i,\delta_j) - b(sd,\sigma_{0i},0)\} \qquad (10)$$

In the case of a non polar solvent $(d = 0)$ eq.10 becomes eq. 11:

$$\Delta\nu = \beta a(0,\sigma_{0i},0)\eta_S \qquad (11)$$

When considering the theory of universal interactions for the description of the spectral shift in non-polar solvents, the following functions are used (Bakhshiev 1972):

$$f(n_p) = (n_p^2-1)/(n_p^2+2) \qquad (12)$$

$$g(n_p) = (n_p^2-1)/(2n_p^2+1) \qquad (13)$$

where n_p - refractive index of a solvent. The spectral shift, which is determined by dispersion and induction parameters, is proportional to $f(n_p)$. A spectral shift which is dependent on inductive-resonance interactions, is proportional to $g(n_p)$ (Bakhshiev 1972). Hence eq.14:

$$\eta_S = C_1 f(n_p) + C_2 g(n_p) \qquad (14)$$

where C_1 and C_2 – parameters that are dependent on the properties of solute molecules. The $g(n_p)$ function has been used in many studies since it takes into account the bathochromic shift. Therefore:

$$\eta_S = (C_1(2n_p^2+1)/(n_p^2+2)+C_2)g(n_p) \qquad (15)$$

Within the interval of 1.3 to 1.6, function $(2n_p^2+1)/(n_p^2+2)$ can be considered as constant. Hence eq.16:

$$\eta_S = \Gamma g(n_p) \qquad (16)$$

where Γ- parameter depending on the solute molecule. It should be mentioned that with regard to the theory of universal interactions (Bakhshiev 1972) the dependency of the spectral shift on the dipole moment of the solvent is determined by orientational forces. In our model such interactions are presented explicitly in functions $a(sd,\sigma_i,\delta_j)$ and $b(sd,\sigma_i,\delta_j)$. Therefore eq. 16 is correct for solvents with arbitrary dipole moment.

2 Functional method of least squares (FMLS).

The energy of spectral transition of a molecule in a solvent i depends linearly on the difference of appropriate roots of the characteristic equation $\triangle x_i$:

$$\triangle E_i = \beta \times \triangle x_i + \gamma \qquad (17)$$

Since the values of RI for intermolecular H-bonds within a sensitizer-solvent complex are fixed, $\triangle x_i$ can be presented as:

$$\triangle x_i = a(\sigma_i)\Gamma g(n_p) + b(\sigma_i) \qquad (18)$$

Combining eq. 17 and eq. 18 we obtain:

$$\triangle E_i = \beta(a(\sigma_i)\Gamma g(n_p) + b(\sigma_i)) + \gamma \qquad (19)$$

In the presence of intermolecular H-bonds, various types of solvents have different influence on electronic parameters. In many cases both the enthalpy and RI value of such H-bonds are not known. Therefore, we use polynomial interpolation for coefficients $a(\sigma)$ and $b(\sigma)$:

$$a(\sigma) = \sum_{i=0}^{N} A_i \sigma^i, b(\sigma) = \sum_{i=0}^{N} B_i \sigma^i \qquad (20)$$

where A_i and B_i- coefficients of decomposition, σ_i – RI for intramolecular H-bond whose value varies during the search of the optimal solution. For the construction of function $\triangle x_i$ we used N = 5. To find the values of unknown parameters in eq. 19 we used all experimental $\triangle E_i$. Application of least squares method results in:

$$\beta_0 = \frac{\sum_{i=1}^{N}(\Delta x_i - \langle x_i \rangle)\Delta E_i}{\sum_{i=1}^{N}(\Delta x_i - \langle x_i \rangle)^2} = \beta_0(\Gamma, \sigma_i) \qquad (21)$$

$$\gamma = \langle \Delta E_i \rangle - \beta_0 \langle \Delta x_i \rangle = \gamma(\Gamma, \sigma) \qquad (22)$$

where i – solvent number N - total number of solvents, Δx_i - MO energy gap corresponding to the solvent i. For characterization of experimental points deviations from the straight line the following function Φ was introduced:

$$\Phi = \sum_{i=1}^{N}(\Delta E_i - \beta_0 \Delta x_i - \gamma)^2 = \Phi(\Gamma, \sigma) \qquad (23)$$

In the context of this model, it is logic to suppose that optimal values of parameters Γ and σ_i correspond to global minimum of the function Φ in three dimensional space (Φ, Γ, σ). This method has enabled us to analyse the presence of intramolecular H-bonds in tetrapyrrole ring (TPR) of three compounds.

MATERIAL AND METHODS

2.1. Chemicals

The photosensitizers Foscan® (mTHPC, temoporfin) and mTHPBC were kindly provided by Biolitec AG (Jena, Germany) and mTHPP was purchased from Sigma (USA). Solvents dichlormethane, hexane, heptane, acetone, benzene, methanol, water, acetonitrile, toluene, ethanol, trichlormethane, dimethylsulfoxide, tetrahydrofuran were purchased from Sigma (USA).

2.2. Spectroscopic measurements.

Upon dilution of sensitizer powder in a solvent the absorption spectra were recorded on a Perkin-Elmer Lambda 35 spectrophotometer (Perkin-Elmer, USA), using a 10 mm quartz cuvette. Data were collected with a 0.1 nm interval using 0.5 nm bandpasses. The absorption spectra of dimers were obtained in ethanol-water mixtures by gradually increasing the water content till the appearance of a new band. The calculations were performed using Matlab 4.0 software and the fitting was obtained with Origin 7.5.

RESULTS AND DISCUSSION

On the basis of an electrostatic model, we can assume that intermolecular H-bond formation in TPR of the three compounds is unfavorable. Consequently, for the construction

of Hamiltonians of complexes, we hypothesized that intermolecular H-bonds could only arise on hydroxyl groups. Accordingly, RI values of intramolecular H-bond should not depend on the solvent. The hydrogen atoms can form four intramolecular H-bonds between imide groups and adjacent nitrogen atoms in TPR. The parameter σ is RI for intramolecular H-bond. Variation of σ in Hamiltonian permits to obtain the dependency $\triangle x = \triangle x(\sigma)$. This curve was fitted to the polynomial equation (eq. 18). For calculations we used the values of 58, 56 and 54 π-electrons in conjugated system for mTHPP, mTHPC and mTHPBC, respectively. Table 1 represents the values of parameters d – dipole moments, parameter s×d and RI (δ) values for intermolecular H-bonds of sensitizer molecules according to the solvent.

Simple electrostatic model of H-bonds, applied to specific intermolecular interactions of TPR with solvent molecules showed that due to steric factors the formation of such intermolecular H-bonds is impeded. This conclusion was derived from the analysis of enthalpy dependence of H-bonds formation on polar angles.

Functions $\triangle x_i = \triangle x_i(\Gamma, \sigma)$ obtained by FMLS method using polynomial interpolation (eq. 20), that describe the position of mTHPC Soret band maximum in various solvents, are represented in Table 2.
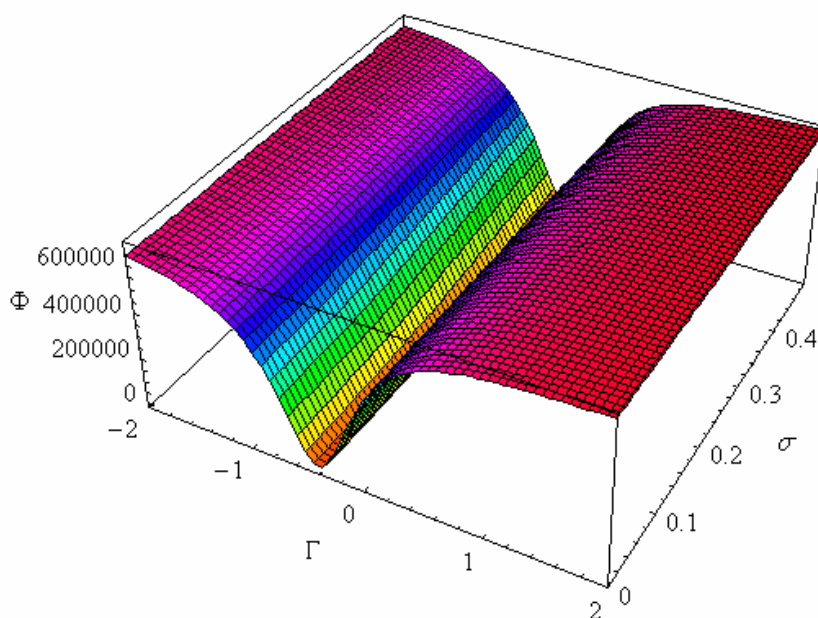
Figure 3. Graphical presentation of function $\Phi(\Gamma, \sigma)$ for mTHPC.

Table 1. Solvents parameters: function g (eq. 13), s×d (d - dipole moment) and intermolecular H-bonds RI (δ) values.

Solvent	g	s×d	δ
aniline	0.251	0.130	0.20
acetone	0.180	0.234	0.20
acetonitrile	0.175	0.307	0.10
benzole	0.228	0	0
dichlormethane	0.203	0.135	0
dimethylsulfoxide	0.221	0.351	0.20
ethanol	0.181	0.151	0.20
fluorobenzene	0.218	0.128	0.25
methanol	0.169	0.148	0.20
pyridine	0.230	0.206	0.20
tetrahydrofuran	0.198	0.151	0.20
toluene	0.226	0.0260	0
ethanol-water[*]	0.171	0.154	0.20

[*] water content – 86 % (v/v).

The global minimum of the function $\Phi(\Gamma,\sigma)$ allows us to obtain the values of semi-empirical parameters for the three sensitizer used. Figure 3 represents these data for mTHPC. The optimal values for mTHPC are $\Gamma = -0.357$, $\sigma = 0,301$ and $\Phi = 6597 cm^{-2}$. For mTHPP $\Gamma = 0.151$, $\sigma = 0,387$ and $\Phi = 8474 cm^{-2}$, and for mTHPBC $\Gamma = 0.289$, $\sigma = 0,405$ and $\Phi = 153522 cm^{-2}$. The value of RI for intermolecular H-bond $\sigma = 0,301$, indicates the existence of strong H-bonds. High RI values for all three compounds point out that the enthalpy of H-bond formation is high, about 10 kcal/mole.

The calculated dependency of Soret band maxima transition energy on MO energy levels difference for mTHPC, mTHPP and mTHPBC are described by eq. 24, 25 and 26, respectively (eq. 7):

$$\Delta E = -51508x - 6462 \ (cm^{-1}) \qquad (24)$$

$$\Delta E = 150814x + 141881 \ (cm^{-1}) \qquad (25)$$

$$\Delta E = 86952x + 81854 \ (cm^{-1}) \qquad (26)$$

Table 2 Function $\triangle x_i = \triangle x_i(\Gamma, \sigma)$ describing the position of mTHPC Soret band maximum in various solvents.

Solvent	$\triangle x_i = \triangle x_i(\Gamma, \sigma)$
aniline	$-0.609203 + 0.000645167\,\sigma - 0.0427875\,\sigma^2 + 0.213042\,\sigma^3 - 0.78625\,\sigma^4 + 0.894167\,\sigma^5 + 0.251\,\Gamma\,(-0.31331 + 0.012695\,\sigma - 0.266125\,\sigma^2 + 1.52958\,\sigma^3 - 3.0875\,\sigma^4 + 2.09167\,\sigma^5)$
acetone	$-0.613381 + 0.00200317\,\sigma - 0.0564292\,\sigma^2 + 0.321875\,\sigma^3 - 0.977083\,\sigma^4 + 0.980833\,\sigma^5 + 0.18\,\Gamma\,(-0.36116 + 0.01363\,\sigma - 0.292417\,\sigma^2 + 1.61792\,\sigma^3 - 3.05833\,\sigma^4 + 1.90833\,\sigma^5)$
acetonitrile	$-0.617197 + 0.00278317\,\sigma - 0.0617625\,\sigma^2 + 0.373875\,\sigma^3 - 1.04375\,\sigma^4 + 0.980833\,\sigma^5 + 0.175\,\Gamma\,(-0.40482 + 0.0141467\,\sigma - 0.31675\,\sigma^2 + 1.7125\,\sigma^3 - 3.075\,\sigma^4 + 1.78333\,\sigma^5)$
benzole	$-0.605438 - 0.00129617\,\sigma - 0.0198375\,\sigma^2 + 0.0387917\,\sigma^3 - 0.43625\,\sigma^4 + 0.6825\,\sigma^5 + 0.228\,\Gamma\,(-0.26888 + 0.0106617\,\sigma - 0.223792\,\sigma^2 + 1.33375\,\sigma^3 - 2.82083\,\sigma^4 + 2.00833\,\sigma^5)$
dichlormethane	$-0.609434 + 0.0007355\,\sigma - 0.0445958\,\sigma^2 + 0.224333\,\sigma^3 - 0.810417\,\sigma^4 + 0.911667\,\sigma^5 + 0.203\,\Gamma\,(-0.31526 + 0.01338\,\sigma - 0.280083\,\sigma^2 + 1.605\,\sigma^3 - 3.24167\,\sigma^4 + 2.2\,\sigma^5)$
dimethylsulfoxide	$-0.620023 + 0.00308533\,\sigma - 0.0618\,\sigma^2 + 0.386583\,\sigma^3 - 1.035\,\sigma^4 + 0.938333\,\sigma^5 + 0.221\,\Gamma\,(-0.43692 + 0.0141367\,\sigma - 0.32825\,\sigma^2 + 1.74042\,\sigma^3 - 2.975\,\sigma^4 + 1.59167\,\sigma^5)$
ethanol	$-0.609967 + 0.0009865\,\sigma - 0.0469208\,\sigma^2 + 0.242583\,\sigma^3 - 0.842917\,\sigma^4 + 0.926667\,\sigma^5 + 0.181\,\Gamma\,(-0.32191 + 0.0134733\,\sigma - 0.280583\,\sigma^2 + 1.59625\,\sigma^3 - 3.19167\,\sigma^4 + 2.14167\,\sigma^5)$
fluorobenzene	$-0.609182 + 0.000601833\,\sigma - 0.0427125\,\sigma^2 + 0.211375\,\sigma^3 - 0.78375\,\sigma^4 + 0.894167\,\sigma^5 + 0.218\,\Gamma\,(-0.31248 + 0.0129467\,\sigma - 0.27025\,\sigma^2 + 1.54917\,\sigma^3 - 3.125\,\sigma^4 + 2.11667\,\sigma^5)$
methanol	$-0.609858 + 0.000936167\,\sigma - 0.0464625\,\sigma^2 + 0.239625\,\sigma^3 - 0.83875\,\sigma^4 + 0.925833\,\sigma^5 + 0.169\,\Gamma\,(-0.32065 + 0.01285\,\sigma - 0.271917\,\sigma^2 + 1.55417\,\sigma^3 - 3.10833\,\sigma^4 + 2.08333\,\sigma^5)$
pyridine	$-0.612151 + 0.00168583\,\sigma - 0.0540958\,\sigma^2 + 0.300167\,\sigma^3 - 0.945417\,\sigma^4 + 0.975\,\sigma^5 + 0.23\,\Gamma\,(-0.34683 + 0.0138233\,\sigma - 0.291583\,\sigma^2 + 1.6275\,\sigma^3 - 3.14167\,\sigma^4 + 2.01667\,\sigma^5)$
tetrahydrofuran	$-0.609989 + 0.000908667\,\sigma - 0.0461\,\sigma^2 + 0.238417\,\sigma^3 - 0.835\,\sigma^4 + 0.921667\,\sigma^5 + 0.198\,\Gamma\,(-0.32188 + 0.0127017\,\sigma - 0.269625\,\sigma^2 + 1.54417\,\sigma^3 - 3.0875\,\sigma^4 + 2.06667\,\sigma^5)$
toluene	$-0.606113 - 0.000905833\,\sigma - 0.0248542\,\sigma^2 + 0.07625\,\sigma^3 - 0.514583\,\sigma^4 + 0.733333\,\sigma^5 + 0.226\,\Gamma\,(-0.27671 + 0.0116917\,\sigma - 0.241542\,\sigma^2 + 1.42458\,\sigma^3 - 2.99583\,\sigma^4 + 2.125\,\sigma^5)$
ethanol-water[*]	$-0.591467 - 0.00162949\,\sigma + 0.00951584\,\sigma^2 - 0.141044\,\sigma^3 + 0.0913168\,\sigma^4 + 0.17035\,\sigma^5 + 0.171\,\Gamma\,(-0.30092 + 0.00122416\,\sigma - 0.0370449\,\sigma^2 + 0.221648\,\sigma^3 - 0.230899\,\sigma^4 - 0.0524347\,\sigma^5)$

[*] water content – 86 % (v/v).

Using proposed model the electronic transitions of sensitizer aggregates can be calculated. The magnitude and the sign of aggregates spectral shift depend on their structure. Depending on the steric factors and the origin of interactions between tetrapyrrolic molecules, several types of aggregates can be formed. The most widely reported are H- and J-aggregates. Both of them are linear aggregate, for which the angle between monomer transition dipoles in the aggregate is zero (Fig. 4a). For J-aggregates the angle (φ) between the line connecting the centers and the direction of transition dipoles in the two neighboring molecules varies from 0 to π/2. For H-aggregates the angle φ is equal to π/2 (Parkash et al. 1998) (Fig. 4a). Another type of aggregates are "zigzag" aggregates, where photosensitizer molecules' planes are not parallel to each other (Parkash et al. 1998) (Fig. 4b).

a)

$\varphi = 0$ (J-aggregate) $\varphi = \pi/2$ (H-aggregate)
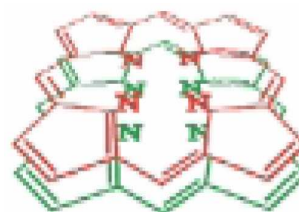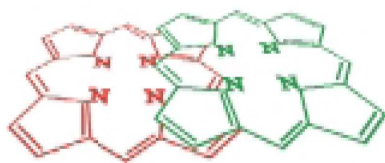
b)
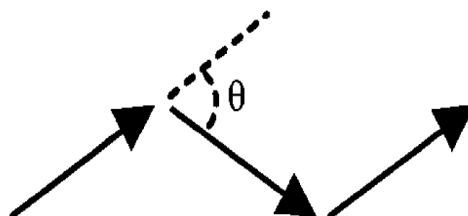
Fig. 4. The structure of typical molecular aggregates.

Using ethanol-water mixtures we obtained the dimers of sensitizers by gradual increase of water content. Non-covalent dimerization has a big impact on the electronic properties of molecules. Two molecules without interactions have identical arrays of MO {x_1, x_2, x_3, x_4 ...., x_n}. Dimerization leads to different MO arrays {x_1-a, x_1+a, x_2-b, x_2+b, x_3-c, x_3+c, x_4-d, x_4+d ...., x_n-t, x_n+t }. In other words, where two monomers show two identical MO levels x_k (HUMO), x_m (LUMO), dimers produce four different MO levels: x_k-r, x_k+r, x_m-p, x_m+p (Gurinovich et al. 1969). The most probable are the transitions { x_k-r $\longrightarrow$ x_m+p }and{ x_k+r $\longrightarrow$ x_m-p}, or the most blue or red shifted (Terenin 1967). With the current proposed ω approach, we were able to calculate and to confirm the existence of both energy levels. Direct calculations using modified ω-technique without any additional assumptions do not suggest the existence of the remaining two intermediate transitions.

The final decision about the type of dimers (one or two MO levels) for different molecules depends on parameter β, the number of experimental maxima in the Soret band and the direction of the shift as compared to the monomer solution. One maximum with red or

blue shift corresponds to J and H aggregates respectively, whereas two maxima correspond to zigzag aggregates.

To establish the nature of mTHPC, mTHPP and mTHPBC dimers in water/ethanol solutions, we undertook spectroscopic studies of these compounds in different solvents. Fig. 5 represents the experimental (points) and calculated (line) dependency of Soret band maximum transition energy on MO energy difference ($\triangle$x) for mTHPC, mTHPP and mTHPBC. For mTHPC and mTHPP only the experimental transitions for J-type dimers coincide well with the calculated values (Fig 5A, 5B). According to the Davidov theory (Davidov 1971) mTHPC and mTHPP dimers undergo $\{x_k\text{-}r \longrightarrow x_m\text{+}p\}$ transitions resulting in linear J-type dimer structure. The Soret band of mTHPBC dimers has two experimental maxima, thus its dimers have two MO levels suggesting a zigzag structure of linear aggregates (Terenin 1967). For calculation we considered that dimers of all three sensitizers were connected by means of hydrogen bonds between phenyl OH groups. The experimental data confirm this proposition. As shown in Fig 5C, experimental data do not exactly coincide with the theoretical cure, indicating that our model is more appropriate for J dimmers than zigzag dimers. This can probably be attributed to the presence of different angles between molecular planes in zigzag aggregates that are not taken into account in the present model.
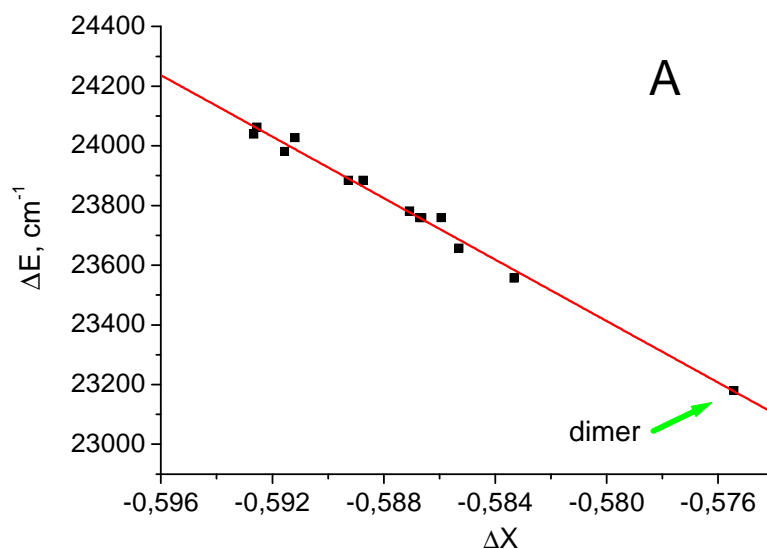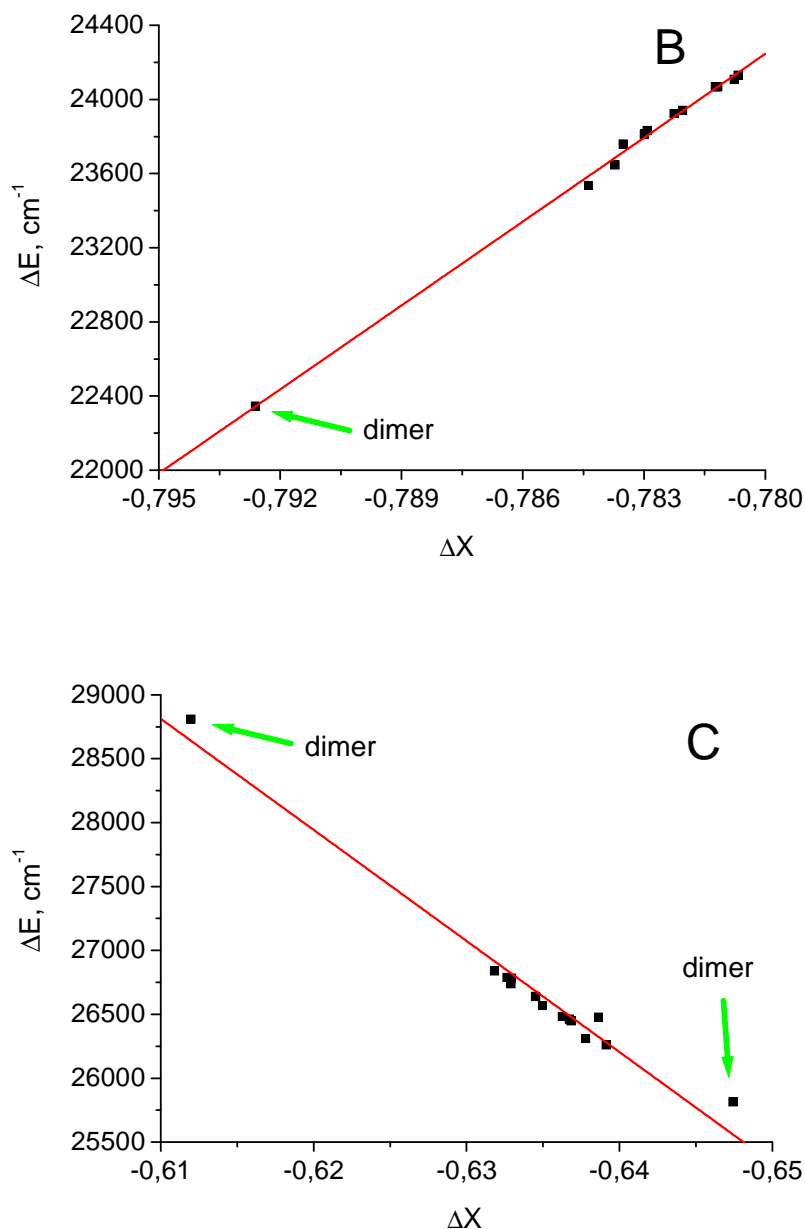
Figure 5. Dependency of Soret band maximum transition energy on MO energy levels difference for mTHPC (A), mTHPP (B) and mTHPBC (C).

4. Conclusions

The relatively good coincidence of calculated and experimental values of Soret band transitions for monomers and dimers of three tetrapyrrole compounds clearly shows the validity of modified ω-technique. Among the advantages of the theory is the fact that using only a personal compute, it is possible to calculate the electronic transitions of molecular systems with thousands of atoms in solution. The model predicts high values for the enthalpy of intramolecular H-bonds formation (about 10 kcal/mole) in all three sensitizers. We can also

conclude that intermolecular H-bonds have little influence on the spectral characteristics of the studied compounds. The study showed the formation of J-type dimers in water-ethanol mixtures for mTHPC and mTHPP, whereas mTHPBC forms zigzag aggregates. The close proximity of experimental points to the calculated curve (Fig. 5) for both monomers and dimers indicates the preservation of molecular characteristics in the dimeric forms. Information concerning the type of dimers and their spectroscopic properties was deduced from this theoretical model.

References

Bakhshiev, N. G. (1972). "Spectroscopy of intermolecular interactions." Nauka, Leningrad [in Russian].

Bezdetnaya, L., N. Zeghari, I. Belitchenko, M. Barberi-Heyob, J. L. Merlin, A. Potapenko and F. Guillemin (1996). "Spectroscopic and biological testing of photobleaching of porphyrins in solutions." Photochem. Photobiol. **64**(2): 382-6.

Davidov, A. S. (1971). "Theory of Molecular Excitons." Plenum, New York.

Dewar, M. J. S. (1969). "The molecular orbital theory of organic chemistry." McGraw-Hill.

Freitas, L. C. G., R. L. Longo and A. M. Simas (1992). "Reaction-field–supermolecule approach to calculation of solvent effects." J. Chem. Soc., Faraday Trans. **88**: 189 - 193.

Gurinovich, G. P., A. N. Sevchenko and K. N. Solov'ev (1969). "Spectroscopy of Chlorophyll and Related Compounds." Nauka i Teknika, Minsk.

Henderson, B. W. and T. J. Dougherty (1992). "How does photodynamic therapy work?" Photochem Photobiol **55**(1): 145-57.

Hückel, E. (1931). "Quantum-theoretical contributions to the benzene problem. I. The electron configuration of benzene and related compounds." Z. Physik **71**: 204-286.

Krivulko, K. F. and A. P. Klishchenko (2006). "Consideration of universal intermolecular interactions using molecular orbital Huckel method." J. Appl. Spectr. **73**(5): 666-669.

Mulliken, R. S., C. A. Rieke, D. Orloff and H. Orloff (1949). "Formulas and Numerical Tables for Overlap Integrals." J. Chem. Phys. **17**: 1248-1267.

Murrell, J. N., S. F. A. Kettle and J. M. Tedder (1970). "Valence Theory." John Wiley and Sons Ltd.

Parkash, J., J. H. Robblee, J. Agnew, E. Gibbs, P. Collings, R. F. Pasternack and J. C. de Paula (1998). "Depolarized resonance light scattering by porphyrin and chlorophyll a aggregates." Biophys. J. **74**(4): 2089-99.

Pimentel, G. C. and A. L. McLellan (1960). "The Hydrogen Bond." W. H. Freeman and Co., San Francisco.

Redmond, R. W., E. J. Land and T. G. Truscott (1985). "Aggregation effects on the photophysical properties of porphyrins in relation to mechanisms involved in photodynamic therapy." Adv. Exp. Med. Biol. **193**: 293-302.

Reichardt, C. (1988). "Solvents and Solvent Effects in Organic Chemistry." John Wiley & Sons Inc.

Streitwieser, A. (1961). "Molecular Orbital Theory for Organic Chemists." John Wiley & Sons Inc.

Terenin, A. N. (1967). "Photonics of Dye Molecules and Related Organic Compounds." Nauka, Leningrad.

Wheland, G. W. and D. E. Mann (1949). "The Dipole Moments of Fulvene and Azulene." J. Chem. Phys. **17**(3): 264-268.

V GENRAL DISCUSSION

Photosensitizer can be delivered to the tumor in different ways. The most widely used mode is intravenous injection, which leads to PS distribution throughout the organism and topical administration for skin and bladder treatments. A third technique, direct intratumor injection, has been proposed by some authors (Hebeda et al. 1998; Gupta et al. 2004; Bao et al. 2006).

Intratumor injection of photosensitizers into brain tumors in a rat model induced intratumoral concentration with very low PS levels in normal brain and other organs (Kostron et al. 1986; Steichen et al. 1986). An important finding was the absence of PS in the tumor blood vessel, thus preserving oxygen supply (Steichen et al. 1986) (Kostron et al. 1987). However, despite rather selective HpD distribution, random photoinduced damage of both tumour and normal brain was reported (Hebeda et al. 1998). But inhomogeneity of photosensitizer intratumor distribution and PDT damage limits the use of i.t. injection and it has recently been postulated that intratumor injection of photosensitizers is rather ineffective (Brown et al. 2004). Therefore, the transport of photosensitizers in the blood after intravenous injection seems to be an important step in PS delivery to tumors, which greatly affects photodynamic efficiency.

Immediately after IV injection, photosensitizers encounter plasma proteins and their binding affinity plays an important role in drug distribution (Kongshaug 1992). The work of Hopkinson et al showed that mTHPC protein-binding pattern is quite different from other hydrophobic drugs (Hopkinson et al. 1999). Upon addition of to human plasma, about 70 % was associated with an unknown high-density protein fraction. This mTHPC – protein complex was weakly fluorescent, supposedly because of the highly aggregated state of mTHPC (Hopkinson et al. 1999). During the next 6-8 hours the sensitizer associated was

redistributed to plasma lipoproteins. After 24 hours of mTHPC incubation in plasma at 37°C, 17 % of sensitizer was still bound to lipoproteins, whereas 73 % was associated with HDL and 8 % with LDL.

In the first part of our study, we investigated different aggregated fractions of mTHPC in plasma proteins. We demonstrated that just after injection in protein solutions mTHPC forms large-scale and free, not bound to protein, aggregates. This conclusion was based on spectroscopic analysis of mTHPC in different protein solutions (p. 68, Figure 1) and on gel-filtration chromatograpgy (p. 71, Figure 7). Using photon correlation spectroscopy technique we have measured the average size of mTHPC aggregates in aqueous media, which appeared to be about 900 nm thus containing thousands of molecules (the data are not presented in the present manuscript). We therefore attributed the non flurescent product, reported by Hopkinson and Kessel (Hopkinson et al. 1999) to large mTHPC aggregates,not bound to any plasma component. We also demonstrated that after further incubation (several hours) mTHPC disaggregates and binds to albumin and lipoproteins and this process required several hours (p 69, Figure 2).

Potential presence of aggregates in the vasculature may explain the unusual pattern of mTHPC pharmacokinetics observed in human and rabbit plasma, characterized by a secondary peak at about 10h and 6h respectively after IV injection (Ronn et al. 1997; Glanzmann et al. 1998). Indeed, due to the interaction of aggregates with plasma, mTHPC monomerizes and can thus be released into the bloodstream and provoke the appearance of a delayed secondary plasma peak.

The second part of our study was dedicated to the investigation of mTHPC redistribution from plasma proteins to cells and vascular system. The kinetics of sensitizer release from the complexes with plasma proteins to model membranes were assessed by a fluorescence method, based on the fluorescence quenching of Alexa fluor 350 by the

sensitizer. The rates of transfer strongly depend on the type and concentration of protein and acceptor structure.

The computed values of apparent transfer constants k for BSA, HDL and lipoproteins were $(1.69 \pm 0.09) \times 10^{-3}$ s^{-1}, $(1.60 \pm 0.30) \times 10^{-4}$ s^{-1} and 1.84×10^{-5} s^{-1} respectively (Fig 3 page 82). This means that the characteristic time of mTHPC release from BSA is about 10 min, about 100 min from HDL and 15 hours from lipoproteins. Such differences between proteins can partially be explained by a much higher binding capacity of different photosensitizers to lipoproteins compared to albumin (Rosenberger and Margalit 1993). Another possibel explanation could be the deep penetration of photosensitizers into the lipid bilayer of lipoproteins, as was demonstrated for phtalocyanines (Bonneau et al. 2004). The values of mTHPC redistribution rates are much smaller compared to other sensitizers (Kuzelova and Brault 1994; Bonneau et al. 2004) and are only comparable to transfer rates of hemin from the complexes with plasma proteins (Miller and Shaklai 1999). These low redistribution rates can possibly be explained by the rigid fixation of mTHPC in the hydrocarbon part of lipid bilayers and by the high value of its fluorescence polarization in lipoproteins (P = 25 %) together with a high fluorescence lifetime (10.2 ns) (data are not presented in the present manuscript). One of the important parameters that influence the PDT-efficacy of lipophilic sensitizers is their mode of binding and localization in lipid bilayers (Berg and Moan 1997). It was shown that lipid bilayers are the primary site of $^1O_2$ generation and subsequent photodamage by lipophilic porphyrins (Ehrenberg et al. 1993). Furthermore, protoporphyrin derivatives that are inserted deeper and vertically into the lipid bilayer of liposomes have been shown to enhance photodynamic efficacy (Lavi et al. 2002). Recent studies reported deep location of mTHPC within lipid bilayesr and its extremely low mobility in membrane structures (Bombelli et al. 2005; Knyazev et al. 2005), which could account for the high efficiency of mTHPC mediated PDT.

An important finding of this part of the study was that the time to complete mTHPC redistribution from HDL, its main carrier in the blood (Hopkinson et al. 1999), is about 6-8 hours. This time correlates well with the maximum of PDT efficacy as observed in our *in vivo* study. This part of our investigation was focused on the correlation between mTHPC distribution in tumor, plasma and leucocytes at different times after drug delivery and PDT efficacy in tumor-bearing mice over the same time course. Unlike tumor and plasma mTHPC concentrations, photosensitizer accumulation in leucocytes exhibited a good correlation with PDT efficacy (p. 61, Figure 1B and p. 62 Figure 3). We hypothesized that a certain delay is required in order for mTHPC to be released from plasma proteins and enter the target cell population, in particular endothelial cells. This was supported by the low redistribution rates of mTHPC from plasma lipoproteins (6-8 hours). The low redistribution rates of mTHPC compared to other sensitizers are also consistent with its unique binding characteristics to cells. The study of Ball et al has shown that mTHPC is tightly sequestered on entering the cell and not easily removed by serum components (Ball et al. 1999). Mitra et al have reported a 150-fold higher mTHPC concentration in spheroids than that in the incubation medium after 24 h incubation (45 μg ml^{-1} in spheroids compared to 0.3 μg ml^{-1} in the medium), whereas for the Photofrin the increase was only 10-fold (Mitra and Foster 2005). Such outstanding retention properties of mTHPC can be understood on the basis of the mechanism of sensitizer interactions with biological membranes. In spite of slow kinetic of redistribution, the equilibrium of mTHPC transfer is strongly shifted to the accumulation in cells. This is due to the fact that there exists a substantial energetic barrier for membrane-bound lipophilic drugs to partition into the aqueous phase (Fahr et al. 2005). mTHPC molecules further diffuse to intracellular compartments thus decreasing photosensitizer content in the plasma membrane and lowering the possibility of efflux from the cells. Indeed, as we reported earlier, mTHPCs efflux from cells was negligible (Teiten et al. 2001) which is also one of the parameters that

could account for a considerably enhanced potency of this photosensitizer (Mitra and Foster 2005).

The aggregation state of a photosensitizer can also affect its transport to the cells. A monomeric sensitizer is transferred from plasma proteins to the cell surface, from which it can cross the outer membrane by passive diffusion or endocytoses in a protein complex (LDL-mediates endocytosis) (Jori and Reddi 1993). Aggregates can not cross the outer membrane by passive diffusion and must undergo endocytoses (MacDonald et al. 1999). They can than be monomerized owing to interactions with membrane structures and proteinss. This disaggregation process is assumed to take place at the inner cell membrane (Ricchelli et al. 1994; Aveline et al. 1995). Thus, it is clear that a study of intracellular aggregation state of sensitizers is an important step in the investigation of the parameters that influence PDT efficacy. Therefore, in the next part of our study we investigated the influence of mTHPC aggregation state on its photophysical properties and PDT efficacy *in vitro*.

As has been shown earlier (Kress et al. 2003), incubation of epithelial cells with mTHPC from 1h to 6h resulted in a decrease of the fluorescence lifetimes from 7.5 to 5.5 ns. This decrease was attributed to enhanced formation of aggregates during incubation. Using confocal fluorescence microscopy, we have demonstrated a diffuse and relatively homogenous mTHPC localization pattern in MCF-7 cells after 3 h incubation, whereas after 24 h incubation we observed highly fluorescent spots (p 98, Figure 3). The sensitizer fluorescence intensity was about an order of magnitude higher in the spots compared to the diffuse regions. Fluorescence lifetimes of mTHPC, assessed by FLIM technique, were found to be 8.7 ns after 3h incubation. At 24h incubation fluorescence lifetimes were 4 ns in diffuse regions and 2 ns in the spots. The lifetime at 3h incubation is consistent with a monomeric mTHPC lifetime, which was reported to be 10.2 ns (Howe et al. 1999), while shorter lifetimes at 24 h could be attributed to mTHPC aggregation. This assumption was supported by the

intracellular absorption spectra of mTHPC, measured in an integrating sphere at different incubation times. The absorption spectrum of mTHPC in MCF-7 cells showed a significant decrease in molar extinction coefficients in Soret band and first Q-band at 24h compared to 3h. This suggests the formation of mTHPC aggregates at prolonged incubation times.

We further studied mTHPC photobleaching in cells since it is very sensitive to aggregation and monomers show a much faster photobleaching than aggregates (Bezdetnaya et al. 1996). Kinetics of mTHPC photobleaching in cells was monoexponential for 3h incubation with a significant fluorescence increase during the first 30 seconds of irradiation (page 100 Figure 4). At 3 h incubation the primary sites of mTHPC localization and photodamage in MCF-7 cells are ER and Golgi apparatus (Teiten et al. 2003). Therefore, the observed increase of mTHPC fluorescence can be explained by photoinduced relocalization of mTHPC from ER/Golgi apparatus to other intracellular sites, where the PS has a higher fluorescence yield or lower local concentration (Wood et al. 1997; Theodossiou et al. 2004). mTHPC photobleaching at 24 h was bi-exponential with a much lower second rate constant, compared to 3h (page 100 Figure 4). The slower photobleaching kinetics with increasing incubation time, could be related to the formation of PS aggregates that impede oxygen penetrate in the molecules. Thus, our results suggest different PS aggregation states in cells in function of incubation time.

In the next part of our study, we assessed the influence of mTHPC aggregation on its photodynamic activity *in vitro*. We compared mTHPC-based PDT efficacy in MCF-7 cells after 3h and 24h incubation. In order to account for the different intracellular sensitizer concentration at these incubation times, the phototoxicity was calculated in function of the number of absorbed photons. With this aim, we determined intracellular mTHPC concentrations after extraction procedure, molar extinction coefficients at 650 nm derived from true absorption spectra and photobleaching rate constants at both incubation times.

Photoinactivation yield computed in such a way demonstrated that after 3h incubation mTHPC inactivates 2 times more cells compared to 24h incubation. This can be attributed to the low photosensitizing efficiency of PS aggregated species together with low accessibility of oxygen in regions with a high sensitizer content (Ball et al. 1998).

Shorter light drug intervals have several advantages such as reduced sensitizer concentration and almost complete photodestruction of the drug at the end of irradiation (page 100 Figure 4) and thus suggest reduced skin sensitization. Due to slow mTHPC transport, the main target of PDT at low LDI is the tumor vasculature. Conversely, lower quantum yield of cells inctivation at 24h, defined by sensitizer aggregation and low access to oxygen, is accompanied by much slower photobleaching kinetics, and persistence of PS after treatment. Therefore at long LDI the use of low irradiation fluence rates is preferable in order reoxygenate the tissue.

The last part of our study examined the nature of the aggregates of mTHPC and related compounds mTHPP and mTHPBC, in aqueous solutions. Tetrapyrrolic sensitizers tend to aggregate in hydrophilic media (Redmond et al. 1985). Depending on the steric factors and the origin of interactions between tetrapyrrolic molecules, several types of aggregates can be formed. The most widely reported are H-and J-aggregates. Both of them are linear aggregates, for which the angle between monomer transition dipoles in the aggregate is zero ($\theta = 0$). For J-aggregates the angle (φ) between the line connecting the centers and the direction of transition dipoles in the two neighboring molecules varies from 0 to $\pi/2$. For H-aggregates the angle φ is equal to $\pi/2$ (Parkash et al. 1998). Another type of aggregates is a "zigzag" aggregate, where photosensitizer molecules' planes are not parallel to each other (Parkash et al. 1998).

To establish the nature of mTHPC, mTHPP and mTHPBC dimers in water/ethanol solutions, we undertook spectroscopic studies of these compounds in different solvents.

Spectra were analyzed using a newly developed quantum mechanic semi-empirical theory, based on Huckel molecular orbital theory. This approach allowed us to calculate the spectral shifts in different solvents. Spectroscopic and quantum chemical study revealed that mTHPC and mTHPP form J-type dimers with $\varphi=0$ in ethanol-water mixtures whereas mTHPBC forms "zigzag" dimers with an angle inferior to180° between monomer transition dipoles. Dimers of all three sensitizers were connected by means of hydrogen bonds between phenyl OH groups. Information concerning the type of photosensitizers dimers can be used to predict the their photophysical properties which are closely related to their photodynamic activity.

VI CONCLUSION AND PERSPECTIVES

The investigation of the influence of mTHPC distribution in tumor, plasma and leukocytes on PDT response shows that photosensitizer accumulation in leukocytes exhibited a good correlation with PDT efficacy. This result suggests that leukocytes could play an important role in the mechanism of PDT-induced vascular damage either by being one of the main effector compartments or by better reflecting mTHPC accumulation in endothelial cells compared to plasma.

Perspectives:
Study of the subsequent transport and distribution of mTHPC in the vascular system and in tussues.

The study of mTHPC monomerisation in the course of interactions with plasma proteins demonstrate slow rate of disaggregation kinetics that is accompanied by an increase of sensitizer fluorescence quantum yield. The fraction of aggregated mTHPC at equilibrium and sensitizer disaggregation rates strongly depend on protein content and incubation temperature. The low values of mTHPC disaggregation rates can be explained by sensitizer lipophilic nature and the formation of large-scale aggregates with strong interaction between sensitizer molecules. Gel-filtration experiments with monomeric BSA revealed the presence of strongly aggregated free sensitizer aggregates.

- *Perspectives*:
Study of internalisation mechanisms and intracellular transport of mTHPC.

Kinetic analysis based on FRET technique demonstrate that mTHPC is characterized by very slow redistribution rates from the complexes with plasma proteins. Low redistribution rates of mTHPC as compared to other sensitizers are consistent with mTHPC unique binding properties. Thermodynamic and kinetic considerations let us suppose the existence of both collisional and aqueous mediated transfer. The former type of transfer predominates in physiological conditions.

- *Perspectives*:
Comparison of the kinetic parameters of mTHPC redistribution with that of mTHPC liposomal formulation (Foslip®).

Confocal microscopy study reveals diffuse mTHPC localization patterns at 3h and formation of highly fluorescent spots of sensitizer at 24h incubation time point in MCF-7 cells. Sensitizer photophysical characteristics obtained using absorption spectroscopy and FLIM technique have shown that at 24h incubation point mTHPC is much more aggregated compared to 3h. This data were confirmed by measurements of sensitizer photobleaching kinetic. Quantum yield of cells photoinactivation is about 3 times higher for 3h time point. Such difference is attributed to sensitizer self-quenching effect due to different aggregation state and interactions with cellular components.

- *Perspectives*:

Assessment of mTHPC photophysical characteristics and aggregation state in tussues *in vivo* using FLIM technique.

The theoretical and spectroscopic study of mTHPC, mTHPP and mTHPBC allowed us to define their aggregates structure in aqueous media. For this purpose the qauntum mechanic semi-empirical method was developed on the basis of which the spectral shifts in different solvents were calculated. mTHPC and mTHPP form J-type dimers in ethanol-water mixtures, whereas mTHPBC form linear dimers with an angle inferior 180 degrees between monomers molecular planes.

- *Perspectives*:

This approach can be used to calculate the electronic density maps of sensitizer molecules in biological solutions and allow to predict the sensitizer photosensitivity.

References

Agostinis, P., E. Buytaert, H. Breyssens and N. Hendrickx (2004). "Regulatory pathways in photodynamic therapy induced apoptosis." Photochem. Photobiol. Sci. 3(8): 721-9.

Allison, R. R., G. H. Downie, R. Cuenca, X.-H. Hu, C. J. Childs and C. H. Sibata (2004). "Photosensitizers in clinical PDT." Photodiagnosis and Photodynamic Therapy 1(1): 27-42.

Almeida, R. D., B. J. Manadas, A. P. Carvalho and C. B. Duarte (2004). "Intracellular signaling mechanisms in photodynamic therapy." Biochim. Biophys. Acta 1704(2): 59-86.

Ambroz, M., A. J. MacRobert, J. Morgan, G. Rumbles, M. S. Foley and D. Phillips (1994). "Time-resolved fluorescence spectroscopy and intracellular imaging of disulphonated aluminium phthalocyanine." J. Photochem. Photobiol. B 22(2): 105-17.

Andrade, S. M. and S. M. Costa (2002). "Spectroscopic studies on the interaction of a water soluble porphyrin and two drug carrier proteins." Biophys. J. 82(3): 1607-19.

Atkins, P. W. (1990). "Physical Chemistry (4th ed.)." Oxford Univ. Press, Oxford.

Auler, H. and G. Banzer (1942). "Untersuchungen über die Role der Porphyrine bei geschwultstkranken Menchen und Tieren." Z. Krebsforsch. 53: 65-68.

Aveline, B., T. Hasan and R. W. Redmond (1994). "Photophysical and photosensitizing properties of benzoporphyrin derivative monoacid ring A (BPD-MA)." Photochem. Photobiol. 59(3): 328-35.

Aveline, B. M., T. Hasan and R. W. Redmond (1995). "The effects of aggregation, protein binding and cellular incorporation on the photophysical properties of benzoporphyrin derivative monoacid ring A (BPDMA)." J. Photochem. Photobiol. B 30(2-3): 161-9.

Aveline, B. M. and R. W. Redmond (1999). "Can cellular phototoxicity be accurately predicted on the basis of sensitizer photophysics?" Photochem. Photobiol. 69(3): 306-16.

Aveline, B. M., R. M. Sattler and R. W. Redmond (1998). "Environmental effects on cellular photosensitization: correlation of phototoxicity mechanism with transient absorption spectroscopy measurements." Photochem. Photobiol. 68(1): 51-62.

Bacia, K., S. A. Kim and P. Schwille (2006). "Fluorescence cross-correlation spectroscopy in living cells." Nat. Methods 3(2): 83-9.

Baker, A. and J. R. Kanofsky (1992). "Quenching of singlet oxygen by biomolecules from L1210 leukemia cells." Photochem Photobiol 55(4): 523-8.

Ball, D. J., S. Mayhew, S. R. Wood, J. Griffiths, D. I. Vernon and S. B. Brown (1999). "A comparative study of the cellular uptake and photodynamic efficacy of three novel zinc phthalocyanines of differing charge." Photochem. Photobiol. 69(3): 390-6.

Ball, D. J., D. I. Vernon and S. B. Brown (1999). "The high photoactivity of m-THPC in photodynamic therapy. Unusually strong retention of m-THPC by RIF-1 cells in culture." Photochem. Photobiol. 69(3): 360-3.

Ball, D. J., S. R. Wood, D. I. Vernon, J. Griffiths, T. M. Dubbelman and S. B. Brown (1998). "The characterisation of three substituted zinc phthalocyanines of differing charge for use in photodynamic therapy. A comparative study of their aggregation and photosensitising ability in relation to mTHPC and polyhaematoporphyrin." J. Photochem. Photobiol. B 45(1): 28-35.

Bao, A., W. T. Phillips, B. Goins, X. Zheng, S. Sabour, M. Natarajan, F. Ross Woolley, C. Zavaleta and R. A. Otto (2006). "Potential use of drug carried-liposomes for cancer therapy via direct intratumoral injection." Int. J. Pharm. 316(1-2): 162-9.

Bartlett, J. A. and G. L. Indig (1999). "Effect of self-association and protein binding on the photochemical reactivity of triarylmethanes. Implications of noncovalent interactions

on the competition between photosensitization mechanisms type I and type II." Photochem Photobiol 70(4): 490-8.

Becker, W., A. Bergmann, M. A. Hink, K. Konig, K. Benndorf and C. Biskup (2004). "Fluorescence lifetime imaging by time-correlated single-photon counting." Microsc. Res. Tech. 63(1): 58-66.

Belitchenko, I., V. Melnikova, L. Bezdetnaya, H. Rezzoug, J. L. Merlin, A. Potapenko and F. Guillemin (1998). "Characterization of photodegradation of meta-tetra(hydroxyphenyl)chlorin (mTHPC) in solution: biological consequences in human tumor cells." Photochem. Photobiol. 67(5): 584-90.

Bellnier, D. A. and T. J. Dougherty (1996). "A preliminary pharmacokinetic study of intravenous Photofrin in patients." J. Clin. Laser Med. Surg. 14(5): 311-4.

Bellnier, D. A., W. R. Greco, G. M. Loewen, H. Nava, A. R. Oseroff, R. K. Pandey, T. Tsuchida and T. J. Dougherty (2003). "Population pharmacokinetics of the photodynamic therapy agent 2-[1-hexyloxyethyl]-2-devinyl pyropheophorbide-a in cancer patients." Cancer Res. 63(8): 1806-13.

Bellnier, D. A., B. W. Henderson, R. K. Pandey, W. R. Potter and T. J. Dougherty (1993). "Murine pharmacokinetics and antitumor efficacy of the photodynamic sensitizer 2-[1-hexyloxyethyl]-2-devinyl pyropheophorbide-a." J. Photochem. Photobiol. B 20(1): 55-61.

Beltramini, M., P. A. Firey, F. Ricchelli, M. A. Rodgers and G. Jori (1987). "Steady-state and time-resolved spectroscopic studies on the hematoporphyrin-lipoprotein complex." Biochemistry 26(21): 6852-8.

Berenbaum, M. C., S. L. Akande, R. Bonnett, H. Kaur, S. Ioannou, R. D. White and U. J. Winfield (1986a). "meso-Tetra(hydroxyphenyl)porphyrins, a new class of potent tumour photosensitisers with favourable selectivity." Br. J. Cancer 54(5): 717-25.

Berenbaum, M. C., S. L. Akande, R. Bonnett, H. Kaur, S. Ioannou, R. D. White and U. J. Winfield (1986b). "meso-Tetra(hydroxyphenyl)porphyrins, a new class of potent tumour photosensitisers with favourable selectivity." Br J Cancer 54(5): 717-25.

Berg, K., H. Anholt, J. Moan, A. Ronnestad and C. Rimington (1993). "Photobiological properties of hematoporphyrin diesters: evaluation for possible application in photochemotherapy of cancer." J. Photochem. Photobiol. B 20(1): 37-45.

Berg, K., K. Madslien, J. C. Bommer, R. Oftebro, J. W. Winkelman and J. Moan (1991). "Light induced relocalization of sulfonated meso-tetraphenylporphines in NHIK 3025 cells and effects of dose fractionation." Photochem. Photobiol. 53(2): 203-10.

Berg, K. and J. Moan (1997). "Lysosomes and microtubules as targets for photochemotherapy of cancer." Photochem. Photobiol. 65(3): 403-9.

Berland, K. M. (2004). "Fluorescence correlation spectroscopy: a new tool for quantification of molecular interactions." Methods Mol. Biol. 261: 383-98.

Bezdetnaya, L., N. Zeghari, I. Belitchenko, M. Barberi-Heyob, J. L. Merlin, A. Potapenko and F. Guillemin (1996). "Spectroscopic and biological testing of photobleaching of porphyrins in solutions." Photochem. Photobiol. 64(2): 382-6.

Birch, D. J. S. and R. E. Imhof (1991). "Time-domain Fluorescence Spectroscopy Using Time-Correlated Single Photon Counting, in Topics in Fluorescence Spectroscopy: Techniques." Plenum Press, New York.

Bizik, J., E. Kankuri, A. Ristimaki, A. Taieb, H. Vapaatalo, W. Lubitz and A. Vaheri (2004). "Cell-cell contacts trigger programmed necrosis and induce cyclooxygenase-2 expression." Cell Death Differ. 11(2): 183-95.

Bombelli, C., G. Caracciolo, P. Di Profio, M. Diociaiuti, P. Luciani, G. Mancini, C. Mazzuca, M. Marra, A. Molinari, D. Monti, L. Toccacieli and M. Venanzi (2005). "Inclusion of a photosensitizer in liposomes formed by DMPC/gemini surfactant: correlation

between physicochemical and biological features of the complexes." <u>J. Med. Chem.</u> 48(15): 4882-91.

Bonneau, S., P. Morliere and D. Brault (2004). "Dynamics of interactions of photosensitizers with lipoproteins and membrane-models: correlation with cellular incorporation and subcellular distribution." <u>Biochem. Pharmacol.</u> 68(7): 1443-52.

Bonneau, S., C. Vever-Bizet, P. Morliere, J. C. Maziere and D. Brault (2002). "Equilibrium and kinetic studies of the interactions of a porphyrin with low-density lipoproteins." <u>Biophys. J.</u> 83(6): 3470-81.

Bonnett, R., P. charlesworth, B. D. Djelal, S. Foley, D. J. McGarvey and T. G. Truscott (1999). "Photophysical properties of 5,10,15,20-tetrakis(m-hydroxyphenyl)porphyrin (m-THPP), 5,10,15,20-tetrakis(m-hydroxyphenyl)chlorin (m-THPC) and 5,10,15,20-tetrakis(m-hydroxyphenyl)bacteriochlorin (m-THPBC): a comparative study." <u>J. Chem. Soc., Perkin Trans. 2</u> 2: 325 - 328.

Bonnett, R., B. D. Djelal, P. A. Hamilton, G. Martinez and F. Wierrani (1999). "Photobleaching of 5,10,15,20-tetrakis(m-hydroxyphenyl)porphyrin (m-THPP) and the corresponding chlorin (m-THPC) and bacteriochlorin(m-THPBC). A comparative study." <u>J. Photochem. Photobiol. B</u> 53(1-2): 136-143.

Bonnett, R., B. D. Djelal and A. Nguyen (2001). "Physical and chemical studies related to the development of m-THPC (FOSCAN®) for the photodynamic therapy (PDT) of tumours." <u>J. Porphyrins Phthalocyanines</u> 5(8): 652-661.

Bonnett, R. and G. Martínez (2001). "Photobleaching of sensitisers used in photodynamic therapy." <u>Tetrahedron</u> 57(47): 9513-9547.

Bonnett, R., R. D. White, U. J. Winfield and M. C. Berenbaum (1989). "Hydroporphyrins of the meso-tetra(hydroxyphenyl)porphyrin series as tumour photosensitizers." <u>Biochem. J.</u> 261(1): 277-80.

Borissevitch, I. E., T. T. Tominaga and C. C. Schmitt (1998). "Photophysical studies on the interaction of two water-soluble porphyrins with bovine serum albumin. Effects upon the porphyrin triplet state characteristics." <u>J. Photochem. Photobiol. A</u> 114(3): 201-207.

Boyle, R. W. and D. Dolphin (1996). "Structure and biodistribution relationships of photodynamic sensitizers." <u>Photochem. Photobiol.</u> 64(3): 469-85.

Brown, S. B., E. A. Brown and I. Walker (2004). "The present and future role of photodynamic therapy in cancer treatment." <u>Lancet. Oncol.</u> 5(8): 497-508.

Brown, S. B., M. Shillcock and P. Jones (1976). "Equilibrium and kinetic studies of the aggregation of porphyrins in aqueous solution." <u>Biochem. J.</u> 153(2): 279-285.

Brun, A., A. Western, Z. Malik and S. Sandberg (1990). "Erythropoietic protoporphyria: photodynamic transfer of protoporphyrin from intact erythrocytes to other cells." <u>Photochem Photobiol</u> 51(5): 573-7.

Buchholz, J., B. Kaser-Hotz, T. Khan, C. Rohrer Bley, K. Melzer, R. A. Schwendener, M. Roos and H. Walt (2005). "Optimizing photodynamic therapy: in vivo pharmacokinetics of liposomal meta-(tetrahydroxyphenyl)chlorin in feline squamous cell carcinoma." <u>Clin. Cancer Res.</u> 11(20): 7538-44.

Campagnola, P. J. and L. M. Loew (2003). "Second-harmonic imaging microscopy for visualizing biomolecular arrays in cells, tissues and organisms." <u>Nat. Biotechnol.</u> 21(11): 1356-60.

Candide, C., J. C. Maziere, R. Santus, C. Maziere, P. Morliere, J. P. Reyftmann, S. Goldstein and L. Dubertret (1989). "Photosensitization of Wi26-VA4 transformed human fibroblasts by low density lipoprotein loaded with the anticancer porphyrin mixture photofrin II: evidence for endoplasmic reticulum alteration." <u>Cancer Lett</u> 44(2): 157-61.

Castano, A. P., T. N. Demidova and M. R. Hamblin (2005a). "Mechanisms in photodynamic therapy: Part three—Photosensitizer pharmacokinetics, biodistribution, tumor localization and modes of tumor destruction." Photodiagnosis and Photodynamic Therapy 2(2): 91-106.

Castano, A. P., T. N. Demidova and M. R. Hamblin (2005b). "Mechanisms in photodynamic therapy: part two—cellular signaling, cell metabolism and modes of cell death." Photodiagnosis and Photodynamic Therapy 2(1): 1-23.

Castedo, M., J. L. Perfettini, T. Roumier, K. Andreau, R. Medema and G. Kroemer (2004). "Cell death by mitotic catastrophe: a molecular definition." Oncogene 23(16): 2825-37.

Chacon, J. N., J. McLearie and R. S. Sinclair (1988). "Singlet oxygen yields and radical contributions in the dye-sensitised photo-oxidation in methanol of esters of polyunsaturated fatty acids (oleic, linoleic, linolenic and arachidonic)." Photochem. Photobiol. 47(5): 647-56.

Chang, C. K., L. K. Hanson, P. F. Richardson, R. Young and J. Fajer (1981). "pi cation radicals of ferrous and free base isobacteriochlorins: Models for siroheme and sirohydrochlorin." Proc. Natl. Acad. Sci. U S A 78(5): 2652-2656.

Chen, J. Y., N. K. Mak, C. M. Yow, M. C. Fung, L. C. Chiu, W. N. Leung and N. H. Cheung (2000). "The binding characteristics and intracellular localization of temoporfin (mTHPC) in myeloid leukemia cells: phototoxicity and mitochondrial damage." Photochem Photobiol 72(4): 541-7.

Chowdhary, R. K., I. Sharif, N. Chansarkar, D. Dolphin, L. Ratkay, S. Delaney and H. Meadows (2003). "Correlation of photosensitizer delivery to lipoproteins and efficacy in tumor and arthritis mouse models; comparison of lipid-based and Pluronic P123 formulations." J. Pharm. Pharm. Sci. 6(2): 198-204.

Cole, M. J., J. Siegel, S. E. Webb, R. Jones, K. Dowling, M. J. Dayel, D. Parsons-Karavassilis, P. M. French, M. J. Lever, L. O. Sucharov, M. A. Neil, R. Juskaitis and T. Wilson (2001). "Time-domain whole-field fluorescence lifetime imaging with optical sectioning." J. Microsc. 203(Pt 3): 246-57.

Collings, P. J., E. J. Gibbs, T. E. Starr, O. Vafek, C. Yee, L. A. Pomerance and R. F. Pasternack (1999). "Resonance Light Scattering and Its Application in Determining the Size, Shape, and Aggregation Number for Supramolecular Assemblies of Chromophores." J. Phys. Chem. B 103(40): 8474 -8481.

Connelly, J. P., S. W. Botchway, D. P. L. Kunz, A. W. Parker and A. J. MacRobert (2001). "Time-resolved fluorescence imaging of photosensitiser distributions in mammalian cells using a picosecond laser line-scanning microscope." J. Photochem. Photobiol. A 142: 169–175.

Copper, M. P., I. B. Tan, H. Oppelaar, M. C. Ruevekamp and F. A. Stewart (2003). "Meta-tetra(hydroxyphenyl)chlorin photodynamic therapy in early-stage squamous cell carcinoma of the head and neck." Arch. Otolaryngol. Head Neck Surg. 129(7): 709-11.

Coutier, S., L. N. Bezdetnaya, T. H. Foster, R. M. Parache and F. Guillemin (2002). "Effect of irradiation fluence rate on the efficacy of photodynamic therapy and tumor oxygenation in meta-tetra (hydroxyphenyl) chlorin (mTHPC)-sensitized HT29 xenografts in nude mice." Radiat. Res. 158(3): 339-45.

Coutier, S., S. Mitra, L. N. Bezdetnaya, R. M. Parache, I. Georgakoudi, T. H. Foster and F. Guillemin (2001). "Effects of fluence rate on cell survival and photobleaching in meta-tetra-(hydroxyphenyl)chlorin-photosensitized Colo 26 multicell tumor spheroids." Photochem. Photobiol. 73(3): 297-303.

Cunderlikova, B., L. Gangeskar and J. Moan (1999). "Acid-base properties of chlorin e6: relation to cellular uptake." J Photochem Photobiol B 53(1-3): 81-90.

Davila, J. and A. Harriman (1990). "Photoreactions of macrocyclic dyes bound to human serum albumin." Photochem. Photobiol. 51(1): 9-19.

Delaey, E. M., R. Obermueller, I. Zupko, D. De Vos, H. Falk and P. A. de Witte (2001). "In vitro study of the photocytotoxicity of some hypericin analogs on different cell lines." Photochem Photobiol 74(2): 164-71.

dos Remedios, C. G. and P. D. Moens (1995). "Fluorescence resonance energy transfer spectroscopy is a reliable "ruler" for measuring structural changes in proteins. Dispelling the problem of the unknown orientation factor." J. Struct. Biol. 115(2): 175-85.

Dougherty, T. J., C. J. Gomer, B. W. Henderson, G. Jori, D. Kessel, M. Korbelik, J. Moan and Q. Peng (1998). "Photodynamic therapy." J. Natl. Cancer Inst. 90(12): 889-905.

Dougherty, T. J., C. J. Gomer and K. R. Weishaupt (1976). "Energetics and efficiency of photoinactivation of murine tumor cells containing hematoporphyrin." Cancer Res. 36(7 PT 1): 2330-3.

Dougherty, T. J., W. R. Potter and K. R. Weinshaupt (1984). The structure of the active component of hematoporphyrin derivative. Porphyrins in Tumor Phototherapy. A. Andreoni and R. Cubeddu. New-York, Plenum: 23-35.

Dowling, K., S. C. W. Hyde, J. C. Dainty, P. M. W. French and J. D. Hares (1997). "2-D fluorescence lifetime imaging using a time-gated image intensifier." Optics Communications 135(1-3): 27-31.

Dummin, H., T. Cernay and H. W. Zimmermann (1997). "Selective photosensitization of mitochondria in HeLa cells by cationic Zn (II) phthalocyanines with lipophilic side-chains." J. Photochem. Photobiol. B 37(3): 219-29.

Dysart, J. S., G. Singh and M. S. Patterson (2005). "Calculation of singlet oxygen dose from photosensitizer fluorescence and photobleaching during mTHPC photodynamic therapy of MLL cells." Photochem. Photobiol. 81(1): 196-205.

Edwards, L., D. H. Dolphin, M. Gouterman and A. D. Adler (1971). "Porphyrins XVII. Vapor absorption spectra and redox reactions: Tetraphenylporphins and porphin." J. Mol. Spectrosc. 38(1): 16-32.

Egorin, M. J., E. G. Zuhowski, D. L. Sentz, J. M. Dobson, P. S. Callery and J. L. Eiseman (1999). "Plasma pharmacokinetics and tissue distribution in CD2F1 mice of Pc4 (NSC 676418), a silicone phthalocyanine photodynamic sensitizing agent." Cancer Chemother. Pharmacol. 44(4): 283-94.

Ehrenberg, B., E. Gross, Y. Nitzan and Z. Malik (1993). "Electric depolarization of photosensitized cells: lipid vs. protein alterations." Biochim. Biophys. Acta 1151(2): 257-64.

Elson, D., J. Requejo-Isidro, I. Munro, F. Reavell, J. Siegel, K. Suhling, P. Tadrous, R. Benninger, P. Lanigan, J. McGinty, C. Talbot, B. Treanor, S. Webb, A. Sandison, A. Wallace, D. Davis, J. Lever, M. Neil, D. Phillips, G. Stamp and P. French (2004). "Time-domain fluorescence lifetime imaging applied to biological tissue." Photochem. Photobiol. Sci. 3(8): 795-801.

Enderle, T., T. Ha, D. F. Ogletree, D. S. Chemla, C. Magowan and S. Weiss (1997). "Membrane specific mapping and colocalization of malarial and host skeletal proteins in the Plasmodium falciparum infected erythrocyte by dual-color near-field scanning optical microscopy." Proc. Natl. Acad. Sci. U S A 94(2): 520-5.

Eyring, H. and E. M. Eyring (1963). "Modern Chemical Kinetics." Reinhold Publishing Company, New York.: 29-50.

Fahr, A., P. van Hoogevest, S. May, N. Bergstrand and S. L. ML (2005). "Transfer of lipophilic drugs between liposomal membranes and biological interfaces: consequences for drug delivery." Eur. J. Pharm. Sci. 26(3-4): 251-65.

Fernandez, J. M., M. D. Bilgin and L. I. Grossweiner (1997). "Singlet oxygen generation by photodynamic agents." J. Photochem. Photobiol. B 37(1-2): 131-140.

Fiedler, D. M., F. Wierrani, G. Schnitzhofer, J. C. Stewart, K. Gharehbaghi, W. Grunberger and B. Krammer (1997). "Does the in-vitro efficiency of meso-tetrahydroxy-phenyl-chlorin depend on pre-treatment of sensitizer?" J. Photochem. Photobiol. B 38(2-3): 241-4.

Fingar, V. H., S. W. Taber, P. S. Haydon, L. T. Harrison, S. J. Kempf and T. J. Wieman (2000). "Vascular damage after photodynamic therapy of solid tumors: a view and comparison of effect in pre-clinical and clinical models at the University of Louisville." In Vivo 14(1): 93-100.

Fingar, V. H., T. J. Wieman, S. A. Wiehle and P. B. Cerrito (1992). "The role of microvascular damage in photodynamic therapy: the effect of treatment on vessel constriction, permeability, and leukocyte adhesion." Cancer Res. 52(18): 4914-21.

Finlay, J. C., D. L. Conover, E. L. Hull and T. H. Foster (2001). "Porphyrin bleaching and PDT-induced spectral changes are irradiance dependent in ALA-sensitized normal rat skin in vivo." Photochem Photobiol 73(1): 54-63.

Finlay, J. C., S. Mitra and T. H. Foster (2002). "In vivo mTHPC photobleaching in normal rat skin exhibits unique irradiance-dependent features." Photochem Photobiol 75(3): 282-8.

Firey, P. A., T. W. Jones, G. Jori and M. A. Rodgers (1988). "Photoexcitation of zinc phthalocyanine in mouse myeloma cells: the observation of triplet states but not of singlet oxygen." Photochem. Photobiol. 48(3): 357-60.

Foley, M. S., A. Beeby, A. W. Parker, S. M. Bishop and D. Phillips (1997). "Excited triplet state photophysics of the sulphonated aluminium phthalocyanines bound to human serum albumin." J. Photochem. Photobiol. B 38(1): 10-7.

Foote, C. S. (1991). "Definition of type I and type II photosensitized oxidation." Photochem Photobiol 54(5): 659.

Foster, T. H., M. C. Primavera, V. J. Marder, R. Hilf and L. A. Sporn (1991). "Photosensitized release of von Willebrand factor from cultured human endothelial cells." Cancer Res. 51(12): 3261-6.

Gantchev, T. G., R. Ouellet and J. E. van Lier (1999). "Binding interactions and conformational changes induced by sulfonated aluminum phthalocyanines in human serum albumin." Arch. Biochem. Biophys. 366(1): 21-30.

Georgakoudi, I. and T. H. Foster (1998). "Singlet oxygen- versus nonsinglet oxygen-mediated mechanisms of sensitizer photobleaching and their effects on photodynamic dosimetry." Photochem. Photobiol. 67(6): 612-25.

Georgakoudi, I., M. G. Nichols and T. H. Foster (1997). "The mechanism of Photofrin photobleaching and its consequences for photodynamic dosimetry." Photochem. Photobiol. 65(1): 135-44.

Gerritsen, H. C., R. Sanders, A. Draaijer, C. Ince and Y. K. Levine (1997). "Fluorescence Lifetime Imaging of Oxygen in Living Cells." J. Fluoresc. 7: 11-16.

Geze, M., P. Morliere, J. C. Maziere, K. M. Smith and R. Santus (1993). "Lysosomes, a key target of hydrophobic photosensitizers proposed for photochemotherapeutic applications." J. Photochem. Photobiol. B 20(1): 23-35.

Glanzmann, T., C. Hadjur, M. Zellweger, P. Grosiean, M. Forrer, J. P. Ballini, P. Monnier, H. van den Bergh, C. K. Lim and G. Wagnieres (1998). "Pharmacokinetics of tetra(m-

hydroxyphenyl)chlorin in human plasma and individualized light dosimetry in photodynamic therapy." <u>Photochem. Photobiol.</u> 67(5): 596-602.

Glasstone, S., K.J. Laidler and H. Eyring (1941). "The Theory of Rate Processes." <u>McGraw-Hill, New York</u>.

Gollnick, K., T. Franken, M. F. R. Fouda, H. R. Paur and S. Held. (1992). "Merbromin (mercurochrome) and other xanthene dyes: quantum yields of triplet sensitizer generation and singlet oxygen formation in alcoholic

solutions." <u>J. Photochem. Photobiol. B</u> 12: 57-81.

Gollnick, S. O., X. Liu, B. Owczarczak, D. A. Musser and B. W. Henderson (1997). "Altered expression of interleukin 6 and interleukin 10 as a result of photodynamic therapy in vivo." <u>Cancer Res.</u> 57(18): 3904-9.

Gupta, S., A. K. Mishra, K. Muralidhar and V. Jain (2004). "Improved targeting of photosensitizers by intratumoral administration of immunoconjugates." <u>Technol. Cancer Res. Treat.</u> 3(3): 295-301.

Hadjur, C., N. Lange, J. Rebstein, P. Monnier, H. van den Bergh and G. Wagnières (1998). "Spectroscopic studies of photobleaching and photoproduct formation of meta(tetrahydroxyphenyl) chlorin (m-THPC) used in photodynamic therapy. The production of singlet oxygen by m-THPC." <u>J. Photochem. Photobiol. B</u> 45(2-3).

Harpur, A. G., F. S. Wouters and P. I. Bastiaens (2001). "Imaging FRET between spectrally similar GFP molecules in single cells." <u>Nat. Biotechnol.</u> 19(2): 167-9.

Haussman, W. (1911). "Die sensibilisierende Wirkung des hämatoporphyrins." <u>Biochem. Z.</u> 30: 276-316.

Hebeda, K. M., W. Kamphorst, H. J. Sterenborg and J. G. Wolbers (1998). "Damage to tumour and brain by interstitial photodynamic therapy in the 9L rat tumour model comparing intravenous and intratumoral administration of the photosensitiser." <u>Acta Neurochir (Wien)</u> 140(5): 495-501.

Henderson, B., T. Dougherty and P. Malone (1984). "Studies on the

mechanism of tumor destruction by photoirradiation

therapy." <u>In: Porphyrin Localization and Treatment of Tumors. Doiron DR, Gomer CJ. (eds.) Alan R. Liss: New York</u>: 601–612.

Henderson, B. W. and T. J. Dougherty (1992). "How does photodynamic therapy work?" <u>Photochem. Photobiol.</u> 55(1): 145-57.

Henderson, B. W. and V. H. Fingar (1987). "Relationship of tumor hypoxia and response to photodynamic treatment in an experimental mouse tumor." <u>Cancer Res.</u> 47(12): 3110-4.

Henderson, B. W., S. M. Waldow, T. S. Mang, W. R. Potter, P. B. Malone and T. J. Dougherty (1985). "Tumor destruction and kinetics of tumor cell death in two experimental mouse tumors following photodynamic therapy." <u>Cancer Res.</u> 45(2): 572-6.

Herman, B., P. Wodnicki, S. Kwon, A. Periasamy, G. W. Gordon, N. Mahajan and W. X. Feng (1997). "Recent Developments in Monitoring Calcium and Protein Interactions in Cells Using Fluorescence Lifetime Microscopy." <u>J. Fluoresc.</u> 7: 85–92.

Hopkinson, H. J., D. I. Vernon and S. B. Brown (1999). "Identification and partial characterization of an unusual distribution of the photosensitizer meta-tetrahydroxyphenyl chlorin (temoporfin) in human plasma." <u>Photochem. Photobiol.</u> 69(4): 482-8.

Hopper, C., A. Kubler, H. Lewis, I. B. Tan and G. Putnam (2004). "mTHPC-mediated photodynamic therapy for early oral squamous cell carcinoma." <u>Int. J. Cancer</u> 111(1): 138-46.

Howe, L., A. Sucheta, O. Einarsdottir and J. Z. Zhang (1999). "Time-resolved studies of the excited-state dynamics of meso-tetra(hydroxylphenyl)chlorin in solution." Photochem. Photobiol. 69(6): 617-23.

Howe, L. and J. Z. Zhang (1998). "The effect of biological substrates on the ultrafast excited-state dynamics of zinc phthalocyanine tetrasulfonate in solution." Photochem. Photobiol. 67(1): 90-6.

Hsieh, Y. J., C. C. Wu, C. J. Chang and J. S. Yu (2003). "Subcellular localization of Photofrin determines the death phenotype of human epidermoid carcinoma A431 cells triggered by photodynamic therapy: when plasma membranes are the main targets." J. Cell. Physiol. 194(3): 363-75.

Iinuma, S., S. S. Farshi, B. Ortel and T. Hasan (1994). "A mechanistic study of cellular photodestruction with 5-aminolaevulinic acid-induced porphyrin." Br. J. Cancer 70(1): 21-8.

Imamura, M. and M. Koizumi (1955). "Irreversible photobleaching of the solution of fluorescent dyes. I. Kinetic studies on the primary process." Bull. Chem. Soc. Jpn. 28: 117-124.

Jiang, F., L. Lilge, B. Logie, Y. Li and M. Chopp (1997). "Photodynamic therapy of 9L gliosarcoma with liposome-delivered photofrin." Photochem. Photobiol. 65(4): 701-6.

Jo, J. A., Q. Fang, T. Papaioannou and L. Marcu (2004). "Fast model-free deconvolution of fluorescence decay for analysis of biological systems." J. Biomed. Opt. 9(4): 743-52.

Jones, H. J., D. I. Vernon and S. B. Brown (2003). "Photodynamic therapy effect of m-THPC (Foscan) in vivo: correlation with pharmacokinetics." Br. J. Cancer 89(2): 398-404.

Jones, J. D. and T. E. Thompson (1989). "Spontaneous phosphatidylcholine transfer by collision between vesicles at high lipid concentration." Biochemistry 28(1): 129-34.

Jones, R. M., Q. Wang, J.H. Lamb, B.D. Djelal, R. Bonnet and C. K. Lira (1996). "Identification of photochemical oxidation products of 5,10,15,20-tetra(m-hydroxyphenyl)chlorin by on-line high performance chromatography-electrospray ionization tandem mass spectroscopy." J. Chromatography A 722: 257-265.

Jori, G. (1989). "In vivo transport and pharmacokinetic behavior of tumour photosensitizers." Ciba. Found. Symp. 146: 78-94.

Jori, G. and E. Reddi (1993). "The role of lipoproteins in the delivery of tumour-targeting photosensitizers." Int. J. Biochem. 25(10): 1369-75.

Keene, J. P., D. Kessel, E. J. Land, R. W. Redmond and T. G. Truscott (1986). "Direct detection of singlet oxygen sensitized by haematoporphyrin and related compounds." Photochem. Photobiol. 43(2): 117-20.

Kelbauskas, L. and W. Dietel (2002). "Internalization of aggregated photosensitizers by tumor cells: subcellular time-resolved fluorescence spectroscopy on derivatives of pyropheophorbide-a ethers and chlorin e6 under femtosecond one- and two-photon excitations." Photochem. Photobiol. 76(6): 686-94.

Kerr, J. F., A. H. Wyllie and A. R. Currie (1972). "Apoptosis: a basic biological phenomenon with wide-ranging implications in tissue kinetics." Br. J. Cancer 26(4): 239-57.

Kessel, D. (1986a). "Porphyrin-lipoprotein association as a factor in porphyrin localization." Cancer Lett. 33(2): 183-8.

Kessel, D. (1986b). "Sites of photosensitization by derivatives of hematoporphyrin." Photochem Photobiol 44(4): 489-93.

Kessel, D. (1999). "Transport and localisation of m-THPC in vitro." Int. J. Clin. Pract. 53(4): 263-7.

Kessel, D. (2002). "Relocalization of cationic porphyrins during photodynamic therapy." Photochem. Photobiol. Sci. 1(11): 837-40.

Kessel, D. and E. Sykes (1999). "Transport, localization, and phototoxicity of m-THPC,." Proc. SPIE 3592: 37–42.

Kessel, D. and Y. Luo (1999). "Photodynamic therapy: a mitochondrial inducer of apoptosis." Cell Death Differ. 6(1): 28-35.

Kessel, D., Y. Luo, Y. Deng and C. K. Chang (1997). "The role of subcellular localization in initiation of apoptosis by photodynamic therapy." Photochem. Photobiol. 65(3): 422-6.

Kessel, D. and R. D. Poretz (2000). "Sites of photodamage induced by photodynamic therapy with a chlorin e6 triacetoxymethyl ester (CAME)." Photochem. Photobiol. 71(1): 94-6.

Kessel, D., P. Thompson, K. Saatio and K. D. Nantwi (1987). "Tumor localization and photosensitization by sulfonated derivatives of tetraphenylporphine." Photochem. Photobiol. 45(6): 787-790.

Kim, H. K. and J. Storch (1992). "Free fatty acid transfer from rat liver fatty acid-binding protein to phospholipid vesicles. Effect of ligand and solution properties." J. Biol. Chem. 267(1): 77-82.

Knyazev, D., S.Sosnovsky, V. Zorin, L. Bolotine and F. Guillemin (2005). "Evaluation of meta-tetra (hydroxiphenil)chlorin incorporation into lipid bilayer." Joint Conference of the German Society of Applied Optics and the Section of Optics of the Polish Physical Society. Wroclaw, Poland, Abstract: 26-27.

Kohen, E., R. Santus and J. Hirschberg (1995). Photobiology. San Diego, Academic Press.

Kongshaug, M. (1992). "Distribution of tetrapyrrole photosensitizers among human plasma proteins." Int. J. Biochem. 24(8): 1239-1265.

Konig, K. (2000). "Multiphoton microscopy in life sciences." J. Microsc. 200 (Pt 2): 83-104.

Konig, K., H. Meyer, H. Schneckenburger and A. Ruck (1993). "The study of endogenous porphyrins in human skin and their potential for photodynamic therapy by laser induced fluorescence spectroscopy." Lasers Med. Sci. 8: 127-132.

Korbelik, M. (1996). "Induction of tumor immunity by photodynamic therapy." J. Clin. Laser Med. Surg. 14(5): 329-34.

Korbelik, M. and G. J. Dougherty (1999). "Photodynamic therapy-mediated immune response against subcutaneous mouse tumors." Cancer Res. 59(8): 1941-6.

Korbelik, M. and J. Hung (1991). "Cellular delivery and retention of Photofrin II: the effects of interaction with human plasma proteins." Photochem. Photobiol. 53(4): 501-510.

Korbelik, M. and G. Krosl (1995). "Photofrin accumulation in malignant and host cell populations of a murine fibrosarcoma." Photochem. Photobiol. 62(1): 162-8.

Kostron, H., D. A. Bellnier, C. W. Lin, M. R. Swartz and R. L. Martuza (1986). "Distribution, retention, and phototoxicity of hematoporphyrin derivative in a rat glioma. Intraneoplastic versus intraperitoneal injection." J. Neurosurg. 64(5): 768-74.

Kostron, H., G. Weiser, E. Fritsch and V. Grunert (1987). "Photodynamic therapy of malignant brain tumors: clinical and neuropathological results." Photochem. Photobiol. 46(5): 937-43.

Kress, M., T. Meier, R. Steiner, F. Dolp, R. Erdmann, U. Ortmann and A. Ruck (2003). "Time-resolved microspectrofluorometry and fluorescence lifetime imaging of photosensitizers using picosecond pulsed diode lasers in laser scanning microscopes." J. Biomed. Opt. 8(1): 26-32.

Kubat, P., K. Lang and P. Anzenbacher, Jr. (2004). "Modulation of porphyrin binding to serum albumin by pH." Biochim. Biophys. Acta 1670(1): 40-8.

Kuzelova, K. and D. Brault (1994). "Kinetic and equilibrium studies of porphyrin interactions with unilamellar lipidic vesicles." Biochemistry 33(32): 9447-59.

Lang, K., P. Kubat, J. Mosinger and D. M. Wagnerova (1998). "Photochemical consequences of porphyrin and phthalocyanine aggregation on nucleoprotein histone." J. Photochem. Photobiol. A 119(1): 47-52.

Lang, K., J. Mosinger and D. M. Wagnerováa (2004). "Photophysical properties of porphyrinoid sensitizers non-covalently bound to host molecules; models for photodynamic therapy." Coord. Chem. Rev. 248(3-4): 321-350.

Lange, Y., A. L. Molinaro, T. R. Chauncey and T. L. Steck (1983). "On the mechanism of transfer of cholesterol between human erythrocytes and plasma." J. Biol. Chem. 258(11): 6920-6.

Lavi, A., H. Weitman, R. T. Holmes, K. M. Smith and B. Ehrenberg (2002). "The depth of porphyrin in a membrane and the membrane's physical properties affect the photosensitizing efficiency." Biophys. J. 82(4): 2101-10.

Ledoux-Lebards, C. (1902). Annales de l'institut Pasteur 16: 593.

Leist, M. and M. Jaattela (2001). "Triggering of apoptosis by cathepsins." Cell Death Differ. 8(4): 324-6.

Leung, W. N., X. Sun, N. K. Mak and C. M. Yow (2002). "Photodynamic effects of mTHPC on human colon adenocarcinoma cells: photocytotoxicity, subcellular localization and apoptosis." Photochem Photobiol 75(4): 406-11.

Lin, C. W., J. R. Shulok, S. D. Kirley, C. M. Bachelder, T. J. Flotte, M. E. Sherwood, L. Cincotta and J. W. Foley (1993). "Photodynamic destruction of lysosomes mediated by Nile blue photosensitizers." Photochem Photobiol 58(1): 81-91.

Lin, H. J., P. Herman and J. R. Lakowicz (2003). "Fluorescence lifetime-resolved pH imaging of living cells." Cytometry A 52(2): 77-89.

Ma, L., J. Moan and K. Berg (1994). "Evaluation of a new photosensitizer, meso-tetra-hydroxyphenyl-chlorin, for use in photodynamic therapy: a comparison of its photobiological properties with those of two other photosensitizers." Int. J. Cancer 57(6): 883-888.

MacDonald, I. J. and T. J. Dougherty (2001). "Basic principles of photodynamic therapy." J. Porphyrins Phthalocyanines 5(2): 105 - 129.

MacDonald, I. J., J. Morgan, D. A. Bellnier, G. M. Paszkiewicz, J. E. Whitaker, D. J. Litchfield and T. J. Dougherty (1999). "Subcellular localization patterns and their relationship to photodynamic activity of pyropheophorbide-a derivatives." Photochem. Photobiol. 70(5): 789-97.

Malik, Z., A. Faraggi and N. Savion (1992). "Ultrastructural damage in photosensitized endothelial cells: dependence on hematoporphyrin delivery pathways." J Photochem Photobiol B 14(4): 359-68.

Mang, T. S., T. J. Dougherty, W. R. Potter, D. G. Boyle, S. Somer and J. Moan (1987). "Photobleaching of porphyrins used in photodynamic therapy and implications for therapy." Photochem. Photobiol. 45(4): 501-6.

Marchal, S., A. Fadloun, E. Maugain, M. A. D'Hallewin, F. Guillemin and L. Bezdetnaya (2005). "Necrotic and apoptotic features of cell death in response to Foscan photosensitization of HT29 monolayer and multicell spheroids." Biochem. Pharmacol. 69(8): 1167-76.

McLean, L. R. and M. C. Phillips (1981). "Mechanism of cholesterol and phosphatidylcholine exchange or transfer between unilamellar vesicles." Biochemistry 20(10): 2893-900.

McMahon, K. S., T. J. Wieman, P. H. Moore and V. H. Fingar (1994). "Effects of photodynamic therapy using mono-L-aspartyl chlorin e6 on vessel constriction, vessel leakage, and tumor response." Cancer Res. 54(20): 5374-9.

Melnikova, V. O., L. N. Bezdetnaya, C. Bour, E. Festor, M. P. Gramain, J. L. Merlin, A. Potapenko and F. Guillemin (1999). "Subcellular localization of meta-tetra (hydroxyphenyl) chlorin in human tumor cells subjected to photodynamic treatment." J. Photochem. Photobiol. B 49(2-3): 96-103.

Melnikova, V. O., L. N. Bezdetnaya, A. Y. Potapenko and F. Guillemin (1999). "Photodynamic properties of meta-tetra(hydroxyphenyl)chlorin in human tumor cells." Radiat Res. 152(4): 428-35.

Merchan, M., E. Orti and B. O. Roos (1994). "Theoretical determination of the electronic spectrum of free base porphin." Chem. Phys. Lett. 226(1-2): 27-36.

Meyer-Betz, F. (1913). "Untersuchungen über die biologische (photodynamische) Wirkung des Hämatoporphyrins und andere Derivate des Blut- und Gallenfarbstoffes." Dtsch. Arch. Klin. Med. 112: 476-503.

Michael-Titus, A. T., R. Whelpton and Z. Yaqub (1995). "Binding of temoporfin to the lipoprotein fractions of human serum." Br. J. Clin. Pharmacol. 40(6): 594-7.

Miller, Y. I. and N. Shaklai (1999). "Kinetics of hemin distribution in plasma reveals its role in lipoprotein oxidation." Biochim. Biophys. Acta 1454(2): 153-64.

Mitra, S. and T. H. Foster (2005). "Photophysical parameters, photosensitizer retention and tissue optical properties completely account for the higher photodynamic efficacy of meso-tetra-hydroxyphenyl-chlorin vs Photofrin." Photochem. Photobiol. 81(4): 849-59.

Moan, J. (1986). "Effect of bleaching of porphyrin sensitizers during photodynamic therapy." Cancer Lett. 33(1): 45-53.

Moan, J. (1990). "On the diffusion length of singlet oxygen in cells and tissues." J. Photochem. Photobiol. B 6: 343-344.

Moan, J. and H. Anholt (1990). "Phthalocyanine fluorescence in tumors during PDT." Photochem Photobiol 51(3): 379-81.

Moan, J., H. Anholt and Q. Peng (1990). "A transient reduction of the fluorescence of aluminium phthalocyanine tetrasulphonate in tumours during photodynamic therapy." J Photochem Photobiol B 5(1): 115-9.

Moan, J. and K. Berg (1991). "The photodegradation of porphyrins in cells can be used to estimate the lifetime of singlet oxygen." Photochem. Photobiol. 53(4): 549-53.

Moan, J., K. Berg, H. Anholt and K. Madslien (1994). "Sulfonated aluminium phthalocyanines as sensitizers for photochemotherapy. Effects of small light doses on localization, dye fluorescence and photosensitivity in V79 cells." Int J Cancer 58(6): 865-70.

Moan, J., K. Berg, E. Kvam, A. Western, Z. Malik, A. Ruck and H. Schneckenburger (1989). Intracellular localization of photosensitizers. Photosensitizing compounds: their Chemistry, Biology and Clinical Use. G. Bock and S. Harnett. Chichester, Wiley. 146: 95-107.

Moan, J. and E. Boye (1981). "Photodynamic effect on DNA and cell survival of human cells sensitized by hematoporphyrin." Photobiochem. Photobiophys. 2: 301–307.

Moan, J., V. Iani and L. W. Ma (1998). "In vivo fluorescence of phthalocyanines during light exposure." J. Photochem. Photobiol. B 42(2): 100-3.

Moan, J., P. Juzenas and S. Bagdonas (2000). "Degradation and transformation of photosensitizers during light exposure." Recent Res. Devel. Photochem. Photobiol. 4: 121-132.

Moan, J. and S. Sommer (1984). "Action spectra for hematoporphyrin derivative and Photofrin II with respect to sensitization of human cells in vitro to photoinactivation." Photochem. Photobiol. 40(5): 631-4.

Moan, J., G. Streckyte, S. Bagdonas, O. Bech and K. Berg (1997). "Photobleaching of protoporphyrin IX in cells incubated with 5-aminolevulinic acid." Int. J. Cancer 70(1): 90-7.

Moan, J., A. Western and C. Rimington (1988). Photomodification of porphyrins in biological systems. Photosensitization. G. Moreno, R. H. Pottier and T. G. Truscott. Berlin,

Heidelberg, New York, London, Paris, Tokyo, Springer-Verlag. NATO ASI Series, vol H 15: 407-418.

Morgan, J. and A. R. Oseroff (2001). "Mitochondria-based photodynamic anti-cancer therapy." Adv. Drug Deliv. Rev. 49(1-2): 71-86.

Morgan, J., W. R. Potter and A. R. Oseroff (2000). "Comparison of photodynamic targets in a carcinoma cell line and its mitochondrial DNA-deficient derivative." Photochem. Photobiol. 71(6): 747-57.

Morliere, P., E. Kohen, J. P. Reyftmann, R. Santus, C. Kohen, J. C. Maziere, S. Goldstein, W. F. Mangel and L. Dubertret (1987). "Photosensitization by porphyrins delivered to L cell fibroblasts by human serum low density lipoproteins. A microspectrofluorometric study." Photochem. Photobiol. 46(2): 183-91.

Morliere, P., J. C. Maziere, R. Santus, C. D. Smith, M. R. Prinsep, C. C. Stobbe, M. C. Fenning, J. L. Golberg and J. D. Chapman (1998). "Tolyporphin: a natural product from cyanobacteria with potent photosensitizing activity against tumor cells in vitro and in vivo." Cancer Res 58(16): 3571-8.

Moser, J. G. (1998). Definition and general properties of 2nd and 3rd generation photosensitizers. Photodynamic tumor therapy. 2nd and 3rd generation photosensitizers. J. G. Moser. Amsterdam, Harwood Academic Publishers: 3-7.

Nagashima, U., T. Takada and K. Ohno (1986). "Ab initio SCF-CI calculation on free base porphin and chlorin; theoretical analysis on intensities of the absorption spectra." J. Chem. Phys. 85(8): 4524-4529.

Nichols, J. W. (1988). "Kinetics of fluorescent-labeled phosphatidylcholine transfer between nonspecific lipid transfer protein and phospholipid vesicles." Biochemistry 27(6): 1889-96.

Niedre, M. J., A. J. Secord, M. S. Patterson and B. C. Wilson (2003). "In vitro tests of the validity of singlet oxygen luminescence measurements as a dose metric in photodynamic therapy." Cancer Res. 63(22): 7986-94.

Obochi, M. O., R. W. Boyle and J. E. van Lier (1993). "Biological activities of phthalocyanines. XIII. The effects of human serum components on the in vitro uptake and photodynamic activity of zinc phthalocyanine." Photochem. Photobiol. 57(4): 634-640.

Oenbrink, G., P. Jurgenlimke and D. Gabel (1988). "Accumulation of porphyrins in cells: influence of hydrophobicity aggregation and protein binding." Photochem. Photobiol. 48(4): 451-6.

Ouedraogo, G., P. Morliere, M. Bazin, R. Santus, B. Kratzer, M. A. Miranda and J. V. Castell (1999). "Lysosomes are sites of fluoroquinolone photosensitization in human skin fibroblasts: a microspectrofluorometric approach." Photochem Photobiol 70(2): 123-9.

Parkash, J., J. H. Robblee, J. Agnew, E. Gibbs, P. Collings, R. F. Pasternack and J. C. de Paula (1998). "Depolarized resonance light scattering by porphyrin and chlorophyll a aggregates." Biophys. J. 74(4): 2089-99.

Pasternack, R. F. and P. J. Collings (1995). "Resonance light scattering: a new technique for studying chromophore aggregation." Science 269(5226): 935-9.

Peng, Q., G. W. Farrants, K. Madslien, J. C. Bommer, J. Moan, H. E. Danielsen and J. M. Nesland (1991). "Subcellular localization, redistribution and photobleaching of sulfonated aluminum phthalocyanines in a human melanoma cell line." Int. J. Cancer 49(2): 290-5.

Peters, T. (1995). "All About Albumin." Academic Press, San Diego.

Plaetzer, K., T. Kiesslich, B. Krammer and P. Hammerl (2002). "Characterization of the cell death modes and the associated changes in cellular energy supply in response to AlPcS4-PDT." Photochem. Photobiol. Sci. 1(3): 172-7.

Pogue, B. W., B. Ortel, N. Chen, R. W. Redmond and T. Hasan (2001). "A photobiological and photophysical-based study of phototoxicity of two chlorins." Cancer Res 61(2): 717-24.

Polo, L., A. Segalla, G. Jori, G. Bocchiotti, G. Verna, R. Franceschini, R. Mosca and P. G. De Filippi (1996). "Liposome-delivered 131I-labelled Zn(II)-phthalocyanine as a radiodiagnostic agent for tumours." Cancer Lett. 109(1-2): 57-61.

Potter, W. R., T. S. Mang and T. J. Dougherty (1987). "The theory of photodynamic therapy dosimetry: consequences of photo-destruction of sensitizer." Photochem. Photobiol. 46(1): 97-101.

Pottier, R. and J. C. Kennedy (1990). "The possible role of ionic species in selective biodistribution of photochemotherapeutic agents toward neoplastic tissue." J. Photochem. Photobiol. B 8(1): 1-16.

Raab, O. (1900). "Ueber die Wirkung fluorescirender Stoffe auf Infusorien." Z. Biol (Munich) 39: 524-546.

Rashid, F. and R. W. Horobin (1990). "Interaction of molecular probes with living cells and tissues. Part 2. A structure-activity analysis of mitochondrial staining by cationic probes, and a discussion of the synergistic nature of image-based and biochemical approaches." Histochemistry 94(3): 303-8.

Reddi, E. (1997). "Role of delivery vehicles for photosensitizers in the photodynamic therapy of tumours." J. Photochem. Photobiol. B 37(3): 189-95.

Reddi, E. and G. Jori (1988). "Steady state and time resolved spectroscopic studies of photodynamic sensitizers: porphyrins and phthalocyanines." Recv. Chem. Intermed. 10: 241-268.

Reddi, E., G. Jori, M. A. J. Rodgers and J. D. Spikes (1983). "Flash photolysis studies of hemato- and copro-porphyrins in homogeneous and microheterogeneous aqueous dispersions." Photochem. Photobiol. 38: 639–645.

Redmond, R. W., E. J. Land and T. G. Truscott (1985). "Aggregation effects on the photophysical properties of porphyrins in relation to mechanisms involved in photodynamic therapy." Adv. Exp. Med. Biol. 193: 293-302.

Ricchelli, F. (1995). "Photophysical properties of porphyrins in biological membranes." J. Photochem. Photobiol. B 29(2-3): 109-18.

Ricchelli, F., P. Nikolov, S. Gobbo, G. Jori, G. Moreno and C. Salet (1994). "Interaction of phthalocyanines with lipid membranes: a spectroscopic and functional study on isolated rat liver mitochondria." Biochim. Biophys. Acta 1196(2): 165-71.

Richter, A. M., E. Waterfield, A. K. Jain, A. J. Canaan, B. A. Allison and J. G. Levy (1993). "Liposomal delivery of a photosensitizer, benzoporphyrin derivative monoacid ring A (BPD), to tumor tissue in a mouse tumor model." Photochem. Photobiol. 57(6): 1000-6.

Ris, H. B., Q. Li, T. Krueger, C. K. Lim, B. Reynolds, U. Althaus and H. J. Altermatt (1998). "Photosensitizing effects of m-tetrahydroxyphenylchlorin on human tumor xenografts: correlation with sensitizer uptake, tumor doubling time and tumor histology." Int. J. Cancer 76(6): 872-4.

Roberts, W. G. and T. Hasan (1992). "Role of neovasculature and vascular permeability on the tumor retention of photodynamic agents." Cancer Res. 52(4): 924-30.

Robinson, D. J., H. S. de Bruijn, N. van der Veen, M. R. Stringer, S. B. Brown and W. M. Star (1998). "Fluorescence photobleaching of ALA-induced protoporphyrin IX during photodynamic therapy of normal hairless mouse skin: the effect of light dose and irradiance and the resulting biological effect." Photochem. Photobiol. 67(1): 140-9.

Ronn, A. M., J. Batti, C. J. Lee, D. Yoo, M. E. Siegel, M. Nouri, L. A. Lofgren and B. M. Steinberg (1997). "Comparative biodistribution of meta-Tetra(Hydroxyphenyl) chlorin

in multiple species: clinical implications for photodynamic therapy." Lasers Surg. Med. 20(4): 437-42.

Roseman, M. A. and T. E. Thompson (1980). "Mechanism of the spontaneous transfer of phospholipids between bilayers." Biochemistry 19(3): 439-44.

Rosenberger, V. and R. Margalit (1993). "Thermodynamics of the binding of hematoporphyrin ester, a hematoporphyrin derivative-like photosensitizer, and its components to human serum albumin, human high-density lipoprotein and human low-density lipoprotein." Photochem. Photobiol. 58(5): 627-30.

Rosenkranz, A. A., D. A. Jans and A. S. Sobolev (2000). "Targeted intracellular delivery of photosensitizers to enhance photodynamic efficiency." Immunol Cell Biol 78(4): 452-64.

Rotomskis, R., S. Bagdonas and G. Streckyte (1996). "Spectroscopic studies of photobleaching and photoproduct formation of porphyrins used in tumour therapy." J. Photochem. Photobiol. B 33(1): 61-7.

Rotomskis, R., G. Streckyte and S. Bagdonas (1997). "Phototransformations of sensitizers 1. Significance of the nature of the sensitizer in the photobleaching process and photoproduct formation in aqueous solution." J. Photochem. Photobiol. B 39(2): 167-171.

Rovers, J. P., M. L. de Jode and M. F. Grahn (2000). "Significantly increased lesion size by using the near-infrared photosensitizer 5,10,15,20-tetrakis (m-hydroxyphenyl)bacteriochlorin in interstitial photodynamic therapy of normal rat liver tissue." Lasers Surg Med 27(3): 235-40.

Rovers, J. P., M. L. de Jode, H. Rezzoug and M. F. Grahn (2000). "In vivo photodynamic characteristics of the near-infrared photosensitizer 5,10,15,20-tetrakis(M-hydroxyphenyl) bacteriochlorin." Photochem. Photobiol. 72(3): 358-64.

Ruck, A., G. Beck, R. Bachor, N. Akgun, M. H. Gschwend and R. Steiner (1996). "Dynamic fluorescence changes during photodynamic therapy in vivo and in vitro of hydrophilic A1(III) phthalocyanine tetrasulphonate and lipophilic Zn(II) phthalocyanine administered in liposomes." J. Photochem. Photobiol. B 36(2): 127-33.

Ruck, A., C. Hildebrandt, T. Kollner, H. Schneckenburger and R. Steiner (1990). "Competition between photobleaching and fluorescence increase of photosensitizing porphyrins and tetrasulphonated chloroaluminiumphthalocyanine." J. Photochem. Photobiol. B 5(3-4): 311-9.

Ruck, A., T. Kollner, A. Dietrich, W. Strauss and H. Schneckenburger (1992). "Fluorescence formation during photodynamic therapy in the nucleus of cells incubated with cationic and anionic water-soluble photosensitizers." J. Photochem. Photobiol. B 12(4): 403-12.

Runnels, J. M., N. Chen, B. Ortel, D. Kato and T. Hasan (1999). "BPD-MA-mediated photosensitization in vitro and in vivo: cellular adhesion and beta1 integrin expression in ovarian cancer cells." Br. J. Cancer 80(7): 946-53.

Sanders, R., A. Draaijer, H. C. Gerritsen, P. M. Houpt and Y. K. Levine (1995). "Quantitative pH imaging in cells using confocal fluorescence lifetime imaging microscopy." Anal. Biochem. 227(2): 302-8.

Savary, J. F., P. Grosjean, P. Monnier, C. Fontolliet, G. Wagnieres, D. Braichotte and H. van den Bergh (1998). "Photodynamic therapy of early squamous cell carcinomas of the esophagus: a review of 31 cases." Endoscopy 30(3): 258-65.

Savary, J. F., P. Monnier, C. Fontolliet, J. Mizeret, G. Wagnieres, D. Braichotte and H. van den Bergh (1997). "Photodynamic therapy for early squamous cell carcinomas of the esophagus, bronchi, and mouth with m-tetra (hydroxyphenyl) chlorin." Arch Otolaryngol Head Neck Surg 123(2): 162-8.

Schneckenburger, H. (2005). "Total internal reflection fluorescence microscopy: technical innovations and novel applications." Curr. Opin. Biotechnol. 16(1): 13-8.

Schneckenburger, H., M. H. Gschwend, R. Sailer, A. Ruck and W. S. Strauss (1995). "Time-resolved pH-dependent fluorescence of hydrophilic porphyrins in solution and in cultivated cells." J. Photochem. Photobiol. B 27(3): 251-5.

Schulthess, G., G. Lipka, S. Compassi, D. Boffelli, F. E. Weber, F. Paltauf and H. Hauser (1994). "Absorption of monoacylglycerols by small intestinal brush border membrane." Biochemistry 33(15): 4500-8.

Scully, A. D., R. B. Ostler, A. J. MacRobert, A. W. Parker, C. de Lara, P. O'Neill and D. Phillips (1998). "Laser line-scanning confocal fluorescence imaging of the photodynamic action of aluminum and zinc phthalocyanines in V79-4 Chinese hamster fibroblasts." Photochem. Photobiol. 68(2): 199-204.

Scully, A. D., R. B. Ostler, D. Phillips, P. O'Neill, A. W. Parker and A. J. MacRobert (1997). "Application of fluorescence lifetime imaging microscopy to the investigation of intracellular PDT mechanisms." Bioimaging 5: 9–18.

Serrano-Andres, L., M. Merchan, M. Rubio and B. O. Roos (1998). "Interpretation of the electronic absorption spectrum of free base porphin by using multiconfigurational second-order perturbation theory." Chem. Phys. Lett. 295(3): 195-203.

Sharkey, S. M., B. C. Wilson, R. Moorehead and G. Singh (1993). "Mitochondrial alterations in photodynamic therapy-resistant cells." Cancer Res 53(20): 4994-9.

Sharman, W. M., C. M. Allen and J. E. van Lier (2000). "Role of activated oxygen species in photodynamic therapy." Methods Enzymol 319: 376-400.

Sheppard, C. J. R. (2003). "Scanning confocal microscopy, in Encyclopedia of Optical Engineering." Marcel Dekker, New York: 22–41.

Singh, G., W. P. Jeeves, B. C. Wilson and D. Jang (1987). "Mitochondrial photosensitization by Photofrin II." Photochem Photobiol 46(5): 645-9.

Sorensen, R., V. Iani and J. Moan (1998). "Kinetics of photobleaching of protoporphyrin IX in the skin of nude mice exposed to different fluence rates of red light." Photochem. Photobiol. 68(6): 835-40.

Spikes, J. D. (1985). "The historical development of ideas on applications of photosensitised reactions in health sciences, In: Bergasson, R.V., Jori, G., Land, E.J., Truscott, T.G. (Eds.) Primary photoprocesses in Biology and Medicine." Plenum Press, New York: 209-227.

Spikes, J. D. (1992). "Quantum yields and kinetics of the photobleaching of hematoporphyrin, Photofrin II, tetra(4-sulfonatophenyl)-porphine and uroporphyrin." Photochem. Photobiol. 55(6): 797-808.

Spikes, J. D. and J. C. Bommer (1993). Photobleaching of mono-L-aspartyl chlorin e6 (NPe6): a candidate sensitizer for the photodynamic therapy of tumors. Photochem Photobiol. 58: 346-50.

Steck, T. L., F. J. Kezdy and Y. Lange (1988). "An activation-collision mechanism for cholesterol transfer between membranes." J. Biol. Chem. 263(26): 13023-31.

Steele, P. M., J. H. Chesebro, A. W. Stanson, D. R. Holmes, Jr., M. K. Dewanjee, L. Badimon and V. Fuster (1985). "Balloon angioplasty. Natural history of the pathophysiological response to injury in a pig model." Circ. Res. 57(1): 105-12.

Steichen, J. D., K. Dashner and R. L. Martuza (1986). "Distribution of hematoporphyrin derivative in canine glioma following intraneoplastic and intraperitoneal injection." J. Neurosurg. 65(3): 364-9.

Streckyte, G. and R. Rotomskis (1993a). "Phototransformation of porphyrins in aqueous and micellar media." J Photochem Photobiol B 18: 259-263.

Streckyte, G. and R. Rotomskis (1993b). "Phototransformation of porphyrins under clinically relevant light irradiation." Biology 3: 26-31.

Stryer, L. (1978). "Fluorescence energy transfer as a spectroscopic ruler." Annu. Rev. Biochem. 47: 819-46.

Suhling, K., P. M. French and D. Phillips (2005). "Time-resolved fluorescence microscopy." Photochem. Photobiol. Sci. 4(1): 13-22.

Sun, X. and W. N. Leung (2002). "Photodynamic therapy with pyropheophorbide-a methyl ester in human lung carcinoma cancer cell: efficacy, localization and apoptosis." Photochem. Photobiol. 75(6): 644-51.

Szeimies, R. M., Dräger, J., Abels, C., Landthaler, M. (2001). "History of photodynamic therapy in dermatology, In: Calzavara-Pinton, P., Szeimies, R.M., Ortel, B. (Eds.) Photodynamic therapy and fluorescence diagnosis in dermatology." Elsevier Science.

Tadrous, P. J., J. Siegel, P. M. French, S. Shousha, N. Lalani el and G. W. Stamp (2003). "Fluorescence lifetime imaging of unstained tissues: early results in human breast cancer." J. Pathol. 199(3): 309-17.

Tanielian, C., C. Schweitzer, R. Mechin and C. Wolff (2001). "Quantum yield of singlet oxygen production by monomeric and aggregated forms of hematoporphyrin derivative." Free Radic. Biol. Med. 30(2): 208-12.

Teiten, M. H., L. Bezdetnaya, J. L. Merlin, C. Bour-Dill, M. E. Pauly, M. Dicato and F. Guillemin (2001). "Effect of meta-tetra(hydroxyphenyl)chlorin (mTHPC)-mediated photodynamic therapy on sensitive and multidrug-resistant human breast cancer cells." J. Photochem. Photobiol. B 62(3): 146-52.

Teiten, M. H., L. Bezdetnaya, P. Morliere, R. Santus and F. Guillemin (2003). "Endoplasmic reticulum and Golgi apparatus are the preferential sites of Foscan localisation in cultured tumour cells." Br. J. Cancer 88(1): 146-52.

Teiten, M. H., S. Marchal, M. A. D'Hallewin, F. Guillemin and L. Bezdetnaya (2003). "Primary photodamage sites and mitochondrial events after Foscan photosensitization of MCF-7 human breast cancer cells." Photochem. Photobiol. 78(1): 9-14.

Theodossiou, T., M. D. Spiro, J. Jacobson, J. S. Hothersall and A. J. Macrobert (2004). "Evidence for intracellular aggregation of hypericin and the impact on its photocytotoxicity in PAM 212 murine keratinocytes." Photochem. Photobiol. 80(3): 438-43.

Thibaut, S., L. Bourre, D. Hernot, N. Rousset, Y. Lajat and T. Patrice (2002). "Effects of BAPTA-AM, Forskolin, DSF and Z.VAD.fmk on PDT-induced apoptosis and m-THPC phototoxicity on B16 cells." Apoptosis 7(2): 99-106.

Thilo, L. (1977). "Kinetics of phospholipid exchange between bilayer membranes." Biochim. Biophys. Acta 469(3): 326-34.

Trivedi, N. S., H. W. Wang, A. L. Nieminen, N. L. Oleinick and J. A. Izatt (2000). "Quantitative analysis of Pc 4 localization in mouse lymphoma (LY-R) cells via double-label confocal fluorescence microscopy." Photochem. Photobiol. 71(5): 634-9.

Tsuchida, T., G. Zheng, R. K. Pandey, W. R. Potter, D. A. Bellnier, B. W. Henderson, H. Kato and T. J. Dougherty (1997). "Correlation between site II-specific human serum albumin (HSA) binding affinity and murine in vivo photosensitizing efficacy of some Photofrin components." Photochem. Photobiol. 66(2): 224-228.

van Lier, J. E. and J. D. Spikes (1989). "The chemistry, photophysics and photosensitizing properties of phthalocyanines." Ciba Found Symp 146: 17-26; discussion 26-32.

van Munster, E. B. and T. W. Gadella (2005). "Fluorescence lifetime imaging microscopy (FLIM)." Adv. Biochem. Eng. Biotechnol. 95: 143-75.

Veenhuizen, R., H. Oppelaar, M. Ruevekamp, J. Schellens, O. Dalesio and F. Stewart (1997). "Does tumour uptake of Foscan determine PDT efficacy?" Int. J. Cancer 73(2): 236-9.

von Hippel, P. H. and O. G. Berg (1989). "Facilitated target location in biological systems." J. Biol. Chem. 264(2): 675-8.

von Smoluchowski, M. (1917). "Veruch einer mathematischen theorie der koagulationskinetik kolloider losungen." Z. Phys. Chem. Leipzig. 92: 129-168.

von Tappeiner, H. and A. Jesionek (1903). "Terapeutische versuche mit fluoreszierenden Stoffen." Münch. Med. Wochenschr. 50: 2042-2044.

von Tappeiner, H. and A. Jodlbauer (1904). "Ueber die Wirkung der photodynamischen (fluorescierenden) Stoffe auf Protozoen und Enzyme." Arch. Klin. Med. 80: 427-487.

Weiss, C., H. Kobayashi and M. Gouterman (1965). "Spectra of porphyrins : Part III. Self-consistent molecular orbital calculations of porphyrin and related ring systems." J. Mol. Spectrosc. 16(2): 415-450.

Wilson, B. C., M. Olivo and G. Singh (1997). "Subcellular localization of Photofrin and aminolevulinic acid and photodynamic cross-resistance in vitro in radiation-induced fibrosarcoma cells sensitive or resistant to photofrin-mediated photodynamic therapy." Photochem. Photobiol. 65(1): 166-76.

Wilson, P. D., R. A. Firestone and J. Lenard (1987). "The role of lysosomal enzymes in killing of mammalian cells by the lysosomotropic detergent N-dodecylimidazole." J. Cell Biol. 104(5): 1223-9.

Wood, S. R., J. A. Holroyd and S. B. Brown (1997). "The subcellular localization of Zn(II) phthalocyanines and their redistribution on exposure to light." Photochem. Photobiol. 65(3): 397-402.

Woodburn, K. W., N. J. Vardaxis, J. S. Hill, A. H. Kaye and D. R. Phillips (1991). "Subcellular localization of porphyrins using confocal laser scanning microscopy." Photochem. Photobiol. 54(5): 725-32.

Wouters, F. S., P. J. Verveer and P. I. Bastiaens (2001). "Imaging biochemistry inside cells." Trends Cell Biol. 11(5): 203-11.

Xavier, K. A. and R. C. Willson (1998). "Association and dissociation kinetics of anti-hen egg lysozyme monoclonal antibodies HyHEL-5 and HyHEL-10." Biophys. J. 74(4): 2036-45.

Xue, L. Y., S. M. Chiu and N. L. Oleinick (2001a). "Photodynamic therapy-induced death of MCF-7 human breast cancer cells: a role for caspase-3 in the late steps of apoptosis but not for the critical lethal event." Exp. Cell Res. 263(1): 145-55.

Xue, L. Y., S. M. Chiu and N. L. Oleinick (2001b). "Photodynamic therapy-induced death of MCF-7 human breast cancer cells: a role for caspase-3 in the late steps of apoptosis but not for the critical lethal event." Exp Cell Res 263(1): 145-55.

Yang, E. and W. H. Huestis (1993). "Mechanism of intermembrane phosphatidylcholine transfer: effects of pH and membrane configuration." Biochemistry 32(45): 12218-28.

Yow, C. M., J. Y. Chen, N. K. Mak, N. H. Cheung and A. W. Leung (2000). "Cellular uptake, subcellular localization and photodamaging effect of temoporfin (mTHPC) in nasopharyngeal carcinoma cells: comparison with hematoporphyrin derivative." Cancer Lett 157(2): 123-31.

Yu, L., M. J. Lenardo and E. H. Baehrecke (2004). "Autophagy and caspases: a new cell death program." Cell Cycle 3(9): 1124-6.

Yuan, F., M. Leunig, D. A. Berk and R. K. Jain (1993). "Microvascular permeability of albumin, vascular surface area, and vascular volume measured in human adenocarcinoma LS174T using dorsal chamber in SCID mice." Microvasc. Res. 45(3): 269-89.

Zilberstein, J., S. Schreiber, M. C. Bloemers, P. Bendel, M. Neeman, E. Schechtman, F. Kohen, A. Scherz and Y. Salomon (2001). "Antivascular treatment of solid melanoma

tumors with bacteriochlorophyll-serine-based photodynamic therapy." Photochem. Photobiol. 73(3): 257-66.

Zucker, R. M. and O. Price (2001). "Evaluation of confocal microscopy system performance." Cytometry 44(4): 273-94.

ANNEXES

French Summary

I INTRODUCTION GENERALE

La thérapie photodynamique (PDT) a été développée comme modalité de traitement pour un certain nombre de pathologies malignes et non-malignes. Le traitement PDT est une combinaison d'une drogue avec des propriétés photosensibilisantes, de lumière visible et d'oxygène. Séparèment, ces trois composés sont sans effet, mais en combinaison ils peuvent détruite le tissu et inactiver les cellules.

La liaison des photosensibilisants aux protéines du sérum semble essentiel pour une PDT efficace, puisque l'injection directe de photosensibilisants dans la lésion a été sans succès. Dans les milieux aqueux comme le plasma sanguin, la plupart des PSs tétrapyrroliques forment des dimères et des agrégats élevés. La dissociation de molécules de PS des agrégats est déterminée par les interactions avec les protéines de plasma. L'agrégation et la désagrégation des porphyrines a lieu dans la circulation sanguine, et la compétition entre ces processus peut affecter l'efficacité *in vivo* de la PDT. Les caractéristiques de la liaison aux protéines du plasma avec les paramètres dynamiques de redistribution entre les protéines du plasma et les biomembranes définit l'interaction des photosensibilisants avec les cellules, leur localisation intracellulaire et les cinétiques de l'accumulation des photosensibilisants dans la tumeur. L'affinité de liaison des protéines du plasma pour différents photosensibilisants peut jouer un rôle important dans la distribution de la drogue et l'efficacité photodynamique.

Meta-tetra(hydroxyphenyl)chlorin (mTHPC) or Foscan® est un photosensibilisant de seconde generation et il est l'un des plus efficace à l'heure actuelle. Son efficacité photodynamique est environ deux fois plus élevée que celle du Photofrin. La mTHPC a reçu l'agrément européen pour le traitement palliatif des patients avec des cancers avancés de la tête et du cou et il est considéré comme une modalité thérapeutique d'autres tumeurs malignes.

II INTRODUCTION BIBLIOGRAPHIQUE
Généralités

La thérapie photodynamique (PDT) est un traitement alternatif employé à des fins curatives pour des tumeurs solides de petites tailles, telles que les tumeurs du poumon, vessie,

tête et cou, œsophage, et de la peau. Elle est aussi utilisée à visée palliative dans le cas de grosses tumeurs infiltrantes ou récidivantes.

Cette technique est basée sur l'activation par la lumière d'une molécule, appelée photosensibilisant, se répartissant de manière prépondérante dans le tissu néoplasique (Kessel and Woodburn, 1993). Le photosensibilisant non toxique à l'obscurité, génère sous l'effet d'une irradiation lumineuse des processus photochimiques produisant des espèces chimiques cytotoxiques.

Trois mécanismes essentiels sont impliqués dans la destruction tumorale par PDT (Dougherty et al., 1998; Peng et al., 1996) :

(i) *destruction directe des cellules tumorales*, conséquence de l'altération des fonctions des organelles cellulaires et des systèmes biomembranaires par effet direct de la PDT ; (ii) *destruction indirecte des cellules tumorales* qui se produit par la destruction première de la néo-vascularisation tumorale ; le processus est suivi par l'hypoxie et finalement aboutit à la mort des cellules néoplasiques dans la tumeur; (iii) *destruction par effets immunologiques*, parce que la PDT cause la libération de cytokines et d'autres médiateurs inflammatoires par les cellules traitées produisant une réponse inflammatoire et recrutant des cellules immunocompétentes (lymphocytes et phagocytes). La contribution de chaque mécanisme à la réponse tumorale générale dépend du photosensibilisant et de la tumeur. Il semble probable que *tous ces mécanismes s'associent pour assurer le contrôle tumoral à long terme.*

Les mechanismes de photosensitization

Les réactions photochimiques caractérisent l'effet direct de la PDT. Après absorption d'un photon d'énergie hv, le photosensibilisant est excité et passe d'un niveau d'énergie fondamental à un niveau singulet excité.

Le retour au niveau singulet fondamental s'effectue en quelques nanosecondes sauf dans le cas d'une transition inter-système, où par rotation de spin le photosensibilisant passe d'un état singulet excité à un état triplet de moindre énergie avec une durée de vie allant jusqu'à la milliseconde. Ce délai permet au photosensibilisant de réagir avec les molécules de son environnement proche avant de redescendre à son niveau d'énergie fondamental.

Ces réactions photochimiques peuvent être de deux types :

La réaction photochimique de type I :

Elle conduit le photosensibilisant dans son état triplet (^{3}P*) à réagir avec un substrat en produisant des radicaux libres, chargés ou neutres. Ces réactions consistent, soit en un transfert d'hydrogène vers le photosensibilisant avec formation de radicaux libres neutres, soit en un transfert d'électron avec formation d'une forme ionique chargée. Les radicaux formés réagissent avec l'oxygène moléculaire (^{3}O$_2$), aboutissant à la formation de produits de photooxydation très puissants. Les espèces réactive de l'oxygène ainsi produites sont l'anion superoxide, le peroxyde d'hydrogène et le radical hydroxyle .

La réaction photochimique de type II :

Ce phénomène est préférentiel dans les tissus bien oxygénés, par transfert d'énergie il y a réaction entre le photosensibilisant dans son état triplet (^{3}P*) et l'oxygène moléculaire (^{3}O$_2$), pour aboutir à l'oxygène singulet (^{1}O$_2$). Ce dernier est une molécule très réactive, hautement toxique et de faible durée de vie. Ce qui lui permet de réagir dans un rayon de 10 à 20 nm avec des substrats cellulaires pour donner principalement des peroxydes.

Propriete photophysique et photochimique de photosensibilisantes

On dénombre aujourd'hui trois classes de photosensibilisants: ceux de première, seconde et troisième génération. Ce qui caractérise les photosensibilisants de seconde génération par rapport à leurs prédécesseurs est une modification des substituants du noyau tétrapyrolique, ce qui à pour effet de changer le spectre d'absorption de la molécule et d'augmenter la sélectivité tumorale. Quant aux photosensibilisants de troisième génération ils sont généralement couplés à une autre molécule (BSA, EGF…) ou encapsulés (liposomes…).

Le photosensibilisant idéal en Thérapie Photodynamique

Bonnett et Mac Robert en 1989 ont défini les caractéristiques d'un photosensibilisant idéal afin aboutir à une action photodynamique efficace (Bonnett et al., 1989; MacRobert et al., 1989).

- Le photosensibilisant recherché en PDT doit avoir un rendement quantique en oxygène singulet élevé, afin d'induire des réactions photochimiques importantes.
  - Il doit posséder une absorption optimale dans le rouge entre 650 et 800 nm, là où les tissus sont les plus transparents à la lumière.
  - -Il doit être sélectif vis-à-vis de la tumeur, en étant de préférence amphiphile, pour une solubilité satisfaisante dans milieux hydrophiles et hydrophobes. Cette caractéristique

va lui permettre de s'incorporer dans les organites cellulaires, ainsi que dans les membranes de ces organites.

- Il doit être pur et non toxique en absence de lumière, pour que la photosensibilisation cutanée soit faible et courte. Le photosensibilisant doit avoir une clairance rapide.

Le Photoblanchiment

La plupart des photosensibilisants utilisés en PDT, tels que les molécules de type porphyrines, chlorines et phtalocyanines, ne sont pas photostables. En solution ou dans un environnement complexe, ils subissent des modifications induites par la lumière qui se traduisent par une diminution de leur intensité initiale d'absorption, et de ce fait une diminution de leurs activités phototoxiques.

Les modifications spectrales de la fluorescence des porphyrines dans les cellules peuvent être dues à trois phénomènes (Bonnett et al., 1999b; Bonnett and Martínez, 2001; Moan et al., 2000) :

-La photodégradation ou « *true photobleaching* », c'est à dire la conversion du photosensibilisant en produits qui n'absorbent pas la lumière visible de manière significative, accompagnée de la destruction de structure macrocyclique.

-La phototransformation ou « *photomodification* », modification photochimique sans destruction du macrocycle, qui conduit à la formation de nouveaux photoproduits absorbant dans le rouge.
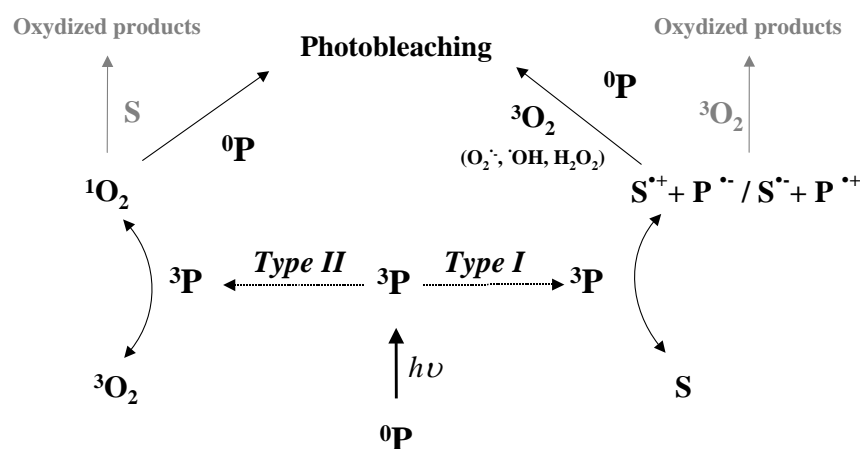
Mécanismes de photoblanchiment

Figure 1. : Mécanismes de photoblanchiment intervenant après l'absorption d'un photon par le photosensibilisant.

Les mécanismes de photoblanchiment empruntent les même voies que les mécanismes de cytotoxicité, c'est à dire les mécanismes de Type I et de Type II, dans ce cas le substrat oxydé se trouve être le photosensibilisant.

De nombreux éléments influencent les mécanismes de photoblanchiment, à savoir :

- L'état d'agrégation, le pH, la force ionique et les surfactants.

- La concentration en oxygène.

- Les « quenchers » de Type I & II.

- Les substrats photo-oxidables.

Paramètres affectant la cinétique photoblanchiment

Le photoblanchiment a longtemps été considéré comme étant un mécanisme uniquement dépendant de la dose de lumière délivrée au tissu, décrit par une décroissance mono-exponentielle de type $e^{-\alpha D}$, ou α représente la constante de photoblanchiment et D représente la fluence (J cm^{-2}) de l'irradiation. Or il est apparu que les cinétiques de photoblanchiment sont des phénomènes complexes qui ne peuvent pas être décrits par une simple décroissance mono-exponentielle (Moan et al., 2000; Sørensen et al., 1998). Plusieurs paramètres peuvent influencer la cinétique du photoblanchiment tels que la présence de différent sites de liaison des photosensibilisants dans les tissus ou cellules, la relocalisation du photosensibilisant pendant l'irradiation et la déplétion en oxygène durant le traitement.

Les propriétés photophysiques du photosensibilisant porphyrinoid avec une liaison non-covalente aux protéines

L'influence de l'environnement biologique sur les propriétés du PS doivent être pris en compte étant donné que pour être photodynamiquement actif, le photosensibilisant doit être associé de façon étroite à la cible. L'influence de l'environnement peut être attribué aux interactions non-covalentes du photosensibilisant avec les molécules biologique. L'interaction non-covalente exerce un grand impact sur les propriétés photophysiques de la molécule de photosensibilisant (Henderson and Dougherty 1992 ; Ricchelli 1995 ; Aveline and Redmond 1999). L'interaction non-covalente des photosensibilisants ne réduit pas la formation des états singulets excités, des états triplets et donc la formation d'$^1O_2$. La liaison influence les propriétés spectroscopiques et les paramètres cinétiques, les durées de vie des états excités et les constantes du taux de quenching collisionel. Le rendement de fluorescence Φ_f, le taux de

formation de l'état triplet Φ_T et le rendement quantique Φ_Δ de formation de $^1O_2$ reste en grande partie inchangé. Mais la prédiction de l'efficacité photosensibilisante dans les systèmes biologiques est difficile car l'effet global des processus photodynamiques est affecté par une combinaison de nombreux facteurs, souvent des facteurs agissant de façon opposée comme l'agrégation, la monomérisation, la compartementalisation, et la restriction des mouvements internes.

Interactions des photosensibilisants avec les proteines de plasma

La liaison des photosensibilisants aux protéines de plasma est le premier pas important pour une PDT efficace car elle détermine le transport du photosensibilisant dans les sites sub-cellulaires sensibles. L'importance des interactions des photosensibilisants avec les protéines du plasma vient du fait que l'injection directe de photosensibilisants dans la lésion est inefficace (Brown et al. 2004). Comme il est montré dans l'étude des pharmacocinétiques, les protéines de plasma jouent un rôle important dans le transport du photosensibilisant et les interactions dans le sang.

Pharmacocinétiques des photosensibilisants

Les différents photosensibilisants ont des pharmacocinétiques et une biodistribution très différents. Avec les possibles exceptions de l'uroporphyrine et quelques-uns des plus grands agrégats présents dans le Photofrin, tous les photosensibilisants tétrapyrroliques, qui ont été suggéré comme drogues en PDT sont plus ou moins étroitement liés aux protéines du sérum après injection intraveineuse. Trois classes de ces composants, qui ont des propriétés de localisation de tumeur, peuvent être déterminées.

(a) les composés relativement hydrophiliques, qui sont liés à l'albumine
(b) les composés amphiphiliques, qui s'insérer dans la couche de phospholipides et apoprotéines des particules de lipoprotéines
(a) composés hydrophobiques, qui nécessitent un véhicule de solubilisation comme les liposomes, crémaphores EL ou Tween 80

Le type de transporteur de protéine influence le transport du photosensibilisant à la tumeur (Jori and Reddi 1993). Comme il a été mentionnée ci-dessus, le transport in vivo de plusieurs dérivés porphyrinoides avec un degré modéré et élevé d'hydrophobicité est effectué par les lipoprotéines (Jori and Reddi 1993). L'albumine du sérum, la protéine la plus abondante dans le plasma sanguin sert comme transporteur pour les photosensibilisants

amphiphiles et hydrophiles (Kessel et al 1987, Peters 1995). Il a été suggéré que le transport des photosensibilisants avec différents systèmes macromoléculaires pouvait conduire à des mécanismes de destruction tumorale différents. L'albumine et les globulines sont connus pour le transport de PS principalement au stroma vasculaire des tumeurs (Jori 1989). Les HDL transfèrent le photosensibilisant aux cellules via un échange non spécifique avec la membrane plasmatique. Le LDL transfèrent probablement une large fraction du PS via une voie médiée par un récepteur actif (Morlière et al, 1987).

Localisation intracellulaire des photosensibilisants

La haute réactivité et la courte demi-vie de l'oxygène singulet et des radicaux hydroxyl déterminent leur action localisée aux molécules biologiques et les structures proches des régions de localisation du PS. Le radius de l'action de l'oxygène singulet dans l'environnement biologique est de l'ordre de 20 nm (Moan and Berg 1991). La localisation subcellulaire est gouvernée par la nature chimique du PS, la lipophilicité, l'amphiphilicité, la charge ionique et les caractéristiques de liaison aux protéines, la concentration du PS, le temps d'incubation, la concentration de sérum et le type de cellule cible (Rosenkranz et al 2000). La façon précise dont la PDT influence la mort cellulaire dépend aussi de la localisation intracellulaire du PS (Kessel et al. 1997). Par conséquent, le site de localisation intracellulaire du PS est un paramètre important en PDT.

Technique pour étudier la localisation intracellulaire et l'état d'agrégation

La microscopie de fluorescence est la principale technique pour étudier la localisation intracellulaire des PSs car l'intensité de fluorescence dépend de différentes influences environnementales, comme le quenching par les autres molécules, l'agrégation, le transfert d'énergie, les effets de l'indice   (Suhling et al. 2005). En utilisant cette technique, l'émission de fluorescence peut être caractérisée par l'intensité et la position, la durée de vie, la polarisation et la longueur d'onde. Les techniques d'imagerie de fluorescence sont des outils puissants dans les sciences biologiques et biomédicales car elles sont peu invasives et peuvent être appliquées aux cellules vivantes et aux tissus (Wouters et al. 2001).

Localisation subcellulaire et dynamique des sensibilisants pendant la PDT

Les distributions intracellulaires in vitro ont été déterminées pour une série de PS avec des structures largement différentes. Un des paramètres structuraux importants qui influence la distribution sont la charge ionique qui varie de –4 à +4, le degré d'hydrophobicité (coefficient de partition octanol-eau) et le degré d'asymétrie présent dans la molécule. Les PSs qui sont hydrophobiques et qui ont deux ou moins de charges négatives peuvent diffuser à travers la membrane plasmatique. Ces PS tendent également à avoir une incorporation plus élevée dans les cellules *in vitro,* spécialement quand ils sont présents en concentrations relativement basses dans le milieu (<1 µM). Les composés moins hydrophobiques et les PSs qui ont plus de deux charges négatives tendent à être trop polaires pour diffuser à travers la membrane plasmatique, et sont par conséquent incorporés par endocytose. La charge, son signe et sa distribution, l'hydrophilicité ou l'hydrophobicité du sensibilisant détermine le mode d'interaction avec les biomolécules et les transporteurs, ses propriétés photophysiques et l'efficacité du photosensibilisant dans un système biologique.

Pendant l'exposition à la lumière, les photosensibilisants peuvent déplacer d'un site de liaison à un autre. Ceci est aussi appelé re-localisation induite par la lumière. Ceci a été montré pour des colorants lysosomotropiques comme TPPS$_4$ (Berg et al. 1991; Rück et al. 1992), le bleu de Nil (Lin et al. 1993), AlPcS$_4$ et AlPcS$_2$ (Rück et al. 1990; Peng et al. 1991; Rück et al. 1996), qui présentent une distribution lysosomiale granulaire dans une region périnucléaire discrete (Rück et al, 1996).

III OBJECTIFS

La première partie du travail a été l'étude de l'influence des concentrations de la mTHPC dans la tumeur, le plasma et les leucocytes à différents temps après l'injection du photosensibilisant sur la réponse PDT in vivo.

Le second objectif de notre travail était d'étudier les interactions mTHPC avec les protéines du plasma et son état d'agrégation. Dans ce but, nous avons étudié les propriétés spectroscopique et cinétique de la mTHPC en solution contenant des protéines du plasma.

Le troisième objectif était d'examiner la cinétique et le mécanisme de redistribution de la mTHPC à partir de complexes avec les protéines du plasma au membranes modèles.

La quatrième partie du travail consiste en l'étude de l'état d'agrégation de la mTHPC intracellulaire en fonction du temps d'incubation et de la localisation des photosensibilisants et de son influence sur le rendement quantique de l'inactivation des cellules.

La cinquième partie du travail a été l'évaluation du solvatochromisme de la mTHPC, mTHPP and mTHPBC dans différents solvants et la détermination de leur structure d'agrégats en milieu aqueux.

IV RESULTATS

Traitement photodynamique in vivo à base de Foscan® : corrélation entre l'efficacité du Foscan® et son accumulation dans la tumeur, le plasma et les leucocytes.

L'effet antitumoral de la thérapie photodynamique médié par le Foscan peut impliquer le destruction à la fois de la vascularisation et des cellules cancéreuses. L'importance de chaque mécanisme semble être définie par l'intervalle de temps entre l'administration du photosensibilisant et l'illumination (intervalle drogue-lumière, DLI). Les intervalles courts drogue-lumière favorisent des dommages vasculaires dus à l'accumulation préférentielle du photosensibilisant dans la vascularisation de la tumeur, tandis que les intervalles longs drogue-lumière déclenchent des dommages directs aux cellules tumorales dus à la localisation du produit dans la tumeur. Les études pharmacocinétiques et de la réponse tumorale ont été effectuées sur des souris nude avec des cellules tumorales Colo26 xénogreffées. A 96 h après injection par i.v. de 0.5 mg/kg Foscan, des animaux ont été exposés à une lumière à 652 nm de 10 J/cm^2 délivrée à 30 mW/cm^2. Le temps moyen de recroissance de la tumeur a été déterminé pour chaque protocole de traitement et corrélé avec la distribution du Foscan dans les compartiments d'intérêt à l'heure de l'irradiation. L'efficacité de la PDT a été plus grande pour des irradiations à 6 et 12h après injection du Foscan et limitée à 96h. A la différence des concentrations du Foscan dans la tumeur et le plasma, l'accumulation du photosensibilisant dans les leucocytes montre une bonne corrélation avec l'efficacité de la PDT. Ces résultats suggèrent que les leucocytes pourraient jouer un rôle important dans le mécanisme de la PDT induisant des dommages vasculaires en étant l'un des compartiments effecteurs principaux ou par une meilleure accumulation du Foscan dans les cellules endothéliales comparées au plasma. La prédominance des dommages indirects a été accentuée par le fait que l'efficacité de la PDT n'a pas été modifiée par l'utilisation d'une valeur plus élevée de fluence (160 mW/cm^2), ce qui a épuisé l'oxygène intratumoral et n'a pas limité la toxicité PDT-induite des cellules.

Investigation des interactions du Foscan® avec les protéines du plasma

Le travail présenté montre l'interaction du Foscan® avec l'albumine et des lipoprotéines de plasma. Les études spectroscopiques ont indiqué la présence d'espèces monomériques et agrégées du Foscan® à l'addition de solutions de protéines plasmatiques. Les cinétiques de désagrégation du Foscan® dans des solutions enrichies en albumine étaient très sensibles à la concentration de la protéine et à la température d'incubation. Les analyses cinétiques ont démontré que deux types d'espèces agrégées du Foscan® pourraient être impliquées dans la désagrégation : des dimères avec une constante $k_1 = (2.3 \pm 0.15) \times 10^{-3}$ s^{-1} et des agrégats plus gros avec des constantes variant de $(0.55 \pm 0.04) \times 10^{-3}$ s^{-1} pour la plus basse concentration d'albumine à $(0.17 \pm 0.02) \times 10^{-3}$ s^{-1} pour la plus haute. La désagrégation augmente considérablement avec l'élévation de la température de 15°C à 37 °C. Comparée à l'albumine, les cinétiques de désagrégation du Foscan® en présence de lipoprotéines ont montré une plus pauvre dépendance à la concentration de lipoprotéines et de plus faible variation des constantes de désagrégations. L'analyse du Foscan® dans les solutions d'albumine par chromatographie par gel-filtration ont démontré la présence de fraction d'agrégats libres, non liés aux protéines-Foscan® et du Foscan® monomérique lié à la protéine.

La redistribution du Foscan® des protéines plasmatiques au modèle membranaire.

La thérapie Photodynamique (PDT) est comparativement une nouvelle modalité de traitement des tumeurs superficielles qui inclut l'action simultanée des photosensibilisants, de la lumière et de l'oxygène. La redistribution du photosensibisant entre les protéines plasmatiques et les biomembranes définit l'interaction des photosensibisants avec les cellules, leur localisation intracellulaire et les cinétiques d'accumulation du photosensibilisant dans la tumeur. Notre travail étudie la cinétique de libération du Foscan® des protéines plasmatique vers les modèles membranaires en utilisant la fluorescence resonance energy transfer (FRET) à partir d'un marqueur, lié à la protéine, au photosensibilisant. Nous avons mis en évidence de très lentes cinétiques de libération du Foscan® du complexe protéique avec des constantes de $(1.7 \pm 0.1) \times 10^{-3}$ s^{-1} pour l'albumine et $(1.6 \pm 0.3) \times 10^{-4}$ s^{-1} pour les HDL. Le Foscan® se redistribue à la fois par une collision et une diffusion par le transfert des complexes avec HDL avec des constantes bimoléculaires $k_{out} = (8.8 \pm 1.4) \times 10^{-2}$ M^{-1}s^{-1}. Les considérations thermodynamiques ont proposé que la redistribution du photosensibilisant depuis les HDL dans le milieu aqueux est non favorable et que le mécanisme de collision apparaissait comme

le mode préféré de transfert dans un environnement biologique. Les faibles taux de redistribution du Foscan® depuis les protéines plasmatiques devraient être considérés lors de la planification des protocoles de dosimétrie pour les PDT avec Foscan®.

Etat d'agrégation et phototoxicité de la mTHPC dans les cellules MCF-7

Les propriétes photophysiques du Foscan® dépendent considérablement du temps d'incubation dans les cellules. Cet effet peut s'expliquer sur la base des différents modèles de localisation et de concentration des PS dans les cellules. Après 3h d'incubation, la mTHPC a diffusé et présente une localisation relativement homogène dans les cellules MCF-7. Le marquage maximal obtenu après 24h d'incubation avec la mTHPC se caractérise par des « spots lumineux ». Il s'accompagne d'une diminution substantielle de l'absorbance dans la bande de Soret, par une cinétique de photoblanchiment plus lente et bi-exponentielle et par une réduction des durées de vie de fluorescence comparée à la mesure à 3h. La durée de vie de la mTHPC était égale à 8.7 ns au point à 3h, 3.9 et 2.0 ns dans les régions diffuses et caractérisées par des spots au point à 24 h respectivement. L'efficacité absolue de la mTHPC à 24h a été déterminée par essai clonogénique 3 fois supérieurs comparée à 3h. Pour comparer les rendements quantiques du photosensibilisant dans les cellules à différents temps d'incubation, le nombre de photons absorbés par le PS intracellulaire a été calculé en fonction du temps d'irradiation. Ensuite, nous avons calculé le phototoxicité cellulaire en terme de nombre de photons absorbé. De cette manière, nous avons obtenu une phototoxicité 3 fois supérieure à 3h comparé a 24h. Cette différence pourrait être expliqué par l'état d'agrégation différent du Foscan. Nous avons observé qu'à 3h d'incubation, le Foscan est plus monomerisé. Cette conclusion est confirmée par l'étude effectuée par FLIM. Le temps durée de vie de fluorescence du PS plus court correspond à un état d'agrégation plus important.

Étude Chimie Quantique de la Structure des Complexes Moléculaire des Composés Tetrapyrrole.

La dernière partie de notre travail était l'étude théorique et spectroscopique de la structure d'agrégats de mTHPC, de mTHPP et de mTHPBC dans des mélanges de eau/ethanol. Pour étudier les propriétés spectroscopiques des composés mentionnés ci-dessus nous avons développé une théorie semi-empirique de mécanique quantique basée sur la théorie de l' orbitale moléculaire de Huckel pour calculer les variations spectrales dans différents solvants.

Lors de l'introduction des photosensibilisants dans le milieu aqueux, les bandes de Soret et dans le rouge de leurs spectres d'absorption subissent des décalages dans le rouge comparés aux solvants non polaires. Ce qui indique la formation d'agrégats. Les études chimie quantique et spectroscopique ont indiqué que la mTHPC et la mTHPP forment des dimères de type J dans les mélanges eau-éthanol. La mTHPBC forme des dimères linéaires avec un angle inférieur à 180° entre les plans moléculaires monomères. Tous les dimères sont reliés au moyen de liaisons hydrogène entre les groupes phényles OH.

V CONCLUSIONS ET PERSPECTIVES

L'étude de l'influence des pharmacocinétiques de la mTHPC dans la tumeur, le plasma et les leucocytes sur la réponse à la PDT ont montré que l'accumulation du photosensibilisant dans les leucocytes exhibaient une bonne corrélation avec l'efficacité de la PDT. Ces résultats suggèrent que les leucocytes pourraient jouer un rôle important dans le mécanisme de la PDT induisant des dommages vasculaires en étant l'un des compartiments effecteurs principaux ou par une meilleure accumulation de la mTHPC dans les cellules endothéliales comparées au plasma.

- *Perspectives*:

Étude du transport par la suite et de la distribution de la mTHPC dans le système vasculaire et dans les tissus.

L'étude de la monomérisation de la mTHPC au cours des interactions avec des protéines plasmatiques démontrent un taux lent de cinétique de désagrégation qui est accompagné d'une augmentation du rendement quantique de fluorescence du photosensibilisant. La fraction de mTHPC agrégée à l'équilibre et le taux de désagrégation du photosensibilisant dépendent fortement de la teneur en protéines et de la température d'incubation. Les valeurs basses des taux de désagrégation de la mTHPC peuvent être expliquées par la nature lipophilique du photosensibilisant et la formation d'agrégats à grande échelle avec une interaction forte entre les molécules du photosensibilisant. Les expériences de Gel-filtration avec de la BSA monomérique ont indiqué la présence d' agrégats libres de photosensibilisant.

- *Perspectives*:

Étude des mécanismes d'internalisation et de transport intracellulaire de la mTHPC.

L'analyse cinétique basée sur la technique de FRET démontre que la mTHPC est caractérisée par des taux très lents de redistribution depuis les complexes avec les protéines plasmatiques. Les faibles taux de redistribution de la mTHPC comparés aux autres photosensibilisants correspondent aux propriétés de liaisons uniques de la mTHPC. Les considérations thermodynamiques et cinétiques nous laissent supposer l'existence à la fois le transfert par collision et par milieu aqueux. Le premier type de transfert prédomine en conditions physiologiques.

- *Perspectives*:

Comparaison des paramètres cinétiques de la redistribution de la mTHPC avec ceux de la formulation liposomale de la mTHPC (Foslip®).

L'étude en microscopie confocale indique des modèles de localisation diffus de la mTHPC à 3h et la formation de taches fortement fluorescentes du photosensibilisant à 24h d' incubation dans des cellules MCF. Les caractéristiques photophysiques du photosensibilisant obtenues en utilisant la spectroscopie d'absorption et la technique de FLIM ont montré qu'à 24h d'incubation la mTHPC est beaucoup plus agrégée qu'à 3h. Ces données ont été confirmées par des mesures des cinétiques de photoblanchiment du photosensibilisant. Le rendement quantique de photoinactivation des cellules est environ 3 fois plus important pour le point à 3h. Une telle différence est attribuée à l'effet d'auto-quenching du photosensibilisant dû aux différents états d'agrégation et interactions avec les composants cellulaires.

- *Perspectives*:

Évaluation des caractéristiques photophysiques de la mTHPC et de l'état d'agrégation dans les tissus *in vivo* en utilisant la technique de FLIM.

L'étude théorique et spectroscopique de la mTHPC, la mTHPP et la mTHPBC nous a permi de définir leur structure agrégée dans des milieux aqueux À cette fin, nous avons développé une méthode semi-empirique de mécanique quantique basée sur le calcul des variations spectrales dans différents solvants. La mTHPC et la mTHPP forment un J-type dimères dans des mélanges d'eau-éthanol, tandis que la mTHPBC forme des dimères linéaires.

- *Perspectives*:

Cette approche peut être employée pour calculer les cartes de densité électroniques des photosensibilisants dans les solutions biologiques et peut permettre de prévoir la photosensibilité de produit.

Abbreviations

HPLC	High-performance liquid chromatography
TIRF	Total internal reflection fluorescence microscopy
FLIM	Fluorescence lifetime imaging
PS	Photosensitizer
LDL	Low density lipoproteins
HDL	High density lipoproteins
FRET	Fluorescence resonance energy transfer
FCS	Fetal calf serum
FDA	Food and Drug Administration
LDI	Light-drug interval
HpD	Haematoporphyrin derivative
HSA	Human serum albumin
IC	Internal conversion
ISC	Intersystem crossing
mTHPBC	5,10,15,20-tetrakis(m-hydroxyphenyl)bacteriochlorin
mTHPC	5,10,15,20-tetrakis(m-hydroxyphenyl)chlorin
mTHPP	5,10,15,20-tetrakis(m-hydroxyphenyl)porphyrin
PBS	Phospate buffer saline
PDT	Photodynamic therapy
TCSPC	Time-correlated single photon counting
TAC	Time to amplitude converter
ADC	Analogue to digital converter
VR	Vibrational relaxation
GFP	Green fluorescent protein
YFP	Yellow fluorescent protein
HP	Hematoporphyrin
PpIX	Protoporphyrin IX
BPD	Benzoporphyrin derivative
RLS	Resonance light scattering
FBP	Free base porphin
MAL	Methylaminolevulinate
HAL	Hexylaminolevulinate
BCC	Basal cell carcinoma
DP	Deuteroporphyrin
BPD-MA	Benzoporphyrin derivative monoacid ring A

Scientific works

Articles in International Reviewed Journals

Maugain E, Sasnouski S, Zorin V, Merlin JL, Guillemin F, Bezdetnaya L.
Foscan-based photodynamic treatment in vivo: correlation between efficacy and Foscan accumulation in tumor, plasma and leukocytes. *Oncol Rep*. 2004, 12:639-45.

Sasnouski S, Zorin V, Khludeyev I, D'Hallewin MA, Guillemin F, Bezdetnaya L.
Investigation of Foscan® interactions with plasma proteins. *Biochim Biophys Acta*. (2005) 1725(3), 394-402.

Sasnouski S, Kachatkou D, Zorin V, Guillemin F, Bezdetnaya L. Redistribution of Foscan® from plasma proteins to model membranes. *Photochem. Photobiol. Sci.*, 2006, *5*, 770–777.

International Meetings and Symposia integrally published in Proceedings

E. Maugain, S. Sasnouski, V. P. Zorin, M. Barberi-Heyob, J. L. Merlin, L. Bezdetnaya, F. Guillemin. Foscan®-based PDT in relation to drug-light interval.
10th Congress of the Europeen Society for Photobiology, Vienne, 2003.
Abstract book., 2003, P93.

E. Maugain, S. Sasnouski, V.P. Zorin, M. Barberi-Heyob, J.L. Merlin., L. Bezdetnaya, F. Guillemin. Thérapie photodynamique des cancers avec le Foscan® : optimisation des protocoles d'irradiation.
Congress Eurocancer 2003 (Paris, 8-10 july 2003)
Abstract book.

Sasnousky S, V. Zorin, I. Hludeev, F. Guillemin, L. Bolotine.
Cinetique de redistribution du Foscan (5, 10, 15, 20-tetrakis(m-hydroxyphenyl)chlorin) entre les proteins du plasma evaluee par FRET (fluorescence resonance energy transfer).
JSTIM (Journees Sciences et TechnologiesIimagerie) , 21-23 mars, 2005, Nancy, France.
Actes STIM, P159.

D. Knyazev, S.Sosnovsky, V. Zorin, L. Bolotine, F. Guillemin Evaluation of meta-tetra (hydroxiphenil)chlorin incorporation into lipid bilayer.

Joint Conference of the German Society of Applied Optics (DGaO) and the Section of Optics of the Polish Physical Society. Wroclaw, Poland, May 17-20, 2005.

Abstract book.

Oral communications

S. Sasnouski, V. Zorin, I. Khludeev, F. Guillemin, L. Bolotine. Meta-tetra(hydroxyphenyl)chlorin (mTHPC) aggregation state and interaction with plasma albumin.

11th Congress of the Europeen Society for Photobiology, 3-8 septembre, Aix-les-Bains, France.

Abstract book, 2005, P105.

S. Sasnouski, I. Khludeev, V. Zorin, L. Bolotine, F. Guillemin, Comparison Foscan® redistribution rates from the complexes with high density lipoproteins and low density lipoproteins, International congress "Molecular, membrane and cellular basis of biosystems function" VII meeting of the belorussian society of photobiology and biophysics, june 21-23 2006 Minsk.

Abstract book.

Acknowledgments